# Appendix 9.C

# Additional Information on Containment Circulation and Stratification

**J. Woodcock**
**M. DzoDzo**

# TABLE OF CONTENTS

| Section | Title | Page |
|---|---|---|
| LIST OF TABLES | | 9.C-iii |
| LIST OF FIGURES | | 9.C-iv |
| 9.C.1 | DEVELOPMENT OF EXPECTED FLOW PATTERNS FOR AP600 AND AP1000 BASED ON SEPARATE FLOW TESTS IN ENCLOSURES | 9.C-1 |
| 9.C.1.1 | STRATIFICATION PHENOMENA | 9.C-1 |
| 9.C.1.1.1 | Static Stratification | 9.C-3 |
| 9.C.1.1.2 | Stratification and Circulation | 9.C-5 |
| 9.C.1.1.3 | References | 9.C-21 |
| 9.C.1.2 | CIRCULATION PHENOMENA | 9.C-25 |
| 9.C.1.2.1 | Circulation Phenomena Due to the Presence of Boundary Layers (Wall Jets) and Buoyant Plumes Formed as a Consequence of Natural Convection Effects | 9.C-26 |
| 9.C.1.2.2 | Circulation Phenomena Due to the Interaction With the Hot Buoyant Plumes and Jets | 9.C-28 |
| 9.C.1.2.3 | References | 9.C-36 |
| 9.C.1.3 | IMPORTANT DIMENSIONLESS GROUPS | 9.C-38 |
| 9.C.1.3.1 | Important Dimensionless Groups for Stratification and Circulation Phenomena Inside Enclosures | 9.C-38 |
| 9.C.1.3.2 | References | 9.C-42 |
| 9.C.1.4 | EXPECTED FLOW PATTERNS FOR AP600 AND AP1000 | 9.C-43 |
| 9.C.1.4.1 | Simplified Representation of Circulation Regions During Post-Blowdown LOCA in AP600 and LST | 9.C-43 |
| 9.C.1.4.2 | A Qualitative Model for Recirculating Stratified Region II | 9.C-46 |
| 9.C.1.4.3 | References | 9.C-58 |
| 9.C.2 | OVERVIEW OF THE INTERNATIONAL CONTAINMENT EXPERIMENTAL DATA BASE | 9.C-59 |
| 9.C.2.1 | DESCRIPTION OF THE AVAILABLE BATTELLE MODEL CONTAINMENT (BMC) DATABASE | 9.C-65 |
| 9.C.2.1.1 | Natural Convection Phenomena Inside the Multi-Compartment Containment (F2 Experiments) | 9.C-66 |
| 9.C.2.1.2 | The Influence of Initial Temperature Distribution, Location of Hydrogen Injection, Duration of Injection, and Size of Vent Openings on the Hydrogen Distribution | 9.C-86 |
| 9.C.2.1.3 | Effects of Sump Heatup on Global Natural Circulation (Experiments RX1 - RX5) | 9.C-98 |
| 9.C.2.1.4 | References | 9.C-111 |

## TABLE OF CONTENTS (Cont.)

| Section | Title | Page |
|---|---|---|
| 9.C.2.2 | DESCRIPTION OF THE AVAILABLE NUPEC DATA BASE | 9.C-112 |
| 9.C.2.2.1 | M-7-1 Test | 9.C-112 |
| 9.C.2.2.2 | M-4-3 Test | 9.C-112 |
| 9.C.2.2.3 | References | 9.C-122 |
| 9.C.2.3 | DESCRIPTION OF THE AVAILABLE CAROLINAS VIRGINIA TUBE REACTOR CONTAINMENT (CVTR) DATABASE | 9.C-123 |
| 9.C.2.4 | DESCRIPTION OF THE AVAILABLE HDR DATABASE | 9.C-139 |
| 9.C.2.4.1 | HDR E11 Test Series | 9.C-139 |
| 9.C.2.4.2 | HDR Large LOCA Experimental Data Base | 9.C-175 |
| 9.C.2.4.3 | References | 9.C-223 |
| 9.C.2.5 | CONCLUSION | 9.C-225 |
| 9.C.3 | APPLICATION OF LUMPED-PARAMETER CODES FOR MODELING LARGE CONTAINMENT FACILITIES | 9.C-227 |
| 9.C.3.1 | VALIDATION OF THE LUMPED PARAMETER CONTAINMENT ANALYSIS COMPUTER CODES BASED ON BMC EXPERIMENTAL RESULTS | 9.C-227 |
| 9.C.3.1.1 | F2 Experiments - Natural Convection Phenomena Inside the Multi-Compartment Containment | 9.C-227 |
| 9.C.3.1.2 | Influence of Initial Temperature Distribution, Location of Hydrogen Injection, Duration of Injection, and Size of Vent Openings on Hydrogen Distribution (BMC Tests 2, 4, 6, 12, and 20) | 9.C-228 |
| 9.C.3.2 | VALIDATION OF THE LUMPED PARAMETER CONTAINMENT ANALYSIS COMPUTER CODES BASED ON NUPEC EXPERIMENTAL RESULTS | 9.C-230 |
| 9.C.3.2.1 | M-7-1 Test | 9.C-230 |
| 9.C.3.2.2 | M-4-1 Test | 9.C-230 |
| 9.C.3.3 | VALIDATION OF THE LUMPED-PARAMETER CONTAINMENT ANALYSIS COMPUTER CODES BASED ON HDR EXPERIMENTAL RESULTS | 9.C-241 |
| 9.C.3.4 | CONCLUSIONS | 9.C-251 |
| 9.C.3.5 | REFERENCES | 9.C-253 |

# LIST OF TABLES

| Table | Title | Page |
|---|---|---|
| Table 9.C-1 | Comparison of Various Facilities | 9.C-61 |
| Table 9.C-2 | Overviewed Tests from International Database | 9.C-62 |
| Table 9.C-3 | Representative Velocity in [m/s] in Opening from R3 to R6 in the Different Experimental Phases of Experiment F2, Phases 2-4 | 9.C-69 |
| Table 9.C-4 | Test Matrix of Battelle Sump Heatup Experiments | 9.C-100 |
| Table 9.C-5 | Events for E11.4 Experiment | 9.C-163 |
| Table 9.C-6 | HDR-V21.1 Test Conditions | 9.C-188 |

## LIST OF FIGURES

| Figure | Title | Page |
|---|---|---|
| Figure 9.C.1-1a | The formation of the horizontal layers of the constant density due to the stratification | 9.C-9 |
| Figure 9C.1-1b | Interaction of jets, plumes and wall boundary layers with stratified regions | 9.C-10 |
| Figure 9C.1-2 | Combination of the constant temperature boundary conditions at the outside and inside surfaces which will produce stratification inside the enclosure | 9.C-11 |
| Figure 9C.1-3 | Stratification inside the upper and lower corners of the romb-shaped enclosure | 9.C-12 |
| Figure 9C.1-4 | Experimental and numerical results for the romb-shaped enclosure with the romb angle 44° and $Ra=3.5*10^4$, Pr=5270 | 9.C-13 |
| Figure 9.C.1-5 | a) The square enclosure with vertical walls at the different temperatures and horizontal walls adiabatic, b) Streamlines for $Ra^6$ and Pr=0.71,c) Isotherms for $Ra=10^6$ and Pr=0.71 | 9.C-14 |
| Figure 9.C.1-6 | Average Nusselt numbers as a function of the Rayleigh numbers for the square enclosure with opposite vertical walls at the different temperature and Pr=0.71 (air) | 9.C-15 |
| Figure 9.C.1-7 | Formation of the stratified core in between two opposite vertical line jets (after Baines and Turner, 1969) | 9.C-16 |
| Figure 9.C.1-8 | Flow in an enclosure with vertical opposite walls at different temperatures ($Ra=10^5$, Pr=0.71) | 9.C-17 |
| Figure 9.C.1-9 | Internal waves in the square cavity - fluctuations in the temperature field at $Ra=2*10^8$ and Pr=0.71 (air) | 9.C-18 |

## LIST OF FIGURES (Cont.)

| Figure | Title | Page |
|---|---|---|
| Figure 9.C.1-10 | Temperatures for the initial solution with the hot and cold intrusions and boundary layer waves presented (after Armfield and Janssen, 1996) | 9.C-19 |
| Figure 9.C.1-11 | Formation of the downward negatively buoyant jets | 9.C-20 |
| Figure 9.C.1-12 | Rayleigh-Benard convection example | 9.C-29 |
| Figure 9.C.1-13 | Hele-Shaw cell | 9.C-30 |
| Figure 9.C.1-14 | Steady and oscillatory convection in Hele-Shaw cell (after Buhler et al., 1987) | 9.C-31 |
| Figure 9.C.1-15 | Turbulent (chaotical) flow with hot and cold plumes interactions (plane cross-section of the three-dimensional enclosure is presented) | 9.C-32 |
| Figure 9.C.1-16 | Interaction of hot and cold plumes (after Aqino et al., 1989) | 9.C-33 |
| Figure 9.C.1-17a | Vertical temperature distribution inside the cylindrical enclosure with lower and upper horizontal plate at higher and lower temperatures, respectively ($Ra=9.38*10^7$, $Pr=200$) | 9.C-34 |
| Figure 9.C.1-17b | Generation of the cold plumes due to the brake (separation) of the vertical boundary layers near the cold vertical walls | 9.C-35 |
| Figure 9.C1-18 | Primary flow regions and volumetric flow rates for quasi-steady containment conditions | 9.C-52 |
| Figure 9.C.1-19 | The volumetric flow between the upper and lower deck regions $Q_e$ | 9.C-53 |

## LIST OF FIGURES (Cont.)

| Figure | Title | Page |
|---|---|---|
| Figure 9.C.1-20 | Primary flow regions and volumetric flow rates for quasi-steady containment conditions in LST case | 9.C-54 |
| Figure 9.C.1-21 | Inflows and outflows from the Region II | 9.C-55 |
| Figure 9.C.1-22 | Recirculating flow paths inside the Region II | 9.C-56 |
| Figure 9.C.1-23 | Mass conservation for thin horizontal layer inside the Region II | 9.C-57 |
| Figure 9.C.2-1 | Comparison of different facilities | 9.C-60 |
| Figure 9.C.2-2 | Model Containment: vertical cross-section 0/180°, horizontal cross-sections at +02 m and +1.7 m for configuration in experiment F2 | 9.C-70 |
| Figure 9.C.2-3 | Model Containment: vertical cross-section 0/180°, horizontal cross-sections at +4.01 m and +5.05 m for configuration in experiment F2 | 9.C-71 |
| Figure 9.C.2-4 | Injections and convective flow loop directions (+ sign for flow indicates the same direction of the flow as arrow in R9) | 9.C-72 |
| Figure 9.C.2-5 | Experiment F2, Phases 2-8, experimental procedures, total and partial pressures | 9.C-73 |
| Figure 9.C.2-6 | Number of compartments, locations of measurement transducers and steam releases | 9.C-74 |
| Figure 9.C.2-7 | Test group F2, Phase 1 (heatup), total pressure in the containment | 9.C-75 |
| Figure 9.C.2-8 | Test group F2 Phase 1 (heatup), atmospheric temperature in the compartment R9, H=1.0 m and 21 m | 9.C-76 |

## LIST OF FIGURES (Cont.)

| Figure | Title | Page |
|---|---|---|
| Figure 9.C.2-9 | Scheme of multi-compartment containment geometry in experiment F2 | 9.C-77 |
| Figure 9.C.2-10 | Test group F2, phase 2: atmospheric temperatures in zones 1, 2 and 3 (R5 + R6, R1 + R4, R7 + R8) | 9.C-78 |
| Figure 9.C.2-11 | Test group F2, phases 3 and 4: atmospheric temperatures in zones 1, 2 and 3 (R5 + R6, R1 + R4, R7 + R8) | 9.C-79 |
| Figure 9.C.2-12 | Thermodynamic state of steam-air atmosphere in R9 top (H=7.6 m) | 9.C-80 |
| Figure 9.C.2-13 | Thermodynamic state of steam-air atmosphere in R9 bottom (H=1 m) | 9.C-81 |
| Figure 9.C.2-14 | Test group F2, phase 2: atmospheric temperatures in R9 (Zone 4) | 9.C-82 |
| Figure 9.C.2-15 | Test group F2, phases 3 and 4: atmospheric temperature in R9 (Zone 4) | 9.C-83 |
| Figure 9.C.2-16 | Velocities in opening from compartment R7 to compartment R9 | 9.C-84 |
| Figure 9.C.2-17 | Velocities in opening from compartment R3 to compartment R6 | 9.C-85 |
| Figure 9.C.2-18 | Vertical cut through BMC with orifice in between R2 and R1 | 9.C-89 |
| Figure 9.C.2-19a | BMC test no. 2: Comparison between experimental data and 2-d GOTHIC computations for hydrogen concentrations | 9.C-90 |
| Figure 9.C.2-19b | BMC test no. 4: Comparison between experimental data and 2-d GOTHIC computations for hydrogen concentrations | 9.C-91 |

## LIST OF FIGURES (Cont.)

| Figure | Title | Page |
|---|---|---|
| Figure 9.C.2-19c | BMC test no. 6: Comparison between experimental data and 2-d GOTHIC computations for hydrogen concentrations | 9.C-92 |
| Figure 9.C.2-20 | BMC test no. 12: Comparison between experimental data and GOTHIC-lp computations for hydrogen concentrations | 9.C-94 |
| Figure 9.C.2-21a | BMC test no. 20: Comparison between experimental data and 2-d GOTHIC computations for hydrogen concentrations | 9.C-95 |
| Figure 9.C.2-21b | BMC test no. 20: Comparison between experimental data and 2-d GOTHIC computations for hydrogen concentrations | 9.C-96 |
| Figure 9.C.2-21c | BMC test no. 20: Comparison between experimental data and 2-d GOTHIC computations for hydrogen concentrations | 9.C-97 |
| Figure 9.C.2-22 | Perspective view, vertical and upper horizontal cross-sections through BMC with main steam feedline | 9.C-101 |
| Figure 9.C.2-23 | Perspective view, vertical and upper horizontal cross-sections through BMC with auxiliary steam feedline | 9.C-102 |
| Figure 9.C.2-24 | Instrumentation plan for BMC - sump heatup test RX4 | 9.C-103 |
| Figure 9.C.2-25 | Battelle-Experiment RX4: Sump and atmospheric temperatures | 9.C-104 |
| Figure 9.C.2-26 | Battelle-Experiment RX4: Velocities in side vents | 9.C-105 |

## LIST OF FIGURES (Cont.)


| Figure | Title | Page |
|---|---|---|
| Figure 9.C.2-27 | Battelle-Experiment RX4: Temperatures in center compartment and dome | 9.C-106 |
| Figure 9.C.2-28 | Battelle-Experiment RX4: Temperatures in external annulus | 9.C-107 |
| Figure 9.C.2-29 | Battelle-Experiment RX4: Hydrogen concentration along circulation path | 9.C-108 |
| Figure 9.C.2-30 | Battelle-Experiment RX4: Hydrogen concentrations in intermediate subcompartments | 9.C-109 |
| Figure 9.C.2-31 | Battelle-Experiment RX4: Relative humidity in the containment atmosphere | 9.C-110 |
| Figure 9.C.2-32 | Model containment used in the test, break-release position, and circulation flow paths (see arrows) | 9.C-115 |
| Figure 9.C.2-33 | Detailed arrangement of each floor | 9.C-116 |
| Figure 9.C.2-34 | Distribution of the compartments at each floor | 9.C-117 |
| Figure 9.C.2-35 | Pressure history | 9.C-118 |
| Figure 9.C.2-36 | Dome temperature history | 9.C-119 |
| Figure 9.C.2-37 | Dome helium concentration history | 9.C-120 |
| Figure 9.C.2-38 | a) Temperature histories for compartments forming a circulation path (8, 15, dome and 7) b) Helium concentration histories for compartments forming a circulation path (8, 15, dome and 7) | 9.C-121 |
| Figure 9.C.2-39 | Carolinas Virginia Tube Reactor (CVTR) containment structure | 9.C-126 |

## LIST OF FIGURES (Cont.)


| Figure | Title | Page |
|---|---|---|
| Figure 9.C.2-40 | CVTR steam line diffuser | 9.C-127 |
| Figure 9.C.2-41a | Steam injection histories test 1 | 9.C-128 |
| Figure 9.C.2-41b | Steam injection histories test 2 | 9.C-129 |
| Figure 9.C.2-41c | Steam injection histories test 3 | 9.C-130 |
| Figure 9.C.2-42 | CVTR containment pressure response (Heise gauge) | 9.C-131 |
| Figure 9.C.2-43 | Atmospheric vertical temperature profile, test 1 | 9.C-132 |
| Figure 9.C.2-44 | Atmospheric vertical temperature profile, test 2 | 9.C-133 |
| Figure 9.C.2-45 | Atmospheric vertical temperature profile, test 3 | 9.C-134 |
| Figure 9.C.2-46 | Surface and atmosphere temperatures - intermediate region, test 1 | 9.C-135 |
| Figure 9.C.2-47 | Surface and atmosphere temperatures - basement region, test 1 | 9.C-136 |
| Figure 9.C.2-48 | Concrete surface temperatures, test 1 | 9.C-137 |
| Figure 9.C.2-49 | Isolated containment region temperatures | 9.C-138 |
| Figure 9.C.2-50 | Cross-sections, elevations and numbers of compartments of the HDR containment, left (180°-0° cross-section), right (270°-90° cross-section) | 9.C-142 |
| Figure 9.C.2-51 | Locations and enumerations of thermocouples (left) and anemomenters (right) of HDR-E-test series | 9.C-143 |
| Figure 9.C.2-52 | HDR-E11.2 sequence of experimental test procedures | 9.C-144 |

## LIST OF FIGURES (Cont.)

| Figure | Title | Page |
|---|---|---|
| Figure 9.C.2-53 | HDR-E11.2 containment pressure history | 9.C-145 |
| Figure 9.C.2-54 | HDR-E11.2 atmospheric temperatures along main stairway | 9.C-146 |
| Figure 9.C.2-55 | HDR-E11.2 steam concentrations along main stairway | 9.C-147 |
| Figure 9.C.2-56 | HDR-E11.2 $H_2$/He Gas concentrations along main stairway | 9.C-148 |
| Figure 9.C.2-57 | HDR-E11.2 Comparison between temperatures in main and spiral stairways at +31.0 m level | 9.C-149 |
| Figure 9.C.2-58 | HDR-E11.2 Comparison between temperatures in main and spiral stairways at +26.5 m level | 9.C-150 |
| Figure 9.C.2-59 | HDR-E11.2 Comparison between temperatures in main and spiral stairways at +16.5 m level | 9.C-151 |
| Figure 9.C.2-60 | HDR-E11.2 Comparison between temperatures in main and spiral stairways at +6 m level | 9.C-152 |
| Figure 9.C.2-61 | HDR-E11.2 Axial temperature profiles in both major flow paths at specific times, left in spiral stairway, right in main stairway | 9.C-153 |
| Figure 9.C.2-62 | HDR-E11.3 Velocities in both major flow paths at different axial positions during containment heatup | 9.C-155 |
| Figure 9.C.2-63 | HDR-E11.3 Velocities in both major flow paths a different axial positions during $H_2$/He gas mixture release | 9.C-156 |
| Figure 9.C.2-64 | HDR-E11.3 Comparison between temperatures in main and spiral stairways at +31.0 m level | 9.C-157 |

## LIST OF FIGURES (Cont.)

| Figure | Title | Page |
|---|---|---|
| Figure 9.C.2-65 | HDR-E11.3 Comparison between temperatures in main and spiral stairways at +26.5 m level | 9.C-158 |
| Figure 9.C.2-66 | HDR-E11.3 Comparison between temperatures in main and spiral stairways at +16.5 m level | 9.C-159 |
| Figure 9.C.2-67 | HDR-E11.3 Comparison between temperatures in main and spiral stairways at +6 m level | 9.C-160 |
| Figure 9.C.2-68 | HDR-E11.3 Axial temperature profiles in both major flow paths at specific times, left in spiral stairway, right in main stairway | 9.C-161 |
| Figure 9.C.2-69 | HDR-E11.4 Sequence of Experimental Test Procedures | 9.C-164 |
| Figure 9.C.2-70 | HDR-E11.4 Containment pressure history | 9.C-165 |
| Figure 9.C.2-71 | HDR-E11.4 Atmospheric temperatures along main stairway | 9.C-166 |
| Figure 9.C.2-72 | HDR-E11.4 Steam concentrations along main stairway | 9.C-167 |
| Figure 9.C.2-73 | HDR-E11.4 $H_2$/He gas concentrations along main stairway | 9.C-168 |
| Figure 9.C.2-74a | HDR-E11.4 Comparison between temperatures in main and spiral stairways at +31.0 m level | 9.C-169 |
| Figure 9.C.2-74b | HDR-E11.4 Comparison between temperatures in main and spiral stairways at +31.0 m level | 9.C-170 |
| Figure 9.C.2-75 | HDR-E11.4 Comparison between temperatures in main and spiral stairways at +26.5 m level | 9.C-171 |
| Figure 9.C.2-76 | HDR-E11.4 Comparison between temperatures in main and spiral stairways at +16.5 m level | 9.C-172 |

## LIST OF FIGURES (Cont.)


| Figure | Title | Page |
|---|---|---|
| Figure 9.C.2-77 | HDR-E11.4 Comparison between temperatures in main and spiral stairways at +6 m level | 9.C-173 |
| Figure 9.C.2-78 | HDR-E11.4 Axial temperature profiles in both major flow paths at specific times, left in spiral stairway, right in main stairway | 9.C-174 |
| Figure 9.C.2-79 | HDR-T31.5 Blowdown mass flow rate into the containment | 9.C-178 |
| Figure 9.C.2-80 | HDR-T31.5 Steam and $H_2$/He gas mass flow rates into containment | 9.C-179 |
| Figure 9.C.2-81 | HDR-T31.5 Pressure history after large LOCA over 1200 minutes | 9.C-180 |
| Figure 9.C.2-82 | HDR-T31.5 Axial temperature profiles along spiral stairway (left) and main stairway (right) for different instants in time | 9.C-181 |
| Figure 9.C.2-83 | HDR-T31.5 Axial gas concentration profiles along spiral stairway (left) and main stairway (right) in upper containment region at different instants in time | 9.C-182 |
| Figure 9.C.2-84 | HDR-T31.5 Gas concentrations inside the containment dome | 9.C-183 |
| Figure 9.C.2-85a | HDR-T31.5 Velocities over 60 minutes along spiral stairways and associated dome regions | 9.C-184 |
| Figure 9.C.2-85b | HDR-T31.5 Velocities over 60 minutes along main stairways and associated dome regions | 9.C-185 |
| Figure 9.C.2-86 | HDR-V21.1 Arrangement of reactor pressure vessel, blowdown pipe and jet impingement plate for water blowdown test | 9.C-189 |

## LIST OF FIGURES (Cont.)


| Figure | Title | Page |
|---|---|---|
| Figure 9.C.2-87 | HDR-V21.1 Containment pressure history | 9.C-190 |
| Figure 9.C.2-88 | HDR-V21.1 Temperatures in the containment dome | 9.C-191 |
| Figure 9.C.2-89 | HDR-V21.1 Temperature along the main staircase at different axial positions | 9.C-192 |
| Figure 9.C.2-90 | HDR-V21.1 Temperatures along spiral staircase at different axial positions | 9.C-193 |
| Figure 9.C.2-91 | HDR-V21.1 Comparison between temperatures in spiral staircase (H=22.5 m) and main staircase (H=25 m) | 9.C-194 |
| Figure 9.C.2-92a | HDR-E11.5 Sequence of Experimental Test Procedures | 9.C-198 |
| Figure 9.C.2-92b | HDR-E11.5 Sequence of Experimental Test Procedures | 9.C-199 |
| Figure 9.C.2-93 | HDR-E11.5 Containment pressure | 9.C-200 |
| Figure 9.C.2-94 | HDR-E11.5 Containment pressure history | 9.C-201 |
| Figure 9.C.2-95 | HDR-E11.5 Containment temperatures along main stairway during containment heatup phase | 9.C-202 |
| Figure 9.C.2-96a | HDR-E11.5 Temperatures in both major flow paths at the same axial positions for three heights in the containment | 9.C-203 |
| Figure 9.C.2-96b | HDR-E11.5 Temperatures in both major flow paths at the same axial positions for three heights in the containment | 9.C-204 |

## LIST OF FIGURES (Cont.)

| Figure | Title | Page |
|---|---|---|
| Figure 9.C.2-96c | HDR-E11.5 Temperatures in both major flow paths at the same axial positions for three heights in the containment | 9.C-205 |
| Figure 9.C.2-97a | HDR-E11.5 Axial steam concentration in spiral (left) and main (right) stairways for different instants in time for large break LOCA release in lower containment region | 9.C-206 |
| Figure 9.C.2-97b | HDR-E11.5 Axial temperature profiles in spiral (left) and main (right) stairways for different instants in time for large break LOCA release in lower containment region | 9.C-207 |
| Figure 9.C.2-98a | HDR-E11.5 Axial $H_2$-He gas mixture concentration profiles along spiral (left) and main (right) stairways during gas release phase (total mass 291 kg) | 9.C-208 |
| Figure 9.C.2-98b | HDR-E11.5 Axial steam concentration profiles along spiral (left) and main (right) stairways during gas release phase (total mass 291 kg) | 9.C-209 |
| Figure 9.C.2-98c | HDR-E11.5 Axial temperature profiles along spiral (left) and main (right) stairways during gas release phase (total mass 291 kg) | 9.C-210 |
| Figure 9.C.2-99a | HDR-E11.5 Gas concentrations in the major flow paths and in regions and subcompartments away from the stairways (H=22m up to 27 m) | 9.C-211 |
| Figure 9.C.2-99b | HDR-E11.5 Gas concentrations in the major flow paths and in regions and subcompartments away from the stairways (H=22m up to 27 m) | 9.C-212 |

## LIST OF FIGURES (Cont.)


| Figure | Title | Page |
|---|---|---|
| Figure 9.C.2-100a | HDR-E11.5 Gas concentrations in the major flow paths and in regions and subcompartments away from the stairways (H=4.5m up to +2.0 m) | 9.C-213 |
| Figure 9.C.2-100b | HDR-E11.5 Gas concentrations in the major flow paths and in regions and subcompartments away from the stairways (H=4.5m up to +2.0 m) | 9.C-214 |
| Figure 9.C.2-101a | HDR-E11.5 Velocities in the main stairway during blowdown | 9.C-215 |
| Figure 9.C.2-101b | HDR-E11.5 Velocities in the spiral stairway during blowdown | 9.C-216 |
| Figure 9.C.2-102a | HDR-E11.5 Velocities in the main stairway during containment heatup phase | 9.C-217 |
| Figure 9.C.2-102b | HDR-E11.5 Velocities in the spiral stairway during containment heatup phase | 9.C-218 |
| Figure 9.C.2-103a | HDR-E11.5 Velocities in the main stairway during $H_2$-He gas mixture release phase | 9.C-219 |
| Figure 9.C.2-103b | HDR-E11.5 Velocities in the spiral stairway during $H_2$-He gas mixture release phase | 9.C-220 |
| Figure 9.C.2-104a | HDR-E11.5 Velocities in the main stairway during sump heatup and boiling phase | 9.C-221 |
| Figure 9.C.2-104b | HDR-E11.5 Velocities in the spiral stairway during sump heatup and boiling phase | 9.C-222 |
| Figure 9.C.3-1 | Dome pressure history | 9.C-232 |
| Figure 9.C.3-2a | Temperature history inside node 8 | 9.C-233 |

## LIST OF FIGURES (Cont.)


| Figure | Title | Page |
|---|---|---|
| Figure 9.C.3-2b | Helium concentration inside node 8 | 9.C-234 |
| Figure 9.C.3-3a | Temperature history inside node 15 | 9.C-235 |
| Figure 9.C.3-3b | Helium concentration inside node 15 | 9.C-236 |
| Figure 9.C.3-4a | Temperature history inside dome | 9.C-237 |
| Figure 9.C.3-4b | Helium concentration history inside dome | 9.C-238 |
| Figure 9.C.3-5a | Temperature history inside node 7 | 9.C-239 |
| Figure 9.C.3-5b | Helium concentration inside node 7 | 9.C-240 |
| Figure 9.C.3-6 | HDR-E11.5: Comparison between measured long-term containment pressure and GOTHIC open post-test prediction | 9.C-243 |
| Figure 9.C.3-7 | HDR-E11.5: Comparison between measured sump temperature and GOTHIC open post-test prediction | 9.C-244 |
| Figure 9.C.3-8 | HDR-E11.5: Comparison between measured temperature in main stairway (6m) and GOTHIC open post-test prediction | 9.C-245 |
| Figure 9.C.3-9 | HDR-E11.5: Comparison between measured temperature in spiral stairway (6m) and GOTHIC open post-test prediction | 9.C-246 |
| Figure 9.C.3-10 | HDR-E11.5: Comparison between measured gas mixture concentration in main stairway (6m) and GOTHIC open post-test prediction | 9.C-247 |
| Figure 9.C.3-11 | HDR-E11.5: Comparison between measured gas mixture concentration in spiral stairway (6m) and GOTHIC open post-test prediction | 9.C-248 |

## LIST OF FIGURES (Cont.)

| Figure | Title | Page |
|---|---|---|
| Figure 9.C.3-12 | HDR-E11.5: Comparison between measured velocity in main stairway (15m) and GOTHIC open post-test prediction | 9.C-249 |
| Figure 9.C.3-13 | HDR-E11.2: Comparison between measured long-term containment pressure and various "optimized" open post-test predictions | 9.C-250 |

# 9.C.1 DEVELOPMENT OF EXPECTED FLOW PATTERNS FOR AP600 AND AP1000 BASED ON SEPARATE FLOW TESTS IN ENCLOSURES

## 9.C.1.1 STRATIFICATION PHENOMENA

Stratification is the formation of horizontal layers of constant density. Stratified layers are stable if the density of the layers decreases in the upward vertical direction (the gradients of density are negative in z direction according to Figure 9.C.1-1a) and if forced convection mixing is not sufficiently strong to disrupt the stable fluid layers.

Another more general definition of stratified conditions is that gradients of density in the horizontal direction are small, except in jets, buoyant plumes, and small regions near the vertical walls inside boundary layers (wall jets). In most of the volume, the density gradients in z direction are negative, while inside the jets, wall jets, and buoyant plumes they could be positive (see Figure 9.C.1-1b).

Stratification occurs as a consequence of the temperature or concentration gradients in the vertical direction. Increasing temperatures or decreasing concentrations of heavier mixture components with increasing elevation promote stratification. The existence of flow structures, such as jets, plumes, and vertical wall boundary layers, decreases the "steepness" of the vertical density gradients.

Examples of stratified conditions are numerous. Stratified layers are observed as large-scale geophysical phenomena (in lakes, sea, and oceans, in atmosphere - stratus clouds), as well as inside the enclosures. For example, warmer air tends to gather below ceilings in energy storage devices, nuclear reactors, solar collectors, and enclosures under the influence of the spread of fire and smoke.

This appendix discusses the stratification phenomena inside a nuclear reactor containment. Possible reasons for the stratification will be specified. Stratification may occur if:

1) The upper boundary is at the higher temperature than the lower boundary (see Figure 9.C.1-2a), as well as for other similar combinations of temperature boundary conditions at the outside and inside surfaces (see Figure 9.C.1-2b - d).

2) A higher concentration of the heavier or lighter components of the mixtures is maintained (by injecting and removing) near the lower or upper boundaries of the enclosure, respectively.

3) A lighter fluid is released (permanently, or from time to time) and captured below the ceiling of the containment.

4) The release point of the lighter/heavier fluid is closer to the top/bottom.

5) The shape of the enclosure promotes stratification (tall elongated enclosure).

6) The distribution of the non-complete vertical partitions suppresses fluid flow in the upper portions of the enclosure.

7) The distribution and size of the horizontal openings suppresses the fluid flow in vertical direction.

8) The internal heat sources (sinks) are positioned in the upper (lower) portions of the enclosure.

Under the conditions above (or a combination of them), the stratification may be stable. The presence of stratified layers inhibits circulation, that otherwise could be induced by a jet, plume, or boundary layers. The conduction and diffusion, heat and mass transfer processes, respectively, are dominant. As a result, the overall heat and mass transfer decreases and the heat transfer through the containment shell is slowed.

One way to avoid the stratification is to generate fluid flow patterns inside the enclosure using forced convection. Additional devices such as fans, sprays, or nozzles are necessary, as well as associated power supplies and controls.

Since the AP600 and AP1000 rely on a passive containment cooling system (PCS), only the effects of fluid circulation due to the interaction of natural convection with the stratified field are discussed.

Modifications to the shape of the enclosure, the distribution and size of the internal partitions, and the openings could be made to avoid stratification. A different distribution of heat sources could also be applied to generate natural convection effects. The fluid flows due to natural convection promote better circulation inside the enclosure. The introduction of jets may also interrupt stably stratified layers through better mixing of the layers of various densities and concentrations. With a jet stratification may become unstable or, at least, the vertical gradient reduced. With only natural convection if the generated buoyancy forces are strong enough, the entire volume of the enclosure will be affected, resulting in the relatively uniform values of temperature and concentration fields. Natural convection heat transfer is dominant and the more intensive circulation improves the transfer of heat from the containment. Natural convection flow effects are generated spontaneously due to the gravity (buoyancy forces) when heated sources exist, so that additional control and other devices are not necessary.

### 9.C.1.1.1 Static Stratification

Static stratification occurs if the upper horizontal boundary of the domain is maintained at a higher temperature than lower boundary, as in Fig. 9.C.1-1a. Stratification also occurs if the concentration of heavy components is low in the mixture in the upper portion of the domain. The fluid layers are undisturbed and fluid motion is negligible. The temperature or density distribution in the vertical direction is linear. Heat transfer is predominantly governed by conduction, while mass transfer is driven by diffusion. The formed fluid layers are stable and communicate only with the neighboring upper and lower layers. The resulting heat and mass transfer rates are low.

Corresponding experimental results are found in Akino et al., 1989 and Hiller et al., 1988. In both papers, stable stratified layers are identified using various colors reflected by liquid crystals (suspended in the fluid).

Static stratification exists inside a containment vessel if the temperature distribution of the vertical walls is the same as in the surrounding stratified fluid (adiabatic vertical walls, as in Fig 9.C.1-1a). Since, the top of the passive containment, as well as the vertical walls, are exposed to the surrounding air and cooled by natural convection, stable stratification is not present. Even small temperature differences between the air inside and outside the containment produce large Grashof (Rayleigh) numbers, due to the height of the containment ($H_t$=109 ft). For example, a temperature difference of 9 °F between the air at the deck level and the air below the dome ceiling results in $Gr_t = 2.2\ 10^{13}$. This is in the range of chaotical turbulent flow, characterized by upward and downward plumes (see experimental results by Akino et al., 1989).

Static stratified layers are also generated by releasing a lighter gas, e.g., steam or hydrogen, into the upper portion of the containment and capturing the gas beneath the dome.

Hydrogen distribution experiments performed in the HDR facility, test group E11, combine high hydrogen release rates with superheated steam injection into the containment (see Wolf et al., 1994a). A comparison of influences of the axial break and gas release positions is obtained with E11.2 (high release position) and E11.4 (low release position) experiments. Although these two specific experiments simulate severe accident scenarios, comparison of results from the two experiments provides insights into the physics of stratification. The tests are characterized by boundary conditions that can promote circulation (especially test E11.4). They also show that relatively small concentration gradients can exist in the presence of circulation.

Steam release from small breaks generates thermal stratification for break positions located at the higher level, with the hot zone above the break locations. Two mechanisms are used to break up the established thermal stratification. The first mechanism used subsequent steam releases at positions lower than the original release to break up the established thermal stratification. This mechanism did not produce

homogeneously mixed conditions. The second method is the application of external sprays on the upper dome. This causes condensation on the inner surface and a decrease in the temperature in the upper part of the dome. Convective flows form and affect the whole volume of the dome and lower compartments, resulting in a completely homogenized atmosphere.

As in the HDR E11.2 experiment, condensation on the dome of the passive containment breaks up stratification. The condensation on the vertical walls also contributes to breaking of stratified layers and to entrainment in the vertical boundary layers. The circulation inside the containment affects the lower compartments and promotes circulation due to the natural convection.

The shape of an enclosure could also promote stratification. One example is natural convection inside romb shaped enclosures (see Figure 9.C.1-3). Stratification is generated if the upper vertical side is at a high temperature and the inclined top and bottom sides are adiabatic (see, Dzodzo, 1993). The overall heat and mass transfer are suppressed by the presence of the stratified fluid in the upper and lower corners of the romb shaped enclosures. When the boundary conditions are reversed, i.e., the lower vertical side is at the higher temperature, the entire volume of the enclosure is effected by circulation. Heat transfer is intensified and stratified layers are not present in the upper and lower corners. A comparison of experimentally and numerically obtained temperature and velocity fields for these two cases is presented in Figure 9.C.1-4. An overview of the numerical results for various angles of the romb (parallelogram-shaped) enclosures, Prandtl numbers, and aspect ratios is presented by (Hyun and Choi, 1990).

Although the top of the passive containment is somewhat conical in shape, stratification in the upper portion of the dome would not exist because of the natural convection due to the lower temperatures of the ceiling and vertical walls. Stratification effects are promoted if the containment ceiling is insulated or at a higher temperature.

The distribution of the internal heat sources in the upper part and heat sinks in the lower part of enclosures promotes the formation of the stratified layers (see Figure 9.C.1-2 b, c, d). Examples of the influence of the position and distance between the heat source and heat sink are provided by A. Kurosawa et al., 1993 and C. J. Ho et al., 1994. An example of the influence of an array of discrete heat sources on natural convection is presented by T. J. Heindel et al., 1995.

Vertical non-complete partitions inside an enclosure contribute to the stratification. If the non-complete vertical partition is positioned near the ceiling, flow in the upper part of the enclosure is obstructed and a stagnant stratified region near the ceiling is formed (see Hanjalic et al., 1996, and Nowak and Novak, 1994 for examples of the two-dimensional numerical simulation, and T. Fusegi et al., 1992, for the three-dimensional

simulation). This is of special interest for the analysis of the spread of fire and smoke inside the buildings. Such partitions do not exist above the operating deck level in the passive containment.

Narrow horizontal openings between upper and lower compartments also suppress circulation and cause stratification. The results of a two-dimensional numerical simulation (R. Frederick and A. Valencia, 1995) show the influence of the size of the horizontal openings on the natural convection inside the vertically connected enclosures.

The potential for stratification in compartments below the operating deck of containments, due to the various sizes of the openings is also studied (see ref. Wolf et al., 1994b).

### 9.C.1.1.2 Stratification and Circulation

Figure 9.C.1-1b illustrates conditions where a portion of an enclosure is stratified and other portions are affected by strong recirculation zones and currents. Due to the circulation effects, shallow vertical density gradients are present inside the stratified portion of the enclosure volume.

Convective heat and mass transfer that results from communication between the stratified and flow-affected zones, contributes to the mixing between the zones with different temperatures, concentrations, and densities. Flow inside the enclosure is promoted by the existence of the entraining wall layers (which are a consequence of the heat transfer), penetrating jets, and buoyant plumes (see reference, Peterson, 1994 and Figure 9.C.1-1b).

To gain insight into passive containment physics, we will start with small-scale enclosure examples and progress to larger scale.

#### 9.C.1.1.2.1 Interaction of Wall Jets (Boundary Layers) with Stratified Layers

One example of interaction of wall jets with stratified layers is the natural convection inside a square enclosure (see Figure 9.C.1-5). The opposite vertical walls of the enclosure are at the different temperatures and the horizontal walls are adiabatic (see Markatos and Pericleous, 1984 and Figure 9.C.1-5a). With high Rayleigh numbers (over $10^{+6}$), Pr=0.71, turbulent flow exists inside the enclosure. Velocity and temperature gradients are large in the boundary layers. Velocities have maximum values near the walls, while inside the core of the enclosure they are small. The temperature (density) field in the core of the enclosure is stratified (see Figure 9.C.1-5c). Communication exists between the boundary layer region and core of the enclosure through the vortices (see Figure 9.C.1-5b), which change in number, position, and intensity for various temperature differences between the opposite walls (various Ra numbers). Temperature gradients are

highest in the boundary layers near the vertical and horizontal walls (see Figure 9.C.1-5c). For the laminar convection ($Ra=10^{+4}$ and $Ra=10^{+5}$), the temperature difference between the highest and lowest points at the vertical axis of the stratified core is $0.6*(T_h - T_c)$, while for the turbulent regime ($Ra= 10^{+8}, 10^{+12}, 10^{+16}$) it is $0.4*(T_h - T_c)$. The decrease in the vertical temperature gradients inside the stratified core for the turbulent regime is the result of higher velocities and stronger circulation inside the cavity. The temperature field inside the core of the enclosure is stratified, while recirculation due to convection inside the enclosure is predominantly near the walls. Despite the presence of the stratified core, for high Ra numbers, a fluid particle travels the entire enclosure (due to the convection) and contributes to better mixing and decreases the vertical gradients inside the core.

The increase of the Rayleigh number corresponds with a decrease in the thickness of the boundary layers, an increase in the temperature gradients inside the boundary layers, and an increase in the heat transfer rate. The dependence of the average Nusselt numbers on the Rayleigh numbers is presented in Figure 9.C.1-6.

A similar two-dimensional flow pattern and stratified temperature (density) field is also obtained between two opposite vertical line jets (see Figure 9.C.1-7) as discussed in Baines and Turner, 1969.

A numerical analysis (Markatos and Pericleous, 1984) is performed for a two-dimensional plane, assuming that the influence of the front and back walls of real three-dimensional enclosures is not significant. For Rayleigh numbers greater than $10^6$, the k-ε turbulence model is used. Due to time-averaging, the numerical results do not show either the instability mechanisms during the transition from laminar to turbulent flow, or the resulting oscillations that would result from solving the time dependent Navier-Stokes equations.

Experimental and numerical results for three-dimensional enclosures are provided by Hiller et al. 1989, Mallinson and de Vhal Davis, 1977, respectively. The results indicate that observed vortices, which affect mixing inside the core of the enclosure, communicate between the front and back walls through the middle of the enclosure, thus enhancing mixing due to three-dimensional circulation effects (see Figure 9.C.1-8).

Reviews of various aspects of confined convective flows, including the interactions between boundary layers near the bounding walls and core and the effects of the cavity aspect ratio, inclination angle, and thermal boundary conditions on flow patterns, are presented by Ostrach 1972, 1982, Catton, 1978, Hoogendoorn, 1986 and Allard, 1992. A state of the art review of the analyses of two-dimensional and three-dimensional transient effects on the natural convection flows in sidewall heated enclosures is presented by T. Fusegi and J. M. Hyun, 1994.

R. J. Janssen and R.A.W.M Henkes, 1995 simulated the instability mechanisms and the transition from laminar to turbulent (oscillatory and finally chaotical) flow regimes inside a two-dimensional square enclosure

with differentially heated vertical walls and adiabatic horizontal walls by solving the time-dependent Navier-Stokes equations. The results indicate that the transition from laminar to chaotic flow (for $Pr < 2.0$) is through periodic and quasi-periodic flow regimes. The periodic, quasi-periodic and chaotic flow regimes are established for Prandtl number 0.71 and Rayleigh numbers $2*10^8$, $3*10^8$ and $7.5*10^8$. Internal waves corresponding to fluctuations in the temperatures at $Ra = 2*10^8$ are presented in Figure 9.C.1-9. The temperature differences in the entire core of the enclosure are small, $0.004*(T_h-T_c)$. The predicted temperature differences inside the core of the enclosure are much smaller than those predicted by k-ε turbulence model (Markatos and Pericleous, 1984). This indicates that temperature gradients inside the boundary layers are greater (isotherms inside the thermal boundary layer are not presented in Figure 9.C.1-9) and heat transfer is more intensive than calculated by k-ε model.

Two instability mechanisms influence the transition to turbulent (chaotical) flow regime. The first instability is a Kelvin-Helmholtz type instability (as in a plane jet with inflection points in the velocity profile) in the fluid layer exiting from the corners (where the vertical boundary layers are turned horizontal). The second source of the instability is related to the instability in the boundary layer near the vertical walls. The instability inside the enclosure vertical boundary layers is mechanically (shear) driven. Both regions of the instability origins (hot and cold intrusions from corners and boundary layer waves) are presented in the Figure 9.C.1-10 (from S. Armfield and R. Janssen, 1996). The figure presents temperatures for the initial solution, i.e., immediately after setting the left and right vertical boundaries to $\Delta T/2$ and $-\Delta T/2$, respectively. For values of Rayleigh numbers greater than $10^9$, the turbulent oscillatory and chaotical flow affects the stratified layers inside the core of the enclosure. If the radius ($H_v$=65 ft) of the containment is taken as a characteristic length (as a distance between the hot buoyant jet plume in the center and cold vertical wall boundary layers), a 9°F temperature difference results in a Grashof number $Gr_v = 4.7*10^{12}$.

### 9.C.1.1.2.2 Interaction of jets or plumes with the stratified layers

The penetration of a stratified layer by a jet is another example where a portion of an enclosure is stratified and another portion is affected by strong recirculating zones (Figure 9.C.1-1b). Depending upon the strength of the jet and the depth of the stratified layers, portions of the enclosure are affected by interaction between the jet and stratified layers. A portion of the stratified fluid is entrained by the jet, decreasing the average jet velocity. The jet penetrates upward (Garrad and Patrick, 1983, So and Aksoy, 1993, and Porterie et al., 1996), or downward (Markatos and Pericleous, 1984, see Figure 9.C.1-5 b and c near the cool wall). A negatively buoyant jet, as presented in Kapoor and Jaluria, 1993, is also possible.

The upward penetrating jet is of interest for LOCA or MSLB accident scenarios. Scaling and analysis of mixing in large stratified volumes for the cases of upward penetrating jets is presented by Peterson, 1994.

If the strength of the jet is strong enough, it produces fluid flow below the ceiling. After reaching the vertical side walls, the flow results in downward negatively buoyant jets (see Figure 9.C.1-11 a and b).

The downward, negatively buoyant penetrating jet (Kapoor and Jaluria, 1993, see Figure 9.C.1-11a and 1-11b) is of interest for the analysis of the flow patterns inside the upper-deck region (Figure 9.C.1-11a), as well as for the compartments below the dome floor (Figure 9.C.1-11b). If the strength of the negatively buoyant jet is not high, it is not able to reach compartments below the deck. The direction of the flow changes as presented in Figure 9.C.1-11a. The redirection of the flow causes additional entrainment of the surrounding fluid, thus contributing towards the increase of the circulation (and mixing) inside the upper-deck region. The correlations for entrainment rates in the negatively buoyant jets are presented in Kapoor and Jaluria, 1993.

If the strength of the negatively buoyant jets is high, it is able to penetrate into the below-deck compartments. There are indications from large-scale tests conducted by Westinghouse (tests 222.3 and 222.4, 3-inch pipe, elevated 6 ft, pointed at the wall and up, respectively, see F. E. Peters, WCAP-14135, July 1994) which simulate the MSLB, that the entire volume of the containment has almost the same steam concentration. This occurs despite the fact that formation of the global circulation loop between the lower-deck compartments and upper dome regions is not possible. An explanation is that the kinetic energy of the jets is high enough to provide downward penetration of the negatively buoyant jets into the below-deck compartments.

Depending upon the distribution of compartments below the dome floor and the number, size and distribution of openings between the compartments and the dome region, various flow patterns are possible inside the compartments. A portion of the downward vertical plumes produced by natural convection (wall boundary layers) or the negatively buoyant jets produced by strong vertical upward penetrating jet into the dome region enters horizontal openings in the compartments, thus promoting circulation and flow inside the compartments below the deck. Fluid flows upward to the dome through other compartment horizontal openings to preserve overall mass continuity and to close the global circulation loop (see Figure 9.C.1-11b).

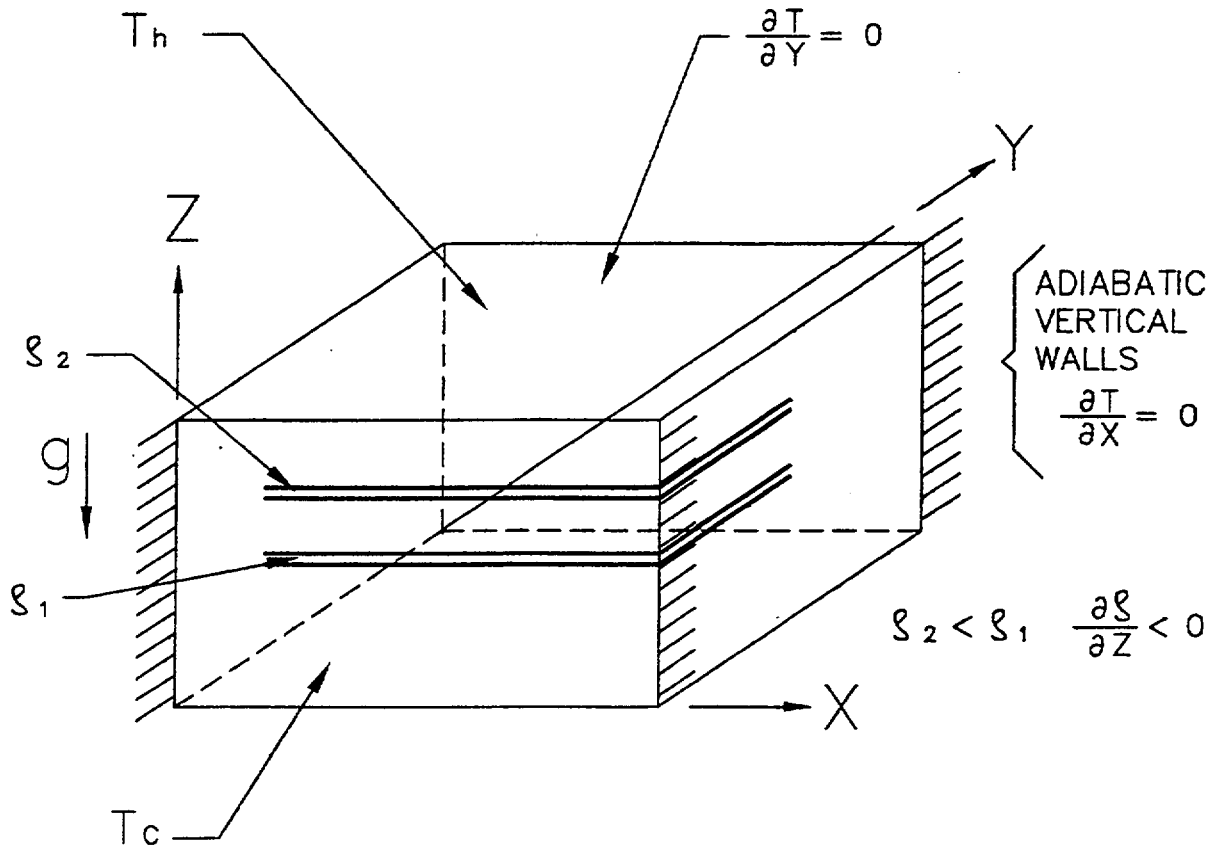


**Figure 9.C.1-1a** **The formation of the horizontal layers of the constant density due to the stratification**

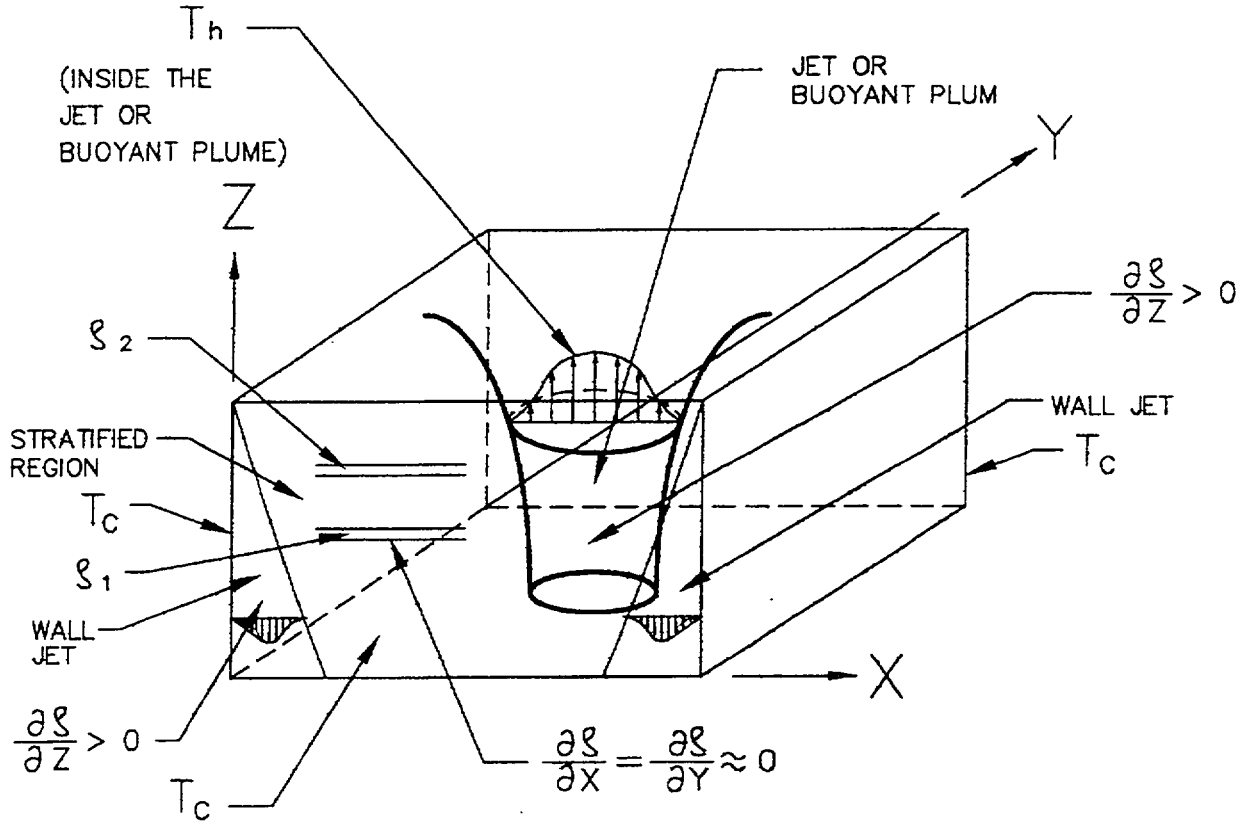


STRATIFIED REGIONS $\left(\frac{\partial \rho}{\partial X} = \frac{\partial \rho}{\partial Y} = 0, \ \frac{\partial \rho}{\partial Z} < 0\right)$ AND

JET REGIONS $\left(\frac{\partial \rho}{\partial X} \neq 0 \quad \frac{\partial \rho}{\partial Y} \neq 0 \quad \frac{\partial \rho}{\partial Z} > 0\right)$ INSIDE

THE ENCLOSURE.

**Figure 9.C.1-1b Interaction of jets, plumes and wall boundary layers with stratified regions**

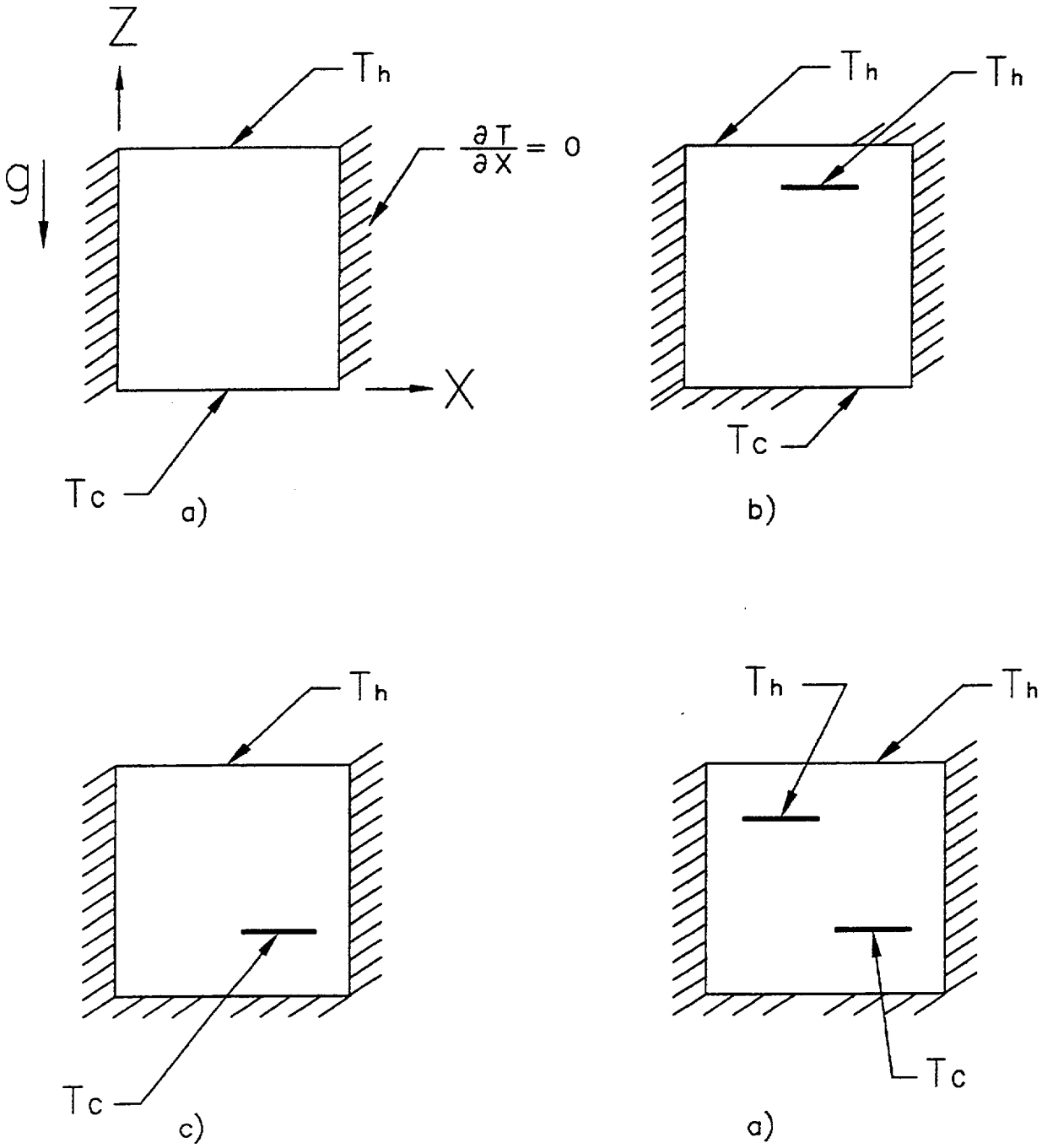


**Figure 9.C.1-2** **Combination of the constant temperature boundary conditions at the outside and inside surfaces which will produce stratification inside the enclosure**

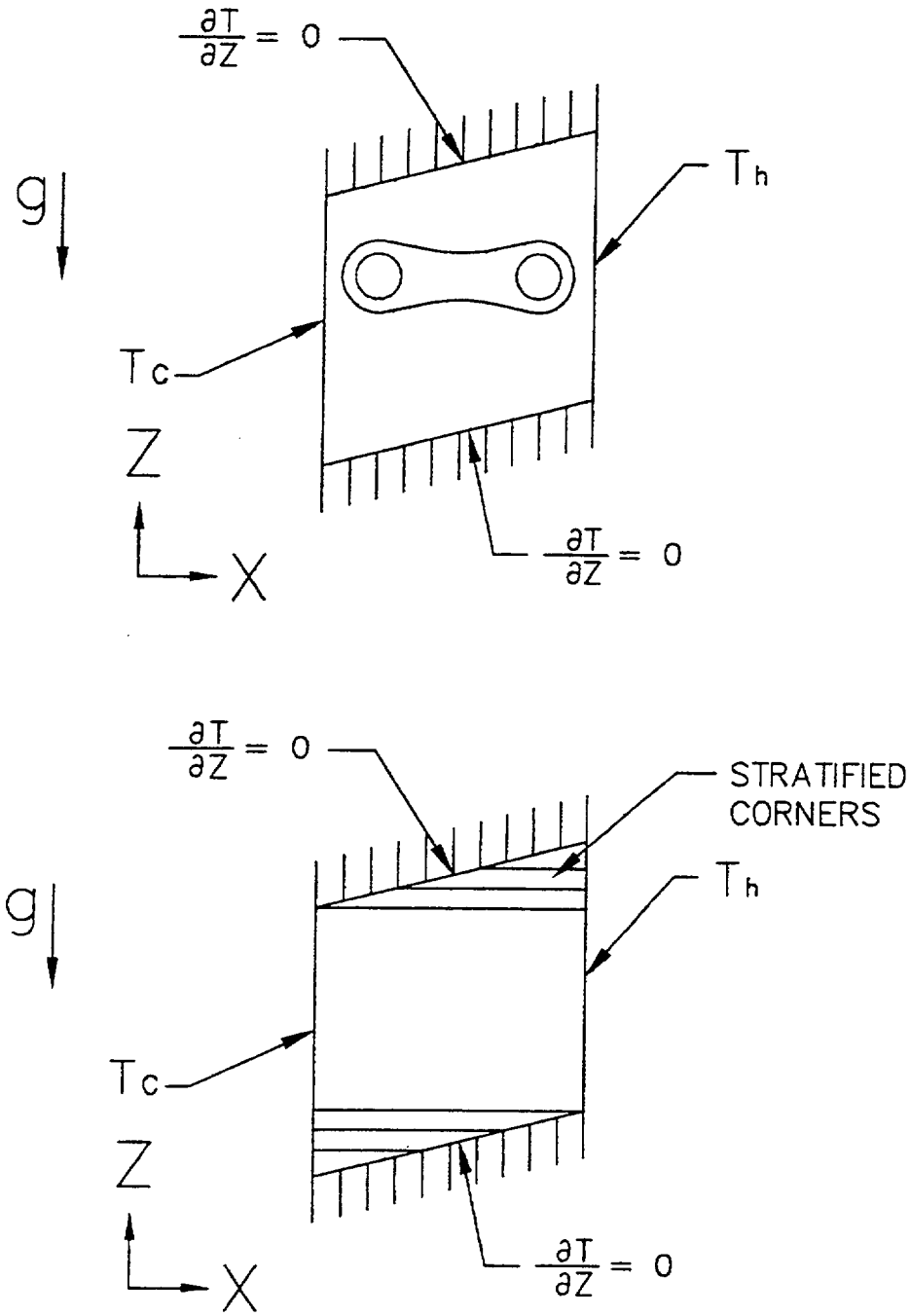


**Figure 9.C.1-3 Stratification inside the upper and lower corners of the romb-shaped enclosure**

**Example of the Stratification Caused by the Shape of the Enclosure and Distribution of the Boundary Conditions**

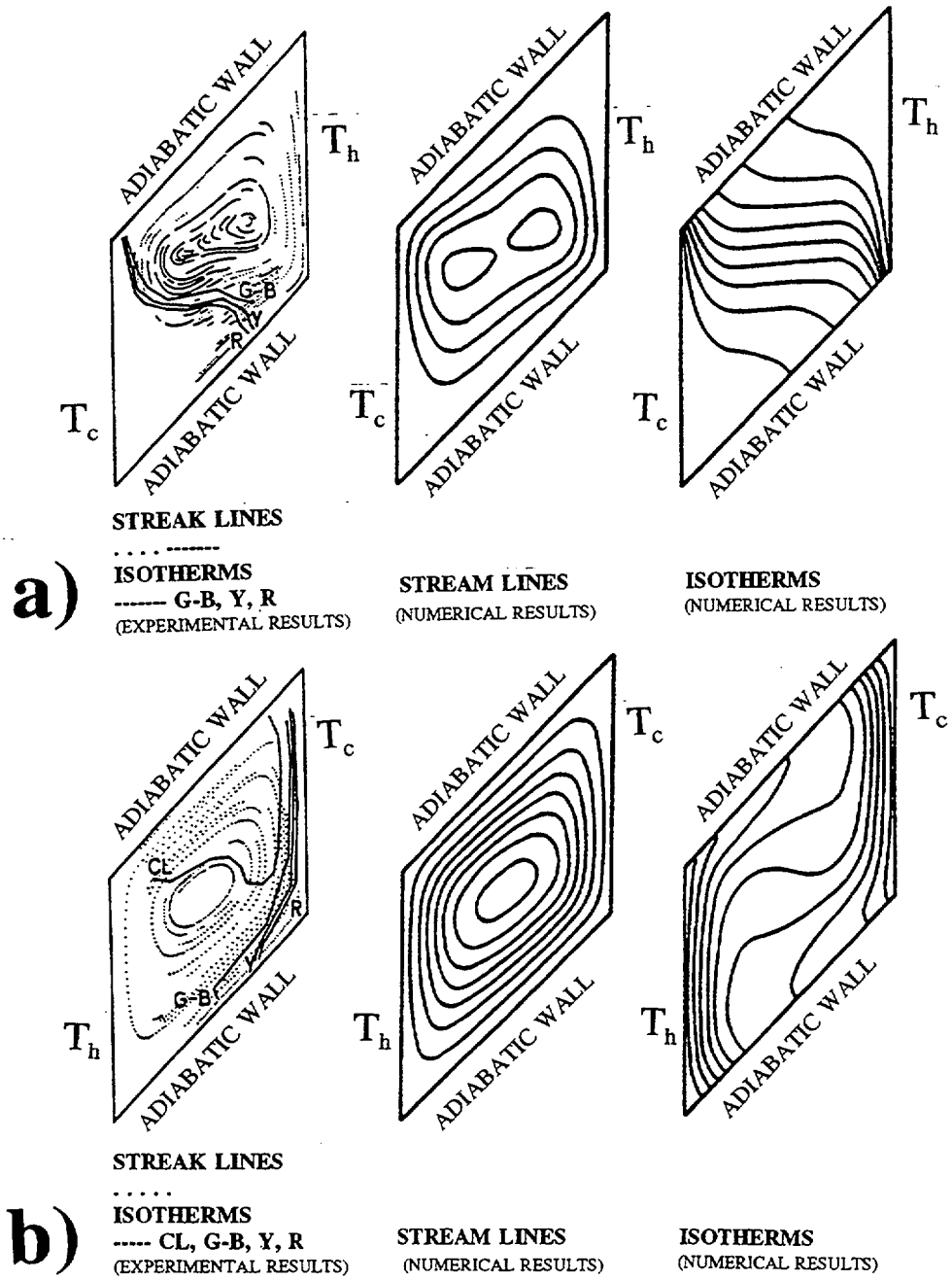


**Figure 9.C.1-4** **Experimental and numerical results for the romb-shaped enclosure with the romb angle 44° and Ra=3.5*10$^4$, Pr=5270.**

**a) results for the upper vertical wall at the higher temperature**
**b) results for the lower vertical wall at the higher temperature**

**(Reprinted from: M.B. Dzodzo, "Visualization of laminar natural convection in romb-shaped enclosures by means of liquid crystals", in Imaging in transport processes (ed. S. Sideman and K. Hijikata), Begel House, Inc., 1993, pp. 183-193)**

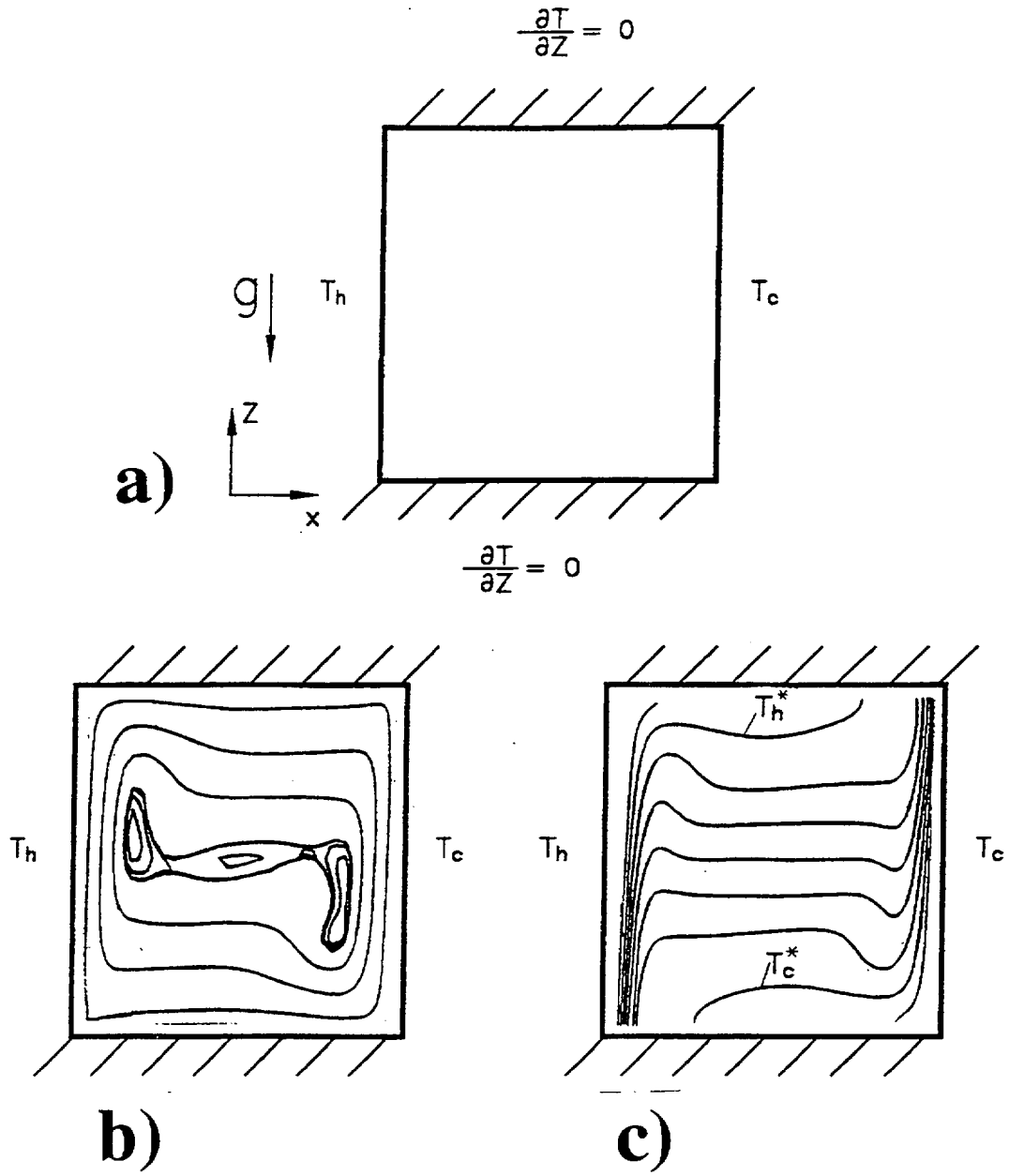


**Figure 9.C.1-5** **a) The square enclosure with vertical walls at the different temperatures and horizontal walls adiabatic, b) Streamlines for Ra=$10^6$ and Pr=0.71,c) Isotherms for Ra=$10^6$ and Pr=0.71**

**"Reprinted from N.C. Markatos and K.A. Pericleous/Laminar and Turbulent Natural Convection in an Enclosed Cavity, Int. J. Heat Mass Transfer, Vol. 27, No. 5, pp. 755-772, 1984, Copyright 1984, Figure 9.C.5(d) and 6(d), with kind permission from Elsever Science Ltd, The Boulevard, Langford Lane, Kidlington OX5 1GB, UK"**

| Ra | $10^3$ | $10^4$ | $10^5$ | $10^6$ | $10^8$ | $10^{10}$ | $10^{12}$ | $10^{14}$ | $10^{16}$ |
|---|---|---|---|---|---|---|---|---|---|
| Nu | 1.108 | 2.201 | 4.430 | 8.754 | 32.045 | 156.85 | 840.13 | 3624.4 | 11226 |

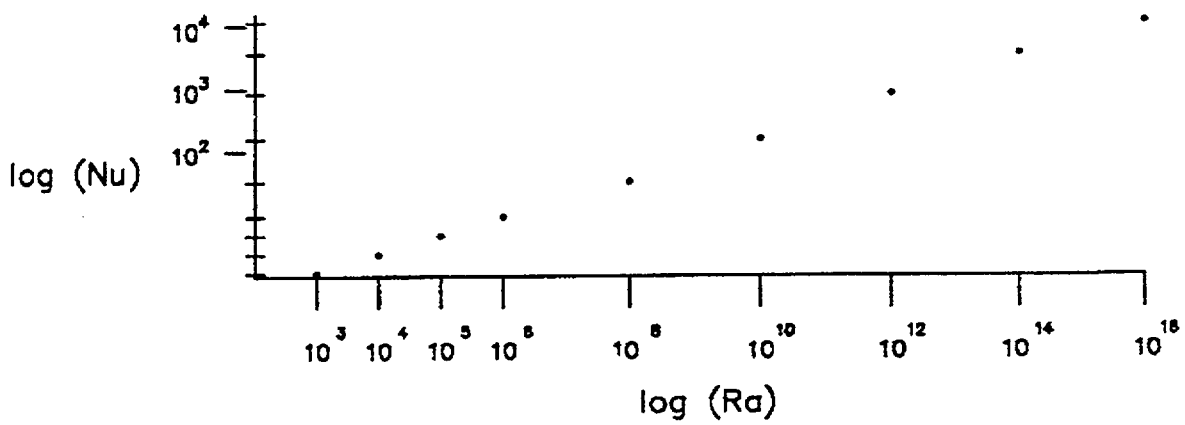


**Figure 9.C.1-6** **Average Nusselt numbers as a function of the Rayleigh numbers for the square enclosure with opposite vertical walls at the different temperature and Pr=0.71 (air)**

**(according to N.C. Markatos and K.A. Pericleous/Laminar and Turbulent Natural Convection in an Enclosed Cavity, Int. J. Heat Mass Transfer, Vol. 27, No. 5, pp. 755-772, 1984)**

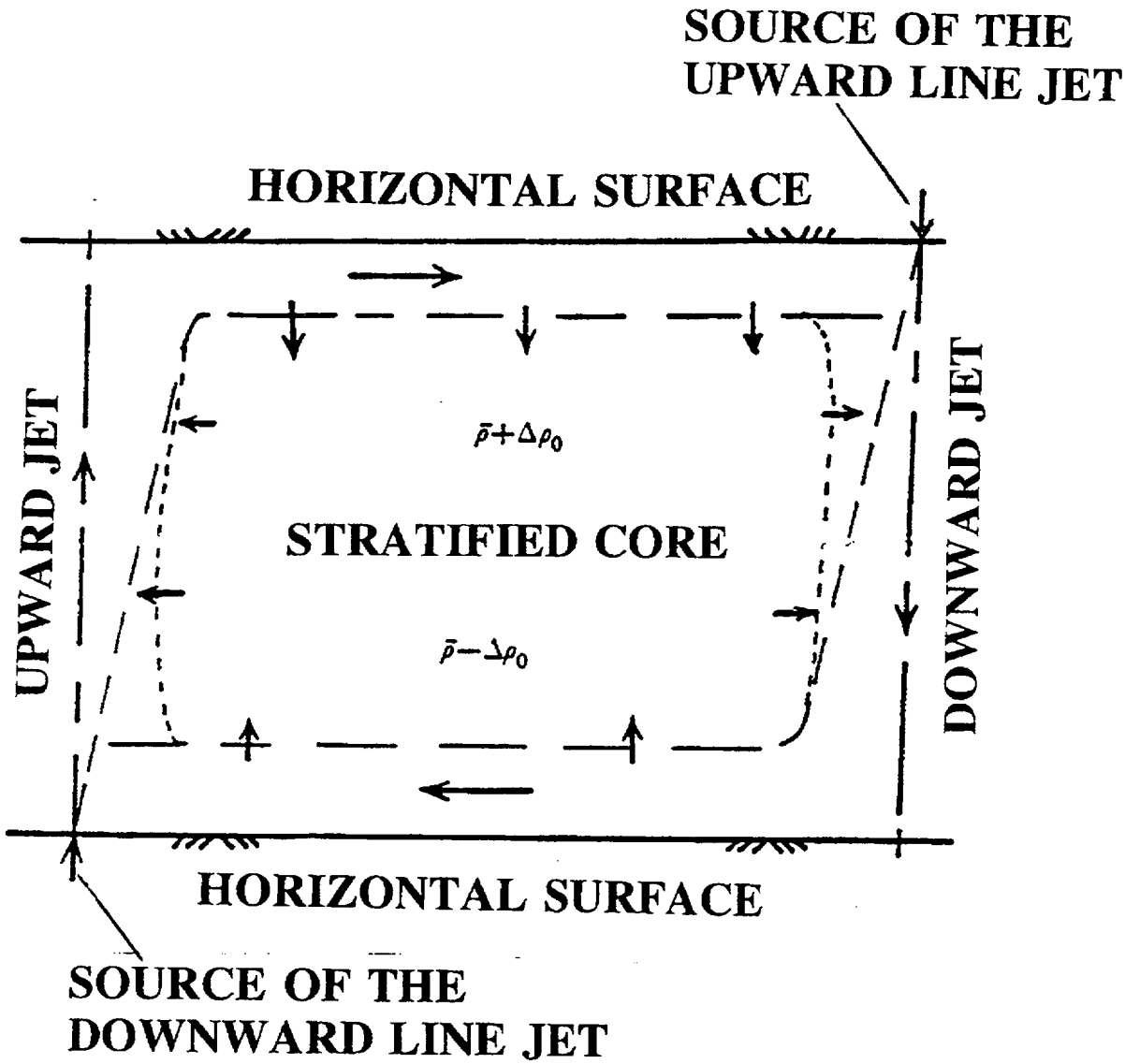


Figure 9.C.1-7 Formation of the stratified core in between two opposite vertical line jets (after Baines and Turner, 1969)

"Reprinted with the permission of Cambridge University Press from Baines W.D. and Turner, J. S./Turbulent buoyant convection from a source in a confined region, Journal of Fluid Mechanics, Vol. 37, 1969; pp. 51-80, Copyright 1969, Figure 9.C.10"

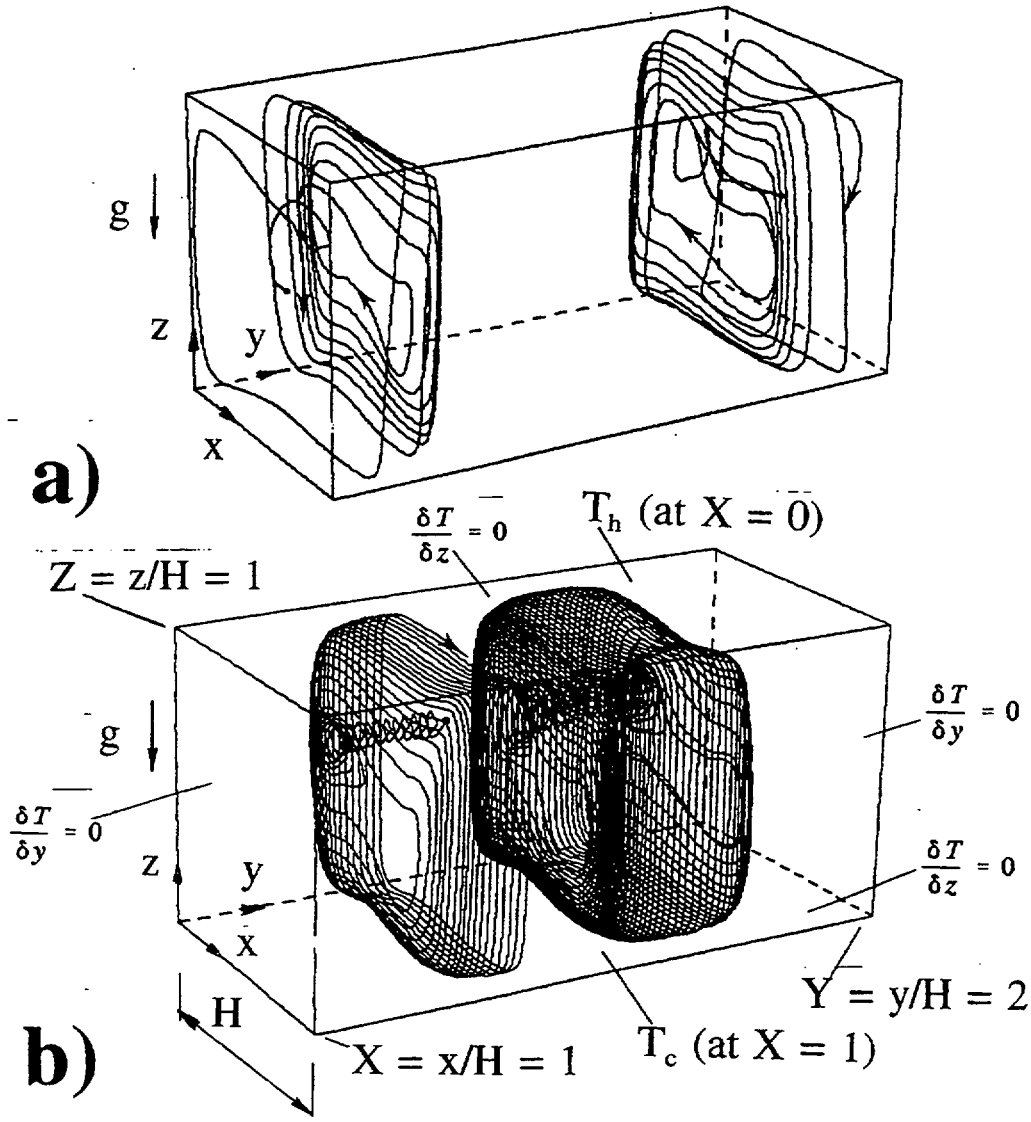


**Figure 9.C.1-8** **Flow in an enclosure with vertical opposite walls at different temperatures ($Ra = 10^5$, $Pr = 0.71$)**

**a) forward flow (towards Y=0 and Y=2) -**
**streamlines through the points**
**(X=0.5, Y=0.1, Z=0.49) and (X=0.5, Y=1.9, Z=0.49)**
**b) reverse flow (towards Y=1.0) -**
**streamlines through the points**
**(X=0.3, Y=0.8, Z=0.65) and (X=0.3, Y=1.2, Z=0.65) after (Mallinson and deVahl Davis, 1977)**

**"Reprinted with the permission of Cambridge University Press from Mallinson, G.D. and G. de Vahl Davis/Three-dimensional natural convection in a box: a numerical study, Journal of Fluid Mechanics, Vol. 83, 1977; pp.1-31, Copyright 1977, Figure 9.C.8"**

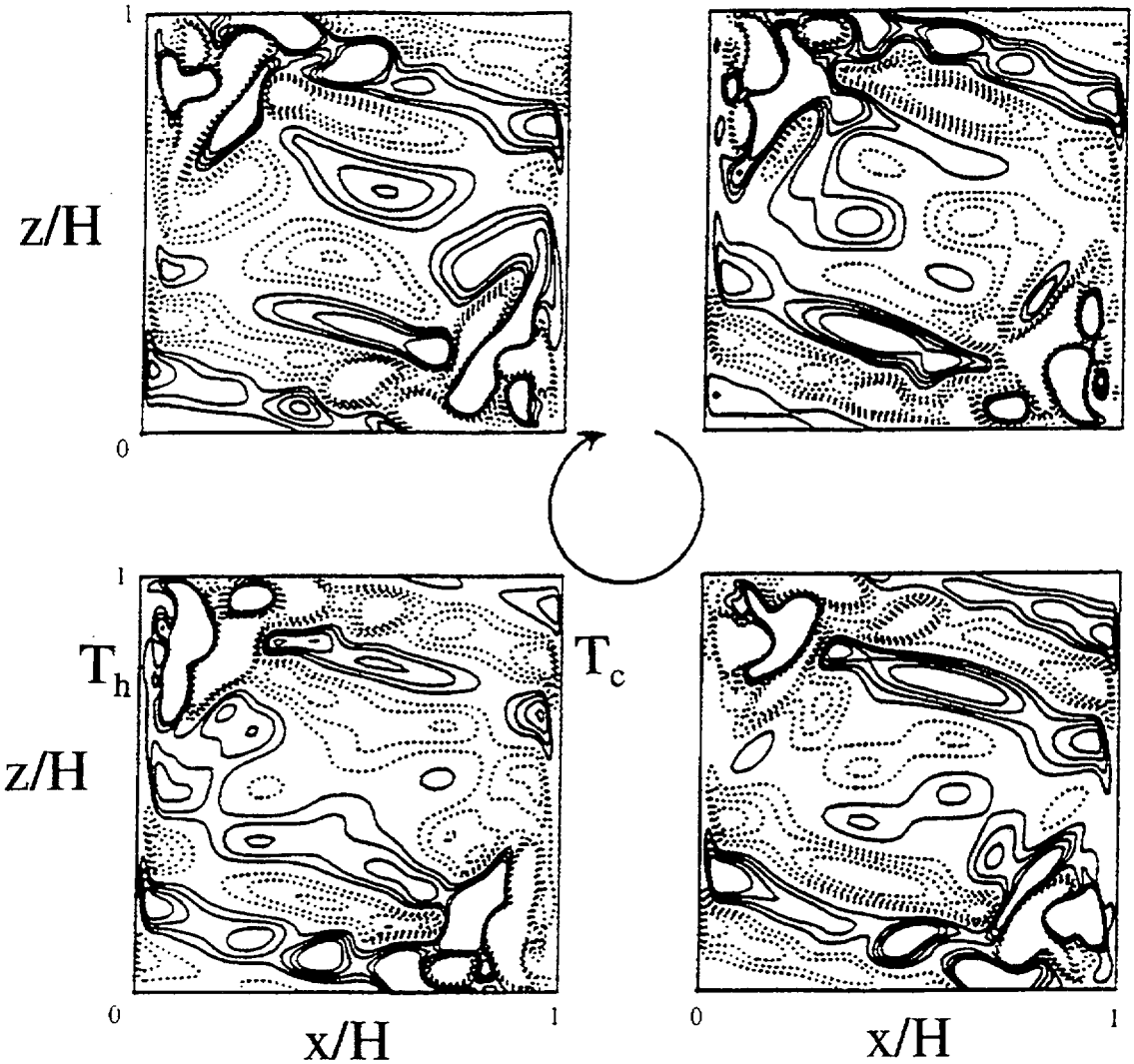


**Figure 9.C.1-9** **Internal waves in the square cavity - fluctuations in the temperature field at Ra = $2*10^8$ and Pr=0.71 (air)**

**Circle with the arrow (in the middle) presents the direction of the consecutive temperature fields.**

**Contour lines correspond to +/-0.0005*ΔT, +/-0.001*ΔT, +/-0.0015*ΔT and +/-0.002*ΔT (the dotted contour lines correspond to negative values, where $T_h$ = ΔT/2 and $T_c$ = -ΔT/2). (After Janssen and Henkes, 1995)**

**"Reprinted with the permission of Cambridge University Press from Jansenn, R.J.A. and R.A.W. Henkes/Influence of Prandtl number on stability mechanisms and transition in a differentially heated square cavity, Journal of Fluid Mechanics, Vol. 290, 1995; pp.319-344, Copyright 1995, Figure 9.C.4"**

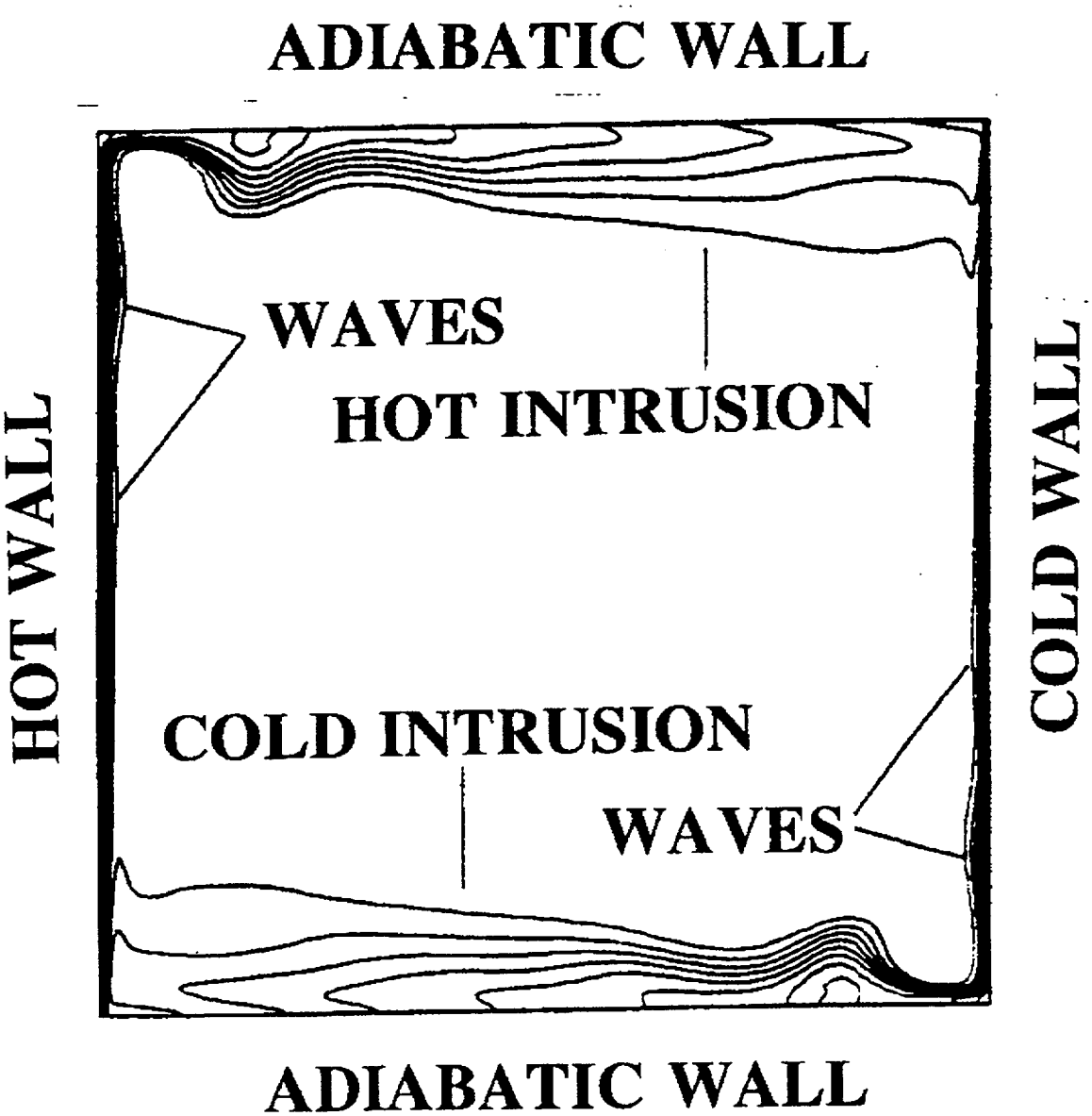


**Figure 9.C.1-10** Temperatures for the initial solution with the hot and cold intrusions and boundary layer waves presented (after Armfield and Janssen, 1996)

**"Reprinted with permission from Int. J. Heat and Fluid Flow, Vol. 17, S. Armfield and R. Janssen/A direct boundary-layer stability analysis of steady-state cavity convection flow, pp. 539-546, 1996. Elsevier Science Inc."**

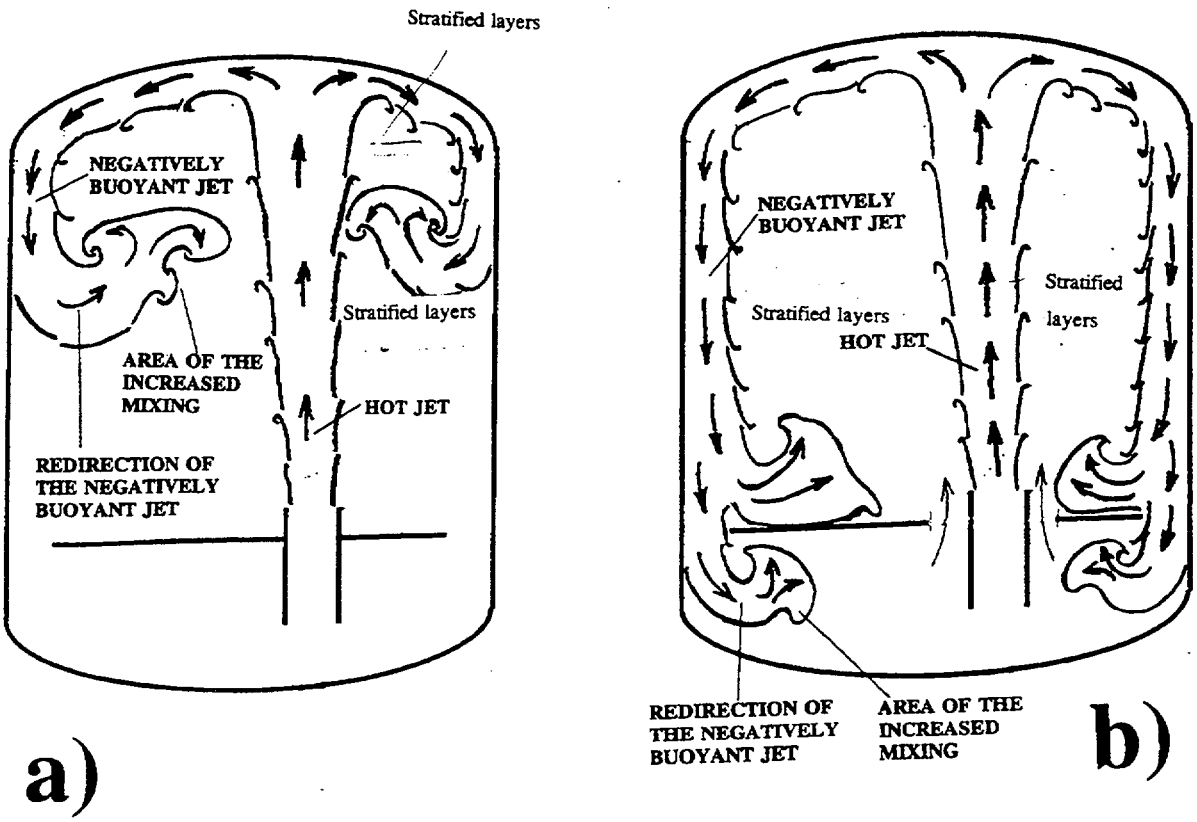


**Figure 9.C.1-11 Formation of the downward negatively buoyant jets**

**a) negatively buoyant jet redirected inside the dome region**
**b) negatively buoyant jet penetrating the below deck region**

### 9.C.1.1.3 References

1. Akino, N., Kunugi, T., Shiina, Y., Seki, M. and Okamoto, Y. (1989)
"Natural convection in a horizontal silicone oil layer in a circular cylinder heated from below and cooled from above", (in Japanese), Trans. Jpn. Soc. of Mech. Eng. 55 509 no. 1989-1), no. 88-0901 B: 152-158, 1989.

2. Allard, F., (1992)
"Effects of thermal boundary conditions on natural convection in thermally driven cavities", in - Turbulent Natural Convection in Enclosures, A Computational and Experimental Benchmark Study, (Eds.) R.A.W.M Henkes and C.J. Hoogendoorn, Editions Europeenns Thermique et Industrie, Paris, pp. 234-256.

3. S. Armfield and R. Janssen (1996)
"A direct boundary-layer stability analysis of steady-state cavity convection flow" Int. J. Heat and Fluid Flow, Vol. 17, No. 6, December 1996.

4. W.D. Baines and J.S. Turner (1969)
"Turbulent buoyant convection from a source in a confined region" J. Fluid Mech., Vol. 37, part 1, pp. 51-80.

5. Catton, I., (1978)
"Natural convection in enclosures" Proc. 6th Int. Heat Transfer Conf., Vol. 6, pp. 13-31.

6. Dzodzo M. B., (1993)
"Visualization of laminar natural convection in romb-shaped enclosures by means of liquid crystals" in "Imaging in transport processes", (ed. S. Sideman and K. Hijikata), Chapter 15, pp. 183-193., Begel House, Inc., 1993.

7. R. Frederick and A. Valencia, (1995), "Natural Convection in Central Microcavities of Vertical Pinned Enclosures of very High Aspect Ratios," Int. J. Heat and Fluid Flow, Vol. 16, No. 2, April 1995, pp. 114-124.

8. T. Fusegi, J. M. Hyun, K. Kuwahara, (1992)
"Numerical simulations of natural convection in a differentially heated cubical enclosure with a partition" Int. J. Heat and Fluid Flow, Vol. 13, No. 2, June 1992, pp 176-183.

9. T. Fusegi, T. M. Hyun, (1994) " Laminat and Transitional Natural Convection in an enclosure with complex and relistic conditions," Int. J. Heat and Fluid Flow, Vol. 15, No. 4, August 1994, pp. 258-268.

10. A. D. Garrad and M.A. Patrick, (1983)
"The velocity field produced by a submerged jet directed upwards at a free surface" Int. J. Heat Mass Transfer, Vol. 26, No. 7, pp. 1029-1036.

11. K. Hanjalic, S. Kernjeres and F. Durst, (1996)
"Natural convection in partitioned two-dimensional enclosures at higher Rayleigh numbers" Int J. Heat Mass Transfer, Vol. 39, No. 7, pp. 1407-1427, 1996

12. T. J. Heindel, S. Ramadhyani, and F. P. Incropera (1995)
"Conjugate natural convection from an array of discrete heat sources: part 1 - two and three-dimensional model validation" Int. J. Heat and Fluid Flow, Vol. 16, No. 6, December 1995, pp. 01-510.

13. Hiller W.J., Koch St., Kowalewski T.A., (1988)
"Simultane erfassung von temperatur und geschwindigkeitsfelden in einer thermischen konvektionsstromung mit ungekapselten flussigkristalltracern, DGLR - Workshop, 2D-Mestechnik, 1988.

14. Hiller W.J., Koch St., Kowalewski T.A., (1989)
"Three-dimensional structures in laminar natural convection in a cube enclosure" Exp. Therm. Fluid Sci., Vol. 2, pp. 34-44.

15. C. J. Ho, Y. T. Cheng and C. C. Wang, (1994)
"Natural convection between two horizontal cylinders inside a circular enclosure subjected to external convection" Int. J. Heat and Fluid Flow, Vol. 15, No. 4, August 1994, pp 299-306.

16. Hoogendoorn, C.J., (1986)
"Natural convection in enclosures" Proc. 8th Int. Heat Transfer Conf., Vol. 1, pp. 111-120.

17. J.M. Hyun and B.S. Choi, (1990)
"Transient natural convection in a parallelogram-shaped enclosure", Int. J. Heat and Fluid Flow, Vol. 11, No. 2, June 1990, pp. 129-134.

18. R. J. A. Janssen and R.A.W.M. Henkes, (1995)
"Influence of Prandtl number on instability mechanisms and transition in a differentially heated square cavity," J. Fluid Mech., Vol. 290, pp. 319-344., 1995

19. K. Kapoor and Y. Jaluria, (1993)
"Penetrative convection of a plane turbulent wall jet in a two-layer thermally stable environment: a problem in enclosure fires" Int. J. Heat Mass Transfer, Vol. 36, No. 1, pp. 155-167, 1993.

20. A. Kurosawa, N. Akino, T. Otsuji, S. Kizu, K. Kobayashi, K. Iwahori, T. Takeda and Y. Ito, (1993)
"Fundamental study on thermo-hydraulic phenomena concerning passive safety of advanced marine reactor" Journal of Nuclear Science and Technology, Vol 30 [2], pp. 131-142, February 1993.

21. G.D. Mallinson and G. de Vahl Davis, (1977)
"Three-dimensional natural convection in a box: a numerical study" J. Fluid Mech., Vol. 83, pp. 1-31.

22. N.C. Markatos and K.A. Pericleous, (1984)
"Laminar and turbulent natural convection in an enclosed cavity" Int. J. Heat Mass Transfer, Vol. 27, No. 5, pp. 755-772.

23. E. S. Nowak and M. H. Novak, (1994)
"Vertical partitions in slender rectangular cavities" Int. J. Heat and Fluid Flow, Vol. 15, No. 2, April 1994, pp. 104-110.

24. Ostrach, S., (1972)
"Natural convection in enclosures" Advances in Heat Transfer, Vol. 8, Academic Press, New York, pp. 161-227.

25. Ostrach, S., (1982)
"Natural convection heat transfer in cavities and cells" Proc. 7th Int. Heat Transfer Conf., Vol 1, pp.365-379.

26. F.E. Peters, (1994)
WCAP-14135, "Final Data Report for PCS Large-Scale Tests, Phase 2 and Phase 3", Revision 1, April 1997.

27. P.F. Peterson, (1994)
"Scaling and analysis of mixing in large stratified volumes" Int. J. Heat Mass Transfer, Vol. 37, Suppl. 1, pp. 97-106.

28. B. Porterie, M. Larini, F. Giroud and J.C. Loraud (1996)
"Solid-propellant fire in an enclosure fitted with a ceiling safety-vent" Int. J. Heat Mass Transfer, Vol. 39, No. 3, pp. 575-601.

29. R.M. C So and H. Aksoy, (1993)
"On vertical turbulent buoyant jets" Int. J. Heat Mass Transfer, Vol. 36, No. 13, pp. 3187-3200.

30. L. Wolf, H. Holzbauer, T. Cron, (1994a)
"Detailed Assessment of the HDR-Hydrogen Mixing Experiments E11" International Conference on New Trends in Nuclear System Thermohydraulics, Pisa, Italy, May 30th - June 2nd, vol. 2, pp. 91--103.

31. L. Wolf, H. Holzbauer, M. Schall, (1994b)
"Comparisons between multi-dimensional and lumped-parameter Gothic-containment analyses with data" International Conference on New Trends in Nuclear System Thermohydraulics, Pisa, Italy, May 30th - June 2nd, vol. 2, pp. 321 - 330.

## 9.C.1.2 CIRCULATION PHENOMENA

Circulation processes inside enclosures are the result of natural or forced convection effects. Forced convection inside an enclosure is promoted using devices such as fans, nozzles, or sprays of liquid droplets. PCS applications are of primary interest, since no credit is taken for active systems in the design basis analysis.

A review of possible flow patterns due to natural convection effects is presented. Natural convection is generated if:

1) The upper boundary is at a lower temperature than the lower boundary or opposite vertical boundaries are at different temperature, as well as for other similar combinations of temperature boundary conditions (or imposed heat flux conditions) at the outside and inside surfaces.

2) A higher concentration of the lighter or heavier components of a mixture is maintained near the lower or upper boundaries of the enclosure, respectively.

3) A lighter fluid is released (permanently, or from time to time) from a source which is closer to the bottom of the enclosure.

4) The shape of the enclosure promotes natural convection (together with the distribution of other boundary conditions).

5) The distribution and size of the horizontal and vertical internal openings allows or enhances (as with a chimney or staircase effects) the formation of fluid flow patterns due to the natural convection.

6) If the internal heat sources (sinks) are positioned in the lower (upper) portions of the enclosure.

Under the conditions above (or a combination of them), natural convection causes circulation inside the enclosure. The convection increases the intensity of heat and mass transfer, therefore increasing the heat released from the containment. The intensity of heat transfer depends upon the location of the heat sinks and sources, which can exchange positions due to the transient effects. The velocity and temperature profiles inside the formed boundary layers (wall jets) influence the rate of heat transfer due to the convection. Wall jets entrain the surrounding atmosphere and contribute to better mixing. In the regions with a higher steam concentration, the increase in the heat transfer rate and the effects of entrainment occur due to the condensation inside the boundary layers.

Another contributing factor that promotes circulation inside an enclosure is the interaction of the enclosure atmosphere with the penetrating buoyant plumes or jets and wall layers. In the case of a containment vessel, the plumes or jets could be generated by a LOCA or MSLB. If the break position is inside a narrow corridor or surrounded by additional equipment, the kinetic energy of the jet is dissipated and steam rises in the form of a buoyant plume. The rising plume entrains the surrounding gas and results in circulation inside the volume of the enclosure.

If the break position is open and the jet is directed upward, both the kinetic energy of the jet and the buoyancy forces contribute to penetration into the atmosphere. The higher speeds of the jet affect a greater portion of the volume and both entrainment of the surrounding gas and circulation is stronger.

### 9.C.1.2.1 Circulation Phenomena Due to the Presence of Boundary Layers (Wall Jets) and Buoyant Plumes Formed as a Consequence of Natural Convection Effects

Natural convection flow is the most often generated by different temperatures or heat fluxes imposed on the boundaries of an enclosure. Various distributions on the boundaries produce various flow patterns and temperature fields.

Section 9.C.1.1 discusses boundary temperature distributions (upper/lower horizontal plates at the higher/lower temperatures) that produce static stratification. Section 9.C1.2 discusses the case where vertical opposite sides are at constant, but different temperatures. If Rayleigh numbers are greater than $10^4$, this condition produces a recirculated region near the walls and a stratified core of the enclosure.

Figure 9.C.1-12 presents a case known as Rayleigh-Benard convection. The upper horizontal boundaries are at the lower temperatures (or cooled). The flow patterns formed depend upon the temperature difference and geometry of the enclosure (in fact the value of the Rayleigh number).

For the smaller Ra numbers, vortical cells are formed. An increase in the Ra numbers produces a greater number of vortical cells that start to oscillate, periodically changing the size and intensity. A further increase in the Ra number results in chaotic flow, and produces vertical plumes which reach the opposing horizontal sides of the enclosure. The flow patterns and possible bifurcations produced during the transition from the laminar to turbulent (chaotical) flow regimes are described in Koschmieder, 1993, Yang, 1988, and Ozawa et al., 1992. Some experimental results (flow patterns and temperature fields) are presented for laminar flow regimes by M. Dzodzo et al., 1994 and M.J. Braun et al., 1993. Flow patterns for turbulent and chaotic flow between two horizontal plates at different temperatures are described in Akino et al., 1989.

Flow in the Hele-Shaw cell is presented as an example of natural convection between two horizontal plates. A Hele-Shaw cell has a square cross-section, but it is narrow in one of the horizontal directions so that three-dimensional convection effects are suppressed (see Figure 9.C.1-13). The upper and lower horizontal sides are at the lower and higher temperatures, respectively.

Consecutive flow patterns and temperature fields for a Hele-Shaw cell with various Rayleigh numbers are presented in Figure 9.C.1-14 (after Buhler et al., 1987). If the value of the Rayleigh number is greater than $4*10^6$, oscillatory flow patterns with four vortical cells are present. The large and small vortices expand and contract periodically (see Figure 9.C.1-14). At high Rayleigh numbers (above $5.9*10^7$), a reverse transition from the oscillatory to the steady flow patterns occurs. This phenomena is probably due to suppressed three-dimensional convection effects.

For cubic or cylindrical enclosures, with the upper and lower horizontal surfaces at the lower and higher temperatures, respectively, three-dimensional convection effects produce turbulent (chaotical) flow (see Figure 9.C.1-15). In the paper by Akino et al., 1989, the turbulent flow regime starts at a Rayleigh number of $2*10^6$ (Pr = 200). For fluids with a Prandtl number close to one, the transition to turbulent flow regime occurs at a smaller Rayleigh number (Ra ~ $10^4$).

The flow pattern consists of vertical buoyant plumes detached from the horizontal sides. The vertical plumes reach opposite sides of the enclosure and generate opposing plumes (see Figure 9.C.1-16). Temperature gradients near the horizontal surfaces are high, while temperatures in the core of the containment are almost uniform. Figure 9.C.1-17a illustrates an example where the temperature in the middle of the enclosure oscillates between 26 and 29 °C with Ra = $9.38*10^7$ ($T_h$=35 °C and $T_c$=20 °C). The highest temperature is registered during the rise of the hot plume and the lowest temperature is registered during the downward penetration of the cold plume. The amplitude of the temperature oscillations in the middle of the enclosure is three degree Celsius. The temperature interval between 26 and 29 °C represents $0.2*(T_h-T_c)$ or 20 percent of the maximum temperature difference. The temperature in the middle of the enclosure is (27.5 °C) +/- 1.5 °C.

Rayleigh-Benard convection is relevant to the containment. In the case of a LOCA or MSLB, the upper portion of the dome and vertical sides are cooled. If the temperature below the ceiling is 9 °F lower than temperature of the incoming steam (at the deck level), the Grashof number (based on the height of the containment, $H_t$=109 ft) is $Gr_t$=2.2 x $10^{13}$. This Grashof number is in the range of the chaotic flow, with the upward and downward plumes (because $Gr_t > 10^4/0.71$).

Maintaining the vertical walls of the containment at the lower temperature also promotes downward vertical plumes near the walls due to separation of the vertical boundary layers (see Figure 9.C.1-17b).

### 9.C.1.2.2 Circulation Phenomena Due to the Interaction With the Hot Buoyant Plumes and Jets

The presence of a hot buoyant plume or a jet of the hot steam during a LOCA or MSLB contributes to the circulation of the containment atmosphere by entraining the surrounding air and other gases. In the case of jet inflow, additional entrainment and circulation are generated by the jet kinetic energy.

Depending upon the strength (initial velocity and mass flow) and direction of the plume or jet, various flow patterns inside the containment are possible. Interaction of the vertical downward plumes generated due to the natural convection (cooling of the shell) produce turbulent flow. This results in good mixing of the dome atmosphere. Examples of vertical plumes and jets are presented by Garrad and Patrick, 1983, So an Aksoy, 1993, and Porterie et al. 1996. The scaling and analysis of circulation in large stratified volumes is presented by Peterson, 1994.

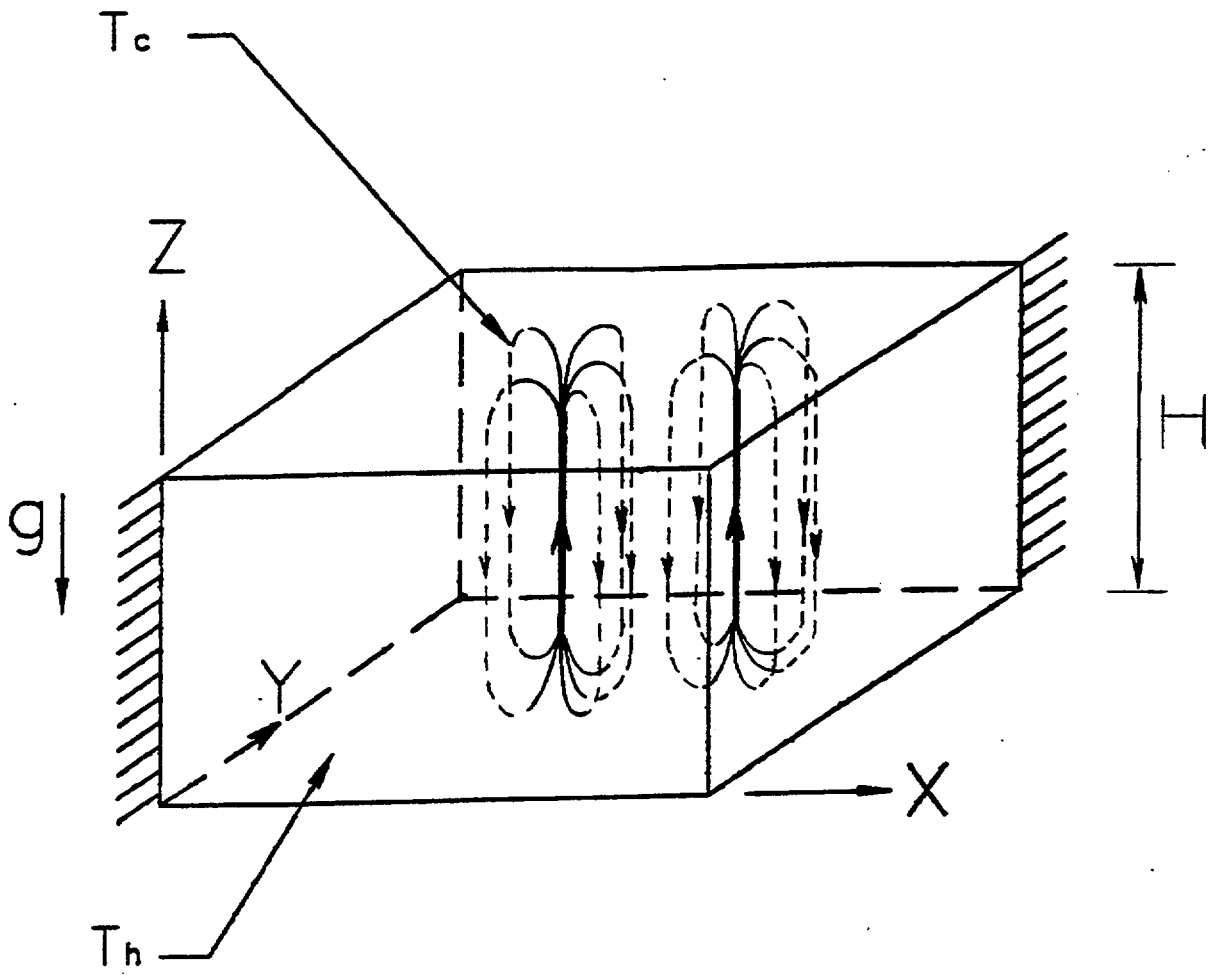


**Figure 9.C.1-12 Rayleigh-Benard convection example**

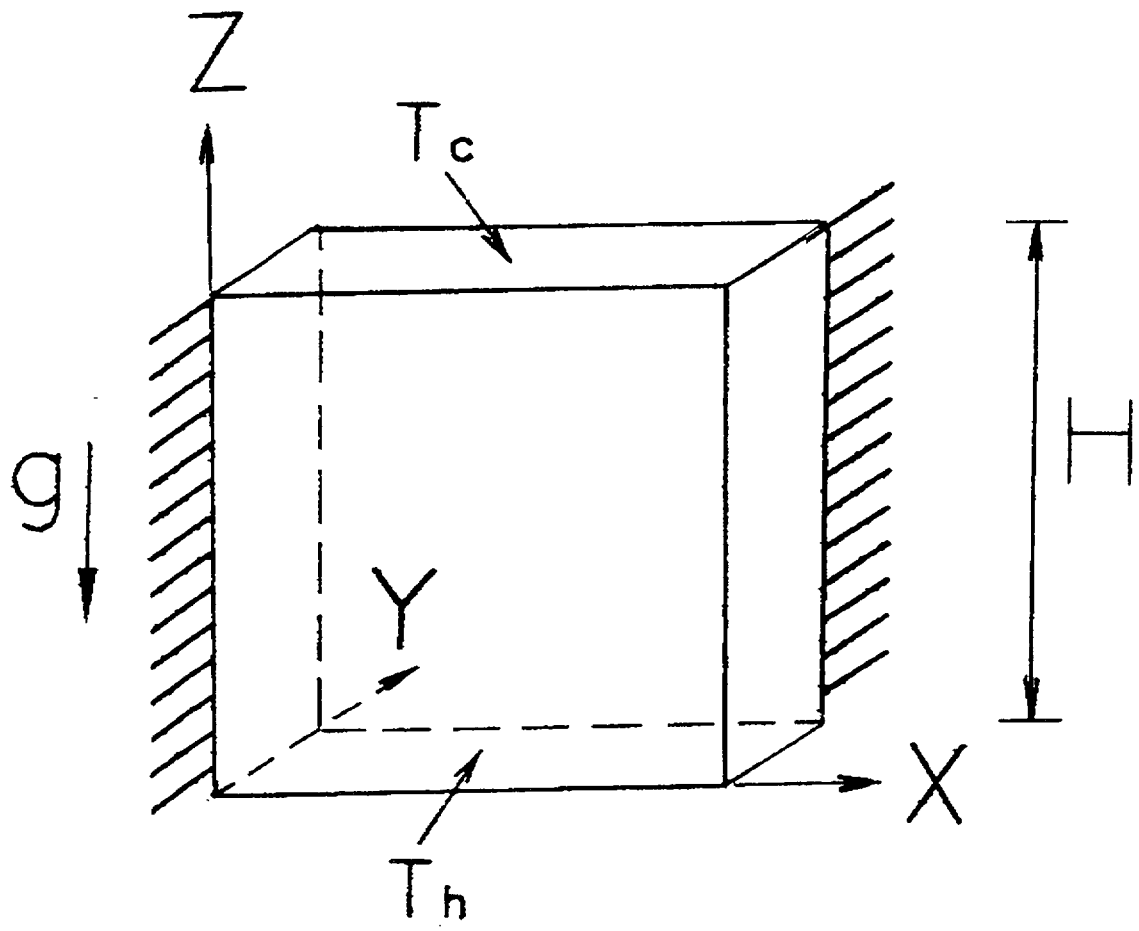


**Figure 9.C.1-13 Hele-Shaw cell**

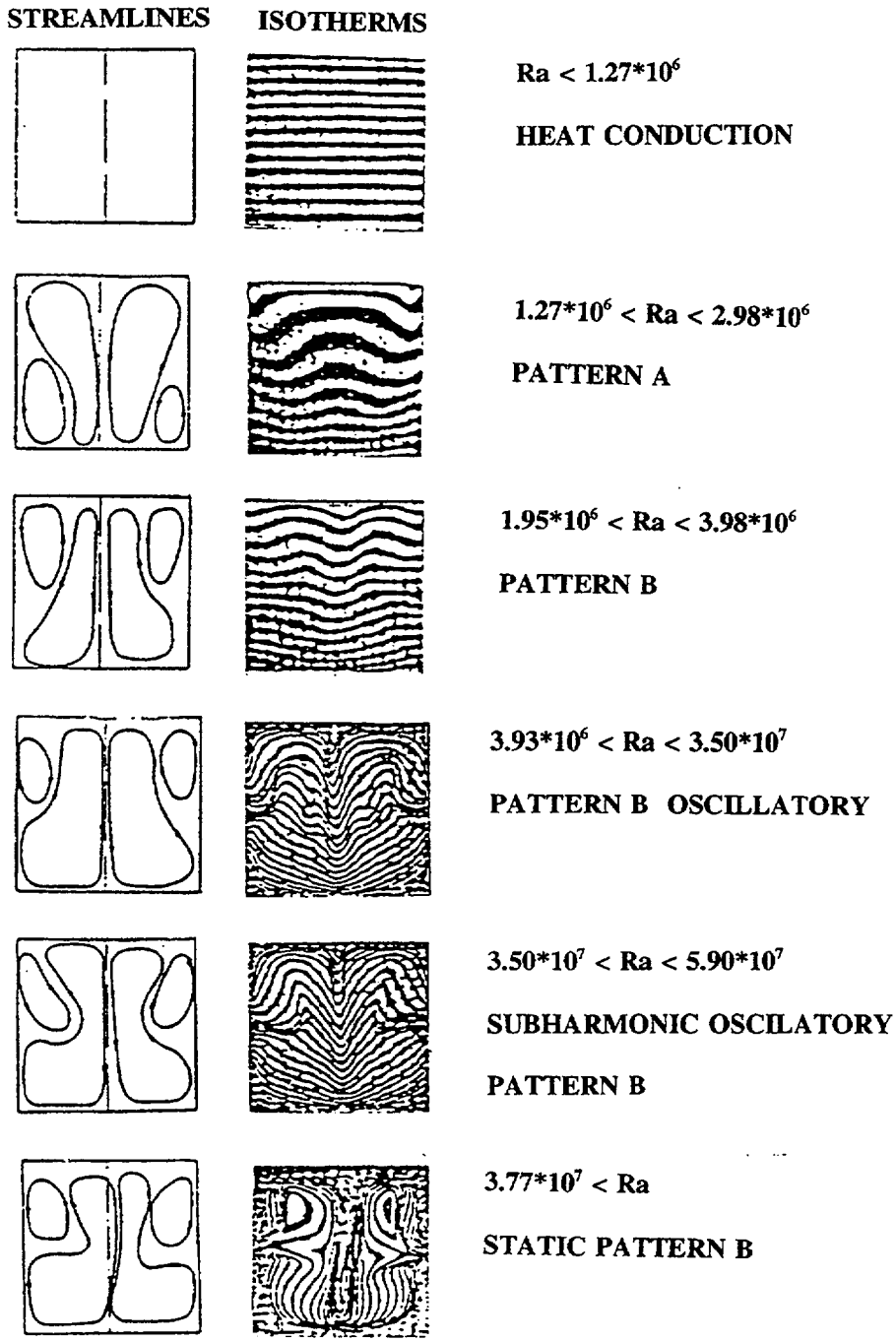


**Figure 9.C.1-14 Steady and oscillatory convection in Hele-Shaw cell (after Buhler et al., 1987)**

**"Reprinted from L.Buhler, P. Ehrhard, C. Gunther, U. Muller and G. Zimmermann/Natural convection in vertical gaps heated at the lower side - en experimental and numerical study, HTD-Vol. 94, AMD-Vol. 89, Bifurcation Phenomena in Thermal Processes and Convection, Winter Annual Meeting of the American Society of Mechanical Engineers, Boston, Massachusetts, December 13-20, 1987"**

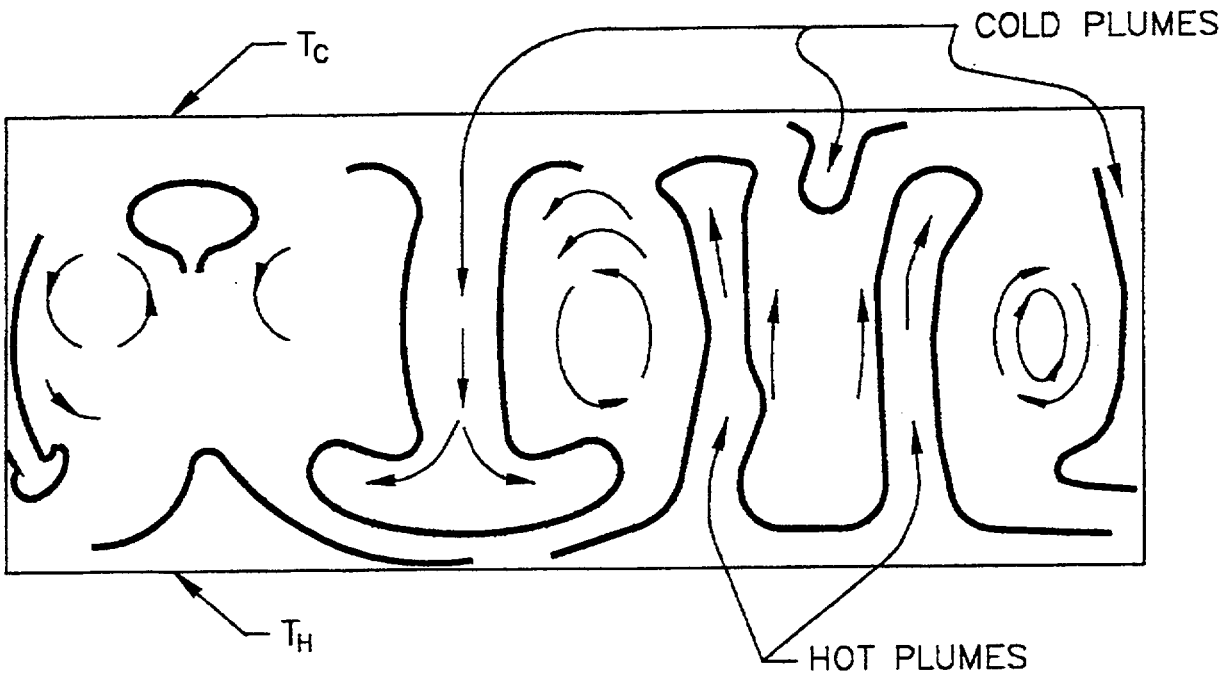


**Figure 9.C.1-15 Turbulent (chaotical) flow with hot and cold plumes interactions (plane cross-section of the three-dimensional enclosure is presented)**

**(according to Figure 6 in N. Akino, T. Kunugi, Y. Shiina, M. Seki, Y. Okamoto/Natural convection in a horizontal silicone oil layer in a circular cylinder heated from below and cooled from above", Trans. Jpn. Soc. of Mech. Eng. 55 509 no. 1989-1), no. 88-0901 B:, pp. 152-158, 1989 -with permission from Norio Akino)**

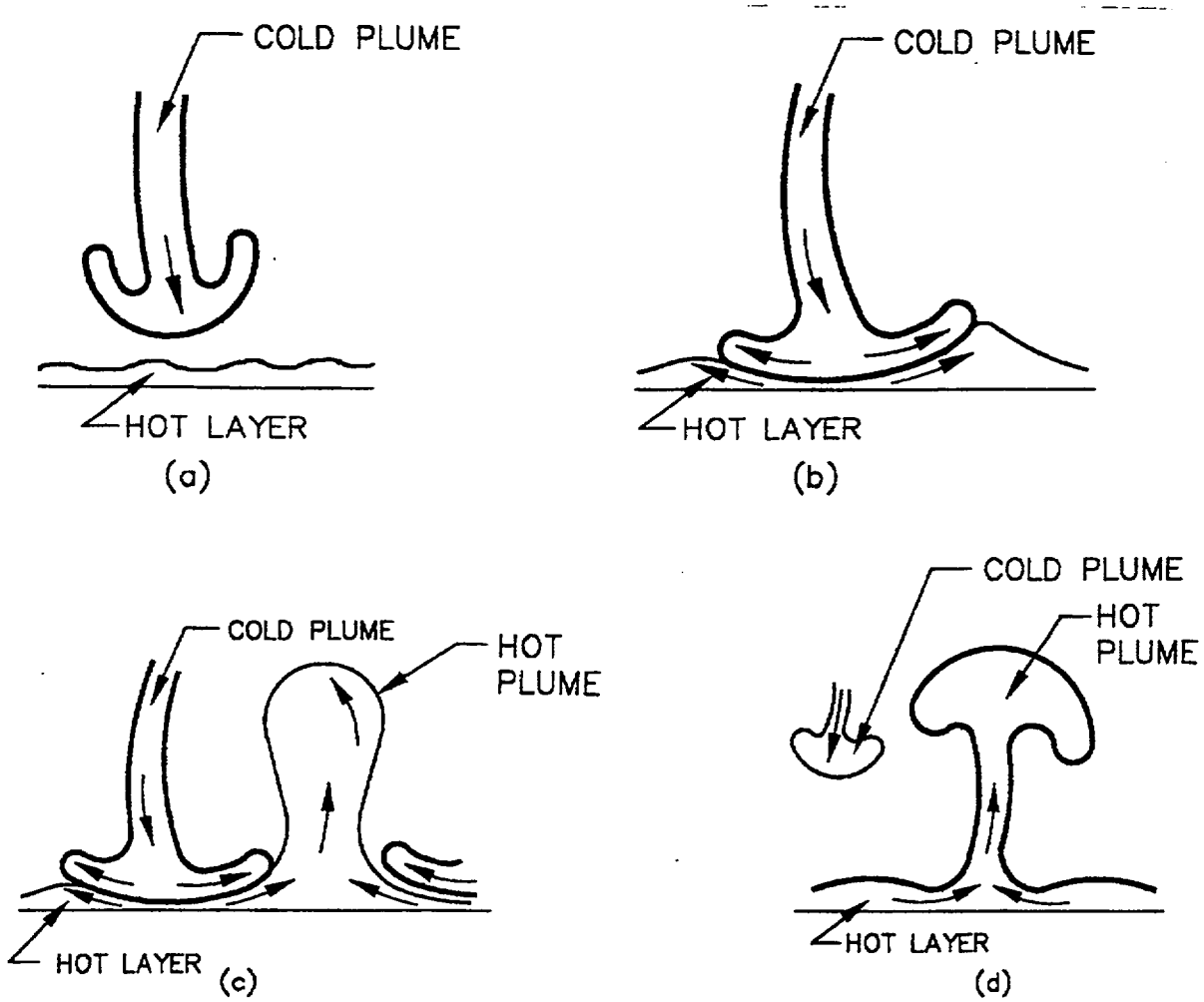


**Figure 9.C.1-16 Interaction of hot and cold plumes (after Aqino et al., 1989)**

**(according to Figure 12 in N. Akino, T. Kunugi, Y. Shiina, M. Seki, Y. Okamoto/Natural convection in a horizontal silicone oil layer in a circular cylinder heated from below and cooled from above", Trans. Jpn. Soc. of Mech. Eng. 55 509 no. 1989-1), no. 88-0901 B:, pp. 152-158, 1989 - with permission from Norio Akino)**

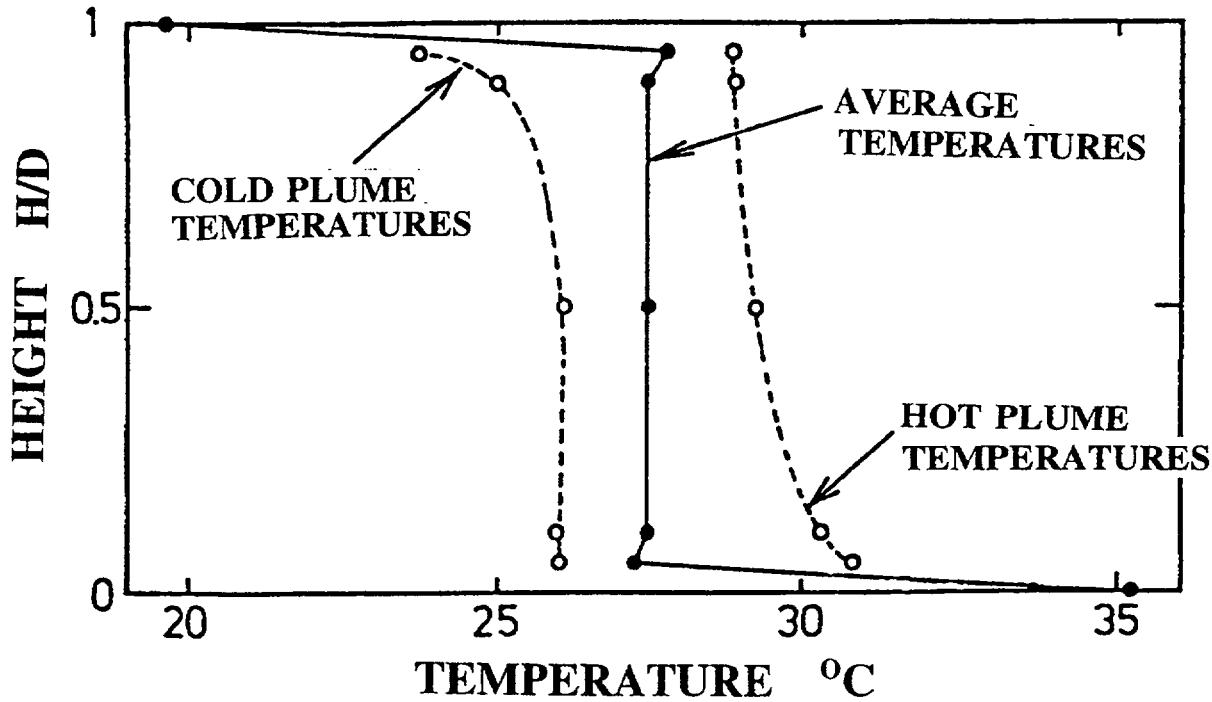


**Figure 9.C.1-17a Vertical temperature distribution inside the cylindrical enclosure with lower and upper horizontal plate at higher and lower temperatures, respectively ($Ra = 9.38*10^7$, $Pr = 200$)**

**(according to Figure 14 in N. Akino, T. Kunugi, Y. Shiina, M. Seki, Y. Okamoto/Natural convection in a horizontal silicone oil layer in a circular cylinder heated from below and cooled from above", Trans. Jpn. Soc. of Mech. Eng. 55 509 no. 1989-1), no. 88-0901 B:, pp. 152-158, 1989 - with permission from Norio Akino)**

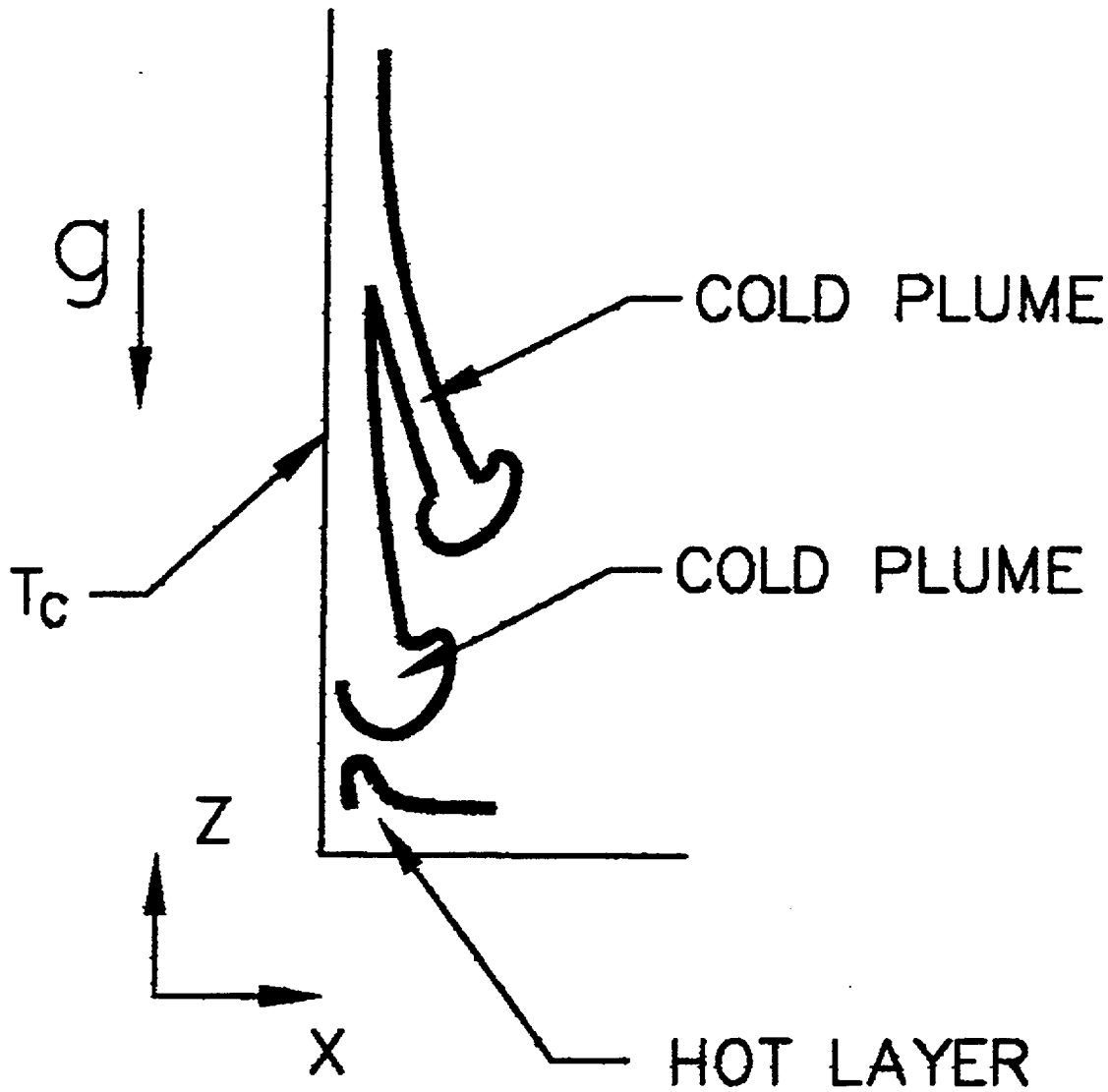


**Figure 9.C.1-17b Generation of the cold plumes due to the brake (separation) of the vertical boundary layers near the cold vertical walls**

### 9.C.1.2.3 References

1. N. Akino, T. Kunugi, Y. Shina, M. Seki, Y. Okamoto, (1989)
"Natural Convection in a Horizontal Silicone Oil Layer in a Circular Cylinder Heated from Below and Cooled from Above" Nippon Kikai Gakkai Ronbunchyu, 55 Vol. 509 (1989-1), pp. 152 -158.

2. M. J. Braun , M. B. Dzodzo, S. B. Lattime, (1993)
"Automatic computer based non-intrusive temperature measurements in laminar natural convection using thermochromic liquid crystals in enclosures with variable aspect ratio" FED-Vol. 172, Experimental and numerical flow visualization, The 1993 ASME Winter Annual Meeting, New Orleans, Louisiana, November 28 - December 3, 1993, pp. 111-119.

3. L. Buhler, P. Erhard, G. Gunther, U. Muller, G. Zimmermann, (1987)
"Natural convection in vertical gaps heated at the lower side - an experimental and numerical study. In: Bifurcation Phenomena in Thermal Processes and Convections (eds.H.M. Bau, L.A. Bertram, S.A. Lorpela) ASME, HTD-Vol. 94/AMD-Vol.89, 67-74.

4. M. Dzodzo, M.J. Braun, S.B. Lattime, (1994)
"A non-intrusive computer automated investigation of natural convection using thermochromic liquid crystals and comparison with numerical simulation" (ed. G.F. Hewitt) Proceedings of The Tenth International Heat Transfer Conference, Brighton, UK, Volume 2, 2-MT-6, pp. 225-230.

5. A.D. Garrad and M.A. Patrick, (1983)
"The velocity field produced by submerged jet directed upwards at a free surface", Int. J. Heat Mass Transfer, Vol. 26, No. 7, pp. 1029-1036.

6. E. L. Koschmieder, (1993)
"Benard Cells and Taylor Vorticies" Cambridge University Press

7. M. Ozawa, U. Muller, I. Kimura and T. Takamori, (1992)
"Flow and temperature measurements of natural convection in a Hele-Shaw cell using a thermo-sensitive liquid-crystal tracer" Experiments in Fluids, Vol 12, pp. 213-222.

8. P.F. Peterson, (1994)
"Scaling and analysis of mixing in large stratified volumes" Int. J. Heat Mass Transfer, Vol. 37, Suppl. 1, pp. 97-106.

9. B. Porterie, M. Larini, F. Giroud and J.C. Loraud, (1996)

"Solid-propellant fire in an enclosure fitted with a ceiling safety-vent" Int. J. Heat Mass Transfer, Vol. 39, No. 3, pp. 575-601.

10. R.M.C. So and H. Aksoy, (1993)
"On vertical turbulent buoyant jets" Int. J. Heat Mass Transfer, Vol. 36, No. 13, pp. 3187-3200.

11. K.T. Yang, (1988)
"Transitions and Bifurcations in Laminar Buoyant Flows in Confined Enclosures" J. of Heat Transfer, November 1988, Vol. 110, pp. 1191-1204.

## 9.C.1.3 IMPORTANT DIMENSIONLESS GROUPS

### 9.C.1.3.1 Important Dimensionless Groups for Stratification and Circulation Phenomena Inside Enclosures

For natural convection, the ratio of the buoyancy to viscosity forces is the most important dimensionless group. The Grashof number defines the ratio of the buoyancy to viscosity forces:

$$Gr = \frac{g\beta(T_h - T_c)H^3}{\nu^2} = \frac{g(\rho_c - \rho_h)H^3}{\rho_c \nu^2}$$

Natural convection correlations often use the Rayleigh number instead of Grashof number, where the Rayleigh number Ra is defined as:

$$Ra = \frac{g\beta(T_h - T_c)H^3}{a\nu} = \frac{g(\rho_c - \rho_h)H^3}{\rho_c a \nu} = Gr\frac{\nu}{a} = GrPr$$

Using the Rayleigh number reduces the number of dimensionless groups in the correlations for natural convection. The appearance of Prandtl number inside some correlations could be avoided.

The Prandtl number is based on fluid properties, i.e., the ratio of kinematic viscosity to thermal diffusivity.

$$Pr = \frac{\nu}{a}$$

When considering the interaction between the hot buoyant plume and the cold vertical wall boundary layer, the Grashof and Rayleigh numbers are defined with $H_v$ as the characteristic length.

$$Gr_v = \frac{g(\rho_v - \rho_o)H_v^3}{\rho_v \nu^2}$$

This applies to flows generated inside the enclosures with the opposite vertical walls at the different temperatures. It also applies to flow caused by two opposing vertical jets (between the two horizontal plates). The AP600 and AP1000 have a combination of the two cases.

Upward flow is caused by the buoyant plume, while downward flow is caused by the lower temperatures of the vertical wall. If the initial kinetic energy of the plume is small, this Grashof number gives an indication of the formed flow pattern and heat transfer due to the two opposing vertical flow paths. The formation of a recirculating stratified core between the vertical jets is related to this parameter as well.

When considering the interaction between the cold ceiling and the hot rising plume (at the bottom of the enclosure), the height of the upper-deck region $H_t$ can be used as a characteristic length. The Grashof number is:

$$Gr_t = \frac{g(\rho_t - \rho_o) H_t^3}{\rho_t \nu^2}$$

The value of this Grashof number indicates the status of the Rayleigh-Benard convection. If the values are above $10^4$, it is possible to form periodic vertical downward plumes which detach from the ceiling.

The conditions described above interact. The overall flow pattern is expected to be a superposition of the flow patterns described for enclosures with horizontal and vertical temperature gradients. The prevailing flow pattern is estimated from the ratio of the two Grashof numbers already defined:

$$\frac{Gr_t}{Gr_v} = \frac{(\rho_t - \rho_o) H_t^3 \rho_v}{(\rho_v - \rho_o) H_v^3 \rho_t}$$

Note that both dimensions of the large-scale test (LST) installation ( $H_t$ and $H_v$) are scaled to AP600 dimensions. Therefore, if the ratio of relative densities (in vertical and horizontal directions) is the same, the flow patterns obtained in LST experiments can be applied to the AP600.

Even small temperature differences between the shell and the atmosphere inside a containment produce large Grashof numbers. For example, a temperature difference of 9°F results in $Gr_t = 2.2*10^{13}$ and $Gr_v = 4.7*10^{12}$ for $H_t$ = 109 ft and $H_v$ = 65 ft, respectively.

In the case of LST, a temperature difference of 9°F results in $Gr_t = 3.9*10^{10}$ and $Gr_v = 7.2*10^9$ for $H_t$ = 13.2 ft and $H_v$ = 7.5 ft, respectively.

If the Grashof numbers are greater than $10^8$, the Nusselt number can be obtained by applying the correlation for turbulent free convection.

For jets and buoyant plumes that penetrate the containment, the ratio of inertia forces and buoyant forces influences the entrainment of surrounding gases. If the initial velocities are high, a constant spreading angle indicates a jet. As the jet velocities decrease, upward motion results from buoyant forces. Buoyant plume behavior is indicated by different spreading angles at each level.

The Froude number represents the ratio of the inertia to gravity forces, or the ratio of kinetic energy to potential energy:

$$Fr = \frac{U^2}{gH} = \frac{\rho U^2}{g\Delta\rho H} = \frac{\left(\frac{U\ H}{\nu}\right)^2}{\frac{g\ \Delta\rho\ H^3}{\rho\nu^2}} = \frac{Re^2}{Gr}$$

For buoyant plumes and jets, the Froude number can be defined as:

$$Fr_{j,o} = \frac{\rho_o U_o^2}{g(\rho_a - \rho_o)d_o}$$

where the characteristic length is the initial diameter of the jet or plume. The source velocity and density have the subscript (o), while the ambient density has the subscript (a). The elevation of the transition from a forced jet to a buoyant plume is calculated (Peterson, 1994 and Spencer, 1997) from the expression:

$$\frac{z_{trans}}{d_o} = Fr_{j,o}^{1/4} \left(\frac{\rho_o}{\rho_a}\right)^{1/4}$$

The ratio of the square of the jet Reynolds number to the containment Grashof number is a volumetric Froude number:

$$Fr_v = \frac{\rho_a U_o^2\ d_o^2}{g(\rho_a - \rho_o)H^3}$$

If the volumetric Froude numbers are much greater than one, the inertia forces dominate. The inertia forces unstabilize stratified layers, promote circulation inside the containment, and contribute towards the better mixing.

However, Peterson, 1994, proposes that the jet or plume is not able to disturb the stratified vertical density gradients if:

$$Fr_v < \left(1 + \frac{d_o}{4\sqrt{2}\,\alpha\,H}\right)^2$$

where ($\alpha$) is Taylor's jet entrainment parameter and where $\alpha = 0.05$ = constant.

For volumetric Froude numbers less then one, the inertia forces are not dominant and are not able to unstabilize stratified layers inside the containment. Therefore, the buoyancy effects are more important than inertia effects. The reciprocal value of the Froude number or Richardson number is the appropriate dimensionless group.

$$Ri_v = \frac{g(\rho_a - \rho_o)H^3}{\rho_a U_o^2\, d_o^2}$$

Since inertia effects of the plume are not important (Reynolds number of the plume is small), only Grashof numbers $Gr_t$ and $Gr_v$ will influence the flow pattern.

Another important factor is the position of the jet (plume) or heat source release location. The ratio of the release point level, $H_r$, to the height of the containment, $H_t$, describes the relative position of the jet (plume) or heat source:

$$\frac{H_r}{H_t}$$

If $H_r/H_t$ is less than 0.2, the release location is considered low. A global circulation flow pattern affecting the entire containment is most likely formed. If $H_r/H_t$ is greater than 0.5, the release elevation is high and stratification effects may occur in a portion of the volume. The result may be that only the upper portion of the enclosure is affected by global circulation, while the lower may be stratified. Such stratification may be stagnant. In stagnantly stratified regions, no entrainment into wall boundary layers or buoyant plumes occurs,

and thus little or no vertical mixing occurs, while in recirculating stratified regions vertical mixing can be strong and can greatly reduce vertical density gradients.

Specified criteria for the $H_r/H_t$ ratio are based on the international experimental database which is presented in the next chapter.

### 9.C.1.3.2 References

P. F. Peterson, (1994), "Scaling and Analysis of Mixing in Large Stratified Volumes," Int. J. of Heat and Mass Transfer, Vol. 37, Supplement 1, pp. 97-106, 1994.

D. R. Spencer, (1997), "Scaling Analysis for AP600 Containments Pressure During Design Basis Accidents," WCAP-14845, Revision 3, March 1998.

## 9.C.1.4 EXPECTED FLOW PATTERNS FOR AP600 AND AP1000

### 9.C.1.4.1 Simplified Representation of Circulation Regions During Post-Blowdown LOCA in AP600 and LST

The AP600 containment and the large-scale test (LST) facility include five primary flow regions (Peterson, 1997 - letter to Woodcock). The regions are presented in Figure 9.C.1-18 showing a control volume that extends to the condensed fluid film surfaces. This figure is useful for structuring a discussion of circulation and stratification phenomena and for relating separate effects of enclosures tests to the various regions.

The volumetric flow rates presented in Figure 9.C.1-18 at "quasi-steady" conditions are:

- $Q_o$, the steam volumetric flow rate from the break,
- $Q_e$, the flow rate of fluid entrained from inside the below-deck region into the steam generator compartment (equivalent to the flow rate delivered to the below-deck region due to the penetration of a portion of the wall boundary layers through the deck gap near the walls),
- $Q_p$, the flow rate of fluid entrained into the plume in the above-deck region,
- $Q_w$, the flow rate of fluid entrained into the vertical wall boundary layers,
- $Q_v$, the flow rate of steam condensed on the vertical walls (shown leaving the control volume), and
- $Q_t$, the flow rate of steam condensed on the dome ceiling (shown leaving the control volume)

For the quasi-steady conditions, the steam flow rate entering in the containment volume $Q_o$ is equal to the summation of the steam flow rates condensed on the dome ceiling $Q_t$ and vertical walls $Q_v$.

The distances presented in Figure 9.C.1-18 are:

- $H_t$, the distance between the jet inflow position into the upper-deck region and the dome springline elevation (in vertical direction),

- $H_{EF}$, the distance between the break location and the jet inflow position into the upper-deck region (in vertical direction), and

- $H_v$, the distance between the vertical wall and the jet center (in horizontal direction).

The definitions of the regions relate well to the separate effects of the enclosure tests.

Region I is below the operating deck level. In the AP600 and AP1000 configuration, connections exist between the below-deck compartments and the upper-deck region (dome). These connections allow the steam jet (plume) generated-entrainment into the break compartment to produce circulation through Region I. The volumetric flow from the lower to the upper deck regions is $Q_e$. Jet entrainment and the slots around the circumference of the deck floor enable this circulation (see Figure 9.C.1-19).

In the LST - LOCA experiments, the release point is also below the operating deck level. However, the compartment containing the release is not connected with the other below-deck compartments (see Figure 9.C.1-20). The simulated steam generator compartment is connected only with the upper portion (dome) of the containment. Therefore, the jet injection location for the LST LOCA experiments is effectively at the top of the simulated steam generator compartment, where the flow enters the above-deck region, and entrained volumetric flow $Q_e$ is equal to zero (see Figure 9.C.1-20). The atmosphere in the below-deck compartment is a stably stratified region without recirculation. The heat and mass transfer in the below deck compartments are governed primarily by molecular diffusion.

Region II is defined as the volume between the springline elevation and a horizontal line above the operating deck elevation, and between the wall boundary layers (Region IV) and the plume (Region III). Two entrainment mechanisms remove fluid from Region II. Entrainments into the vertical jet (or buoyant plume) and the wall boundary layers are compensated for by the inflows from the upper and lower horizontal boundaries. In order to preserve mass continuity and to obtain inflow into Region II, the vertical velocity components (see Figure 9.C.1-21) are negative and positive at the upper and lower horizontal boundaries, respectively. The fluid inside the Region II is recirculating (see Figure 9.C.1-22), yet has a quasi-steady $d\rho/dz$ maintained by balance between the buoyancy and the two entrainment mechanisms. Therefore, Region II can be called a recirculating stratified region. The horizontal density and concentration gradients are small, but significant recirculation flow exists due to the entrainment into the free and wall jets (see Peterson, 1997). Region II can be considered as a region where the vertical density, temperature and concentration gradients are dependent on the values of the volumetric Froude numbers (for free jets or plumes) and Grashof (Rayleigh) numbers (for wall boundary layers). This is similar to the case of an enclosure with opposite vertical walls at different temperatures (see section 9.C.1.1.2.1). The recirculation and entrainment from the Region II contributes to a decrease in the vertical temperature, density, and concentration gradients.

Region III contains free jets (plumes) which transport fluid in the vertical direction. The upward motion of a jet (or plume) produces entrainment from Region II. As a result, the jet (or plume) spreads, reduces velocity, and dilutes (decreases the temperature and concentration difference between the core of the jet and the surrounding atmosphere - Region II).

Region IV contains wall boundary layers which also provide transport in the vertical direction. The entrainment into the wall boundary layer transports steam into Region IV. The entrainment from Region II into the wall boundary layers enhances recirculation inside the Region II. This contributes to a decrease in the vertical temperature, density, and concentration gradients inside Region II.

Region V, the dome region, is between the containment ceiling and the elevation of the springline. Because the temperature of the containment ceiling is lower than the temperature of the atmosphere below the ceiling, downward flowing "ceiling plumes" are formed (see the Rayleigh-Benard convection example of section 9.C.1.2.1). The difference in the steam concentrations between the top of the Region V (immediately below the ceiling where condensation occurs) and the top of Region II are small due to the circulation (interaction) within Region V, caused by cold plumes falling from the ceiling and the hot plume reaching the ceiling of the dome. The downward plumes increase circulation and reduce gradients inside the dome, Region V. The downward "ceiling plumes" interact with the uprising plume (from the Region III). If the strength of the jet (plume) from the Region III is high, interactions occur inside Region V and the influence of the downward plumes does not spread towards the lower regions.

However, if the plume from Region III is not strong enough to produce good mixing inside Region V, the penetration of the downward "ceiling plumes" into the lower regions can disturb (from time to time) the recirculating stratified layers inside Region II. This tends to reduce the vertical gradients within Region II.

If the plume is very weak or does not exist, the vertical downward "ceiling plumes" affect the entire volume of the upper-deck region. The flow patterns formed are the result of superposition of Rayleigh-Benard convection (described for the enclosure with cold upper and hot lower surface) and recirculating stratification (described for the enclosure with opposite vertical walls at different temperatures).

The cold dome ceiling produces downward vertical plumes as in Rayleigh-Benard convection case, while cold vertical walls produce downward wall boundary layers. Due to continuity, the downward wall boundary layers tend to generate upward flow in the middle of the above-deck region. The wall boundary layer and the upward flow in the middle of the containment form a recirculation zone. Between the wall boundary layers and the upward flow in the middle of the containment, a recirculating stratified core is formed. This is similar to enclosures with opposite vertical walls at different temperatures. Note that although there is

evidence from enclosure tests that a stable non-zero vertical density gradient could exist in Region II, entrainment flows cause circulation of fluid. Region II is not considered as stagnant.

The prevailing flow pattern can be postulated (Rayleigh-Benard or recirculating stratified) from the ratio of Grashof numbers $Gr_t/Gr_v$ [defined for vertical $\Delta\rho$ and distance $H_t$ (for $Gr_t$) and horizontal $\Delta\rho$ and distance $H_v$ (for $Gr_v$)]. Note that turbulent Rayleigh-Benard convection starts at $Ra_t = Gr_t Pr > 10^4$ (for $Pr = 0.71$, based on 3D enclosure experiments - see section 9.C.1.2.1), while turbulent flow (with thin boundary layers and recirculating stratified but almost homogenized core) in enclosures with vertical walls at opposite temperatures starts at $Ra_v = Gr_v Pr > 10^8$ (for $Pr = 0.71$, based on 2D numerical simulations, see section 9.C.1.1.2.1). This indicates that for small values of Rayleigh numbers ($10^4 < Ra_v$ and $Ra_t < 10^8$), Rayleigh-Benard convection is dominant. Turbulent and chaotical flow are dominated by falling vertical plumes (see Figure 9.C.1-15).

For higher Rayleigh numbers ($Ra_v$ and $Ra_t > 10^8$) combined with a weak source plume, in fact smaller Rayleigh number in horizontal direction, falling vertical plumes (see Figure 9.C.1-15) dominate the flow patterns. For the dominant jet (or plume), or high Rayleigh number in horizontal direction ($Gr_v$ high) and moderate Froude number, a recirculating stratified flow pattern prevails in Region II (see Figure 9.C.1-5). Higher and similar magnitude values of both Rayleigh numbers (in vertical and horizontal direction) result in a flow pattern that is a superposition of the two described patterns (shown in Figures 9.C.1-15 and 9.C.1-5). Finally, for the case of the momentum-dominated jet (with high Froude number), the circulation flow pattern will be present in the entire volume of the containment (see Figure 9.C.1-11).

### 9.C.1.4.2 A Qualitative Model for Recirculating Stratified Region II

A qualitative model of Region II is used to address the issue of recirculating stratification and circulation (Peterson, 1997). The model is a coarse, first-principle representation of the effects of various volumetric flows and entrainment rates. It qualitatively examines the influence of various parameters on the difference in steam concentrations from the bottom to the top of the Region II ($\Delta X$).

Because of the complexity of the physics, two simplifying assumptions are used. It is assumed that Region II is not influenced by falling plumes from Region V and that the recirculation effects inside Region II can be neglected. Both assumptions cause overestimated vertical steam gradients $\Delta X$. Interactions between Region II and Region V that result from the penetration of the cold falling plumes (from Region V), improve mixing and decrease vertical steam gradients $\Delta X$. Recirculation inside Region II (established experimentally and numerically inside the core of enclosures) further decreases the vertical steam gradients.

Peterson, 1997, provides the following mass conservation equation for the thin horizontal layer inside Region II with area A(z) (see Figure 9.C.1-23):

$$\rho(z)A(z)dv(z) = -\rho_p(z)u_p(z)p_p(z)dz - \rho_w(z)u_w(z)p_w(z)dz$$

where v(z) is the vertical velocity, and $u_p(z)$ and $u_w(z)$ are the entrainment velocities into the steam plume and wall boundary layer, respectively. The vertical coordinate is z, while $p_p$ and $p_w$ are the perimeters of the plume (or jet) and wall boundary layer, respectively.

Since molar densities are dependent only on the temperature (assuming constant pressure in the entire volume), the differences between the molar densities $\rho(z)$, $\rho_p$ and $\rho_w$ are small. To simplify the analysis, the equation is written without densities. A balance of the volumetric flow rates is then used for the remainder of the analysis (instead of a mass balance).

To further simplify the analysis (considering only global effects), $u_p$, $u_w$, $p_p$, $p_w$, and A are assumed to be constant, or independent of z (Peterson, 1997). This assumption results in a linear, vertical velocity distribution. Although the actual entrainment varies with height, the integrated total should be reasonably close to the average constant values.

The calculations of the entrained volumetric flow into the plume $Q_p$ and wall boundary layer $Q_w$ are simplified as:

$$Q_p = \int_0^H u_p(z)p_p(z)dz = u_p\ p_p\ H$$

and

$$Q_w = \int_0^H u_w(z)p_w(z)dz = u_w\ p_w\ H$$

respectively. The total inflow to the top and bottom of Region II (see Figure 9.C.1-21) provides the boundary conditions for the vertical velocities v(0) and v(H) at the bottom and at the top of the Region II, respectively:

$$A\ v(0) = Q_w - Q_v - Q_e$$

$$A\ v(H) = -(Q_v + Q_p + Q_e)$$

where $Q_e$ is the volumetric rate of flow into the below-deck region (see Figures 9.C.1-18 and 9.C.1-19). Due to mass continuity (conservation) for the below-deck region, this flow rate is equal to the volumetric flow rate ($Q_e$) entrained into the steam generator compartment by the steam jet (plume).

The volumetric flow rate of steam condensed on the vertical wall is $Q_v$. $Q_t$ is the flow rate of steam condensed on the dome. The total steam volumetric inflow into the containment is $Q_o = Q_v + Q_t$ (see Figure 9.C.1-18 and 9.C.1-23).

The linear, vertical velocity distribution in Region II is:

$$A\,v(z) = (Q_w - Q_v - Q_e) - \frac{z}{H}(Q_p + Q_w)$$

Downflow exists in the top part of Region II, while in the lower portion, the velocities are positive (upwards flow). This agrees with the previous discussion of Region II inflow horizontal boundaries (see Figure 9.C.1-21). Because the continuity-driven velocities are assumed horizontally uniform upward at the bottom and downward at the top of Region II, there will be an elevation, z, where the two meet and vertical velocity is zero. The z coordinate where the vertical velocity is zero in this model is:

$$z = \frac{Q_w - Q_v - Q_e}{Q_p + Q_w} H$$

The average gas mole fraction in Region II is:

$$\overline{x_g} = \frac{1}{V}\int_0^H A(z)\, x_g(z)\, dz = \frac{1}{H}\int_0^H x_g(z)\, dz$$

The mole fraction of gas at the bottom of Region II is found from a mass balance on the wall boundary layer. (Note that $Q_v$ is the volumetric flow of steam that condenses on the vertical wall. It contains no noncondensible gas.)

$$x_g(0) = \frac{\int_0^H x_g(z)\, u_w(z)\, p_w(z)\, dz}{Q_w - Q_v} = \frac{u_w\, p_w \int_0^H x_g(z)\, dz}{Q_w - Q_v} = \frac{u_w\, p_w\, H\, \overline{x_g}}{Q_w - Q_v} = \frac{Q_w\, \overline{x_g}}{Q_w - Q_v}$$

Similarly the gas mole fraction at the top of the Region II is:

$$x_g(H) = \frac{x_g(0)\ Q_e + \int_0^H x_g(z)u_p(z)p_p(z)dz}{Q_v + Q_p + Q_e} = \frac{\frac{Q_w\ \overline{x_g}}{Q_w - Q_v}Q_e + u_p\ p_p \int_0^H x_g(z)\ dz}{Q_v + Q_p + Q_e} = \frac{\frac{Q_w\ \overline{x_g}}{Q_w - Q_v}Q_e + Q_p\ \overline{x_g}}{Q_v + Q_p + Q_e}$$

The relative difference in the concentrations from the bottom to the top of Region II is:

$$\frac{\Delta x}{\overline{x_g}} = \frac{x_g(0) - x_g(H)}{\overline{x_g}} = \frac{Q_w}{Q_w - Q_v} - \frac{\frac{Q_w Q_e}{Q_w - Q_v} + Q_p}{Q_v + Q_p + Q_e}$$

The final form of the equation, which is more suitable for qualitative understanding of the influence of various volumetric flow rates, is:

$$\frac{\Delta x}{\overline{x_g}} = \frac{x_g(0) - x_g(H)}{\overline{x_g}} = \frac{Q_v\ (Q_w + Q_p)}{(Q_w - Q_v)(Q_p + Q_v + Q_e)}$$

The influence of the various volumetric flow rates under various assumed conditions will now be examined.

### 9.C.1.4.2.1 Case 1: Strong Plume, Wall Boundary Layer and Plume Entrainments are Equal

If the entrainment volumetric flow rates are approximately equal ($Q_p \sim Q_w$) and are large compared to $Q_v$ and $Q_e$, the relative concentration difference is simplified to:

$$\frac{\Delta x}{\overline{x_g}} = \frac{x_g(0) - x_g(H)}{\overline{x_g}} \approx \frac{Q_v\ (2Q_w\ )}{(Q_w)(Q_w)} = \frac{2Q_v}{Q_w}$$

These assumptions are valid for the case of the jet-dominated flow. The large plume and wall boundary layer entrainment volumetric flow rates act to reduce the relative, vertical steam concentration gradient.

Even if the flow pattern cannot be defined as jet-dominated (i.e., the equation for the relative difference in the concentration from the bottom to the top of Region II cannot be simplified), the recirculating stratified Region II interacts with the plume and wall jets, Regions III, and IV (see Figure 9.C.1-23). The relative

concentration difference will still decrease if the entrainments in both the wall layer $Q_w$ and plume $Q_p$ are large.

It has been shown (Enclosure to Westinghouse Letter NSD-NRC-97-4978, February 7, 1997) that during the quasi-steady portion of a LOCA, jet entrainment rates ($Q_p$) in the AP600 are about a factor of 10 greater than the condensation rate ($Q_v$+$Q_t$).

#### 9.C.1.4.2.2 Case 2: Equal Entrainment into the Wall Boundary Layer $Q_w$ and the Rate of the Steam Condensed at the Vertical Walls $Q_v$

A small difference between the entrainment volumetric flow rate into the wall boundary layer $Q_w$ and volumetric flow rate of the steam condensed at the vertical walls $Q_v$ produces an increase in the relative difference of the concentrations. If all the steam entrained into the wall boundary layer is condensed at the vertical walls, nothing is left to be redistributed through the lower horizontal boundary of Region II and contribute towards a decrease in the vertical concentration gradients.

#### 9.C.1.4.2.3 Case 3: High Dome Condensation Rate $Q_t$

The volumetric flow of the steam condensed on the dome of the containment $Q_t$ does not directly affect the relative concentration difference in Region II (it is not present in the equation). However, indirect effects are possible. If the condensation on the dome is high, the ratio of $Q_t/Q_v$ is high, and the volumetric flow of steam condensing on the vertical walls $Q_v$ decreases. In contrast, a small ratio of $Q_t/Q_v$ represents an increased volumetric flow rate condensing on the vertical walls, $Q_v$. A decrease in the rate of steam condensing on the vertical walls $Q_v$ (in fact the increase of steam volumetric flow rate condensing on the dome, $Q_t$), decreases the relative concentration difference.

#### 9.C.1.4.2.4 Case 4: Influence of the Below Deck Entrainment $Q_e$

Region I also interacts with the stratified Region II. The effects of this interaction on the relative concentration difference change are captured by the $Q_e$ term. A large below-deck entrainment, $Q_e$, reduces the concentration difference. In the AP600 and AP1000, below-deck entrainment contributes to a decrease in the relative concentration difference. This effect is not present in the LST case, where $Q_e = 0$.

#### 9.C.1.4.2.5 Case 5: Dominant Entrainment into the Wall Boundary Layer $Q_w$

If $Q_v = 0.5\ Q_o$, as observed in phase 3 of the LST experiments where $Q_v$ is between $0.4Q_o$ and $0.6Q_o$ (see WCAP-14135), and if $Q_w = 2Q_p$, i.e., the wall boundary layer entrainment is twice as strong as plume entrainment (weak plume scenario), if the entrainment in the below-deck region is negligible, $Q_e$=0, and if we assume $Q_p = 10Q_o$ the relative steam concentration is:

$$\frac{\Delta x}{\overline{x_g}} = \frac{x_g(0) - x_g(H)}{\overline{x_g}} = \frac{0.5Q_o\ (2Q_p + Q_p)}{(2Q_p - 0.5Q_o)(Q_p + 0.5Q_o + 0)} = 0.073$$

A further increase in the entrainment into the wall boundary layers causes an additional decrease in the relative difference between steam concentrations in the bottom and the top of Region II (e.g., if $Q_w$=3$Q_p$, the relative concentration is 0.064). The increase in the entrainment into the wall boundary layers contributes to the homogenization of the containment atmosphere.

### 9.C.1.4.2.6 Conclusion

The expected circulation within the AP600 and AP1000 containment is segregated into five regions that relate to separate effects tests (SETs) in enclosures. Given the presence of the externally cooled shell, which is assumed in a DBA analysis, there are no regions of stagnant stratification in containment.

The proposed conceptual model can be used to structure the containment into regions for comparison to relevant enclosures SETs. The mathematical representation provides insight into the influence of various volumetric flows on the axial steam concentration gradients in the AP600 and AP1000.

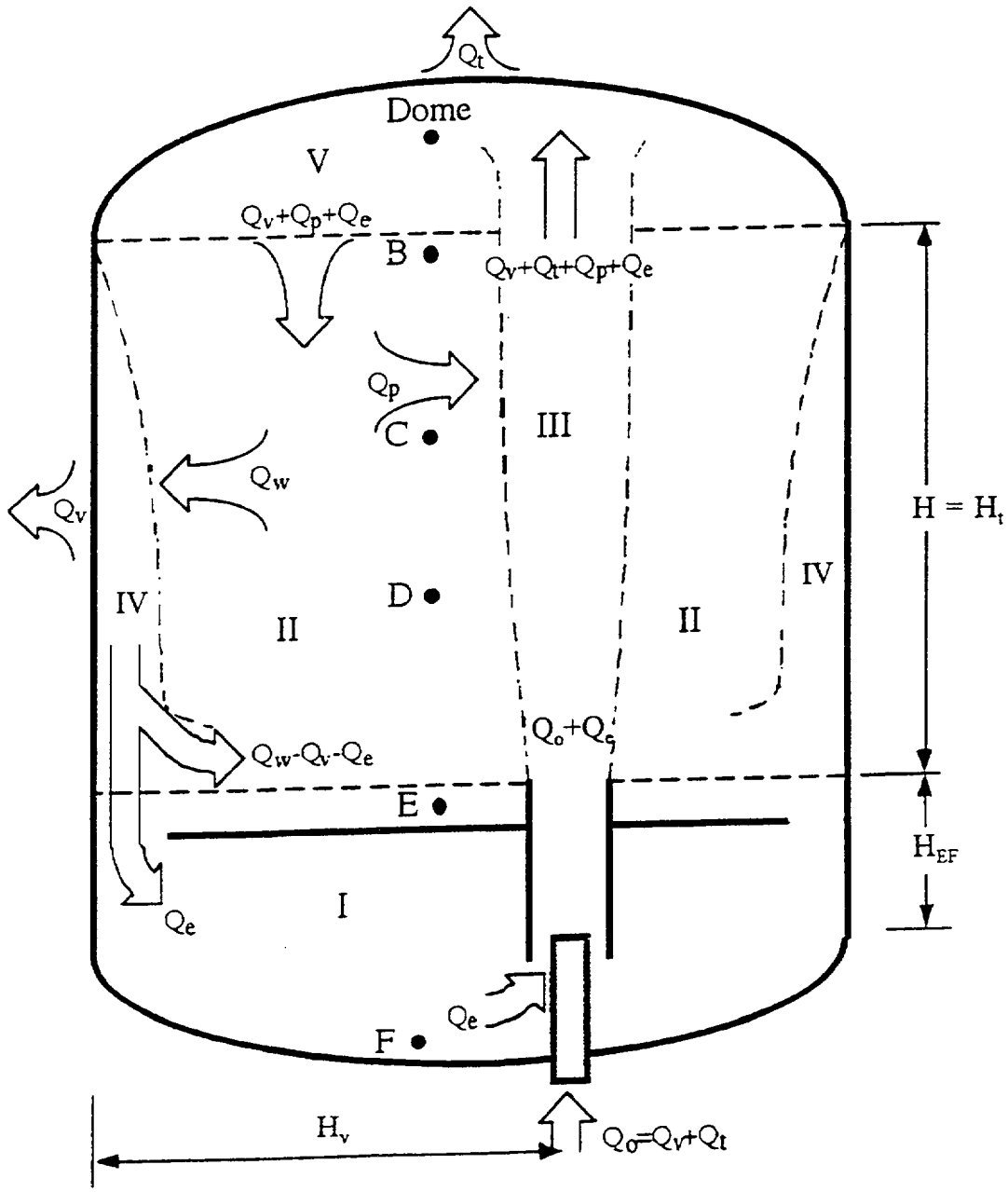


VOLUMETRIC FLOW RATES

$Q_o$ steam volumetric flow rate from the brake
$Q_e$ flow rate entrained by the jet inside the below deck region
$Q_p$ flow rate entrained into the plume in the above deck region
$Q_w$ flow rate entrained into the vertical wall boundary layers
$Q_v$ steam flow rate condensed on the vertical walls
$Q_t$ steam flow rate condensed on the dome ceiling

REGIONS

I below deck region
II region of recirculating stratification
III region of jets or plumes
IV region of wall boundary layers
V region below dome ceiling

**Figure 9.C.1-18** **Primary flow regions and volumetric flow rates for quasi-steady containment conditions**

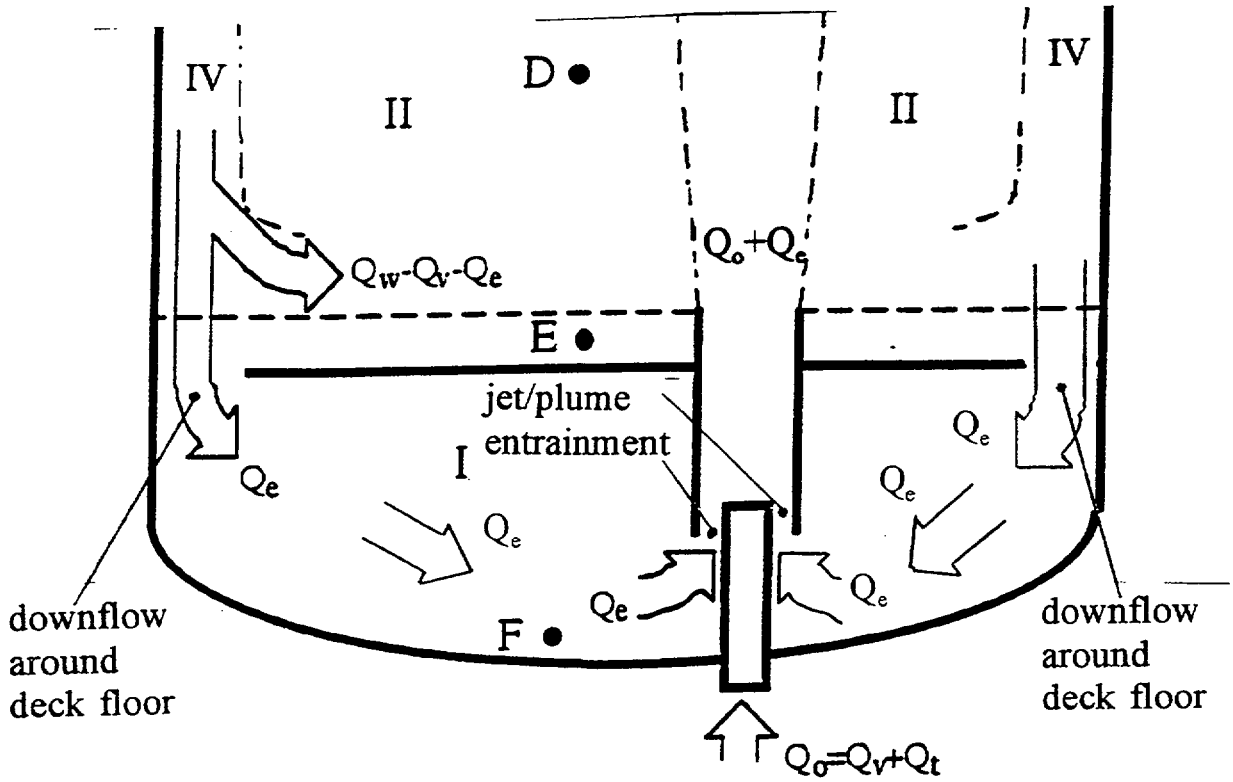


**Figure 9.C.1-19 The volumetric flow between the upper and lower deck regions $Q_e$**

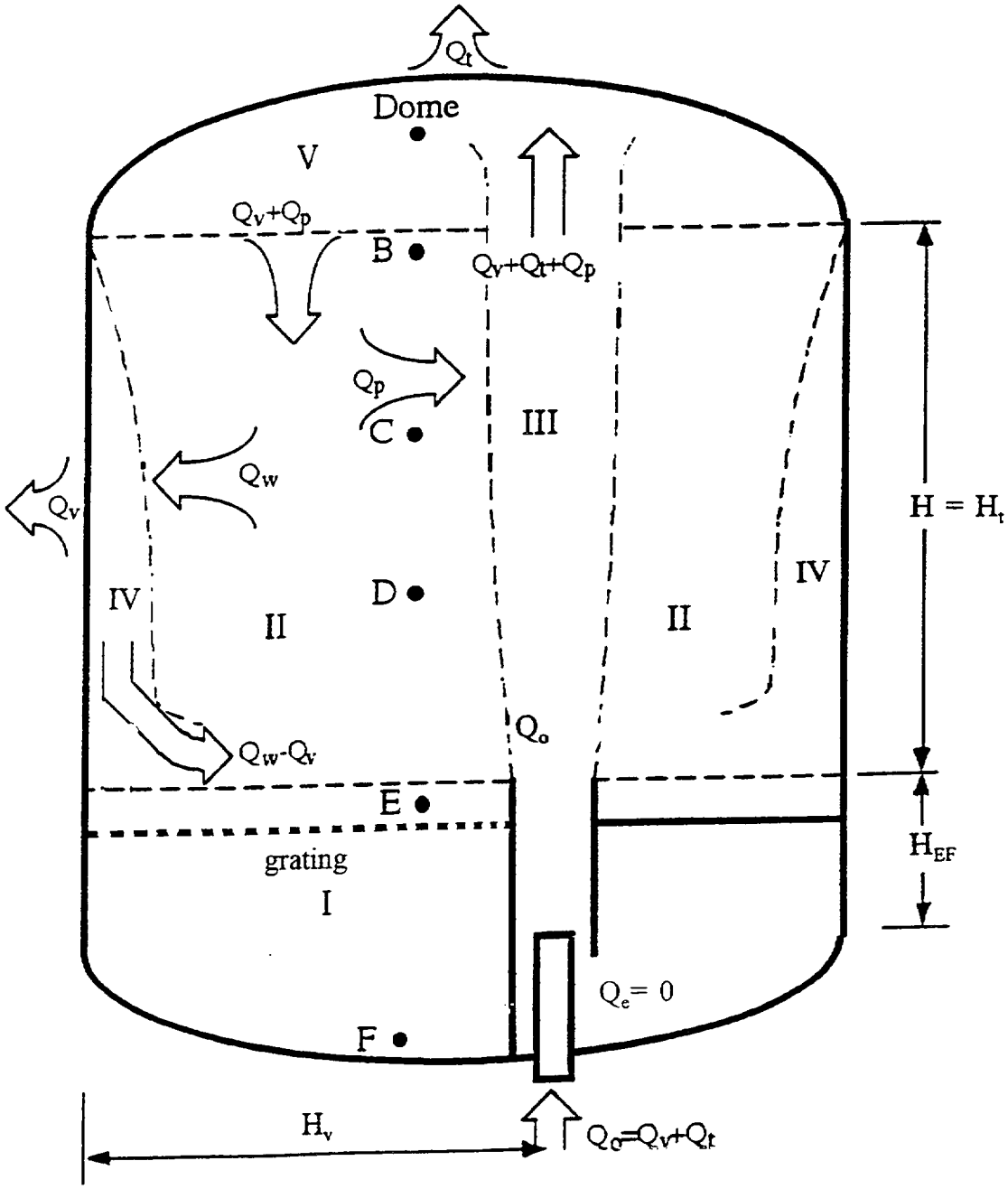


VOLUMETRIC FLOW RATES

$Q_o$ steam volumetric flow rate from the brake
$Q_e = 0$ flow rate entrained by the jet inside the below deck region
$Q_p$ flow rate entrained into the plume in the above deck region
$Q_w$ flow rate entrained into the vertical wall boundary layers
$Q_v$ steam flow rate condensed on the vertical walls
$Q_t$ steam flow rate condensed on the dome ceiling

REGIONS

I below deck region
II region of recirculating stratification
III region of jets or plumes
IV region of wall boundary layers
V region below dome ceiling

**Figure 9.C.1-20 Primary flow regions and volumetric flow rates for quasi-steady containment conditions in LST case**

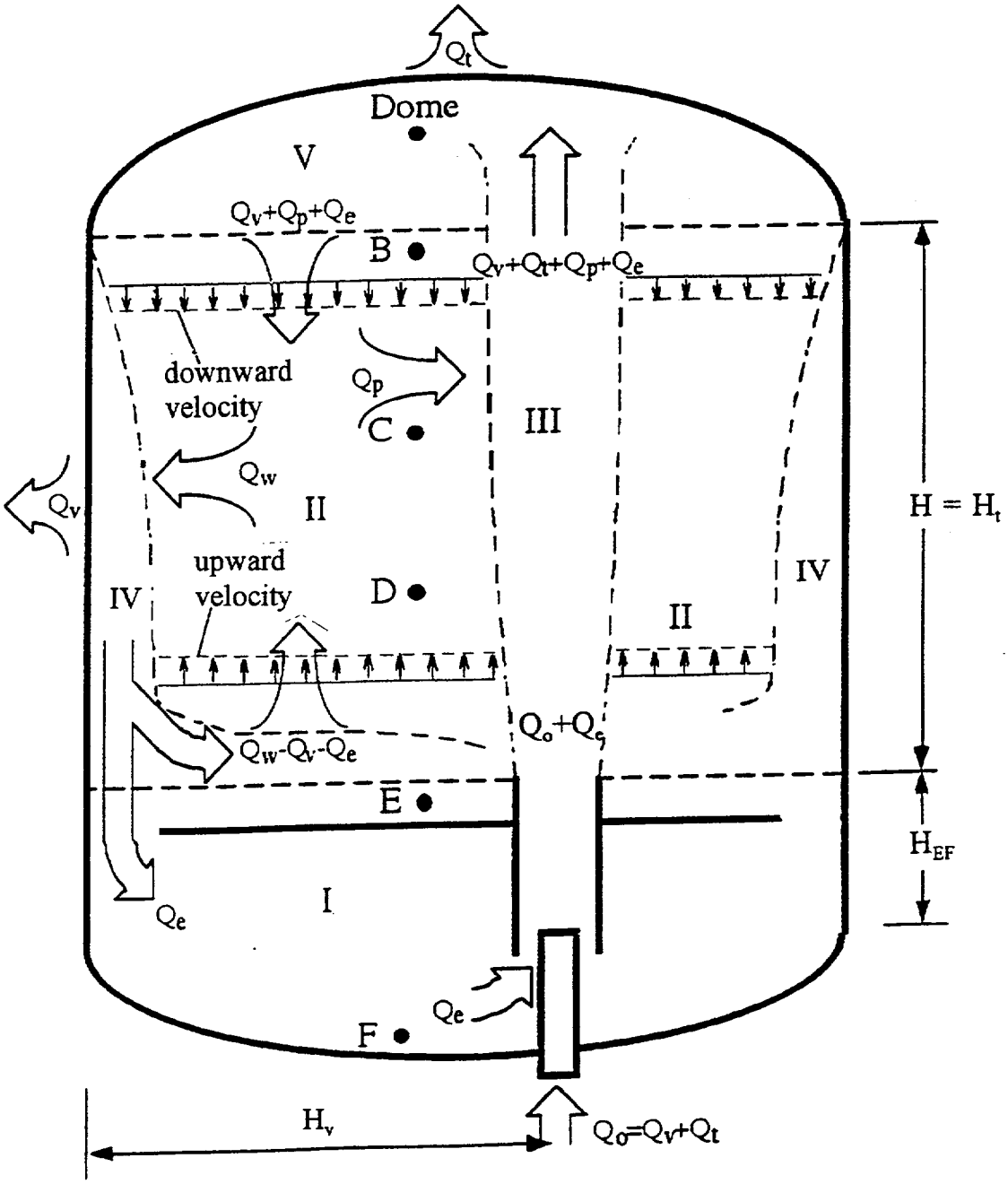


VOLUMETRIC FLOW RATES

$Q_o$ steam volumetric flow rate from the brake
$Q_e$ flow rate entrained by the jet inside the below deck region
$Q_p$ flow rate entrained into the plume in the above deck region
$Q_w$ flow rate entrained into the vertical wall boundary layers
$Q_v$ steam flow rate condensed on the vertical walls
$Q_t$ steam flow rate condensed on the dome ceiling

REGIONS

I below deck region
II region of recirculating stratification
III region of jets or plumes
IV region of wall boundary layers
V region below dome ceiling

**Figure 9.C.1-21 Inflows and outflows from the Region II**

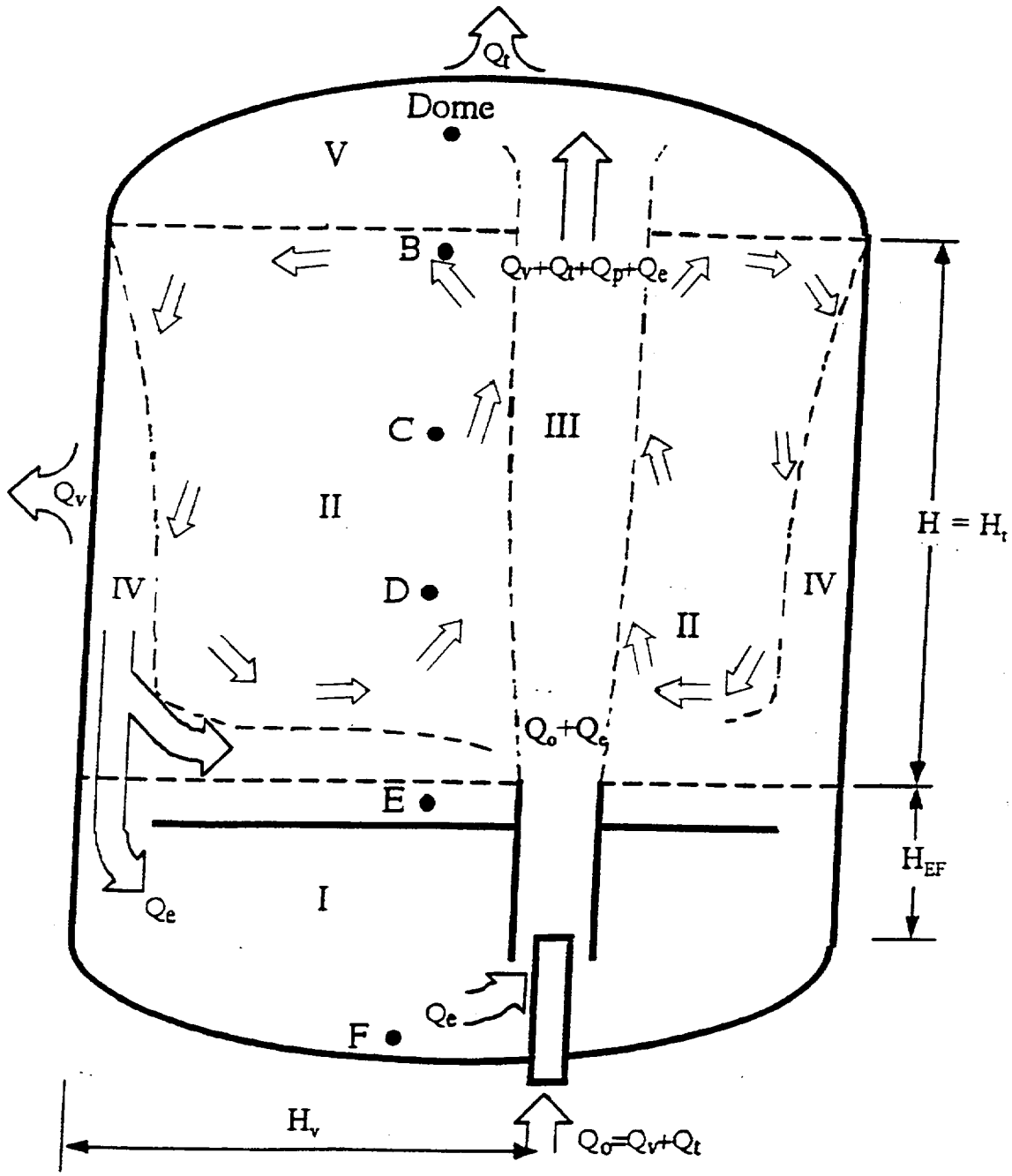


VOLUMETRIC FLOW RATES

$Q_o$ steam volumetric flow rate from the brake
$Q_e$ flow rate entrained by the jet inside the below deck region
$Q_p$ flow rate entrained into the plume in the above deck region
$Q_w$ flow rate entrained into the vertical wall boundary layers
$Q_v$ steam flow rate condensed on the vertical walls
$Q_t$ steam flow rate condensed on the dome ceiling

REGIONS

I below deck region
II region of recirculating stratification
III region of jets or plumes
IV region of wall boundary layers
V region below dome ceiling

**Figure 9.C.1-22 Recirculating flow paths inside the Region II**

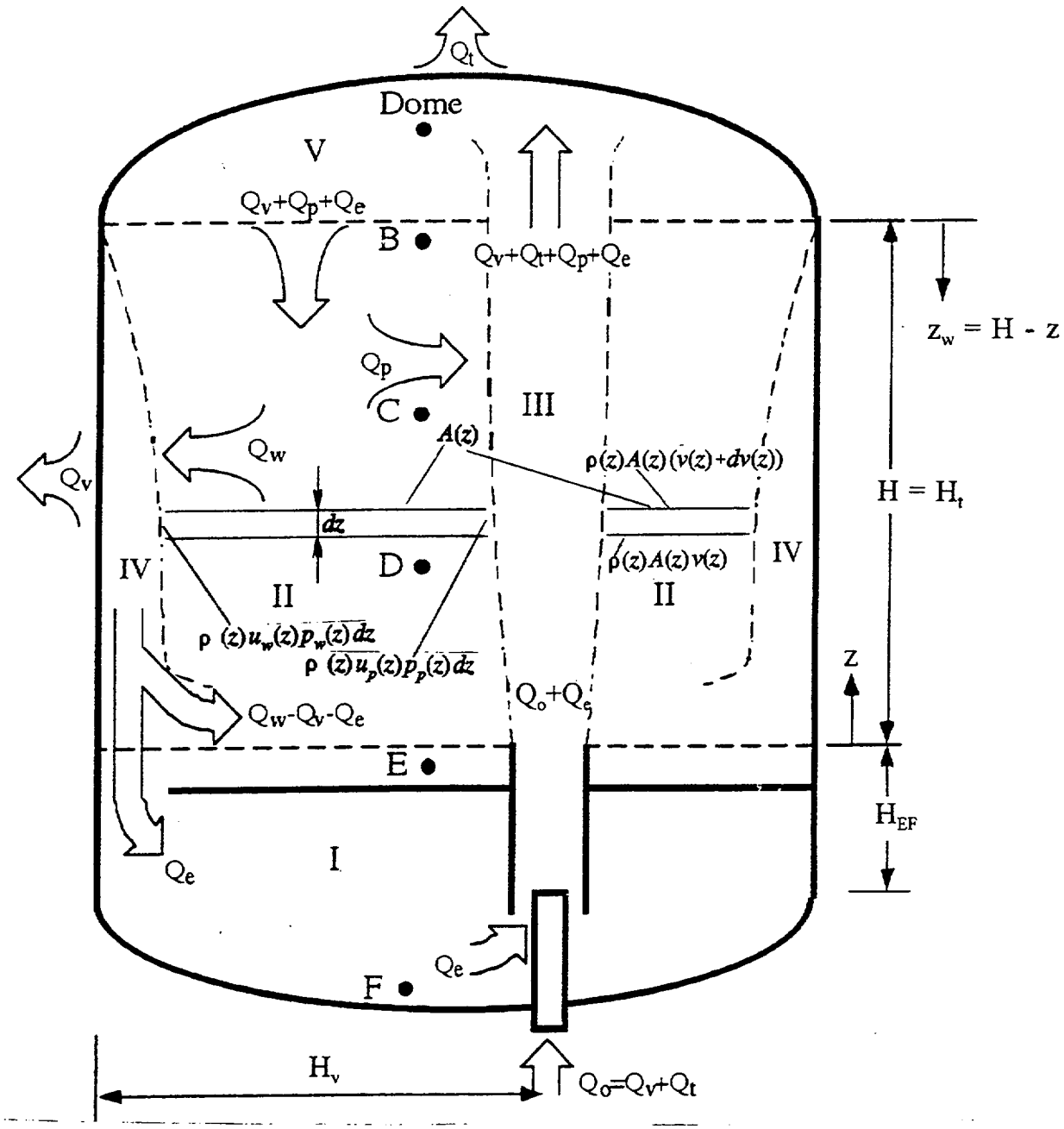


VOLUMETRIC FLOW RATES

$Q_o$ steam volumetric flow rate from the brake
$Q_e$ flow rate entrained by the jet inside the below deck region
$Q_p$ flow rate entrained into the plume in the above deck region
$Q_w$ flow rate entrained into the vertical wall boundary layers
$Q_v$ steam flow rate condensed on the vertical walls
$Q_t$ steam flow rate condensed on the dome ceiling

REGIONS

I below deck region
II region of recirculating stratification
III region of jets or plumes
IV region of wall boundary layers
V region below dome ceiling

**Figure 9.C.1-23 Mass conservation for thin horizontal layer inside the Region II**

### 9.C.1.4.3 References

1. P.F. Peterson, 1997
LST Mixing Model Writeup - letter to J. Woodcock, 02/24/97

2. Enclosure to Westinghouse Letter NSD-NRC-97-4978
Subject: Position paper in support of the assumption of complete mixing of aerosols in the AP600 containment atmosphere following a loss of coolant accident
February 7, 1997

3. WCAP-14135, F. E. Peters, April 1997
"Final Data Report for PCS Large-Scale Tests, Phase 2 and Phase 3", Revision 1
Westinghouse Energy Systems

## 9.C.2 OVERVIEW OF THE INTERNATIONAL CONTAINMENT EXPERIMENTAL DATA BASE

Tests from the available international containment experimental database that are relevant to the passive containment design, are presented in this chapter. Some tests are very close to possible passive containment cases. Others are presented to emphasize the difference between the passive containment design and the test conditions that lead towards stratification.

Four experimental facilities are considered to supplement LST data. Table 9.C-1 specifies characteristics of each experimental facility and provides a comparison with the LST, the AP600 and the AP1000. A comparison of the sizes of various test facilities is provided in Figure 9.C.2-1. Scaled cross-sections of each facility are shown.

A list of the facilities and the overviewed experiments is provided in Table 9.C.2-2, as well as the main characteristics of each experiment.

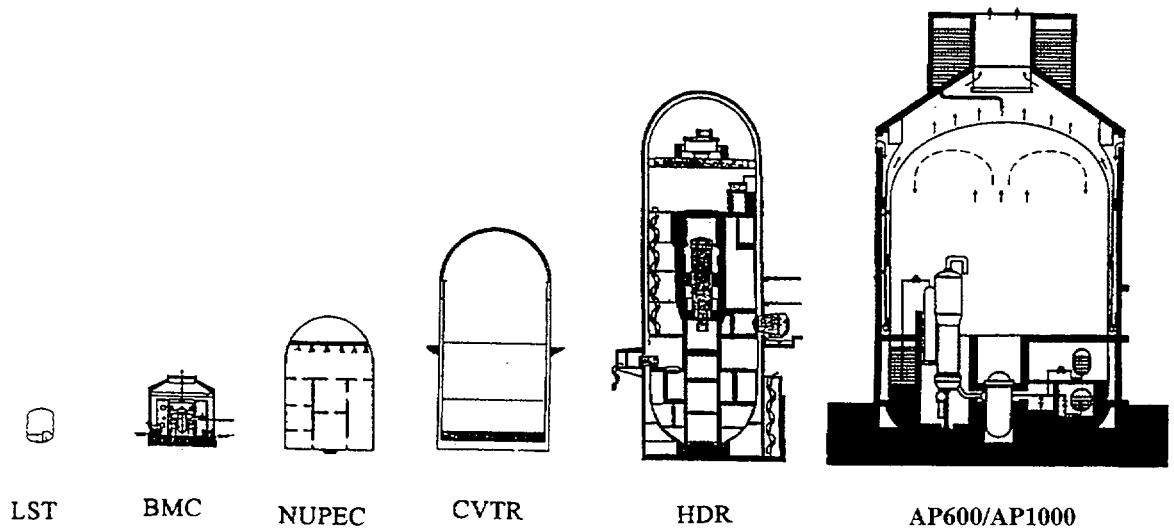


**Figure 9.C.2-1 Comparison of different facilities**

**Table 9.C-1 Comparison of Various Facilities**

| Facility | LST | BMC | NUPEC | CVTR | HDR | AP600 | AP1000 |
|---|---|---|---|---|---|---|---|
| Volume $m^3$ | 83.1 | 640 | 1300 (used) | 6428 | 11300 | 48710 | 58333 |
| Height m | 6.1 | 9 | 17.4 | 34.7 | 60 | 57.9 | 65.6 |
| Diameter m | 4.57 | 11.25 | 10.8 | 17.7 | 20 | 39.6 | 39.6 |
| Number of compartments | 3 | 9 | 25 | 3 | 62-72 | 11 | 11 |
| Volume of the dome | 79% | | 70% | 41% | 44% | 81% | 83% |
| Containment walls | steel | concrete | steel | concrete | steel shell concrete and steel | steel shell concrete and steel | steel shell concrete and steel |

**Table 9.C-2 Overviewed Tests from International Database**

| Facility | Experiment | Main Feature | Position of the Release Point and Other Relevant Data | Stratification or Circulation |
|---|---|---|---|---|
| BMC | F2 set First Phase | stepwise steam addition | release point is high Hr/Ht=0.444 | circulation through the majority of compartments, external annulus stratified |
| BMC | F2 set Phase 2 | inducing the natural circulation with steam injection | steam release point is low Hr/Ht = 0.111 | circulation through the majority of compartments, external annulus stratified |
| BMC | F2 set Phase 3 | heater on in R6 to reverse circulation | heat source location is low Hr/Ht = 0.111 | circulation through the majority of compartments, external annulus stratified |
| BMC | F2 set Phase 4 | steam injection in R6 compartment | steam release point is low Hr/Ht = 0.111 | circulation through the majority of compartments, external annulus stratified |
| BMC | Test 2 Two compartments (Phase I) | hydrogen injection, uniform initial temperature, orifice present, low feed rate | low position of hydrogen source Hr/Ht = 0.06 | hydrogen uniformly distributed, circulation present |
| BMC | Test 4 Two compartments (Phase I) | hydrogen injection, uniform initial temperature, no orifice | high position of hydrogen source Hr/Ht = 0.57 | concentration stratification occurs |
| BMC | Test 6 Two compartments (Phase I) | hydrogen injection, stratified initial temperature, orifice present | low position of hydrogen source Hr/Ht = 0.06 | stratification present, highest hydrogen concentration in the lower compartments |

**Table 9.C-2 (cont.) Overviewed Tests from International Database**

| Facility | Experiment | Main Feature | Position of the Release Point and Other Relevant Data | Stratification or Circulation |
|---|---|---|---|---|
| BMC | Test 12<br>Six compartments<br>(Phase II) | hydrogen injection in R2 room (high), uniform initial temperatures | high release point<br>$H_r/H_t = 0.69$ | hydrogen uniformly distributed, circulation present |
| BMC | Test 20<br>Six compartments<br>(Phase II) | hydrogen injection in R6 room (low), stratified initial temperature | low position of hydrogen source<br>$H_r/H_t = 0.06$ | stratification present, highest hydrogen concentration in the lower compartments |
| BMC | RX4 | sump heat up and three hydrogen injections | low position of the heat and hydrogen source<br>$H_r/H_t = 0.0$ | circulation present, homogenization of temperature and concentrations |
| NUPEC | M-4-3 | simulated break inside the low steam generator compartment, steam and hydrogen release, containment shell insulated | low position of the heat and hydrogen source<br>$H_r/H_t = 0.0$ | circulation present during release, temperature stratifies and concentration homogenizes after the end of release |
| CVTR | First test without the internal water sprays | steam release in the upper compartment, concrete shell | high position of the steam release<br>$H_r/H_t = 0.525$ | temperature field stratifies |
| CVTR | The second and third test with internal water sprays | steam release in the upper compartment, concrete shell | high position of the steam release<br>$H_r/H_t = 0.525$ | temperature field stratifies<br>but not as strong as in the previous case |
| HDR | E11.2 | high positioned release point (small break) and active external spray | high position of the steam release<br>$H_r/H_t = 0.555$ | stratification exists, external sprays promoted circulation |
| HDR | E11.3 | low positioned small break closed spiral stairway entrance | | global circulation pattern formed |

**Table 9.C-2 Overviewed Tests from International Database (cont.)**

| Facility | Experiment | Main Feature | Position of the Release Point and Other Relevant Data | Stratification or Circulation |
|---|---|---|---|---|
| HDR | E11.4 | low positioned release point (small break) and active external spray | low position of the steam release $H_r/H_t = 0.18$ | global circulation formed almost uniform temperature distribution except below release point |
| HDR | T31.5 | simulates DBA large LOCA in the upper section of the containment | high position of the steam release $H_r/H_t = 0.526$ | temperatures and gas concentrations first stratify and latter homogenize |
| HDR | V21.1 | simulates DBA large LOCA in the middle section of the containment (in both staircases) | middle position of the steam release $H_r/H_t = 0.38$ | Equal heating of both staircases first suppressed circulation. Slight global circulation was generated later. |
| HDR | E11.5 | simulates DBA large LOCA in the lowest section of the containment with effects of dry heat release and sump boiling | low position of the steam release $H_r/H_t = 0.18$ | global circulation due to the steam release, gas mixture injection and sump boiling contributed towards homogenization |

## 9.C.2.1 DESCRIPTION OF THE AVAILABLE BATTELLE MODEL CONTAINMENT (BMC) DATABASE

The objective of the Battelle Model Containment (BMC) tests is to obtain data to analyze design basis accidents (DBAs), hydrogen distribution, and aerosol depletion. The total volume of the containment is 640 $m^3$ and represents 1/64 of the BIBLIS B containment. Its interior is divided into nine compartments and its walls are made of reinforced concrete. The sizes and locations of openings between the compartments can be adjusted by opening (or closing) the openings with steel plates or mobile concrete structures.

Three sets of tests are presented.

- The first set, the F2 experiments, tests natural convection as a function of release location and type of release (steam, air, dry heat).
- The second set of tests studies the influence of the initial temperature distribution, the location of hydrogen injection, the injection rates, and the size of the vent openings on hydrogen distribution, stratification and global circulation.
- The third set of tests examines the effect of sump heatup on global natural circulation.

### 9.C.2.1.1 Natural Convection Phenomena Inside the Multi-Compartment Containment (F2 Experiments)

The F2 experiments, performed by Kanzleiter in 1988, study natural convection inside a multi-compartment containment as a function of release location (room) and type (steam, air, dry heat). The BMC configuration used for experiment F2 is shown in Figures 9.C.2-2 and 9.C.2-3. A 48-hour heatup period is the first phase of the experiment - see Figure 9.C.2-4, (Fischer et al., 1989, and Fischer et al., 1991). This is followed by a three-part, natural circulation phase (phases 2, 3, and 4) within the 48- to 75-hour time period see Figure 9.C.2-5, (Fischer et al., 1990 and Fischer et al., 1993).

An overview of the results and a comparison with analysis codes is presented by Wolf et al, 1996. Data for pressure, temperature, sump temperature, and liquid level, as well as partial steam pressure is presented for phases 1-4 (up to 75 hours).

#### 9.C.2.1.1.1 F2 - Experiment Heatup Phase - Phase 1

Phase 1 is from 0-48 hours. A steam release inside the R2 compartment provides the heatup (see Figures 9.C.2-6 and 9.C.2-4). The stepwise steam addition results in a stepwise increase of the containment pressure (see Figure 9.C.2-7 for GP 9117 location).

During the 48 hours of heatup, the atmosphere in the external annulus (the lower portion of R9 surrounding compartment) stratifies, Figure 9.C.2-8. Since there is no driving force for the circulation of steam into the lower air-rich regions of R9, the two experimental curves in Figure 9.C.2-8 (for temperatures GT9004 and GT9037) show that the heatup was delayed in lower positions in the external annulus behind the missile shield. The lower portion of R9 heats up over a longer period (Figure 9.C.2-8) because of global circulation induced by entrainment in the release. The entrainment is fed by flow from R9, R4 and R1.

Over a period of time, the atmosphere of the containment in the external annulus stratifies (after 16 hours it is already stratified). However, after 36 hours the stratification is not as pronounced, i.e., the temperature differences are not greater than 10 °C in the external annulus. The initial stratification in the external annulus results from the high position of the steam release, which is inside the R2 compartment, and the closed circulation paths in the lower portion of the external annulus (see Figure 9.C.2-9).

The experimental curves for temperature histories of the other subcompartments (except for R4 and R3) are not presented in Wolf et al., 1996. However, consecutive phases of other experiments performed in the BMC indicate that natural circulation effects are present and contribute towards homogenization of the temperature fields among the majority of compartments. The only exception is the external annulus.

**Application to the AP600 and AP1000**

There is evidence that a release high in the steam generator compartment can induce global circulation flow by entrainment through the CMT room openings. It is difficult to compare time scales due to significant differences between the BMC and the passive containment compartment arrangement.

### 9.C.2.1.1.2 Phases 2-4 of the F2 Experiment (Natural Circulation)

After the heatup, the experiment continues through three additional phases (see Figures 9.C.2-4 and 9.C.2-5 for phases 2, 3 and 4) that use the following methods to induce or amplify circulation:

- Steam injection to induce natural circulation,
- Activation of the heater to reverse circulation,
- Injection of steam to amplify reversed circulation.

Figure 9.C.2-5 illustrates four additional phases (5, 6, 7, and 8) that are not discussed. The circled numbers in Figure 9.C.2-5 represent the type of injection (see also Figure 9.C.2-4). The flow patterns formed during the particular injection are presented below the circled numbers. Figure 9.C.2-9 shows the two different locations for the steam injection, the location of the heater and the positions of the anemometers.

In addition to the measured velocities in the openings (see Table 9.C-3), the fluctuations in measured temperatures indicate natural circulation (see Figures 9.C.2-10 and 9.C.2-11). Due to natural circulation, complex flow patterns form and temperatures in the compartments are nearly homogeneous (i.e., temperature differences are not greater than 4°C, see Figures 9.C.2-10 and 9.C.2-11). The detailed temperatures and velocities during each subphase are given by Kanzleiter, 1988.

Figure 9.C.2-12 presents the thermodynamic states of the containment dome atmosphere at a high position (H = 7.6 m) during various time periods, while Figure 9.C.2-13 presents the conditions at a low position in the external annulus (H = 1.0 m). Except during air injection times, the steam partial pressure in the high position follows the shape of the total pressure curve (0.5 to 1.0 bar lower values than $p_{tot}$). At the low position, the steam partial pressure is almost constant (0.5 bar) after 60 hours. This indicates steam stratification inside the external annulus (lower portion of the R9 compartment) behind the missile shield.

The temperature distribution inside the external annulus is presented in Figure 9.C.2-14 for the second phase and in Figure 9.C.2-15 for the third and fourth phases. Both figures indicate stratification of the temperature fields. The temperature difference between the upper dome and the lowest position in the external annulus is 30°C at the end of the second phase and 18°C at the end of the fourth phase.

All other compartments have almost homogeneous temperatures (the greatest temperature differences are 4°C), which indicate the presence of the natural circulation (see Figures 9.C.2-10 and 9.C.2-11).

The values of the measured velocities in the vent between the R3 and R6 compartments during the individual phases are presented in Table 9.C-3. The histories of the velocities in the R7-R9 and R3-R6 vent paths are presented in Figures 9.C.2-16 and 9.C.2-17, respectively. The directions of the convective flow loops as a function of steam and air injections into the various compartments and the applications of the dry heater are presented in Figure 9.C.2-4 (arrow in R9 compartment represents positive flow loop direction). The upward (positive) velocities in Figure 9.C.2-16 produce a positive flow direction loop. The upward (positive) velocities in Figure 9.C.2-17 produce a negative flow direction loop.

The various injections and the application of the dry heat source generate natural circulation and homogenize temperatures in the majority of the containment compartments.

**Table 9.C-3 Representative Velocity in [m/s] in Opening from R3 to R6 in the Different Experimental Phases of Experiment F2, Phases 2-4**

| | Phase No. | | | | | | | | | | |
|---|---|---|---|---|---|---|---|---|---|---|---|
| | **2.1** | **2.2** | **2.3** | **2.4** | **3.1** | **3.2** | **3.3** | **4.1** | **4.2** | **4.3** | **4.4** |
| | 0.35 | -0.4 | 0.4 | -0.4 | +/-0.1 | +/-0.1 | +/-0.1 | -0.35 | 0./0.6 | 0.35 | -0.4 |

(reprinted from L. Wolf, M. Gavrilas, K. Mun, "Overview of experimental results for long-term, large-scale natural circulations in LWR-containments after large LOCAS," University of Maryland at College Park, Final Report for DOE - Project, Order Number: DE-AP07-96ID10765")

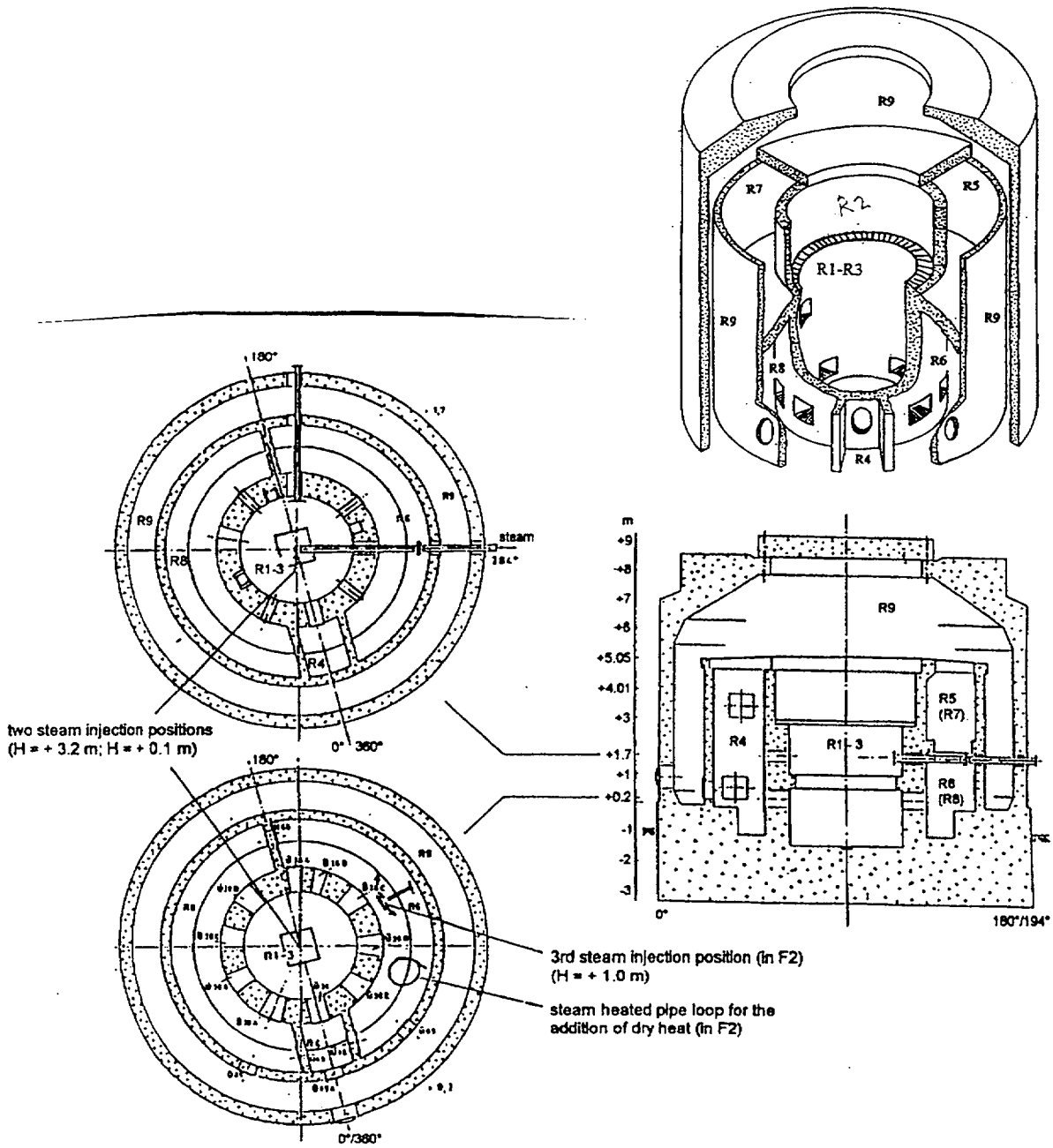


**Figure 9.C.2-2 Model Containment: vertical cross-section 0/180°, horizontal cross-sections at +0.2 m and +1.7 m for configuration in experiment F2**

**(reprinted from L.Wolf, M.Gavrilas, K. Mun, "Overview of experimental results for long-term, large-scale natural circulations in LWR-containments after large LOCAs", University of Maryland at College Park, Final Report for DOE - Project, Order Number: DE-AP07-96ID10765")**

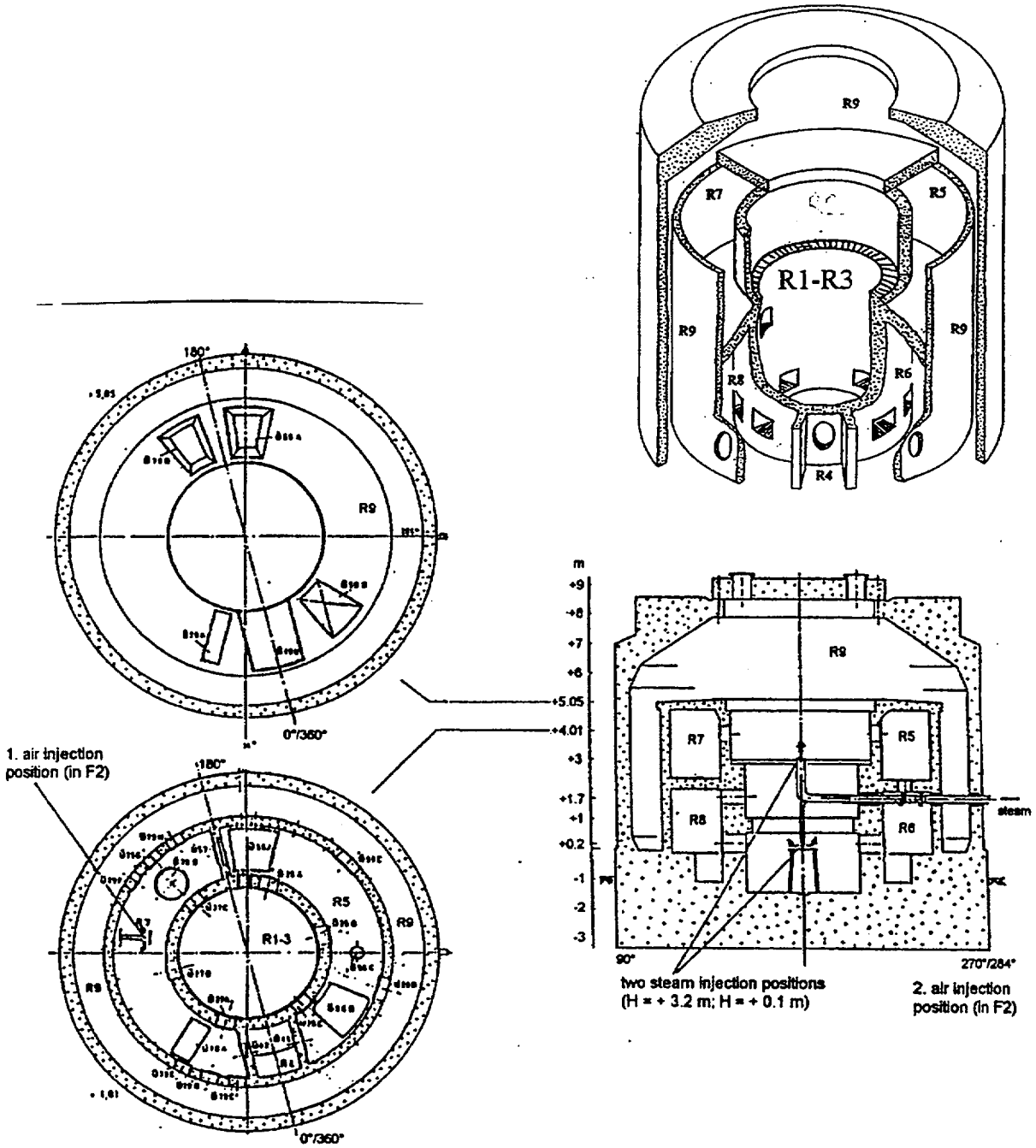


**Figure 9.C.2-3 Model Containment: vertical cross-section 0/180°, horizontal cross-sections at +4.01 m and +5.05 m for configuration in experiment F2**

**(reprinted from L.Wolf, M.Gavrilas, K. Mun, "Overview of experimental results for long-term, large-scale natural circulations in LWR-containments after large LOCAS", University of Maryland at College Park, Final Report for DOE - Project, Order Number: DE-AP07-96ID10765")**

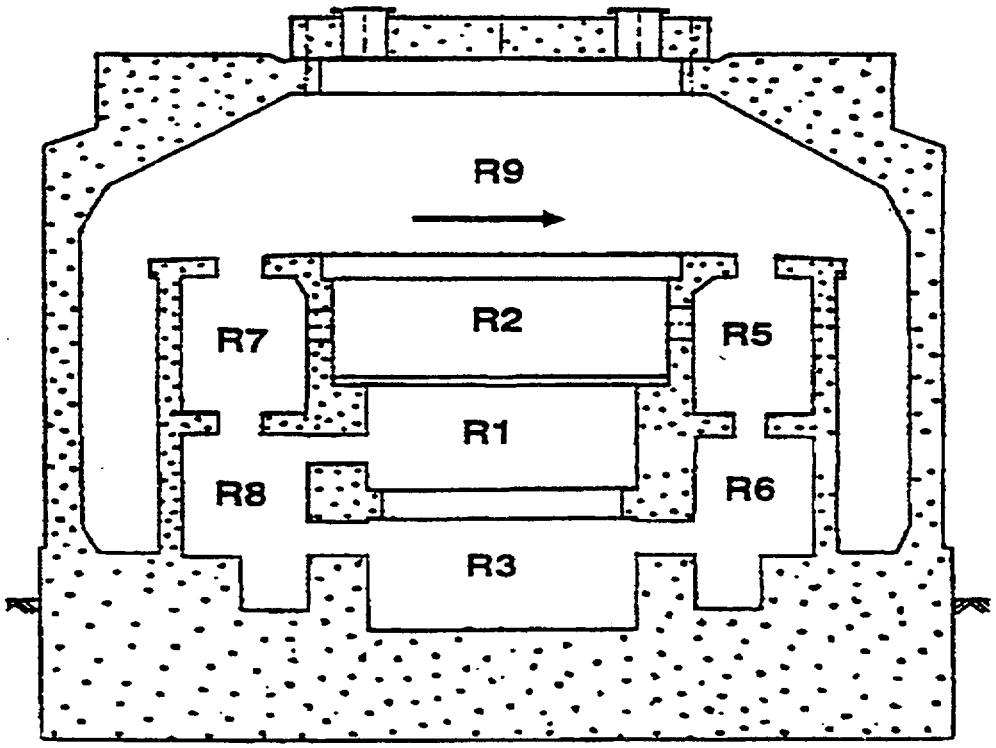


| Phase | Pressure | Steam | Air | Heat | Drainage | Flow | Injection |
|---|---|---|---|---|---|---|---|
| 1 | 1-3 bar | R2 | | | R9 | | |
| 2.1 | 3 bar | R3 | R7 | | R3 | - | 1 + |
| 2.2 | 3 bar | R3 | | R6 | R3 | + | 2 |
| 2.3 | 3 bar | R6 | | | | - | 3 |
| 2.4 | 3 bar | R3 | | | | + | 1 |
| 3.1 | 3 bar | | | | | | |
| 3.2 | to | | | R6 | | - | 2 |
| 3.3 | 1.8 bar | | | | | - | |
| 4.1 | 1.8 bar | R3 | | | | + | 2 |
| 4.2 | 1.8 bar | R3 | | R6 | | + - | 1 |
| 4.3 | 1.8 bar | R6 | | | | - | 2 |
| 4.4 | 1.8 bar | R3 | | | | + | 3 |
| | | | | | | | 4 |

**Figure 9.C.2-4 Injections and convective flow loop directions (+ sign for flow indicates the same direction of the flow as arrow in R9)**

**(reprinted from L.Wolf, M.Gavrilas, K. Mun, "Overview of experimental results for long-term, large-scale natural circulations in LWR-containments after large LOCAS", University of Maryland at College Park, Final Report for DOE - Project, Order Number: DE-AP07-96ID10765")**

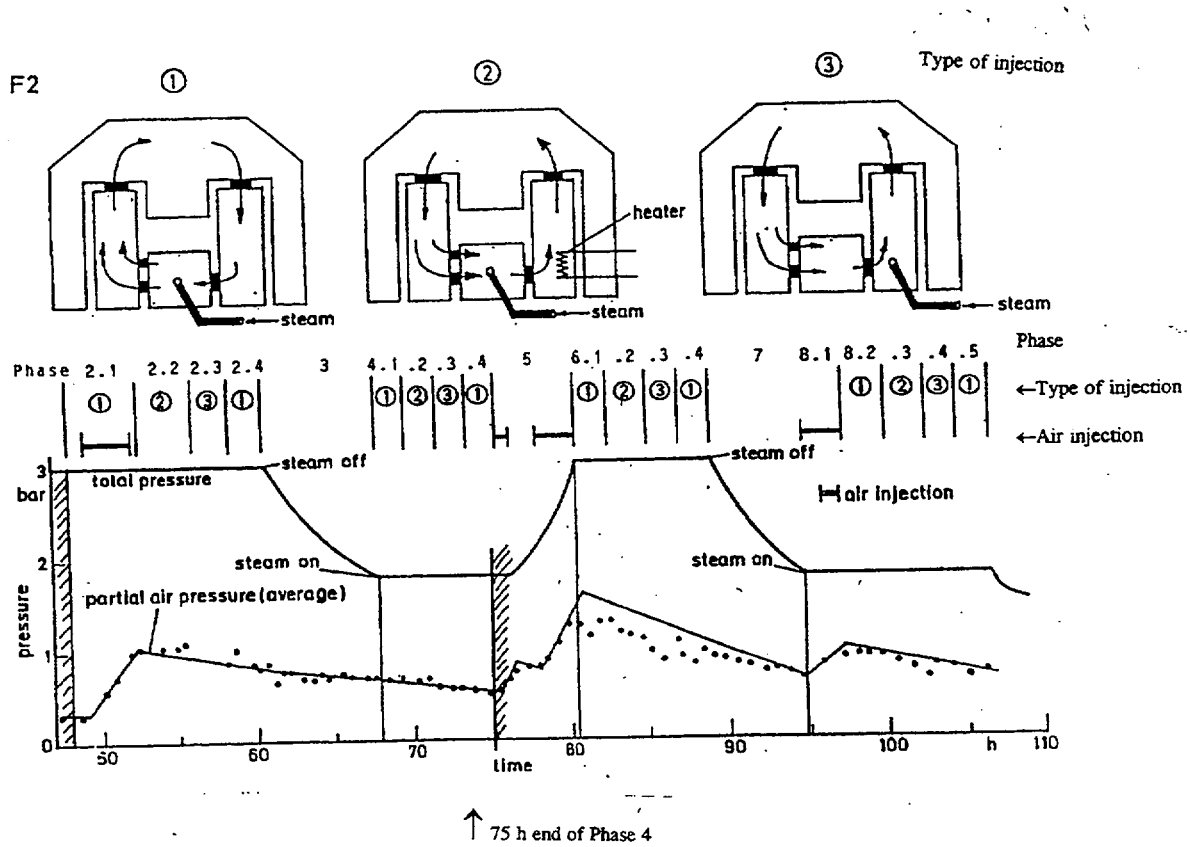


**Figure 9.C.2-5 Experiment F2, Phases 2-8, experimental procedures, total and partial pressures**

**(reprinted from L.Wolf, M.Gavrilas, K. Mun, "Overview of experimental results for long-term, large-scale natural circulations in LWR-containments after large LOCAS", University of Maryland at College Park, Final Report for DOE - Project, Order Number: DE-AP07-96ID10765")**

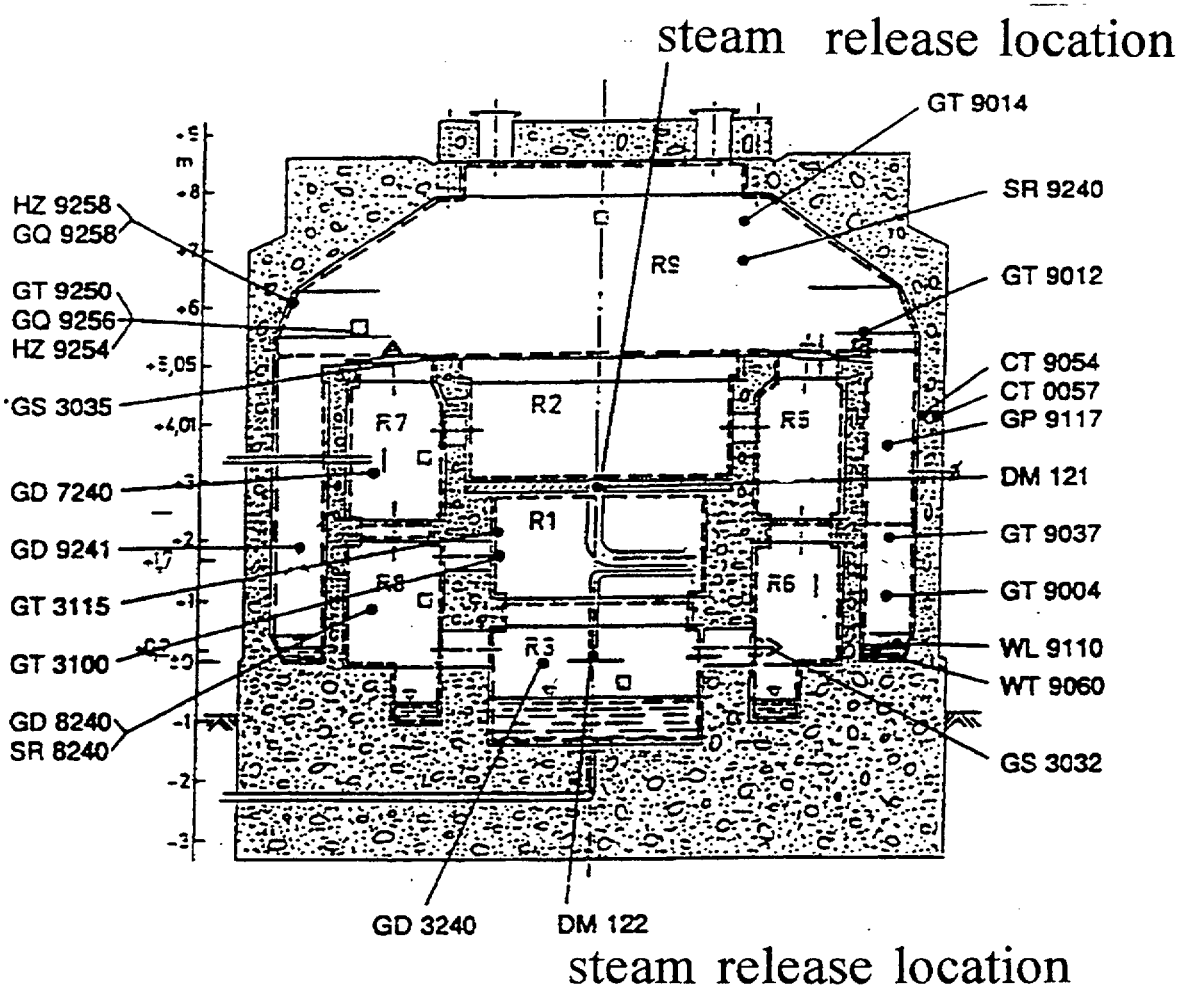


**Figure 9.C.2-6 Number of compartments, locations of measurement transducers and steam releases**

**(reprinted from L.Wolf, M.Gavrilas, K. Mun, "Overview of experimental results for long-term, large-scale natural circulations in LWR-containments after large LOCAS", University of Maryland at College Park, Final Report for DOE - Project, Order Number: DE-AP07-96ID10765")**

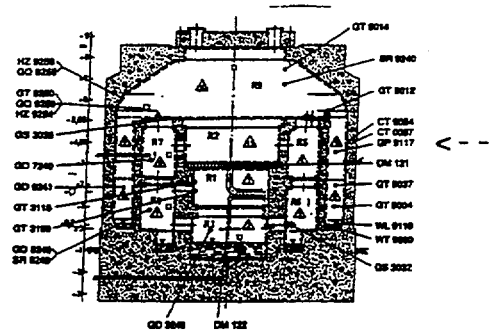

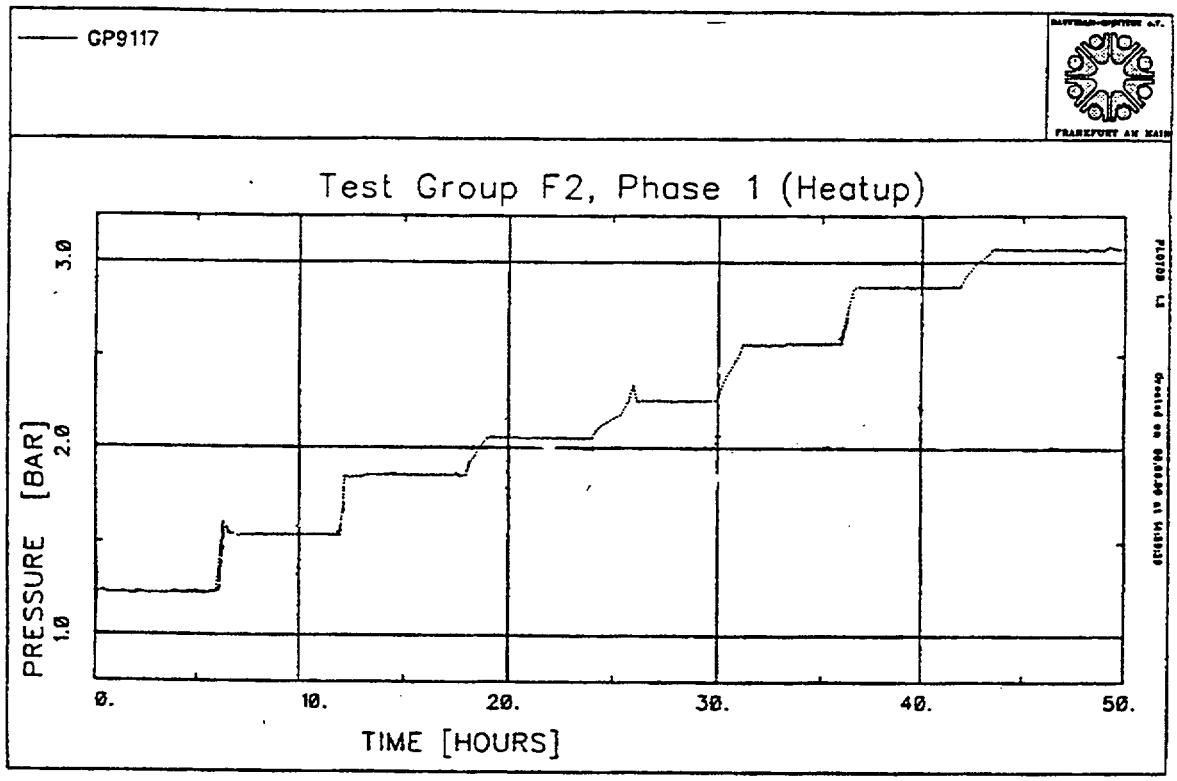


**Figure 9.C.2-7 Test group F2, Phase 1 (heatup), total pressure in the containment**

**(reprinted from L.Wolf, M.Gavrilas, K. Mun, "Overview of experimental results for long-term, large-scale natural circulations in LWR-containments after large LOCAS", University of Maryland at College Park, Final Report for DOE - Project, Order Number: DE-AP07-96ID10765")**

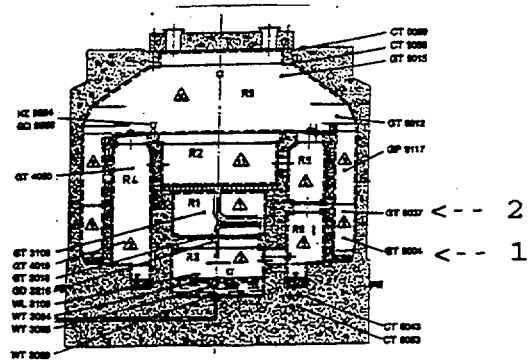


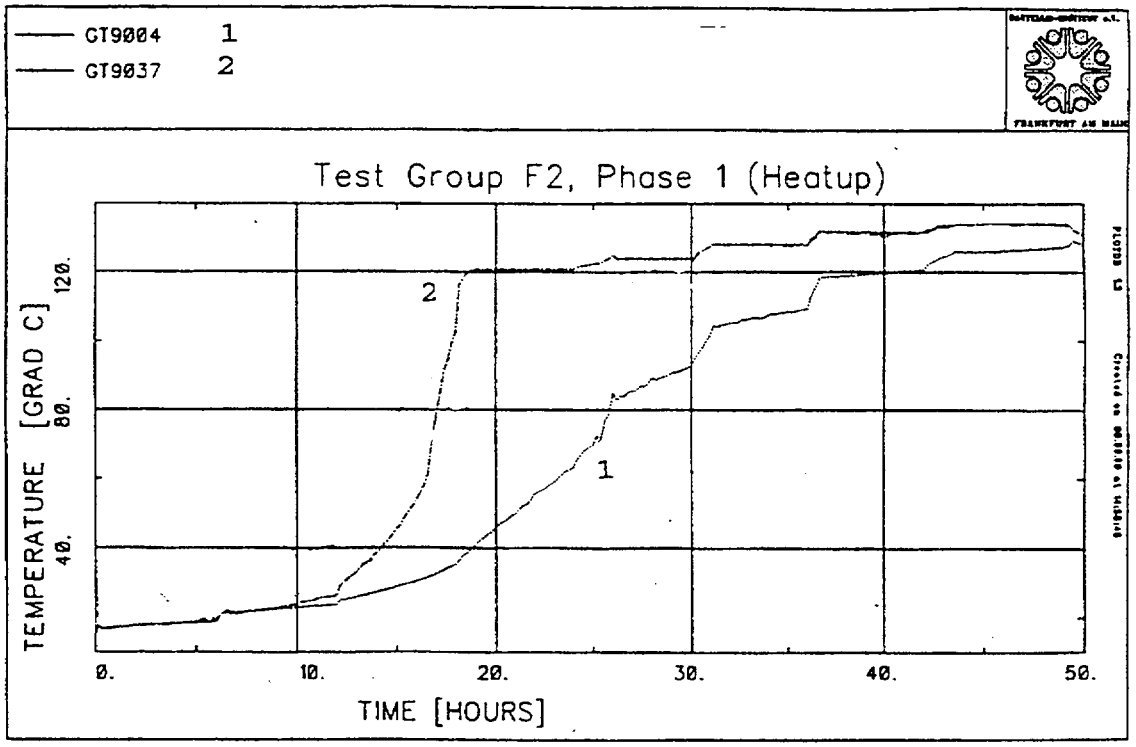


**Figure 9.C.2-8 Test group F2, Phase 1 (heatup), atmospheric temperature in the compartment R9, H=1.0 m and 2.1 m.**

**(reprinted from L.Wolf, M.Gavrilas, K. Mun, "Overview of experimental results for long-term, large-scale natural circulations in LWR-containments after large LOCAS", University of Maryland at College Park, Final Report for DOE - Project, Order Number: DE-AP07-96ID10765")**

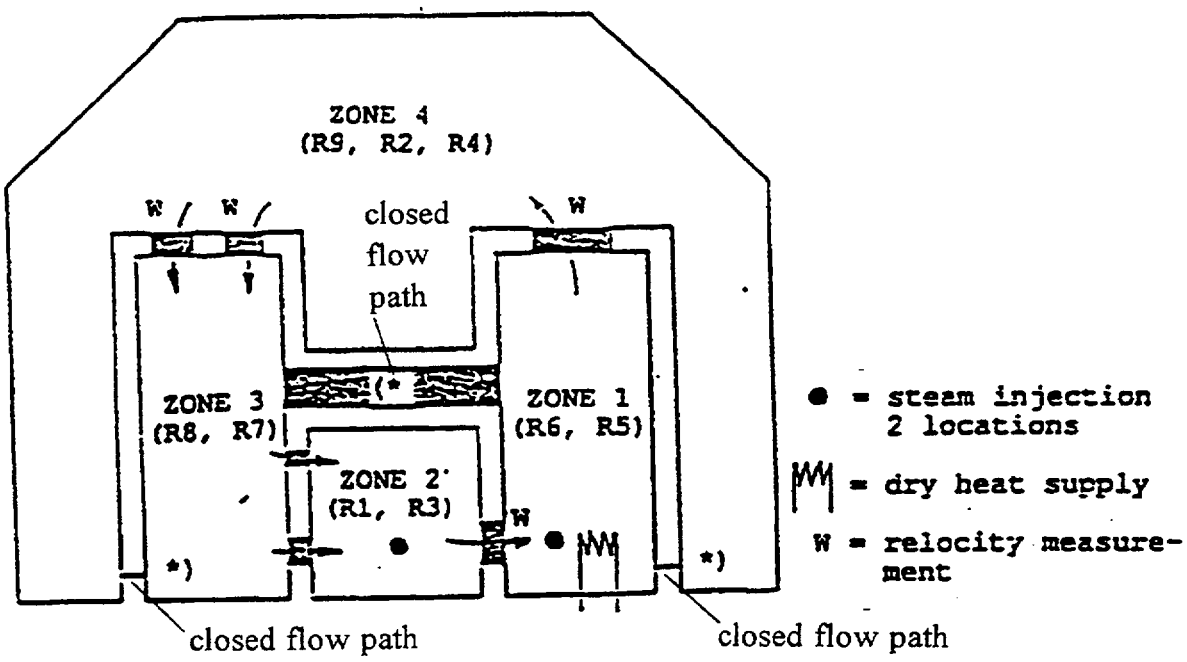


circulation for phases 3 and 4 are shown

**Figure 9.C.2-9 Scheme of multi-compartment containment geometry in experiment F2**

**(reprinted from L.Wolf, M.Gavrilas, K. Mun, "Overview of experimental results for long-term, large-scale natural circulations in LWR-containments after large LOCAS", University of Maryland at College Park, Final Report for DOE - Project, Order Number: DE-AP07-96ID10765")**

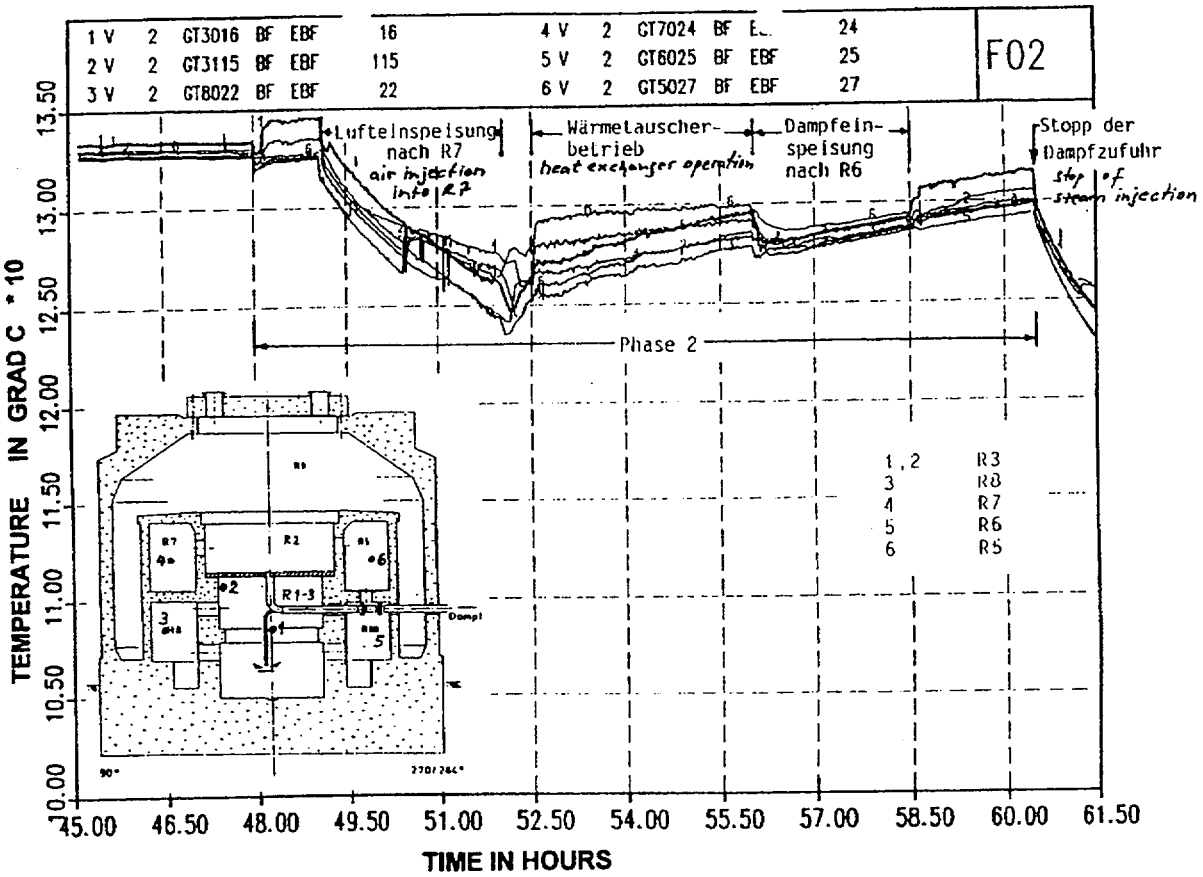


**Figure 9.C.2-10 Test group F2, phase 2: atmospheric temperatures in zones 1, 2 and 3 (R5 + R6, R1 + R4, R7 + R8)**

**(reprinted from L.Wolf, M.Gavrilas, K. Mun, "Overview of experimental results for long-term, large-scale natural circulations in LWR-containments after large LOCAS", University of Maryland at College Park, Final Report for DOE - Project, Order Number: DE-AP07-96ID10765")**

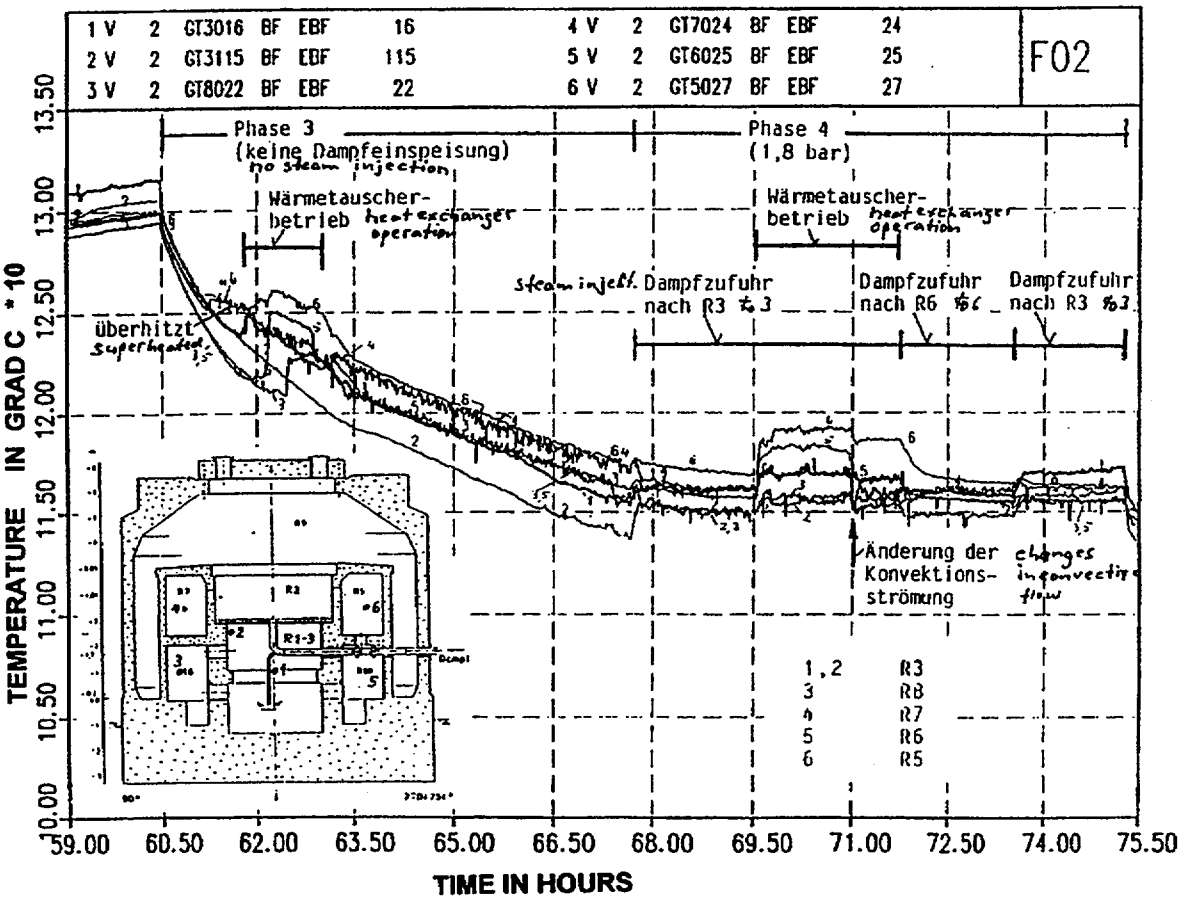


**Figure 9.C.2-11** **Test group F2, phase 3 and 4: atmospheric temperatures in zone 1, 2 and 3 (R5 + R6, R1 + R4, R7 + R8)**

**(reprinted from L.Wolf, M.Gavrilas, K. Mun, "Overview of experimental results for long-term, large-scale natural circulations in LWR-containments after large LOCAS", University of Maryland at College Park, Final Report for DOE - Project, Order Number: DE-AP07-96ID10765")**

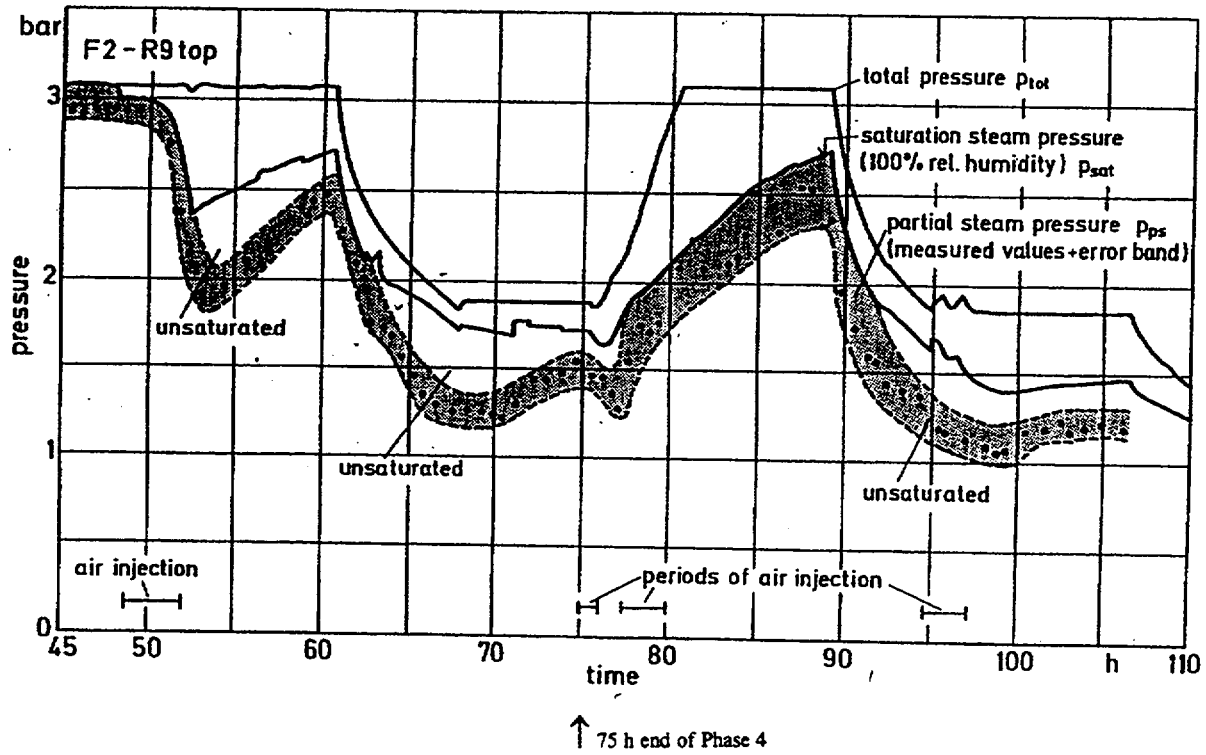


**Figure 9.C.2-12 Thermodynamic state of steam-air atmosphere in R9 top (H=7.6 m)**

**(reprinted from L.Wolf, M.Gavrilas, K. Mun, "Overview of experimental results for long-term, large-scale natural circulations in LWR-containments after large LOCAs", University of Maryland at College Park, Final Report for DOE - Project, Order Number: DE-AP07-96ID10765")**

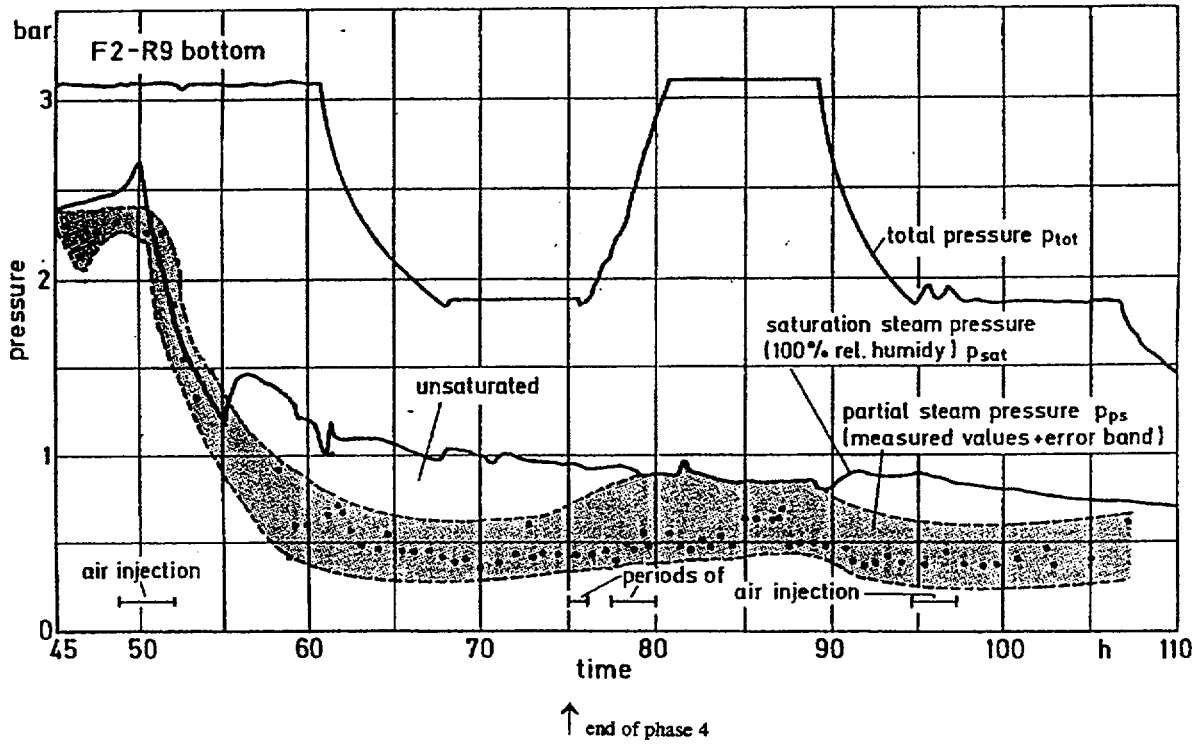


**Figure 9.C.2-13 Thermodynamic state of steam-air atmosphere in R9 bottom (H=1 m)**

**(reprinted from L.Wolf, M.Gavrilas, K. Mun, "Overview of experimental results for long-term, large-scale natural circulations in LWR-containments after large LOCAS", University of Maryland at College Park, Final Report for DOE - Project, Order Number: DE-AP07-96ID10765")**

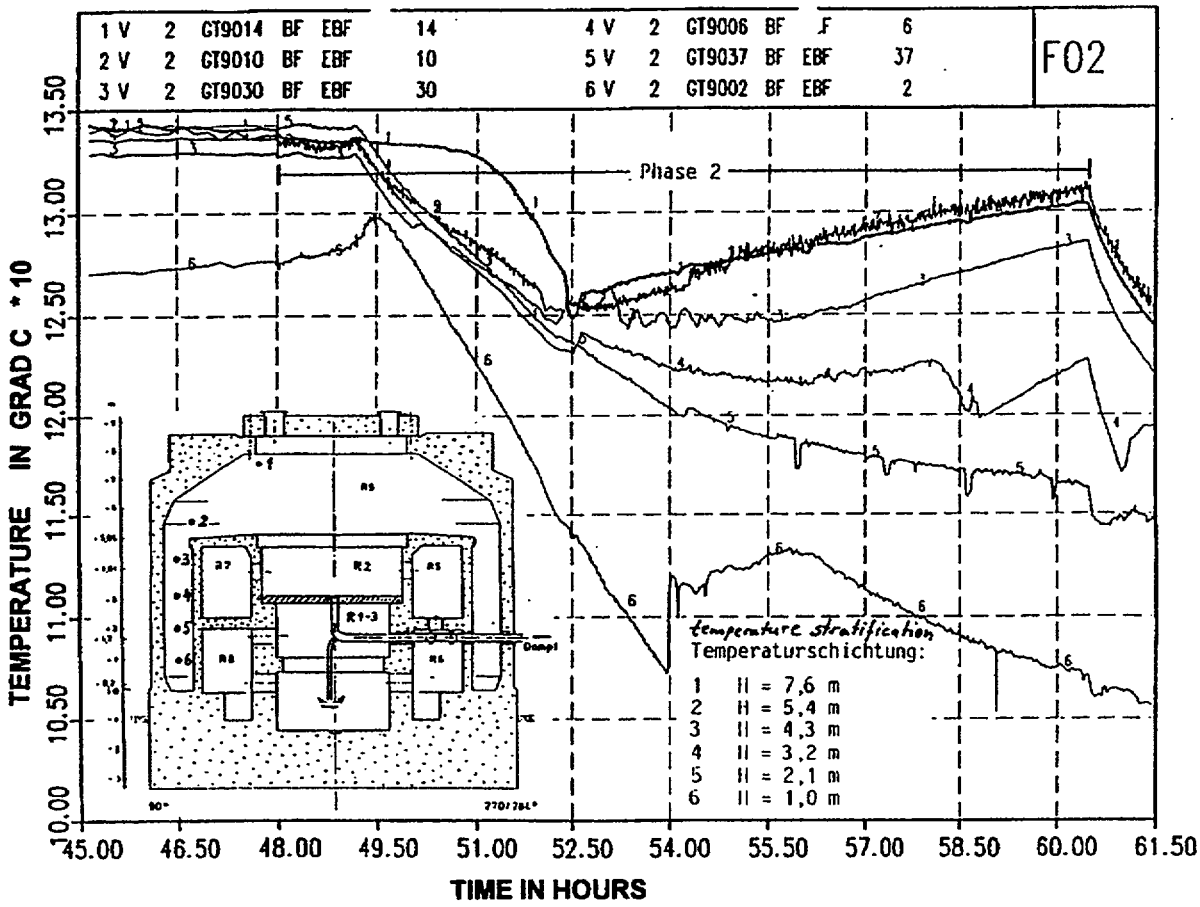


**Figure 9.C.2-14 Test group F2, phase 2: atmospheric temperatures in R9 (Zone 4)**

**(reprinted from L.Wolf, M.Gavrilas, K. Mun, "Overview of experimental results for long-term, large-scale natural circulations in LWR-containments after large LOCAS", University of Maryland at College Park, Final Report for DOE - Project, Order Number: DE-AP07-96ID10765")**

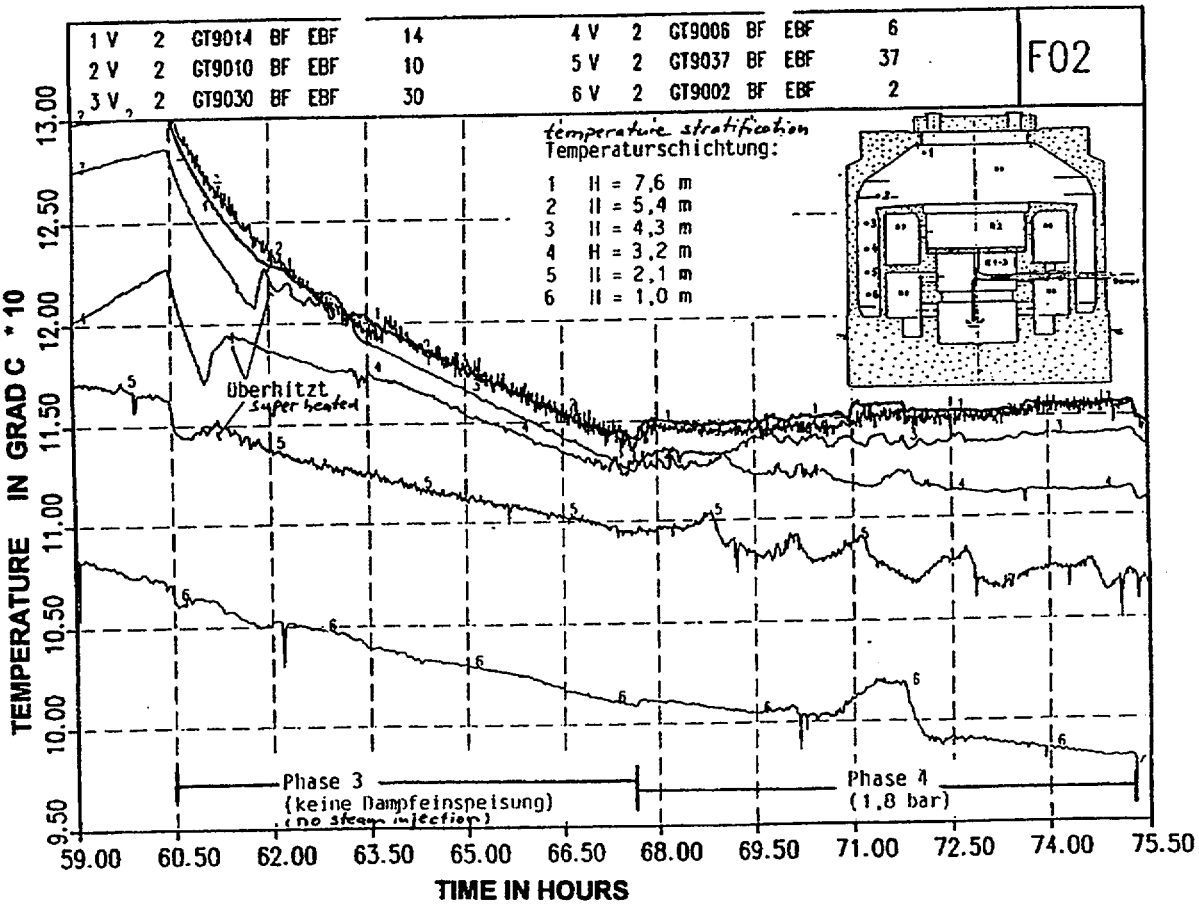


**Figure 9.C.2-15 Test group F2, phase 3 and 4: atmospheric temperatures in R9 (Zone 4)**

**(reprinted from L.Wolf, M.Gavrilas, K. Mun, "Overview of experimental results for long-term, large-scale natural circulations in LWR-containments after large LOCAS", University of Maryland at College Park, Final Report for DOE - Project, Order Number: DE-AP07-96ID10765")**

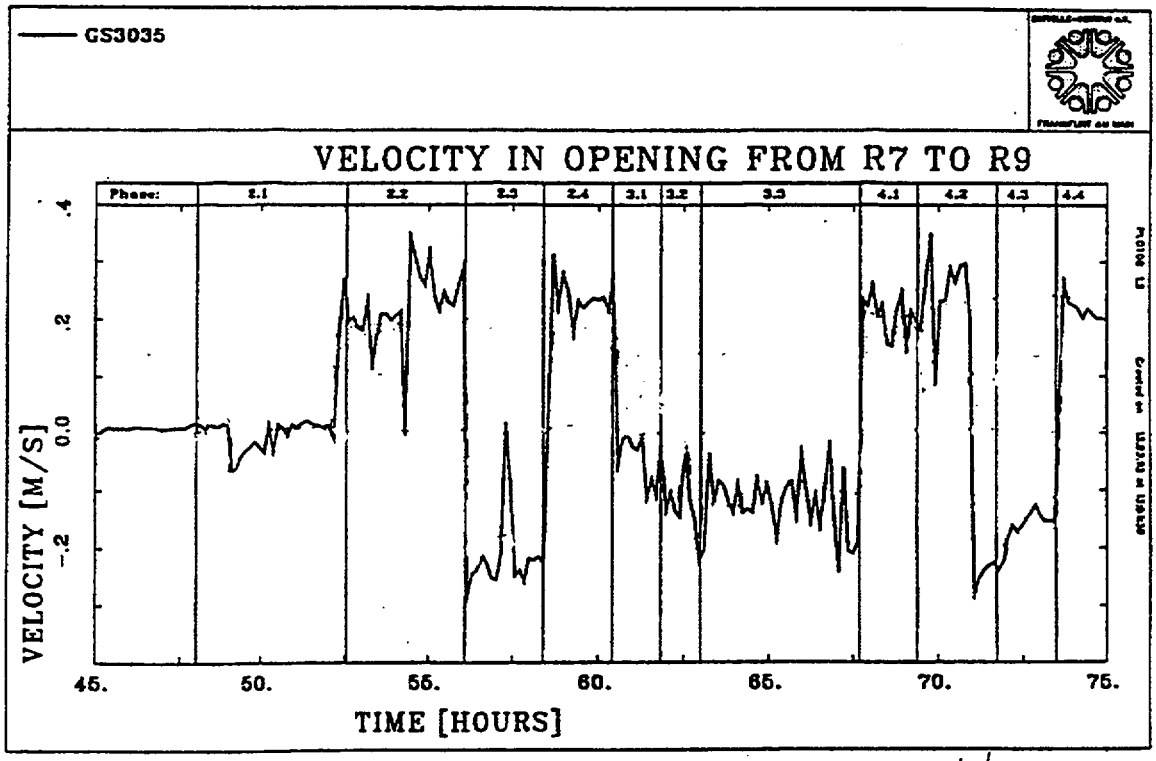


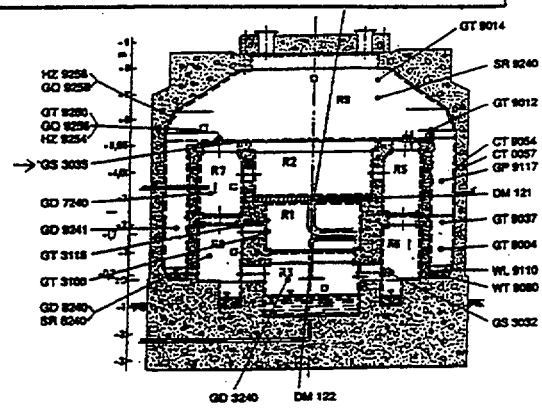


**Figure 9.C.2-16 Velocities in opening from compartment R7 to compartment R9**

**(reprinted from L.Wolf, M.Gavrilas, K. Mun, "Overview of experimental results for long-term, large-scale natural circulations in LWR-containments after large LOCAs", University of Maryland at College Park, Final Report for DOE - Project, Order Number: DE-AP07-96ID10765")**

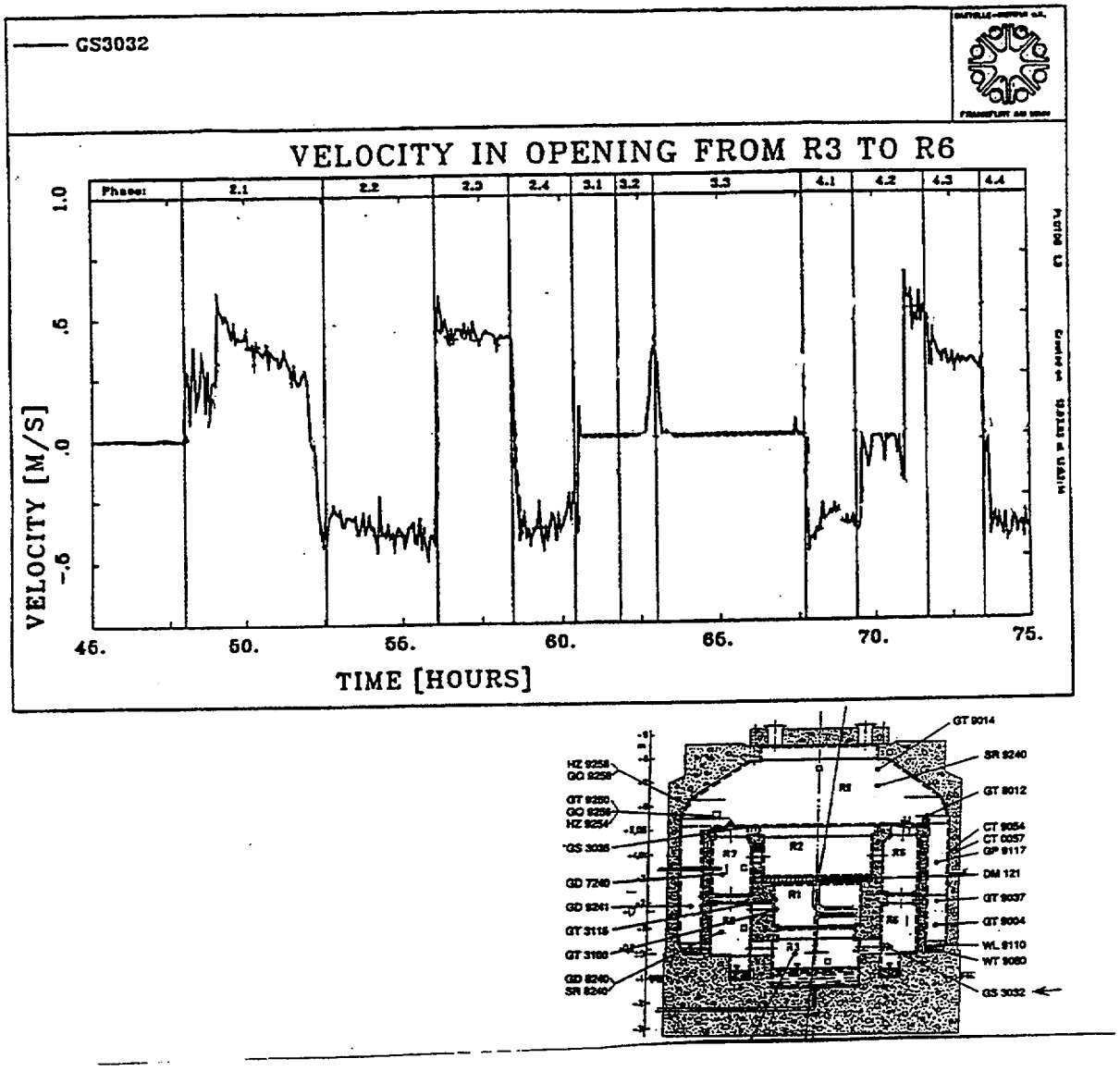


**Figure 9.C. 2-17 Velocities in opening from compartment R3 to compartment R6**

**(reprinted from L.Wolf, M.Gavrilas, K. Mun, "Overview of experimental results for long-term, large-scale natural circulations in LWR-containments after large LOCAs", University of Maryland at College Park, Final Report for DOE - Project, Order Number: DE-AP07-96ID10765")**

### 9.C.2.1.2 The Influence of Initial Temperature Distribution, Location of Hydrogen Injection, Duration of Injection, and Size of Vent Openings on the Hydrogen Distribution (BMC Tests 2, 4, 6, 12 and 20)

Another set of experimental results obtained in BMC is presented in Wolf et al., 1994. The temperature and hydrogen distribution are studied first for two compartments (Phase I) and later for the whole containment (Phase II). These experiments are not directly related to LOCA and MSLB situations, but contribute toward a better understanding of the influence of stratification and circulation phenomenas on the hydrogen distribution inside containments. Although Wolf et al., 1994, compared the experimental results with the GOTHIC containment code, the comparisons are not discussed because of the non-prototypical nature of the experiment relative to the passive containment design.

The results of the experiments with only two compartments (upper and lower) are first presented by Langer et al., 1979. The total volume of the two compartments is 72 $m^3$. The central compartments R1, R3 (form lower compartment) and R2 (upper - see Figure 9.C.2-2, 9.C.2-3 and 9.C.2-18) are used for the test. The opening size between the two compartments can be adjusted. Experiments are performed both with and without orifice (with an effective circular opening of 1 $m^2$) between compartments R1 and R2 (see Fig 9.C.2-18). Uniform injection of hydrogen-nitrogen gas is provided by a flat circular plate with a diameter of 2.5 m. The upper containment is preheated with warm air for several days before the start of some experiments to provide stratification .

Tests 2, 4 and 6 (presented by Wolf et al., 1994) investigate the effects of the vertical hydrogen distribution. The measurement positions are located near the bottom (levels 1 m and 1.85 m) and at the top (levels 5 and 5.5 m) of the containment.

The experiments study the effects of

- The hydrogen injection rates
  - Test 2 has a longer time duration than test 6
- The locations of hydrogen injections
  - The hydrogen-nitrogen source is located above the pool surface in tests 2 and 6
  - The hydrogen-nitrogen source is at the 3.4 m elevation (above the mid-elevation of room R1) in test 4
- The vent flow area (between two compartments)

- An orifice plate is present between R1 and R2 in tests 2 and 6
- Test 4 is performed without the orifice plate

- The initial temperature distribution in the containment (homogeneous versus stratified)

  - A uniform temperature of 19°C is applied in test 2
  - The temperature is a uniform 22°C in test 4
  - A temperature stratification of 19°C in the R3 and R1 (lower rooms) and 35°C in the R2 (upper room) exist in test 6

The hydrogen pressure ratios at the top and bottom of the compartments are presented in Figure 9.C.2-19a, b, c for the second, fourth, and sixth experiments. A comparison of the hydrogen partial pressures shows the effects of the hydrogen release position (test 4) and the initially stratified temperature field (test 6) on the hydrogen concentration stratification.

The experimental findings presented in Wolf et al., 1994 are:

1) The hydrogen is homogeneously distributed through a compartment if the hydrogen source is at the floor and the feed rate is low, even if an orifice plate is installed (see the results for test 2, Figure 9.C.2-19a). Note that the feed rate in the second experiment is lower than in the fourth and sixth experiment. Also, hydrogen is released for 225 minutes in test 2 and for 125 minutes in test 4 and 6.

2) Vertical concentration stratification occurs if the source is located above the floor (see results for test 4, Figure 9.C.2-19b). For low kinetic energy, the diffusion process slowly equalizes concentrations.

3) If the openings between compartments are relatively small, the transport of hydrogen may be obstructed (see results for test 6, Figure 9.C.2-19c).

4) If an initial thermal stratification of air exists and an orifice is installed between the lower and upper compartments, the transport of the lighter $H_2/N_2$ gas mixture is prevented. The highest hydrogen concentrations exist in the lower, cooler part of the compartments, where circulation and mixing occurs (see results for test 6, Figure 9.C.2-19c). The initially stratified temperature field is provided by keeping the upper compartment R2 at a higher temperature ( 35°C ) for several days before the start of the experiment.

Figure 9.C.2-19a (see results for test 2) shows that the buoyancy of the rising plume and the circulation resulting from entrainment into the introduced lighter $H_2/N_2$ gas mixture lead to a relatively homogenized atmosphere. Circulation and mixing are present in both the upper and lower compartments.

Test 4, with an elevated source and reasonably low kinetic energy (Fr is not reported for the tests), shows that there is no significant driving force for circulation below the break elevation. Stratification into two regions occurs, one below and one above the break elevation. The lower region is almost stagnant, while circulation and mixing is present in the upper region (see GOTHIC numerical simulation results by L.Wolf, H. Holzbauer, M. Schall, 1994).

In comparison, test 6, which includes an orifice between R1 and R2 and a stratified temperature field in the upper R2 compartment, shows an almost stagnant upper region. It also shows an increase in the concentration of the lighter $H_2/N_2$ gas mixture in the lower region (a result of the circulation and mixing in the lower regions R1 and R3). The lighter gas mixture is not able to penetrate into the upper stratified layers due to the presence of the narrow orifice. The circulation cell formed by the gas mixture injection into the lower compartments does not communicate with the stratified layers in the upper compartment (see also GOTHIC numerical simulation results by L.Wolf, H. Holzbauer, M. Schall, 1994).

**Application to the AP600 and AP1000**

These tests are not relevant to the passive containment design. The cold dome prevents the stratification that results from higher temperatures of either the vertical walls at the high elevations or the ceiling. In the BMC case, the higher temperatures of the wall surfaces are maintained for a long period of time due to the heat accumulated in the concrete walls (which are heated for several days before the start of the experiment). The passive containment shell is made of steel. Natural convection at the outer surface of the containment walls keeps their temperature low, so that a highly stratified initial temperature field is not possible. Even if initial stratification exists, the application of water on the outer containment surface decreases wall temperatures and causes circulation inside the containment.

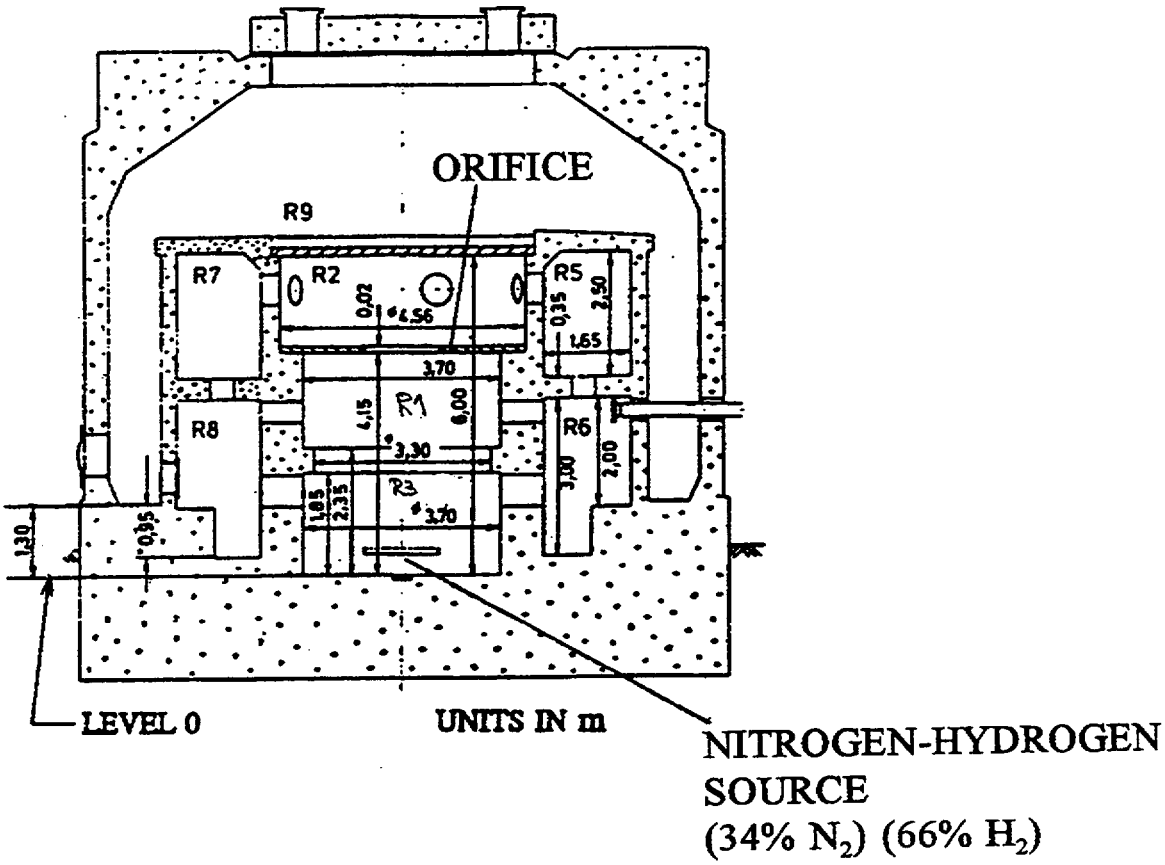


**Figure 9.C.2-18 Vertical cut through BMC with orifice in between R2 and R1**

**(reprinted with permission from authors from L.Wolf, H. Holzbauer, M. Schall, "Comparison between multi-dimensional and lumped-parameter GOTHIC-containment analyses with data", Proceedings, Volume II - Thermohydraulics of Containment and Severe Accidents, May 30th - June 2nd, 1994, pp. 321-330.)**

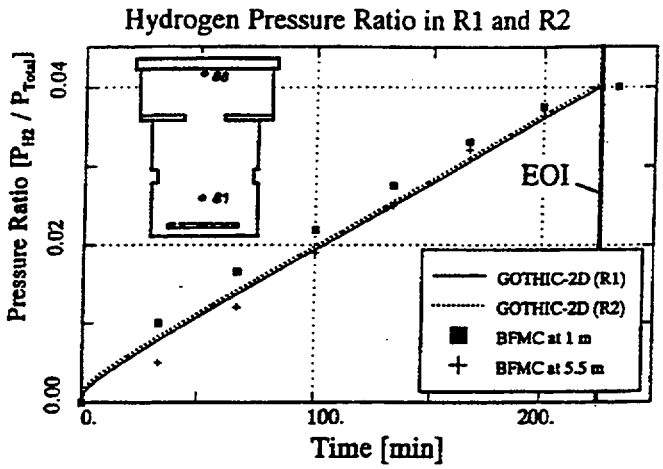


Battelle Test No. 2

EOI - End of Injection

**Figure 9.C.2-19a BMC test no. 2: Comparison between experimental data and 2-d GOTHIC computations for hydrogen concentrations**

**(reprinted with permission from authors from L.Wolf, H. Holzbauer, M. Schall, "Comparison between multi-dimensional and lumped-parameter GOTHIC-containment analyses with data", Proceedings, Volume II - Thermohydraulics of Containment and Severe Accidents, May 30th - June 2nd, 1994, pp. 321-330.)**

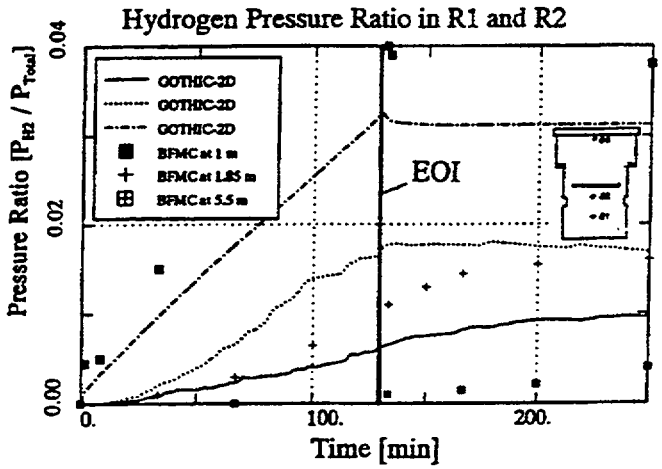


Battelle Test No. 4

EOI - End of Injection

**Figure 9.C.2-19b** **BMC test no. 4: Comparison between experimental data and 2-d GOTHIC computations for hydrogen concentrations**

**(reprinted with permission from authors from L.Wolf, H. Holzbauer, M. Schall, "Comparison between multi-dimensional and lumped-parameter GOTHIC-containment analyses with data", Proceedings, Volume II - Thermohydraulics of Containment and Severe Accidents, May 30th - June 2nd, 1994, pp. 321-330.)**

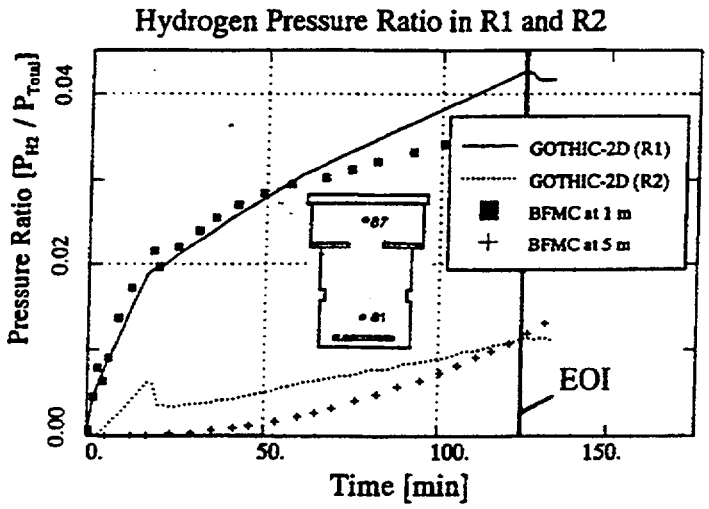


EOI = End of Injection

Battelle Test No. 6

**Figure 9.C.2-19c** **BMC test no. 6: Comparison between experimental data and 2-d GOTHIC computations for hydrogen concentrations**

**(reprinted with permission from authors from L.Wolf, H. Holzbauer, M. Schall, "Comparison between multi-dimensional and lumped-parameter GOTHIC-containment analyses with data", Proceedings, Volume II - Thermohydraulics of Containment and Severe Accidents, May 30th - June 2nd, 1994, pp. 321-330.)**

In the second phase (Langer and Baukal, 1982), the full model containment is used for experiments. The effects of: (1) the initial temperatures and humidities, (2) the geometry of the containment, and (3) the location and rate of hydrogen release are investigated.

The results of tests 12 and 20 are presented in Wolf et al., 1994 and are compared with the results of three GOTHIC modeling strategies. Tests 12 and 20 are performed with six compartments (R1-2, R5-8, see Figures 9.C.2-2 and 9.C.2-3). The hydrogen-nitrogen mixture is injected into rooms R2 and R6 in tests no.12 and 20, respectively.

Test no. 12 is performed with a uniform initial temperature. It results in a homogenized hydrogen distribution in the containment (see Figure 9.C.2-20). The stratified initial temperature distribution in test 20 results in higher hydrogen distribution in the lower level compartments (R1, R6 and R8 - see Figure 9.C.2-21a, b, c). An explanation for this unexpected result is that the circulation cell formed by the injection of the lighter gas mixture is not able to penetrate upper stratified layers at the beginning of the experiment. This is similar to test 6, which includes an orifice and stratified initial temperature field in the upper compartment. After three hours, there is a tendency toward decreased gradients in the concentration field, especially between R1 and R2 compartments. This indicates that global circulation affects the upper stratified layers.

A summary of the experimental results is:

1) If the temperature field was uniform (test 12), hydrogen was homogeneously distributed inside the containments.

2) For an initially thermally stratified field (test 20), higher hydrogen concentrations are present in the lower (cooler) compartments at the beginning of the experiment.

Both groups of experiments indicate that good air circulation inside the containment (in fact a uniform temperature field) is crucial for homogeneous hydrogen distribution. Note that in the first group of tests, the stratification is obtained by preheating the upper room with warm air for several days before the start of the experiments.

A comparison between this experimental data and the numerical results obtained with GOTHIC (with lumped-parameter and multi-dimensional analyses) is presented in Wolf et. al, 1994.

Battelle Test No. 12

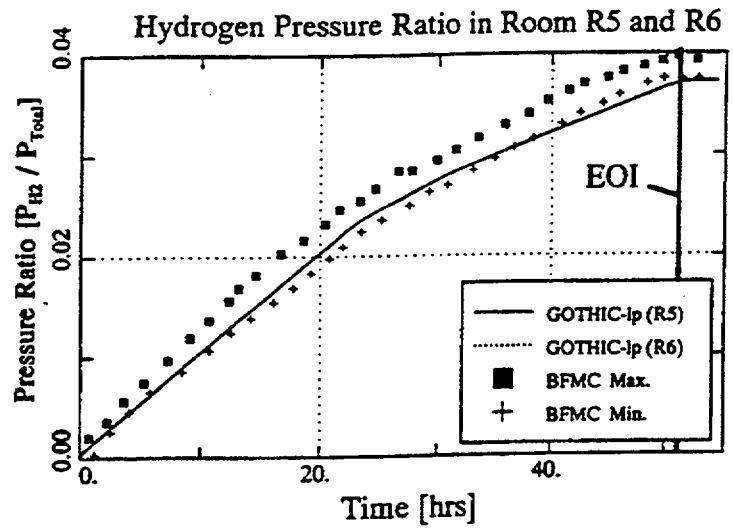


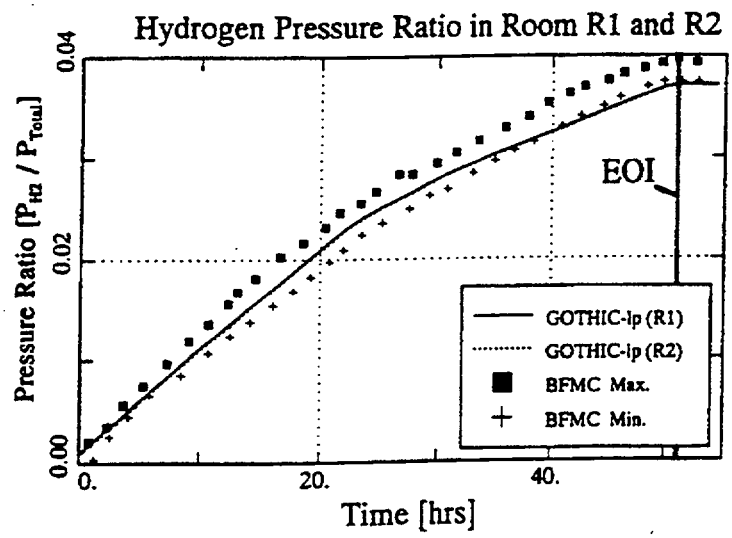


EOI = End of Injection

**Figure 9.C.2-20** **BMC test no. 12: Comparison between experimental data and GOTHIC-lp computations for hydrogen concentrations**

**(reprinted with permission from authors from L.Wolf, H. Holzbauer, M. Schall, "Comparison between multi-dimensional and lumped-parameter GOTHIC-containment analyses with data", Proceedings, Volume II - Thermohydraulics of Containment and Severe Accidents, May 30th - June 2nd, 1994, pp. 321-330.)**

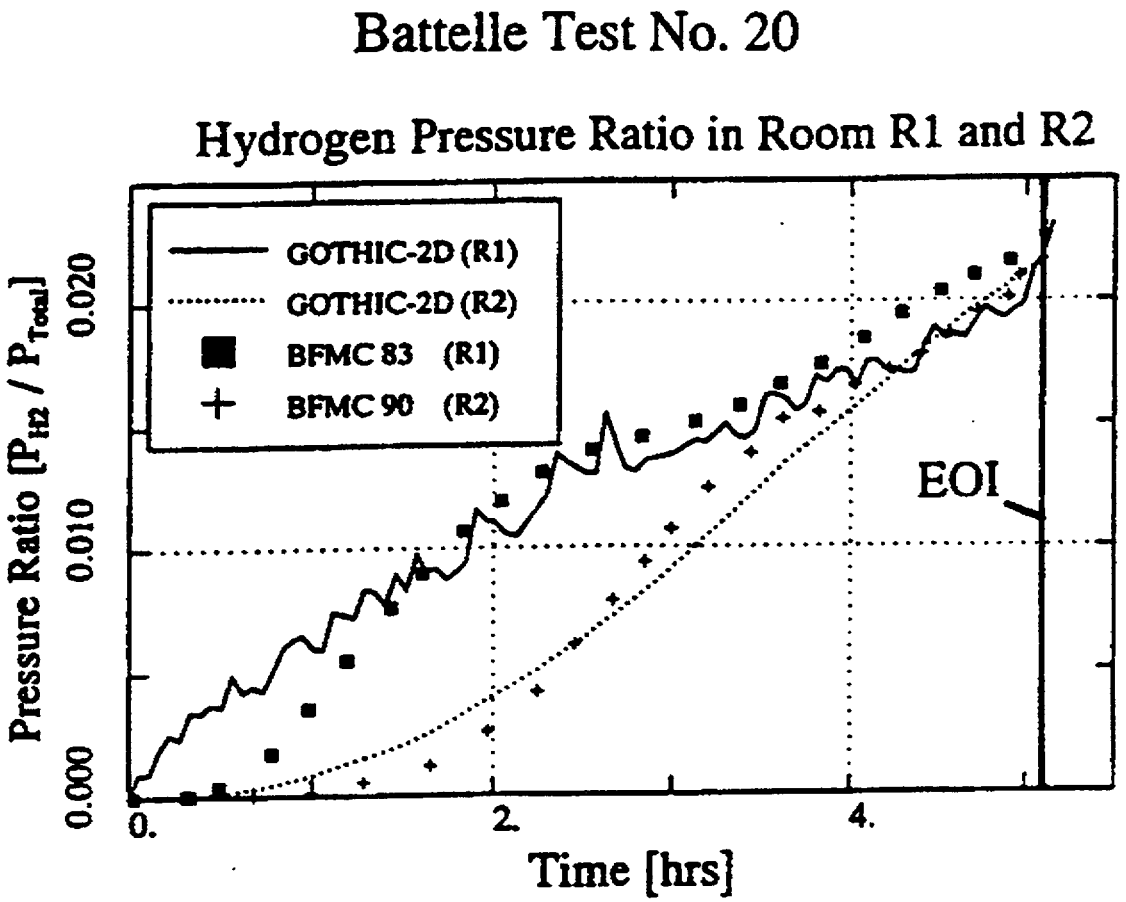


**Figure 9.C.2-21a** **BMC test no. 20: Comparison between experimental data and 2-d GOTHIC computations for hydrogen concentrations**

**(reprinted with permission from authors from L.Wolf, H. Holzbauer, M. Schall, "Comparison between multi-dimensional and lumped-parameter GOTHIC-containment analyses with data", Proceedings, Volume II - Thermohydraulics of Containment and Severe Accidents, May 30th - June 2nd, 1994, pp. 321-330.)**

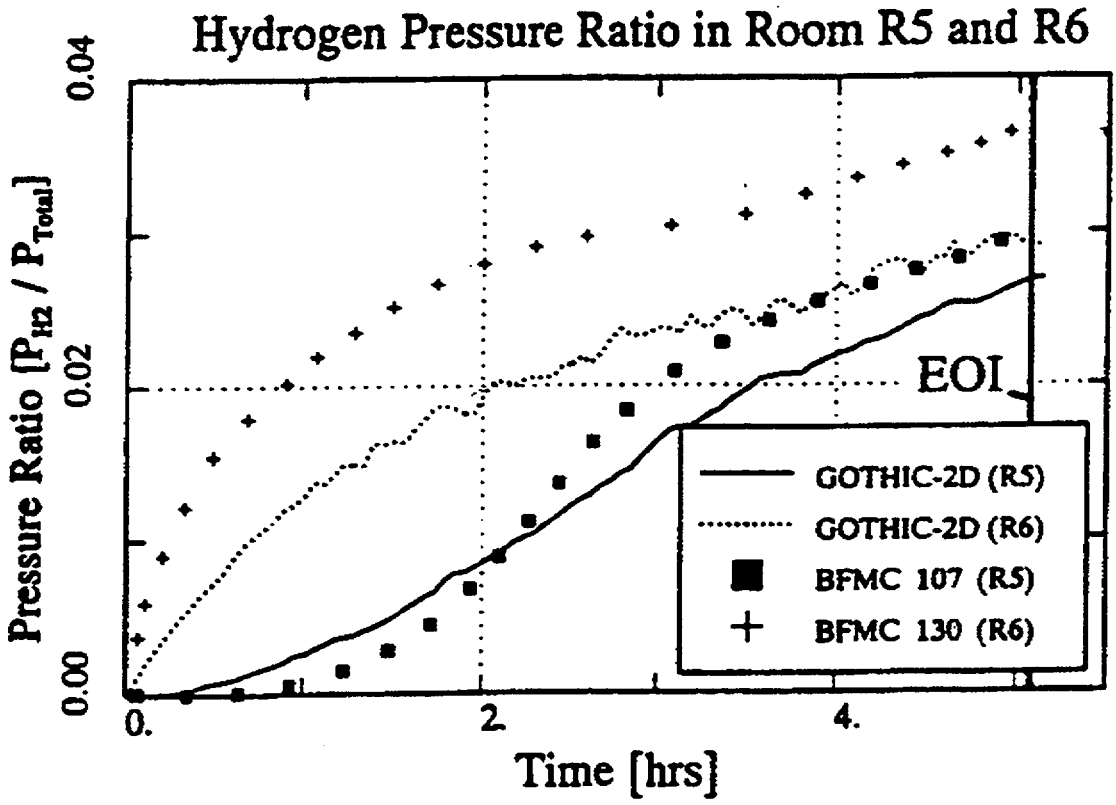


**Figure 9.C.2-21b** **BMC test no. 20: Comparison between experimental data and 2-d GOTHIC computations for hydrogen concentrations**

**(reprinted with permission from authors from L.Wolf, H. Holzbauer, M. Schall, "Comparison between multi-dimensional and lumped-parameter GOTHIC-containment analyses with data", Proceedings, Volume II - Thermohydraulics of Containment and Severe Accidents, May 30th - June 2nd, 1994, pp. 321-330.)**

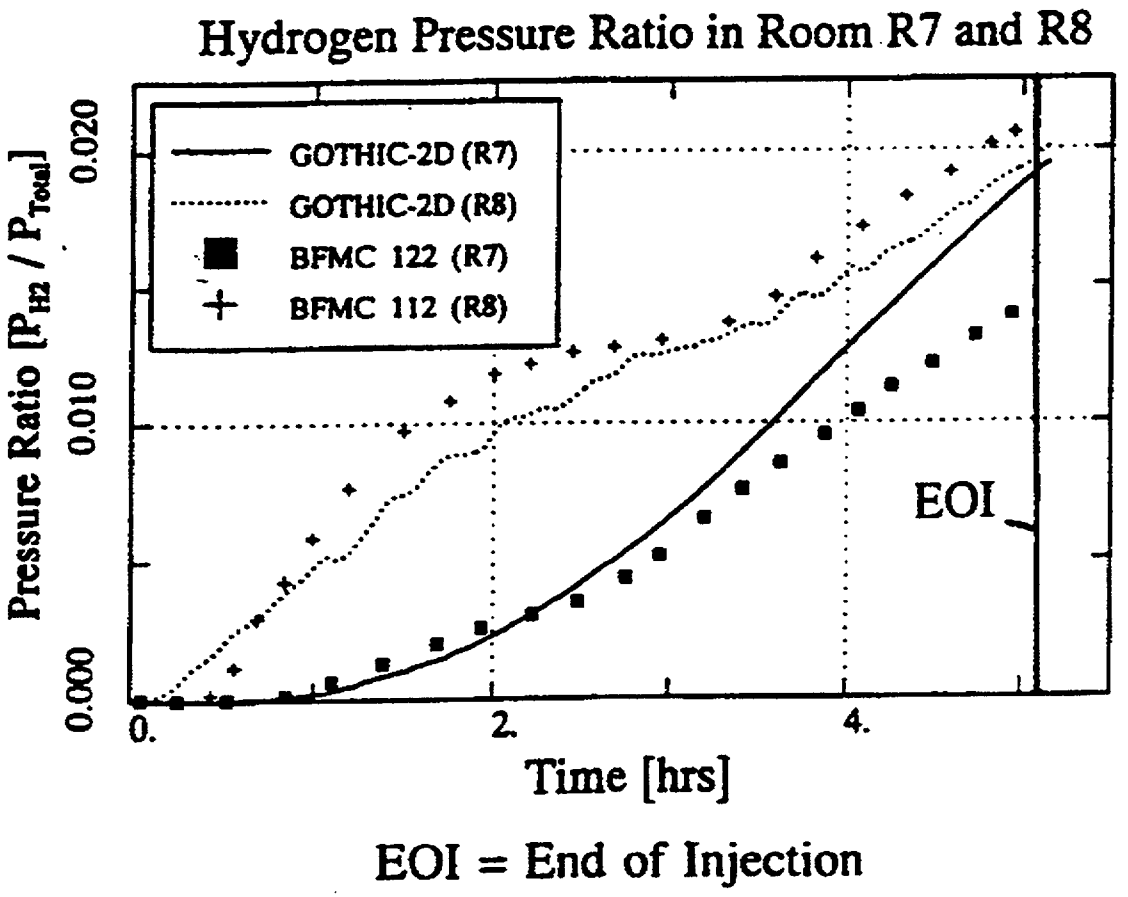


**Figure 9.C.2-21c** **BMC test no. 20: Comparison between experimental data and 2-d GOTHIC computations for hydrogen concentrations**

### 9.C.2.1.3 Effects of Sump Heatup on Global Natural Circulation (Experiments RX1 - RX5)

The third set of experiments performed in the BMC (Fischer et al., 1994 and Petersen et al., 1994) examine the effect of sump heatup on global natural circulation inside the containment. The starting and transient behavior of natural circulation for small temperature differences, the influence of natural circulation on mixing of hydrogen released during accident conditions, and the effects of stratification on the natural convection formation are also studied.

A total of five experiments are performed (RX1 to RX5) at atmospheric pressure. Temperatures are recorded in the sump, in the containment atmosphere, and in the concrete structures. The relative humidity, containment pressure, liquid sump level, velocities (in the vents), and hydrogen concentration are also measured.

The objective of long-term experiments is to establish at what sump temperature global circulation exists. During these experiments, the containment atmosphere, structure, and sump have nearly identical temperatures. Circulation effects inside the containment are already present with a sump temperature as low as 25°C. Experiments RX2 (without hydrogen injection) and RX4 (with multiple hydrogen injections) are performed as long-term tests. The respective initial and boundary conditions for all experiments are given in Table 9.C-4.

Results are provided for only the RX4 experiment, since the hydrogen distribution is available for this test. A summary of the results for the RX4 experiment, with the cold containment and multiple hydrogen injections, is presented in Wolf et al., 1996. The perspective view and cross-sections of the BMC containment, illustrating the compartment numbers and the location of the hydrogen injection, are presented in Figures 9.C.2-22 and 9.C.2-23. The instrumentation plan for the RX4 test is specified in Figure 9.C.2-24.

At the beginning of the experiment, the temperatures of the structure range from 20-26°C. The sump temperature is 20°C (see Figure 9.C.2-25). Several consecutive characteristic periods evolve during the experiment. The sump heat up is divided into three periods:

1) 0 to 1:48 hr - the sump is heated to 50°C
2) 2:43 to 3:39 hr - continuation of sump heating to 60°C
3) 3:34 to 4:52 hr - continued sump heating to maintain the temperature at 60°C until the end of experiment (5 hr)

Three hydrogen injections occur:

1) 1:11-1:24 hr, 236 g of hydrogen is released
2) 2:11-2:23 hr, 215 g of hydrogen is released

3) 4:06-4:33 hr, 319 g of hydrogen is released

At the beginning of the sump heatup, the anemometers register velocities between 0.2-0.3 m/s (for sump temperatures 24-27°C), while at the end of the experiment, velocities are 0.6-0.8 m/s (see Figure 9.C.2-26). At the end, the temperature of the dome is 30°C (see Figure 9.C.2-27). Shaded areas in Figures 9.C.2-26 and 9.C.2-27 represent periods of hydrogen injection. Velocities increase during periods of hydrogen injection.

Sump and atmosphere temperatures are presented in Figures 9.C.2-25, 9.C.2-27, and 9.C.2-28. Temperature differences in the area of the center compartment and dome are not greater than 2°C (Figure 9.C.2-27). The temperature difference in the external annulus is smaller than 3°C (Figure 9.C.2-28), indicating the presence of natural circulation effects.

Due to the natural circulation, the hydrogen distribution is almost uniform in the whole containment, see (Figures 9.C.2-29 and 9.C.2-30). After two hours, the relative humidity of the whole containment atmosphere is 100 percent (see Figure 9.C.2-31). Even low natural circulation flows provide complete mixing of the hydrogen and steam (evaporated from sump). The heated sump provides sufficient buoyancy force for natural circulation flow.

**Table 9.C-4 Test Matrix of Battelle Sump Heatup Experiments**

| Test No. | Containment-Atmosphere | | | Structure-Temperature [°C] | Sump-Temperature [°C] | $H_2$-Mass [g] |
|---|---|---|---|---|---|---|
| | Containment Media | Initial Temperature [°C] | Total Pressure [bar] | | | |
| RX1 | air | 23.5 - 28.5 | 1.011 | 24 - 26 | 1) ≈ 40<br>2) ≈ 50<br>3) ≈ 55<br>4) ≈ 60 | -------- |
| RX2 | air | 22 - 28.5 | 1.009 | 24.5 - 28 | 1) ≈ 40<br>2) ≈ 50<br>3) ≈ 60 | -------- |
| RX3 | air + steam | 48 - 58.5 | 1.008 | 42 - 61 | 60 - 100 | -------- |
| RX4 | air + $H_2$ | 24 - 27 | 1.014 | 22.5 - 26.5 | 1) ≈ 48<br>2) ≈ 60 | 1) 236<br>2) +215<br>3) +319 |
| RX5 | air + steam + $H_2$ | 55 - 69 | 1.001 | 39 - 64 | 1) 62 - 49<br>2) 63 - 58 | 1) 371<br>2) +390<br>3) +406 |

(reprinted from L. Wolf, M. Gavrilas, K. Mun, "Overview of experimental results for long-term, large-scale natural circulations in LWR-containments after large LOCAS," University of Maryland at College Park, Final Report for DOE - Project, Order Number: DE-AP07-96ID10765")

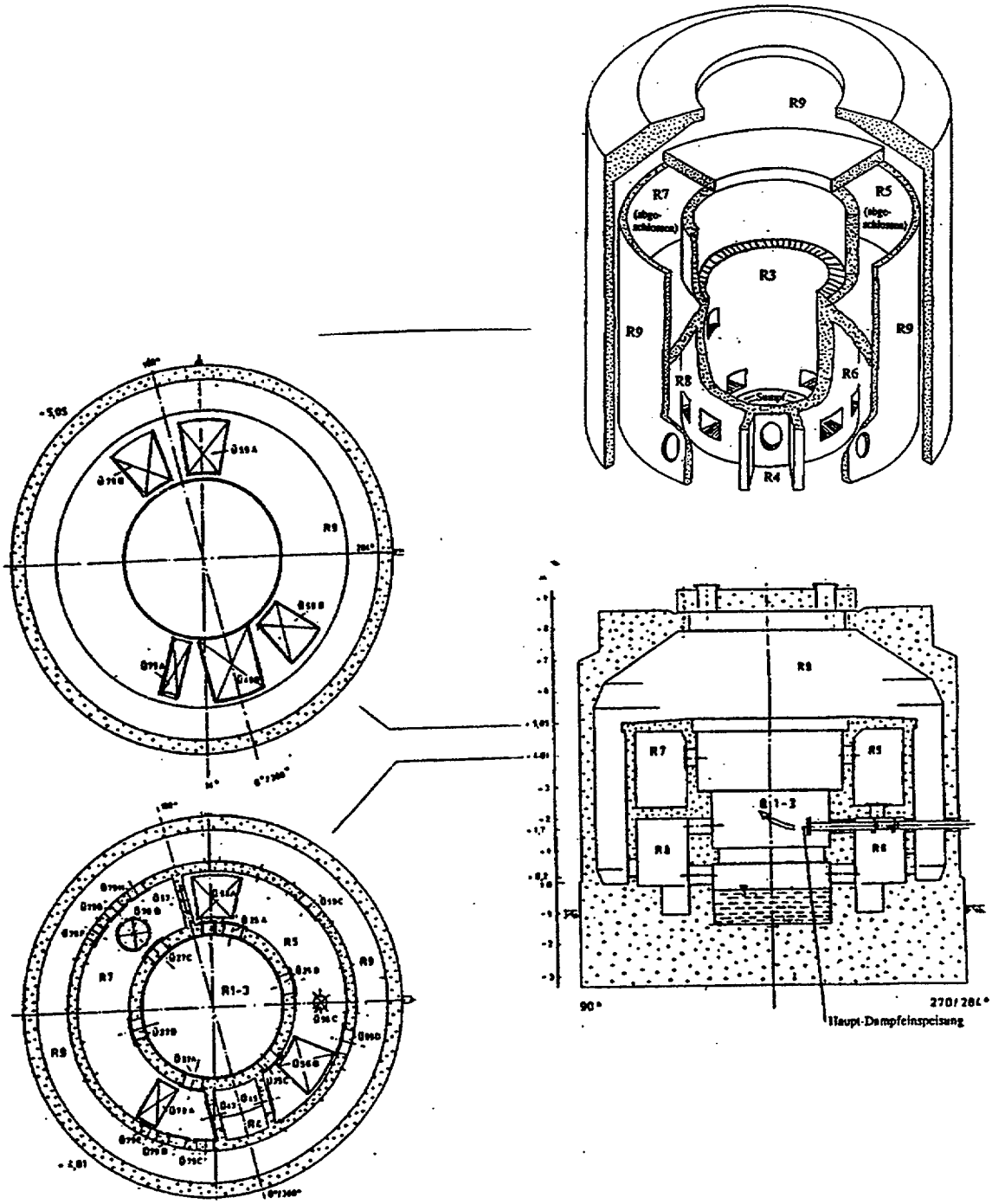


**Figure 9.C.2-22** **Perspective view, vertical and upper horizontal cross-sections through BMC with main steam feedline**

**(reprinted from L.Wolf, M.Gavrilas, K. Mun, "Overview of experimental results for long-term, large-scale natural circulations in LWR-containments after large LOCAS", University of Maryland at College Park, Final Report for DOE - Project, Order Number: DE-AP07-96ID10765")**

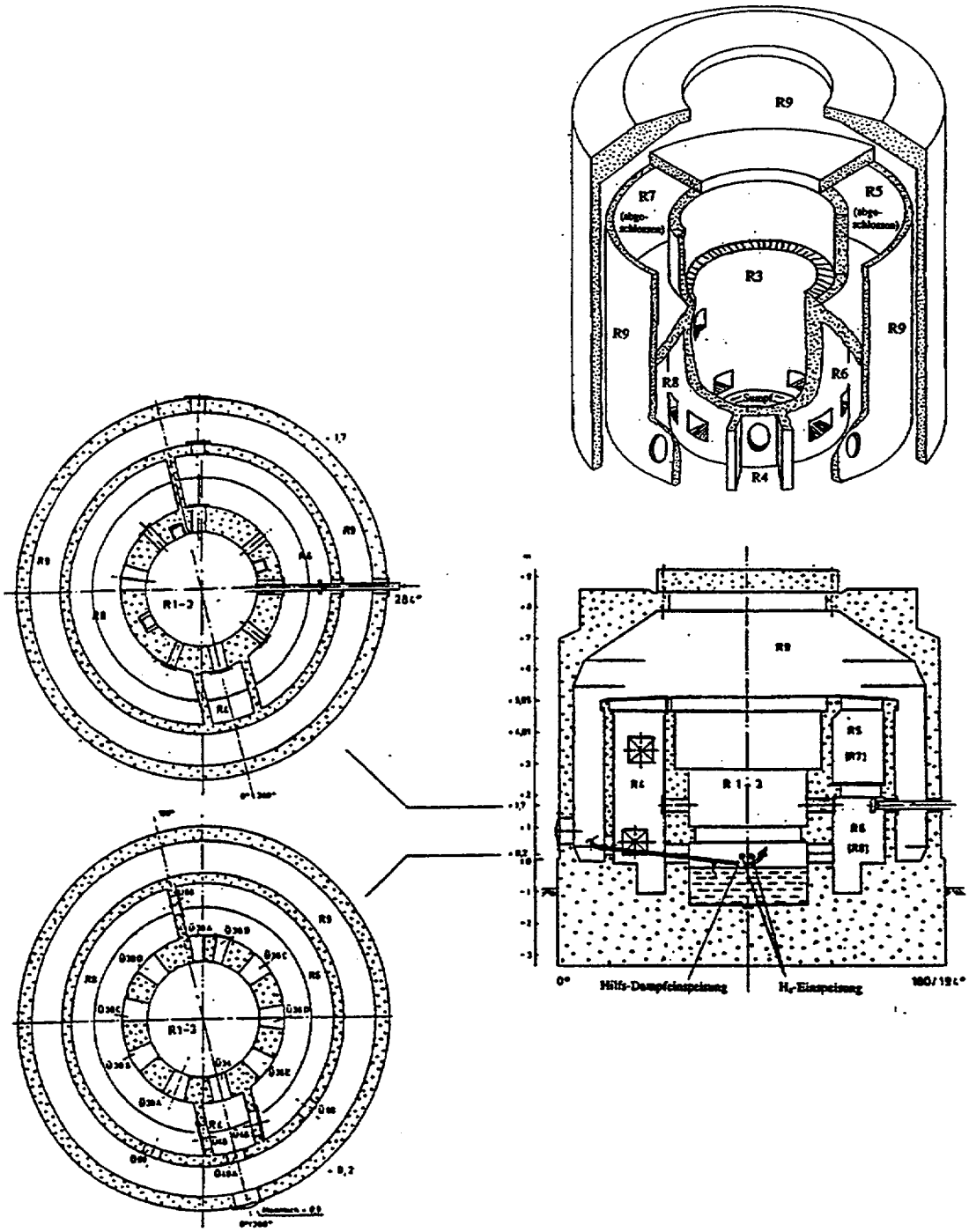


**Figure 9.C.2-23** **Perspective view, vertical and upper horizontal cross-sections through BMC with auxiliary steam feedline**

**(reprinted from L.Wolf, M.Gavrilas, K. Mun, "Overview of experimental results for long-term, large-scale natural circulations in LWR-containments after large LOCAS", University of Maryland at College Park, Final Report for DOE - Project, Order Number: DE-AP07-96ID10765")**

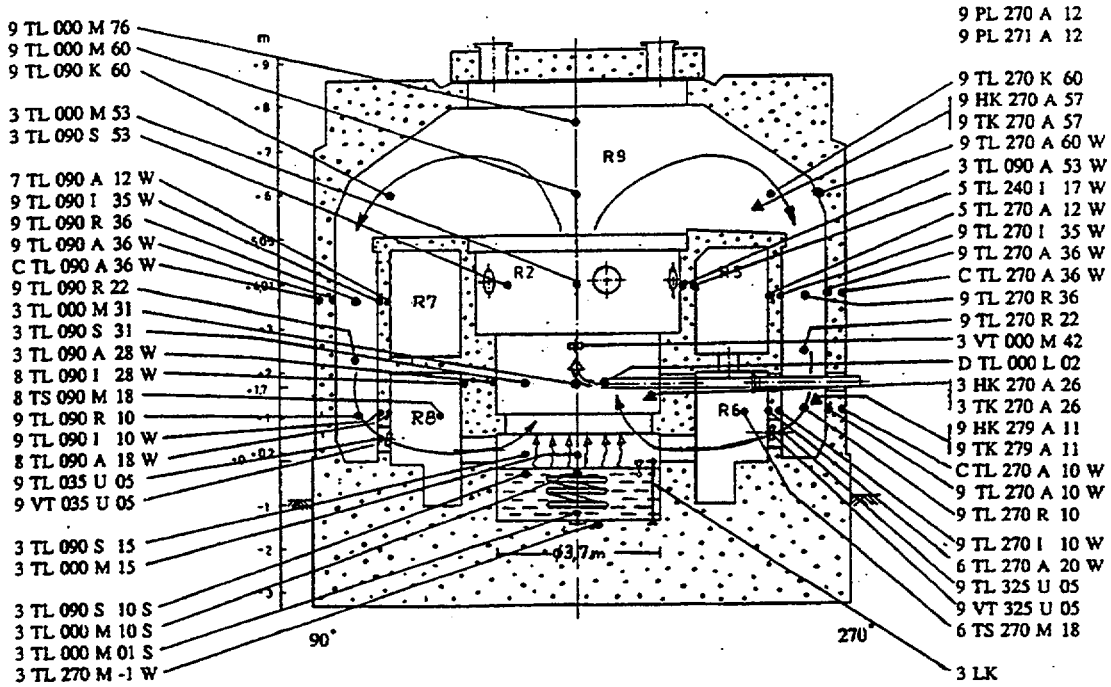


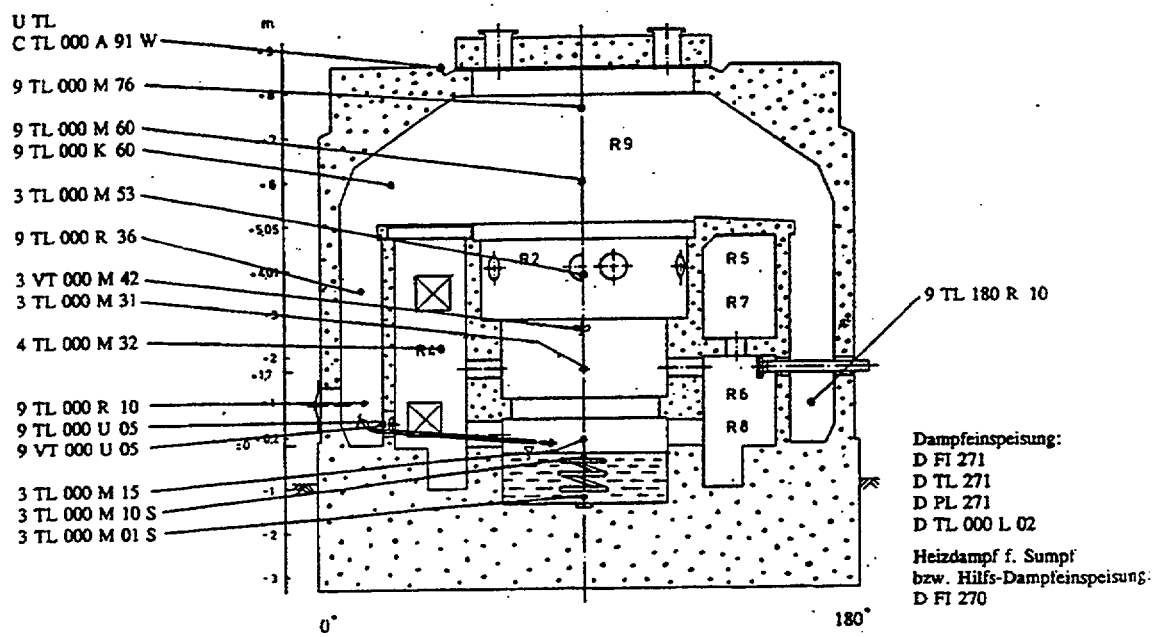


**Figure 9.C.2-24 Instrumentation plan for BMC - sump heatup test RX4**

**(reprinted from L.Wolf, M.Gavrilas, K. Mun, "Overview of experimental results for long-term, large-scale natural circulations in LWR-containments after large LOCAs", University of Maryland at College Park, Final Report for DOE - Project, Order Number: DE-AP07-96ID10765")**

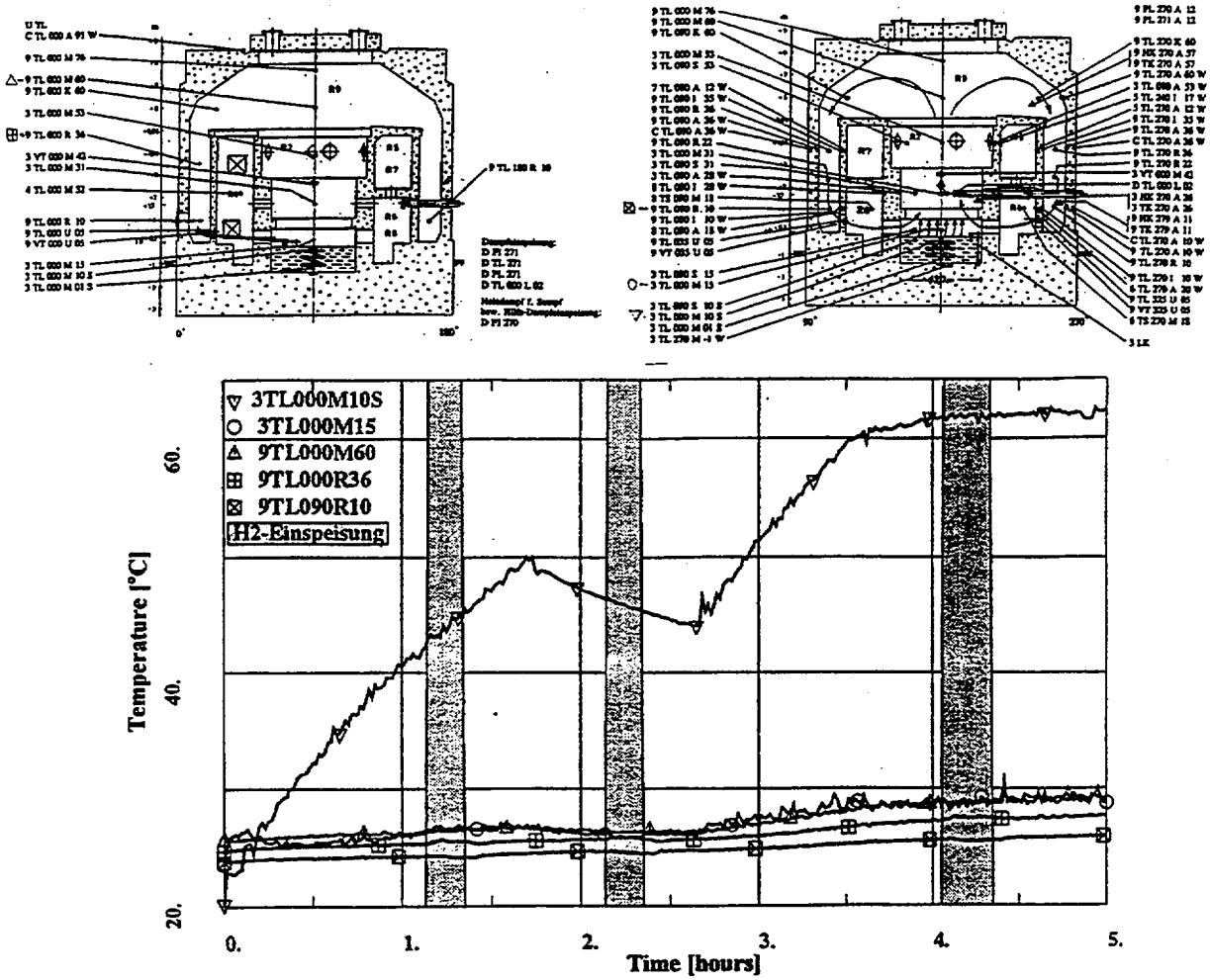


**Figure 9.C.2-25 Battelle-Experiment RX4: Sump and atmospheric temperatures**

**(reprinted from L.Wolf, M.Gavrilas, K. Mun, "Overview of experimental results for long-term, large-scale natural circulations in LWR-containments after large LOCAs", University of Maryland at College Park, Final Report for DOE - Project, Order Number: DE-AP07-96ID10765")**

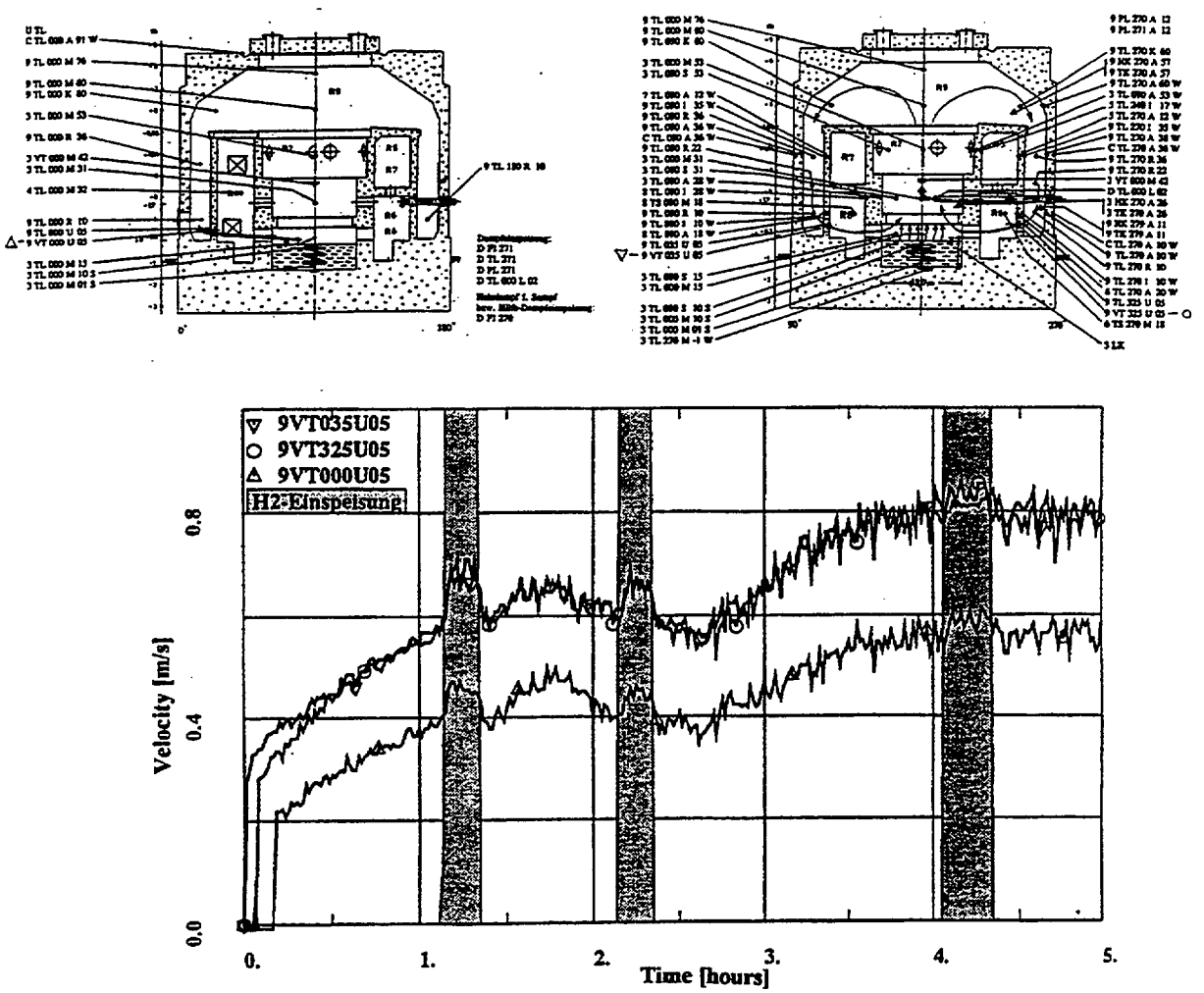


**Figure 9.C.2-26 Battelle-Experiment RX4: Velocities in side vents**

**(reprinted from L.Wolf, M.Gavrilas, K. Mun, "Overview of experimental results for long-term, large-scale natural circulations in LWR-containments after large LOCAs", University of Maryland at College Park, Final Report for DOE - Project, Order Number: DE-AP07-96ID10765")**

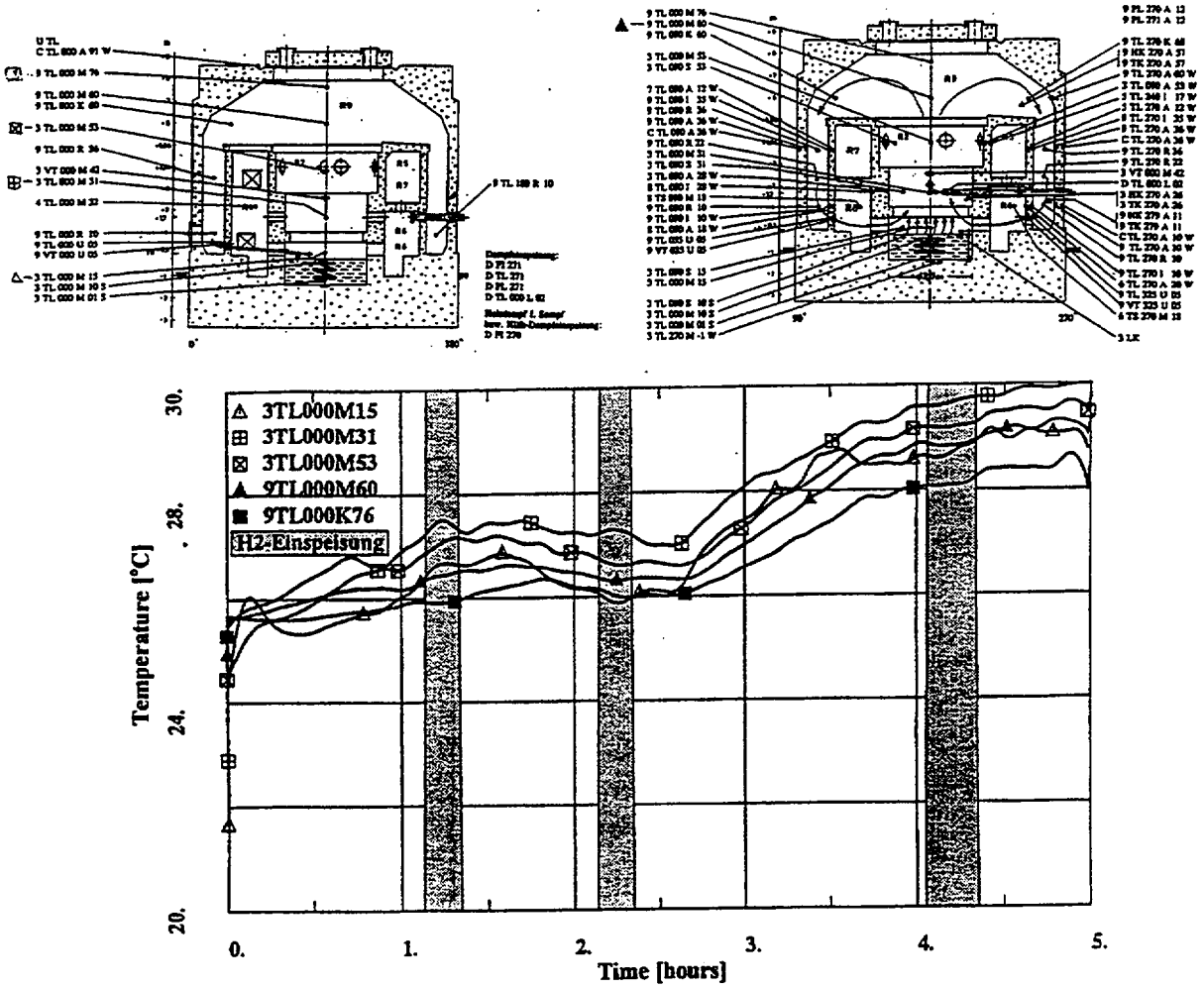


**Figure 9.C.2-27 Battelle-Experiment RX4: Temperatures in center compartment and dome**

**(reprinted from L.Wolf, M.Gavrilas, K. Mun, "Overview of experimental results for long-term, large-scale natural circulations in LWR-containments after large LOCAs", University of Maryland at College Park, Final Report for DOE - Project, Order Number: DE-AP07-96ID10765")**

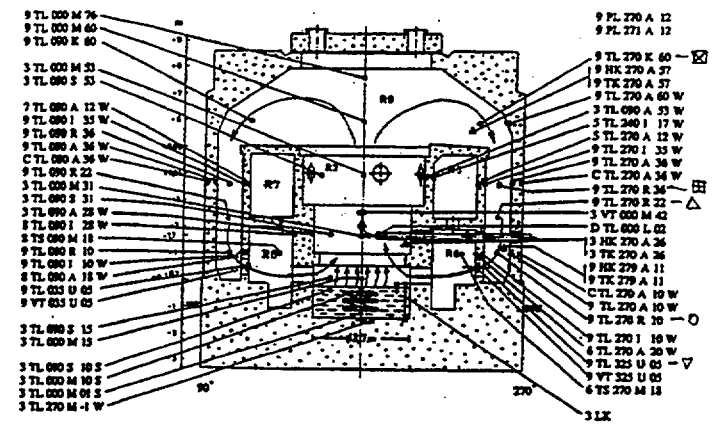

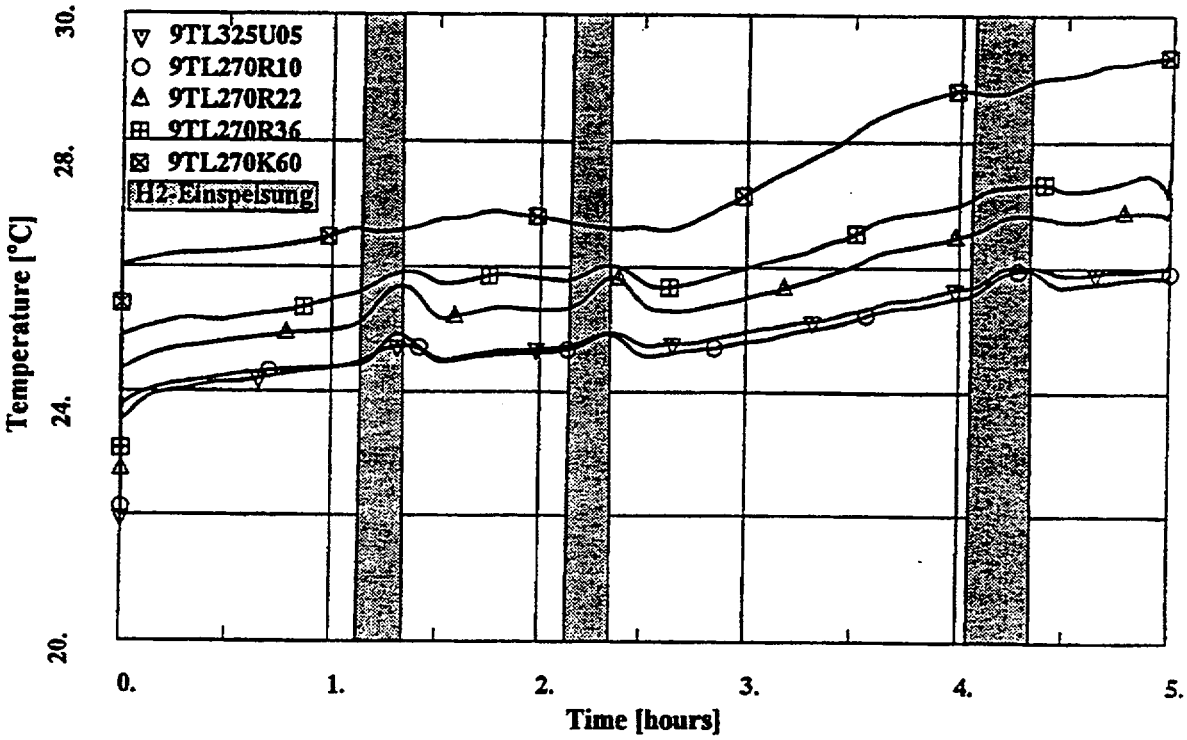


**Figure 9.C.2-28 Battelle-Experiment RX4: Temperatures in external annulus**

**(reprinted from L.Wolf, M.Gavrilas, K. Mun, "Overview of experimental results for long-term, large-scale natural circulations in LWR-containments after large LOCAs", University of Maryland at College Park, Final Report for DOE - Project, Order Number: DE-AP07-96ID10765")**

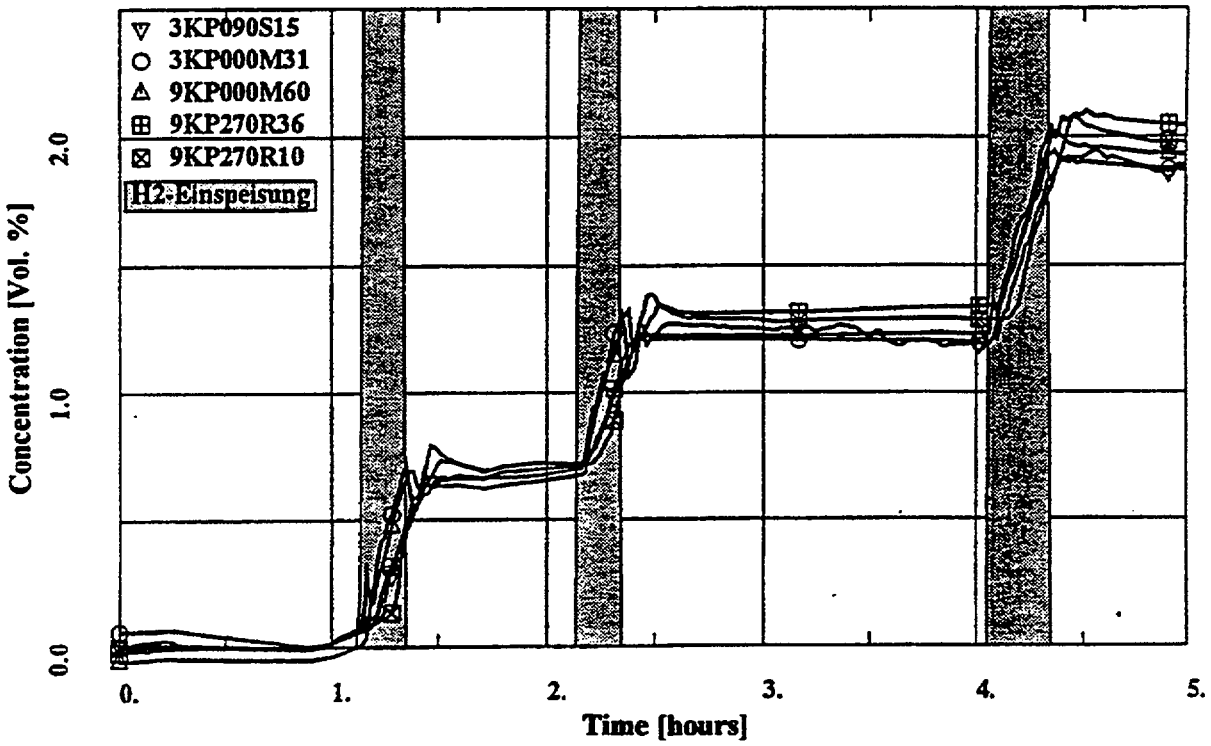


**Figure 9.C.2-29 Battelle-Experiment RX4: Hydrogen concentration along circulation path**

**(reprinted from L.Wolf, M.Gavrilas, K. Mun, "Overview of experimental results for long-term, large-scale natural circulations in LWR-containments after large LOCAs", University of Maryland at College Park, Final Report for DOE - Project, Order Number: DE-AP07-96ID10765")**

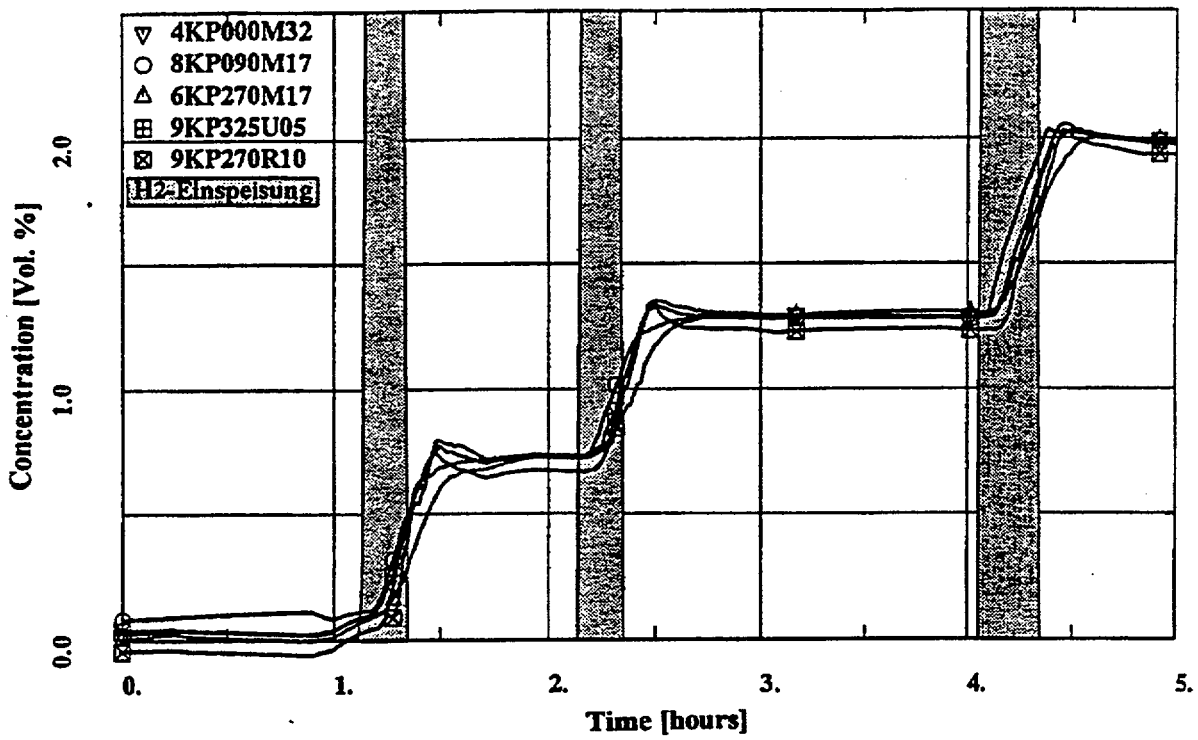


**Figure 9.C.2-30** **Battelle-Experiment RX4: Hydrogen concentrations in intermediate subcompartments**

**(reprinted from L.Wolf, M.Gavrilas, K. Mun, "Overview of experimental results for long-term, large-scale natural circulations in LWR-containments after large LOCAs", University of Maryland at College Park, Final Report for DOE - Project, Order Number: DE-AP07-96ID10765")**

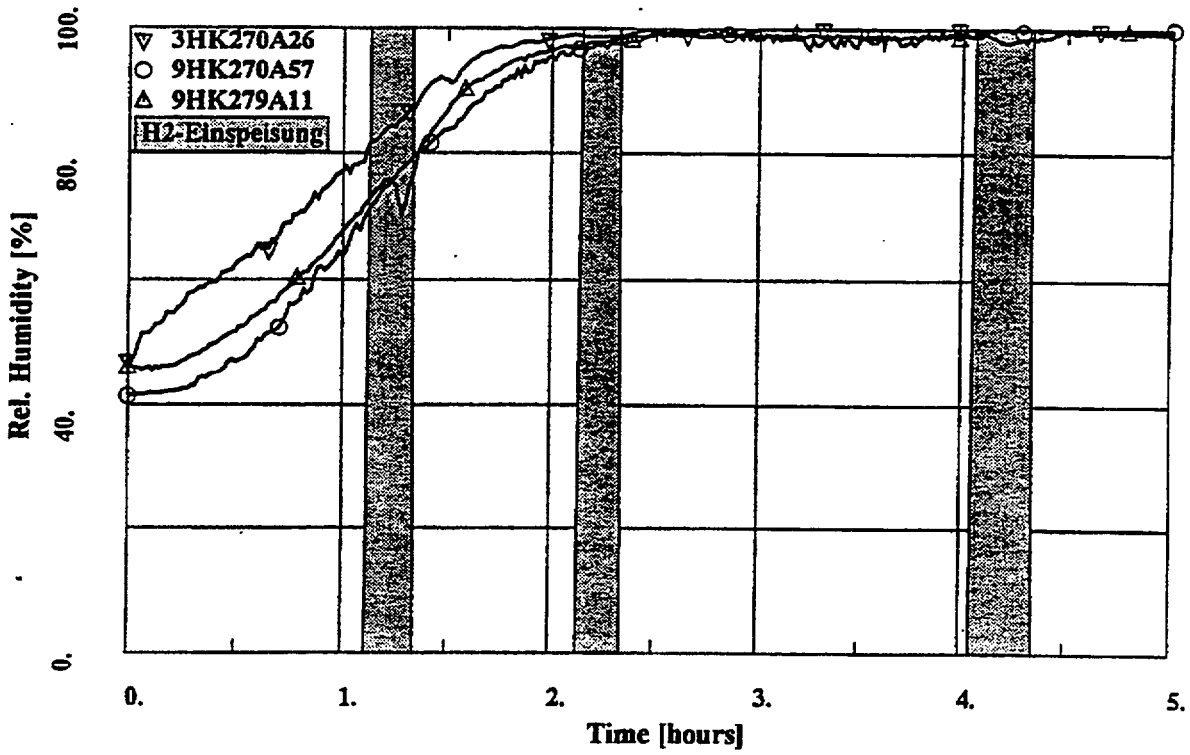


**Figure 9.C.2-31 Battelle-Experiment RX4: Relative humidity in the containment atmosphere**

**(reprinted from L.Wolf, M.Gavrilas, K. Mun, "Overview of experimental results for long-term, large-scale natural circulations in LWR-containments after large LOCAs", University of Maryland at College Park, Final Report for DOE - Project, Order Number: DE-AP07-96ID10765")**

### 9.C.2.1.4 References

1. Fischer, K., Kanzleiter, T., Schall, M., Wolf, L., 1989
"CEC Thermal-Hydraulic Benchmark Exercise on FIPLOC Verification Experiment F2 in BMC-Long-Term Heatup Phase - Specification for Phase I, Battelle-Institut e.V., Frankurt/Main, Germany, Sept. 1989

2. Fischer, K., T., Schall, M., Wolf, L., 1991
"CEC Thermal-Hydraulic Benchmark Exercise on FIPLOC Verification Experiment F2 in BMC-Long-Term Heatup Phase - Results for Phase I, Final Report, EUR 13588 EN, 1991

3. Fischer, K., Kanzleiter, T., Schall, M., Wolf, L., 1990
"CEC Thermal-Hydraulic Benchmark Exercise on FIPLOC Verification Experiment F2 in BMC, Experimental Phases 2, 3, and 4 - Specification for Phase II, Battelle-Institut e.V., Frankurt/Main, Germany, July 1990

4. Fischer, K., T., Schall, M., Wolf, L., 1993
"CEC Thermal-Hydraulic Benchmark Exercise on FIPLOC Verification Experiment F2 in BMC, Experiment F2 in BMC, Experimental Phases - Results for Phase 2, 3 and 4, Results of Comparisons, Final Report, EUR 14454 EN, 1993

5. Fischer, K., Hafner, W., Holzbauer, H., Kanzleiter, T., (1994)
"Experiments for Concerning Natural Convective Flows in Battelle Model Containment, Documentation of Measured Data"
(In German), Battelle Ingenieurtechnik GmbH, Eschborn, Germany, Technical Report V68270.2, Oct. 1994

6. T. Kanzleiter, 1988
"FIPLOC-Verification Experiments",
(In German), Battelle-Institut e. V., Frankfurt/Main, Germany, Final Report BIeV-R-66.614-01, March 1988

7. Langer G., Jenior R., Wentlandt H.G., 1979
"Experimental investigation of the hydrogen distribution in the containment of a LWR following a LOCA"
(In German), Battelle-Institut e. V., Frankfurt/Main, FRG, Report BF-R-63.363-3

8. Langer G., Baukal W., 1982

"Experimental investigation of the hydrogen distribution in a model containment (Preliminary Experiments II)"
(In German), BMFT-Research Contract 150.375, Battelle-Institut e. V., Frankfurt/Main, FRG, Report BF-R-64.036-3

9. Petersen, K., Pamme, H., Seyffarth, L., Wolf, L., (1994)
"Hydrogen Mixing by Natural Convection in PWR Containments"
(In German), atw 39 (1994), 758-769

10. L.Wolf, H. Holzbauer, M. Schall, 1994,
"Comparisons Between Multi-Dimensional and Lumped-Parameter GOTHIC Containment Analyses with Data" International Conference on New Trends in Nuclear System Thermohydraulics, Pisa, Italy, May 30th - June 2nd, vol. 2, pp. 321 - 330.

11. L. Wolf, M. Gavrilas, K. Mun, 1996,
"Overview of Experimental Results for Long-Term, Large-Scale Natural Circulations in LWR-Containments after Large LOCAs"
Final Report for DOE - Project, Order Number: DE-AP07-96ID10765, Department of Materials and Nuclear Engineering, University of Maryland at College Park, July 1996.

## 9.C.2.2 DESCRIPTION OF THE AVAILABLE NUPEC DATA BASE

### 9.C.2.2.1 M-7-1 Test

NUPEC's Hydrogen Mixing and Distribution Test M-7-1 is used as OECD/CSNI sponsored International Standard Problem Exercise ISP-35 ( report NEA/CSNI/R(94)29 ) to compare and validate the performance of various computer codes. The WGOTHIC code is included among the codes that have been compared to this test (see ref. report NEA/CSNI/R(94)29 ). A detailed presentation of the M-7-1 test is not provided because the test is not directly applicable to the AP600 or AP1000. Internal sprays, which are not used in the passive containment design, are active during the M-7-1 test. A more relevant NUPEC experiment, the M-4-3 test (reference T. Hirose, 1993), is performed without internal sprays. This test investigates the mixing behavior of hydrogen and steam injected into the lower containment compartment.

### 9.C.2.2.2 M-4-3 Test

The test facility represents one quarter of a linearly scaled PWR (four-loop) containment model with 25 inner compartments. The approximate volume is 1600 $m^3$ with a height of 17.4 m and an inner diameter 10.8 m. Of the total volume, only 1300 $m^3$ is used. The dome compartment is approximately 70 percent of the total volume. Twenty-four smaller compartments occupy from 0.1 percent to 4 percent of the total volume. The

containment walls are made of steel plates (concrete structures are not present), so that the response of the heat sinks was very fast. The external containment wall is 12 mm thick steel and is insulated. Three floors are located at the 3.2, 5.4, and 7.3 m levels. A large sump is located below the lowest floor. A gas supply system for steam and helium, a containment internal spray supply system, and measuring systems for temperature, helium concentration, and pressure are installed.

The M-4-3 test simulates a break inside the lower D loop of the steam generator compartment. This compartment is at the first level of the containment. Figures 9.C.2-32, 9.C.2-33, and 9.C.2-34 illustrate the containment compartments and their corresponding numbers on each level. Figure 9.C.2-32 also shows the location of the break and typical circulation patterns.

The M-4-3 test starts with a pressure of 101.35 kPa and an initial containment temperature of 30°C. A mixture of steam and helium is injected at a constant flow rate during the first 30 minutes. The mass flow rates simulating a small break are 0.33 kg/s and 0.027 kg/s for the steam and helium, respectively. The inflow temperatures are 140°C and 20°C for the steam and helium, respectively.

Experimental data is recorded for 2 hours. The atmosphere and wall temperatures, the helium concentrations in the various compartments, and the pressure inside the dome are recorded. The pressure inside the dome increases almost linearly during the release and reaches 1.6 bar after 30 minutes (end of the release). The total mass of the steam released is 594 kg. Following the release, pressure decreases slowly to 1.5 bar (after 2 hours - see Figure 9.C.2-35). The dome temperature increases from 303 to 341°K during the release and then decreases to 334°K (see Figure 9.C.2-36). The dome helium concentration history is presented in Figure 9.C.2-37.

The temperature and helium concentrations increase first near the release point and the compartments above it, indicating an upward flow direction. This is followed by increases in the dome and steam generator compartments at the opposite side of the containment, indicating a downward flow loop direction. The global circulation loop is closed in the lower level of the containment. The consecutive positions of the higher temperatures and the helium concentration fronts indicate the flow path due to the global circulation during the break release (see Figure 9.C.2-38, from 0 - 1800 seconds).

A comparison of the temperatures and helium concentration histories in various compartments, Figure 9.C.2-38, shows the direction of the formed global circulation loop during the break release. One flow path starts in compartment 8, followed by compartments 15, 21, 25 (dome), 14, and 7. Following break release, the temperature field stratifies but the temperature difference between the dome and first floor level is not greater than 14°C at the end of the experiment. After the break release, the temperatures in all the compartments slowly decrease, despite the fact that the outer surface of the containment is insulated. Figure 9.C.2-38b shows that the concentration in the containment starts to homogenize after the end of the release (1800 seconds). This indicates that natural circulation effects are active after the end of release.

Note that the external walls of the containment are insulated and the interior walls are made of steel. This limits their ability to accumulate energy and act as a heat sources (which would promote natural circulation) later in the test. The natural circulation that exists after the end of release is most likely formed by the presence of the hot sump at the bottom of the containment.

Throughout the test, global circulation is present inside the containment and contributes to the homogenization of the atmosphere over time.

**Application to AP600 and AP1000**

This test is similar to the AP600 and AP1000 plant configurations in both the position of the injection point (break at the low level) and the geometry of the containment (70 percent of the volume is dome). However, overriding the similarities are the absence of concrete structures (able to store heat and later act as heat sources) and cooling on the outer surface of the containment shell. These features make the test very dissimilar to the passive containment design. The external cooling and the hot concrete structures, positioned in the lower portion of the passive containment produce strong global circulation and decrease the effects of thermal stratification.

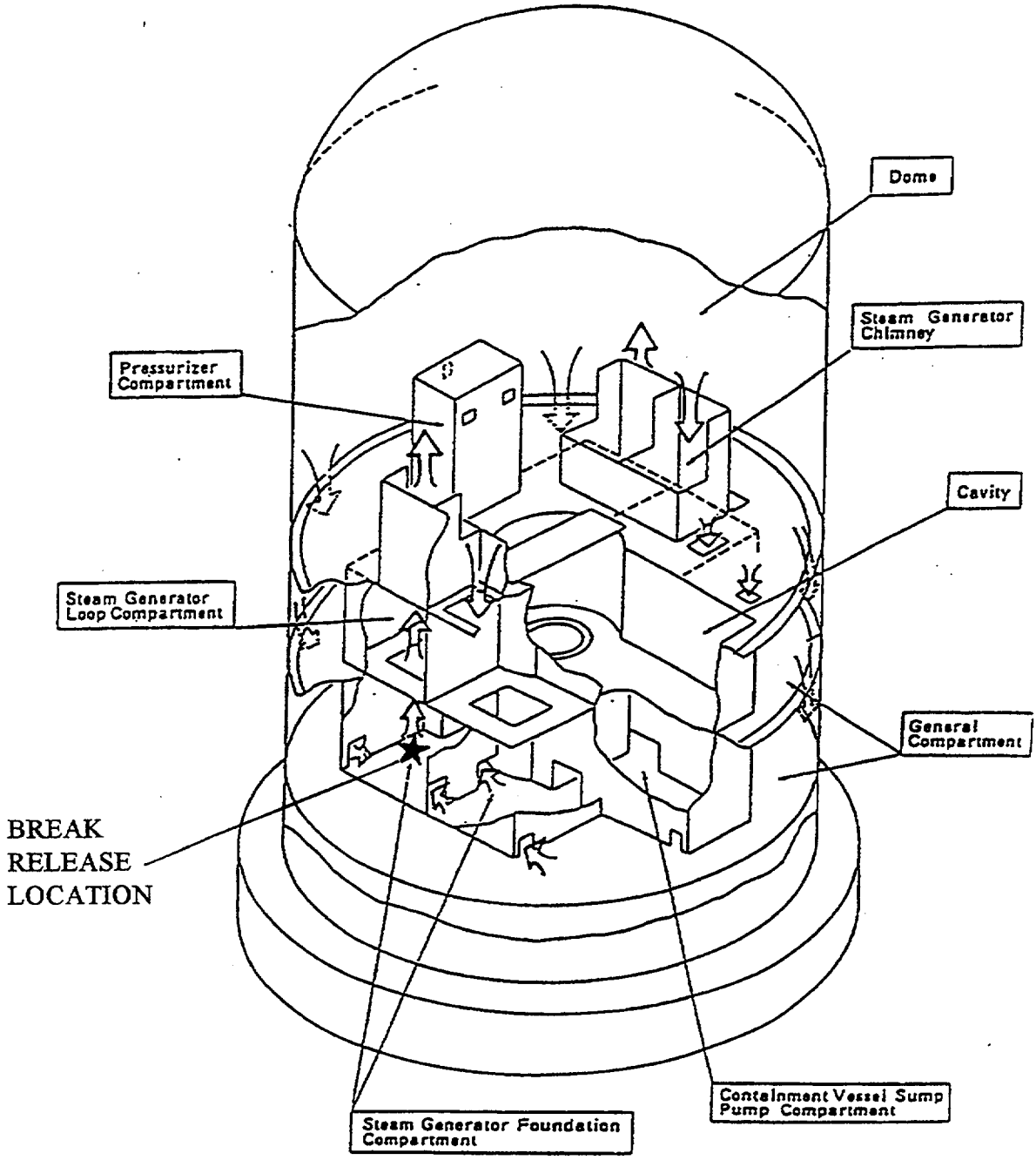


**Figure 9.C.2-32** **Model containment used in the test, break-release position, and circulation flow paths (see arrows)**

**(Figure prepared according to T. Hirose documentation for M-4-3 test data, NUPEC Nuclear Power Engineering Corporation, ISP35-035, 30 April, 1993)**

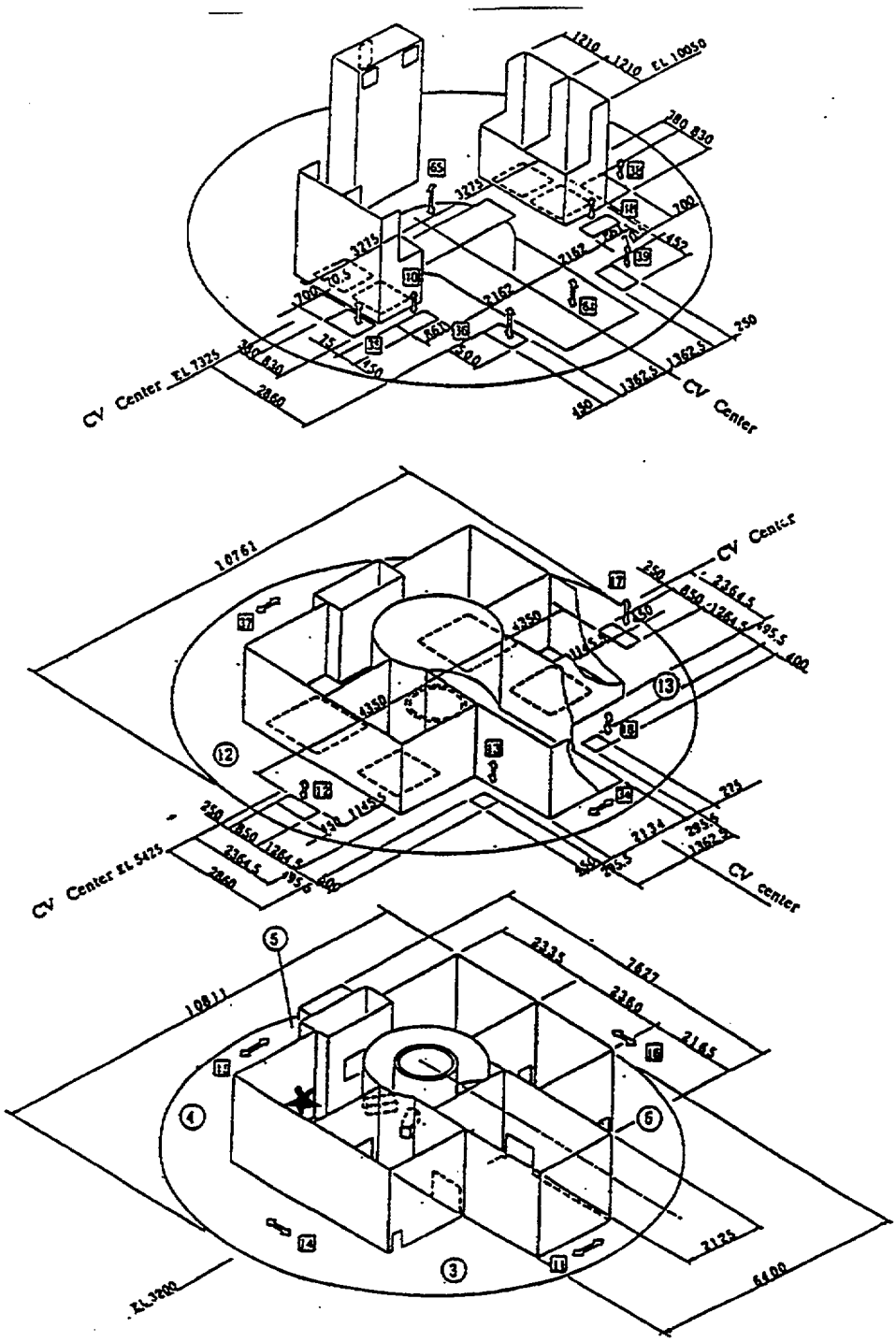


**Figure 9.C.2-33 Detailed arrangement of each floor**

**(Figure prepared according to T. Hirose documentation for M-4-3 test data, NUPEC Nuclear Power Engineering Corporation, ISP35-035, 30 April, 1993)**

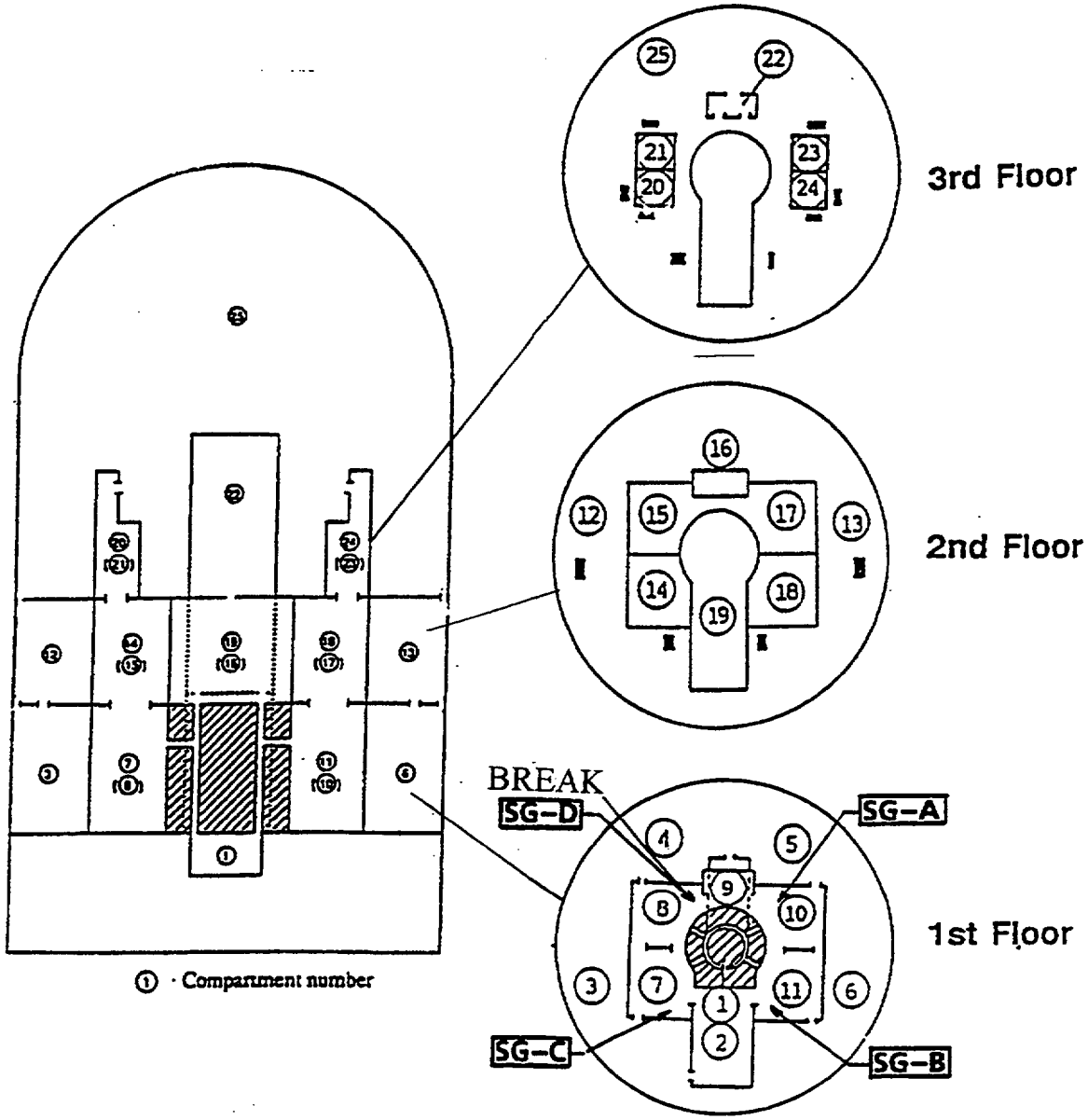


**Figure 9.C.2-34 Distribution of the compartments at each floor**

**(Figure prepared according to T. Hirose documentation for M-4-3 test data, NUPEC Nuclear Power Engineering Corporation, ISP35-035, 30 April, 1993)**

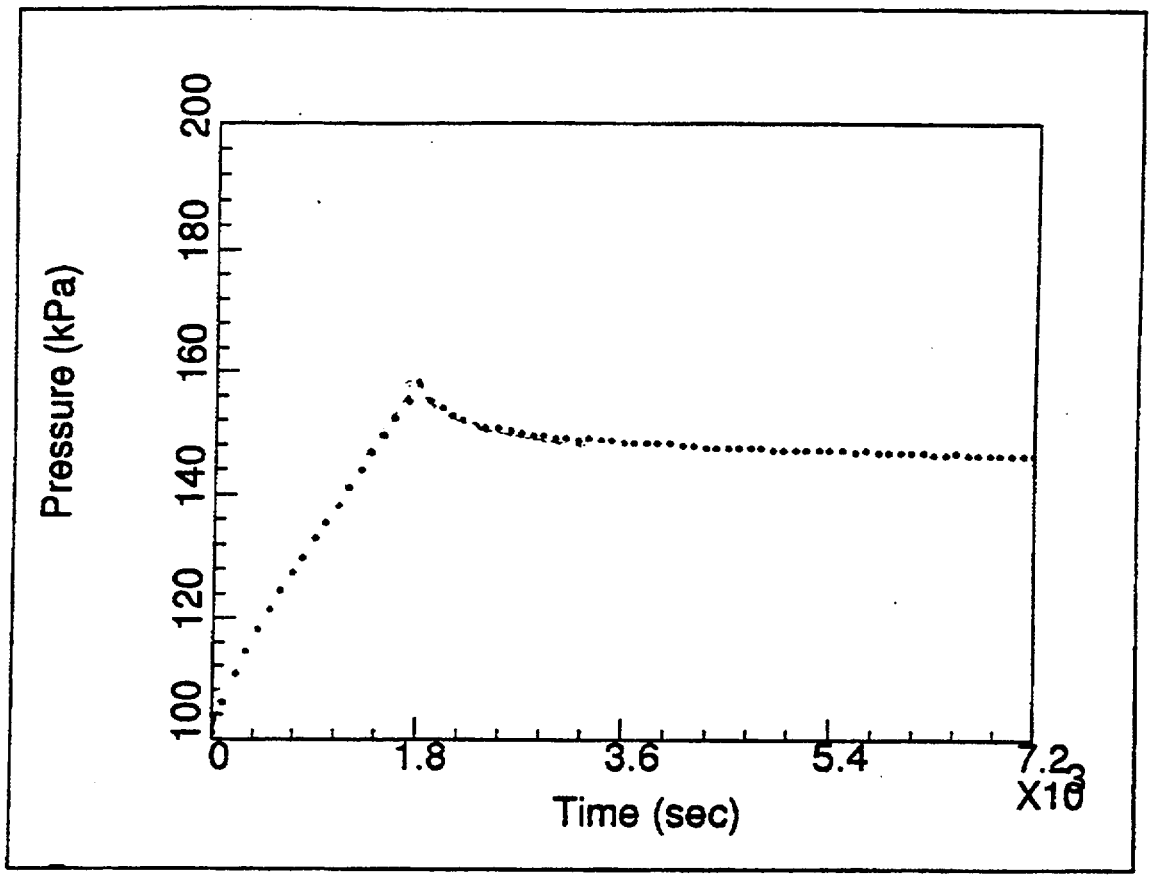


**Figure 9.C.2-35 Pressure history**

**(Figure prepared according to T. Hirose documentation for M-4-3 test data, NUPEC Nuclear Power Engineering Corporation, ISP35-035, 30 April, 1993)**

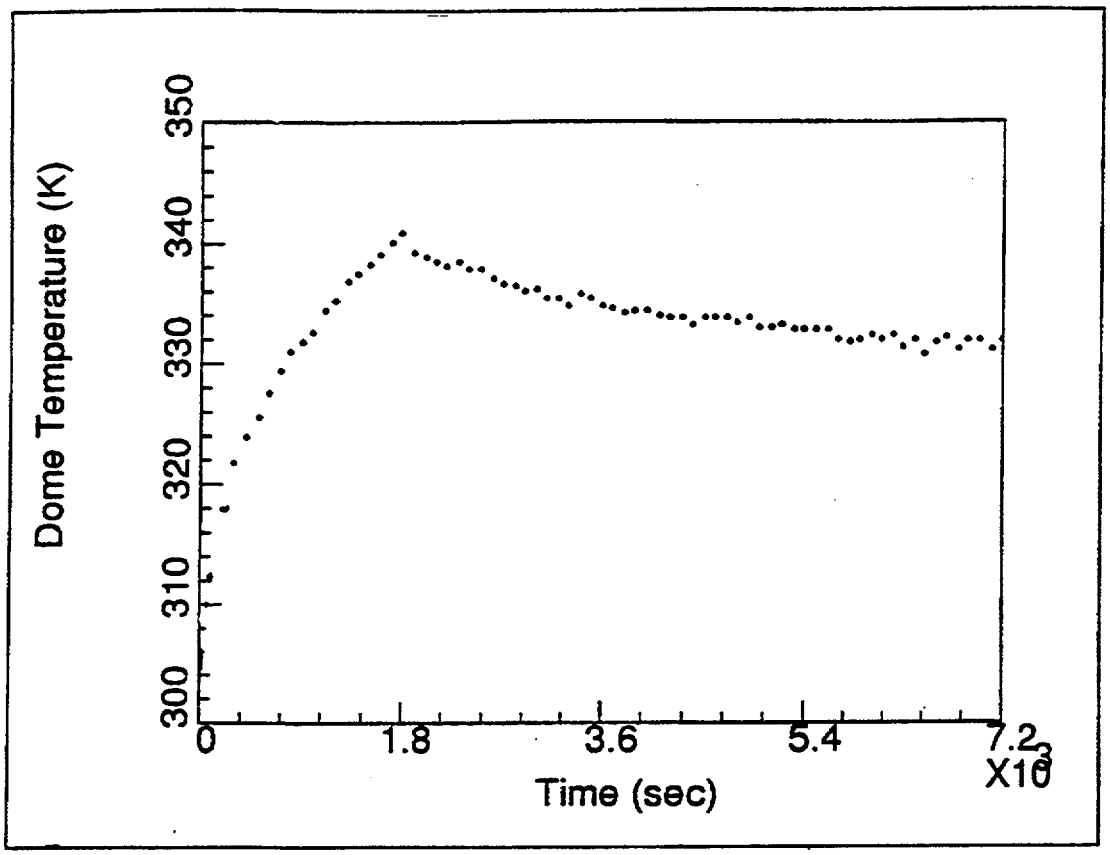


**Figure 9.C.2-36 Dome temperature history**

**(Figure prepared according to T. Hirose documentation for M-4-3 test data, NUPEC Nuclear Power Engineering Corporation, ISP35-035, 30 April, 1993)**

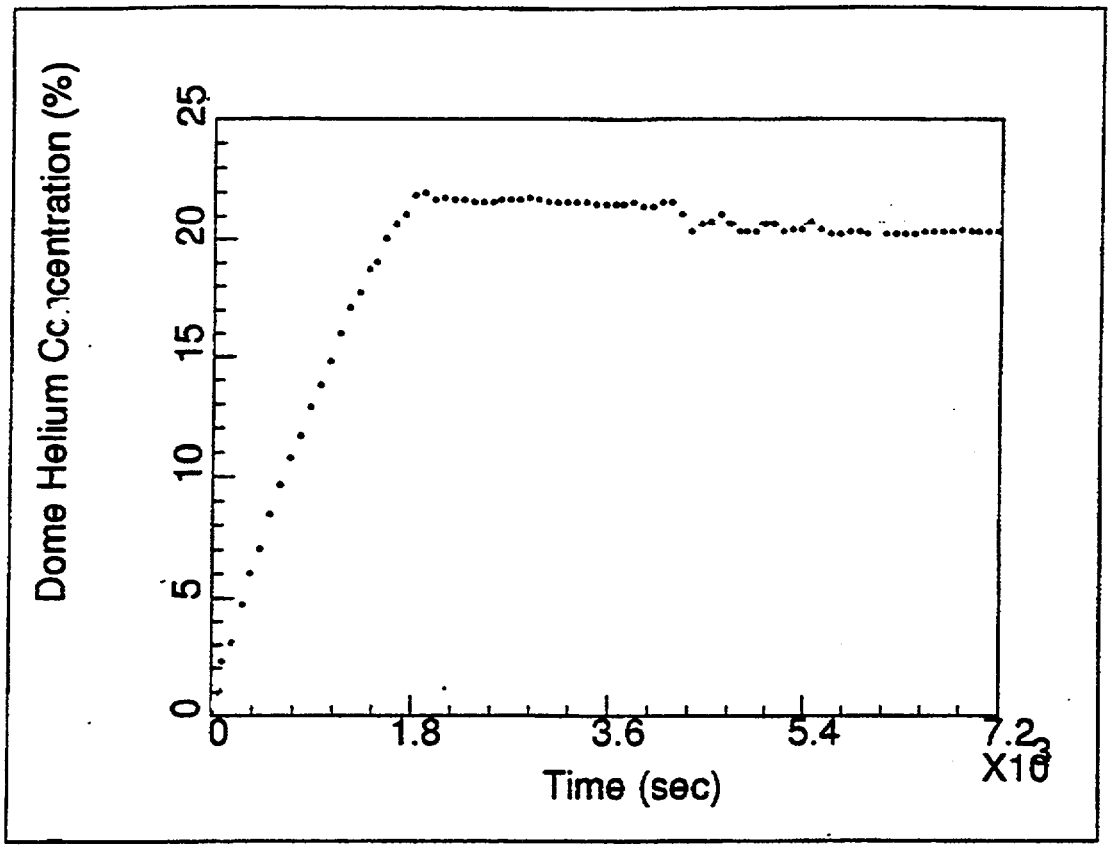


**Figure 9.C.2-37 Dome Helium Concentration history**

**(Figure prepared according to T. Hirose documentation for M-4-3 test data, NUPEC Nuclear Power Engineering Corporation, ISP35-035, 30 April, 1993)**

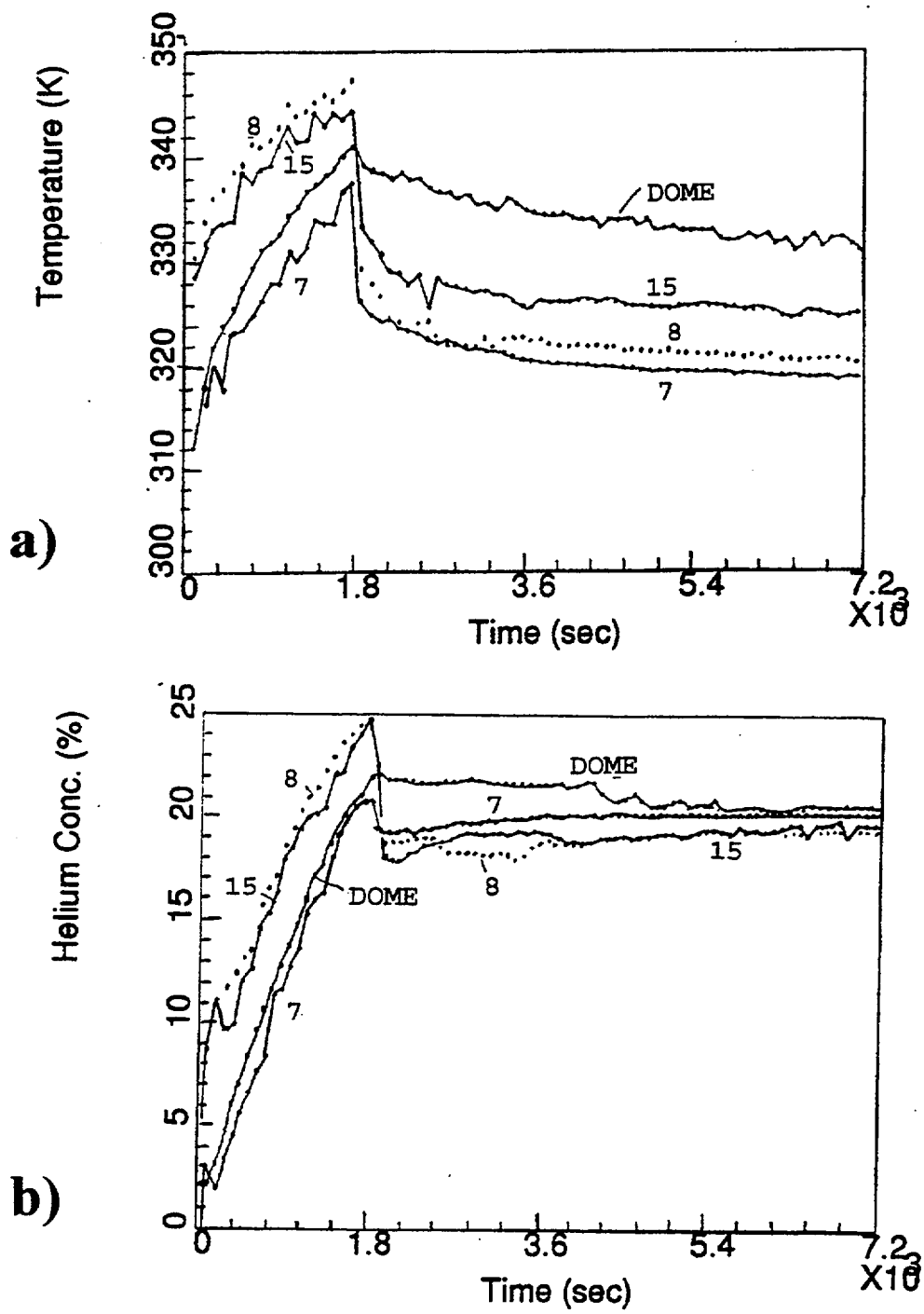


**Figure 9.C.2-38** **a) Temperature histories for compartments forming a circulation path (8, 15, dome and 7) b) Helium concentration histories for compartments forming a circulation path (8, 15, dome and 7)**

**(Figure prepared according to T. Hirose documentation for M-4-3 test data, NUPEC Nuclear Power Engineering Corporation, ISP35-035, 30 April, 1993)**

### 9.C.2.2.3 References

1. NEA/CSNI/R(94)29: Final comparison report on ISP-35: NUPEC hydrogen mixing and distribution test (Test M-7-1), Committee on the safety of nuclear installations OECD Nuclear Energy Agency, December 1994

2. Tadashi Hirose (1993): Letter, floppy disk which contains the M-4-3 test data, an attached document, and a video-cassette, NUPEC Nuclear Power Engineering Corporation, ISP35-035, 30 April, 1993

## 9.C.2.3 DESCRIPTION OF THE AVAILABLE CAROLINAS VIRGINIA TUBE REACTOR CONTAINMENT (CVTR) DATABASE

The results of the simulated DBA of CVTR containment system are presented in (Schmitt et al., 1970). The CVTR containment is made of reinforced concrete (see Figure 9.C.2-39). It is cylindrical in shape with an internal diameter of 57 ft 11 - 1/2 in and an inside height of 114 ft. The cylindrical wall is 2 feet thick. At the top of the cylinder is a hemispherical dome made of 1/2-inch thick steel covered by 20.5 inches of concrete. The structure is divided in three regions (operating, intermediate, and basement). The free volume is about 227,000 $ft^3$. A water spray system is installed at the 360 foot elevation (6 inches above the containment bend line).

Three simulated DBA tests are performed. The first test does not use the water sprays. The pressure and temperature histories are obtained to establish the effects of the sprays on pressure reduction. The remaining tests include active water sprays with flow rates 290 and 500 gpm, respectively. The water spray flow rate is adjusted by changing the total number of nozzles in the spray header. The spray flow is initiated 30 seconds after the end of steam injection and remains in operation for 12 minutes. The second and third tests are not applicable to passive containment DBA situations due to the spray effects.

Superheated steam, at approximately 10°F above the saturation temperature, is injected into the containment. The steam is released above the operating floor through a diffuser made of a 10 foot pipe installed vertically on the discharge nozzle of the steam line (see Figure 9.C.2-40). The end of the pipe is capped. The pipe contains approximately 126 holes (with 1-inch diameter) that direct the steam horizontally (see Figure 9.C.2-40). The injection continues until the containment pressure reaches 17.5 psig above the atmospheric pressure.

To obtain the containment response, measurements of the interior pressure are made using seven fast response pressure transducers and a Heise gauge. The containment atmospheric temperature is measured by 34 thermocouples and 15 resistance thermometers. Two additional thermocouples and pressure transducers are located in two partially isolated regions (the reactor header cavity and the refueling canal) to determine their thermal and pressure response. Twenty three thermocouples are positioned at the containment liner envelope and the interior surfaces to obtain the temperature response of the interior concrete sections. The heat transfer through the liner wall of the operating region of the containment is established using heat flow devices along with thermocouples that measure the temperature distribution in the cross-section of the wall. The weight of condensate collected from the selected areas of the cylindrical liner walls is also measured.

The mass flow rates of steam for the three DBA tests range from 360,000 to 380,000 lb/hr (see Figures 9.C.2-41 a, b, c). The injection steam conditions are near to saturated conditions with an enthalpy of 1196 Btu/lb. The steam is injected in the operating region at 335 ft elevation. The duration of the release

is approximately 180 seconds. The measurements are taken for approximately two hours, but only the first 50 minutes are presented in the report.

Containment pressure histories for the three DBA tests are presented in Figure 9.C.2-24. The influence of the spray application and the intensity of the sprays on the decrease of the containment pressure is obvious.

The containment vertical temperature profiles for various tests are presented in Figures 9.C.2-43, 9.C.2-44 and 9.C.2-45, respectively. For the first test, large vertical temperature gradients exist for the duration of the measurements (about two hours), indicating temperature stratification. The containment air recirculation system is activated one and half hours after the beginning of the first test and it decreases the vertical temperature gradients (but not so efficiently as water sprays).

The spray tests (tests 2 and 3 - which are not applicable for passive containment designs) contribute towards the uniformity of the containment atmosphere by decreasing the dome temperatures. After one hour, the dome temperatures were 177, 155, and 137°F for tests 1, 2, and 3, respectively.

One hundred minutes of test data from thermocouples mounted at the same horizontal level inside the operating region are analyzed. Significant temperature gradients are not established in the horizontal direction. This is consistent with the view that stratification gradients are mainly in a vertical direction, with negligible horizontal gradients, except near plumes and wall boundary layers.

Liner vertical temperatures are almost the same as the temperatures in the upper regions of the containment atmosphere, while they are higher than temperatures in the atmosphere of the lower regions (see Figures 9.C.2-46 and 9.C.2-47 for lower regions). An explanation for the higher liner temperatures in the lower regions is that the steam, in its downward movement, passed through the annular gap near the containment wall (surrounding the operating floor) releasing heat predominantly to the wall instead of the atmosphere.

Data from six thermocouples embedded in concrete surfaces in the containment are presented in Figure 9.C.2-48 for the case without sprays. The operating region structures have a large temperature increase, while the basement region is almost unaffected. The results are in agreement with the atmospheric and liner temperature data and show stratification above the break elevation.

The results from two thermocouples installed in two partially isolated regions (the reactor header cavity and the fuel transfer canal) are presented in Figure 9.C.2-49. A small temperature increase is seen during the steam injection. After the injection, temperatures decrease very fast, resulting in the very small final

temperature increase. The data also indicates that dead-ended compartments get some steam during the pressure increase.

The reasons for the established temperature stratification in the case of the CVTR containment test performed without internal sprays are:

- The position of the release point is above the 335 foot elevation of containment height see Figure 9.C.2-39). This could be considered as a release in the upper region of the containment ($H_r/H_t$ = 0.525).

- The external walls and the dome of the containment were made of 23-3/4" thick concrete which accumulated a portion of the heat released in the upper regions (operational region and intermediate region - see Figure 9.C.2-48 for vertical temperature distribution inside the liner). The upper portions of the walls remain hot as containment cools, producing boundary conditions for a stable stratification.

- External spray cooling of the dome and walls (upper half exposed to the air) is not applied.

- The steam condensate is collected in the buckets so that weight of the condensate can be measured. This eliminated hot sump evaporation and heat source effects. The other experiments (BMC and HDR) indicate that even small temperature differences between the sump (as a heat source at the lowest level) and the containment atmosphere generate global natural circulation inside the containment.

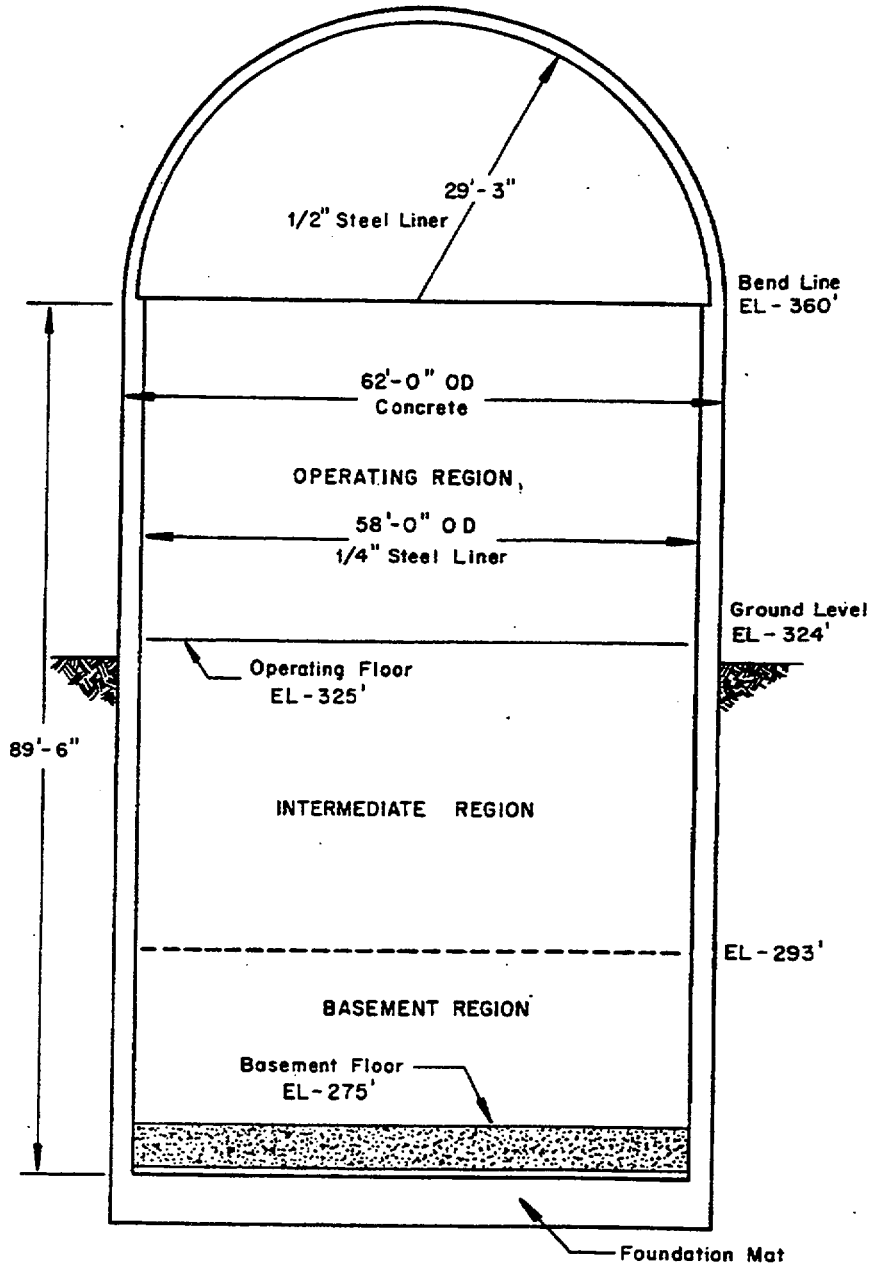


**Figure 9.C.2-39 Carolinas Virginia Tube Reactor (CVTR) containment structure**

**(reprinted from: R.C. Schmitt, G.E. Bingham, J.A. Norberg, "Simulated design basis accident tests of the Carolinas Virginia Tube Reactor Containment - Final report", Prepared for the U.S. Atomic Energy Commission, Idaho Operations Office, Under Contract No. AT(10-1)-1230)**

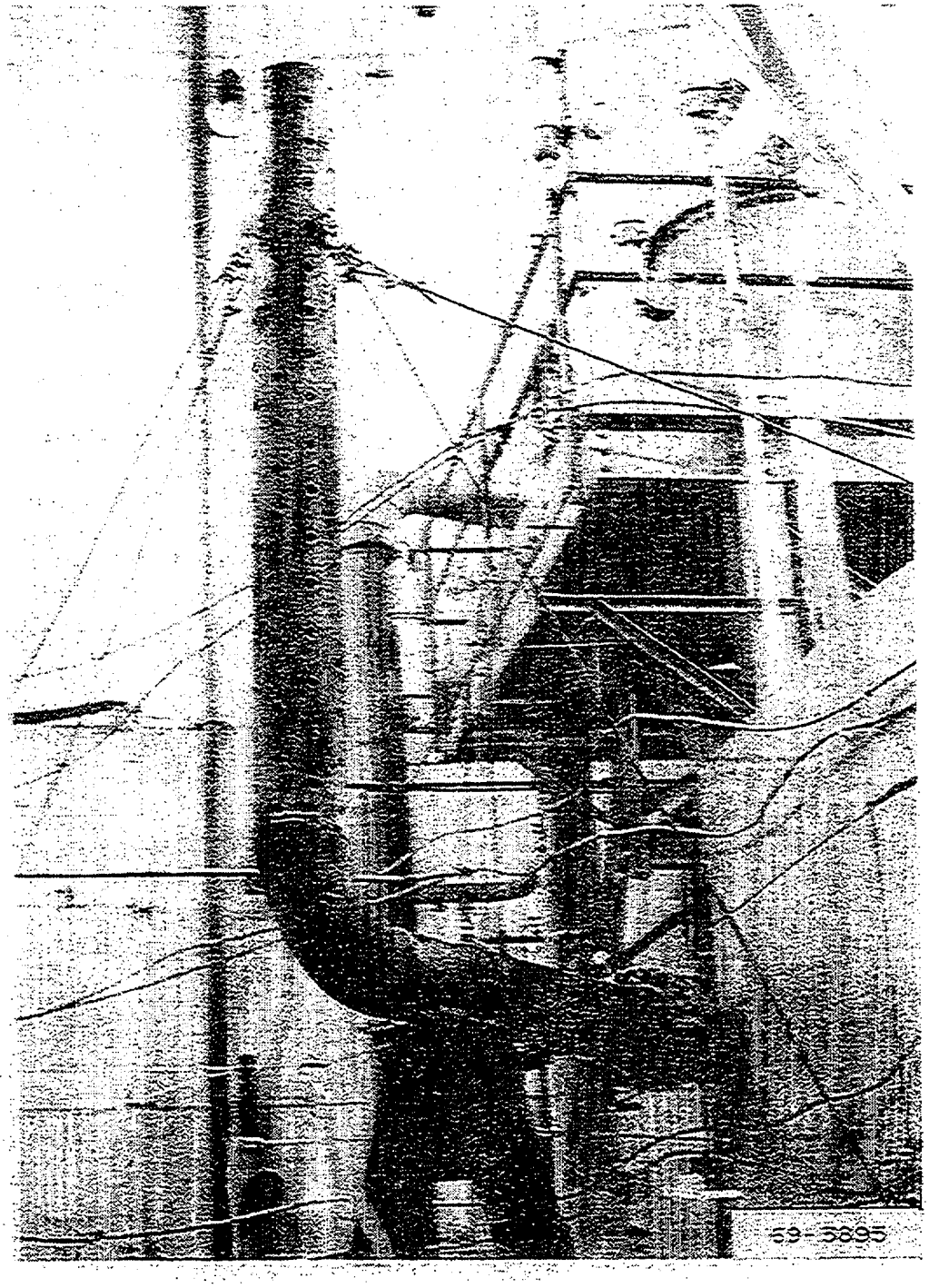


**Figure 9.C.2-40 CVTR steam line diffuser**

**(reprinted from: R.C. Schmitt, G.E. Bingham, J.A. Norberg, "Simulated design basis accident tests of the Carolinas Virginia Tube Reactor Containment - Final report", Prepared for the U.S. Atomic Energy Commission, Idaho Operations Office, Under Contract No. AT(10-1)-1230)**

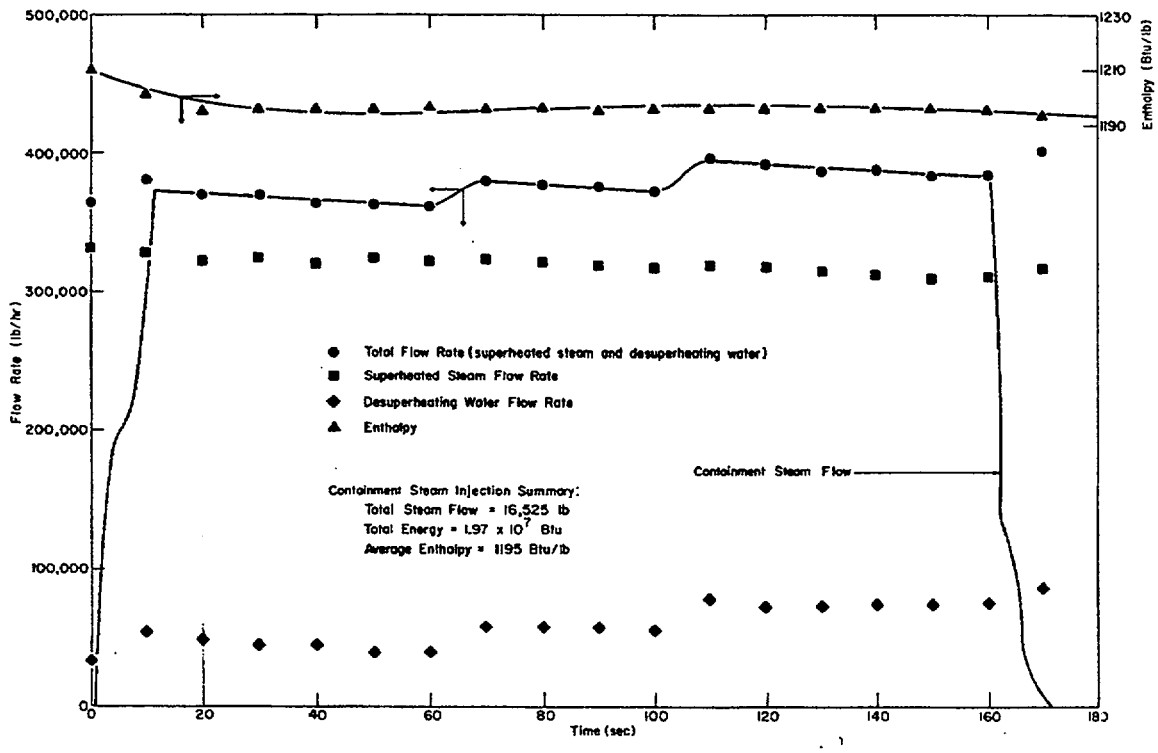


**Figure 9.C.2-41a Steam injection histories test 1**

**(reprinted from: R.C. Schmitt, G.E. Bingham, J.A. Norberg, "Simulated design basis accident tests of the Carolinas Virginia Tube Reactor Containment - Final report", Prepared for the U.S. Atomic Energy Commission, Idaho Operations Office, Under Contract No. AT(10-1)-1230)**

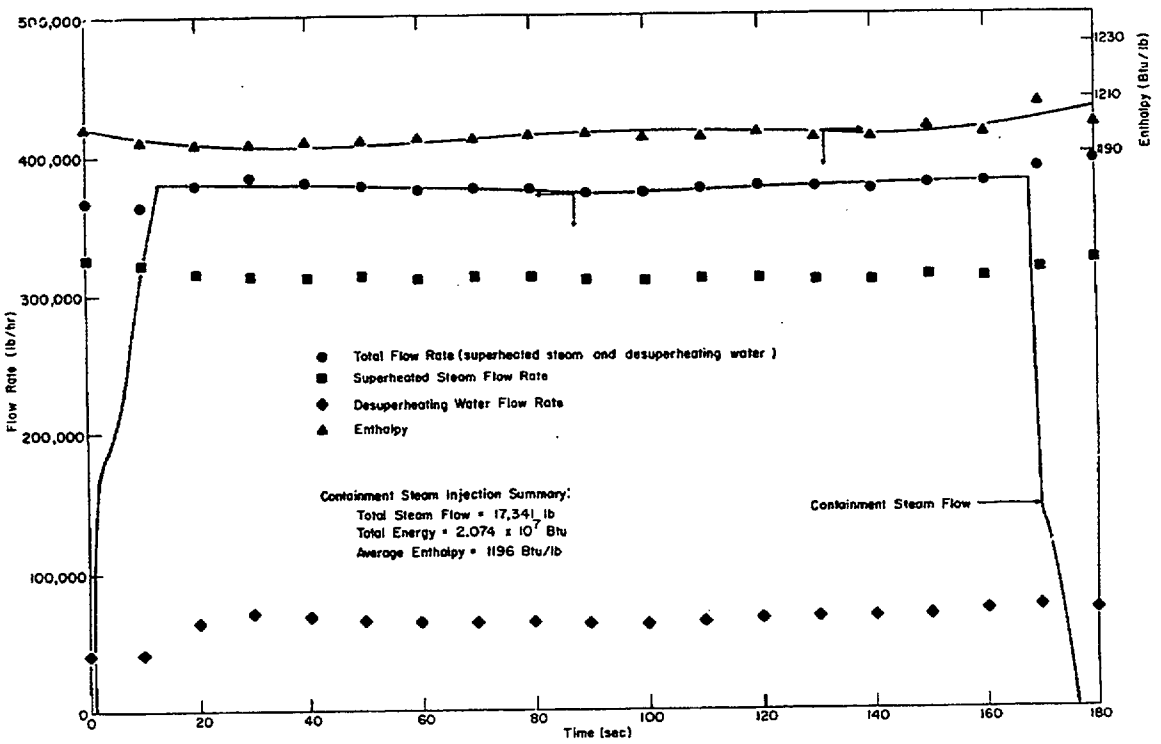


**Figure 9.C.2-41b Steam injection histories test 2**

**(reprinted from: R.C. Schmitt, G.E. Bingham, J.A. Norberg, "Simulated design basis accident tests of the Carolinas Virginia Tube Reactor Containment - Final report", Prepared for the U.S. Atomic Energy Commission, Idaho Operations Office, Under Contract No. AT(10-1)-1230)**

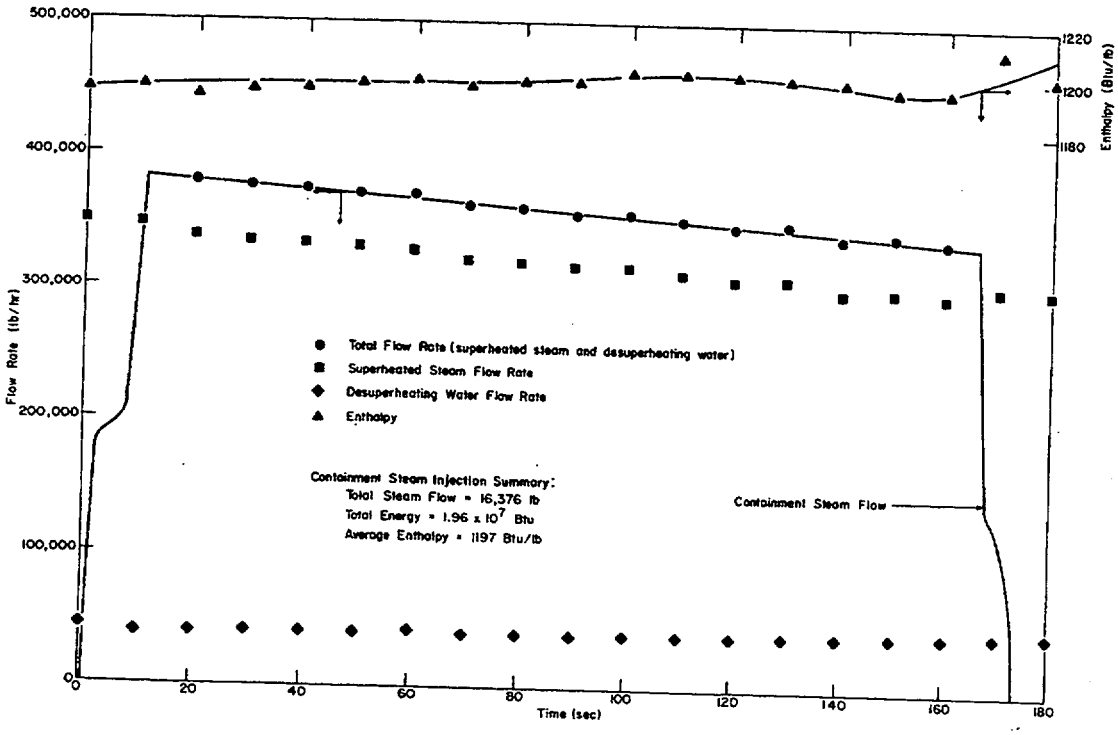


**Figure 9.C.2-41c Steam injection histories test 3**

**(reprinted from: R.C. Schmitt, G.E. Bingham, J.A. Norberg, "Simulated design basis accident tests of the Carolinas Virginia Tube Reactor Containment - Final report", Prepared for the U.S. Atomic Energy Commission, Idaho Operations Office, Under Contract No. AT(10-1)-1230)**

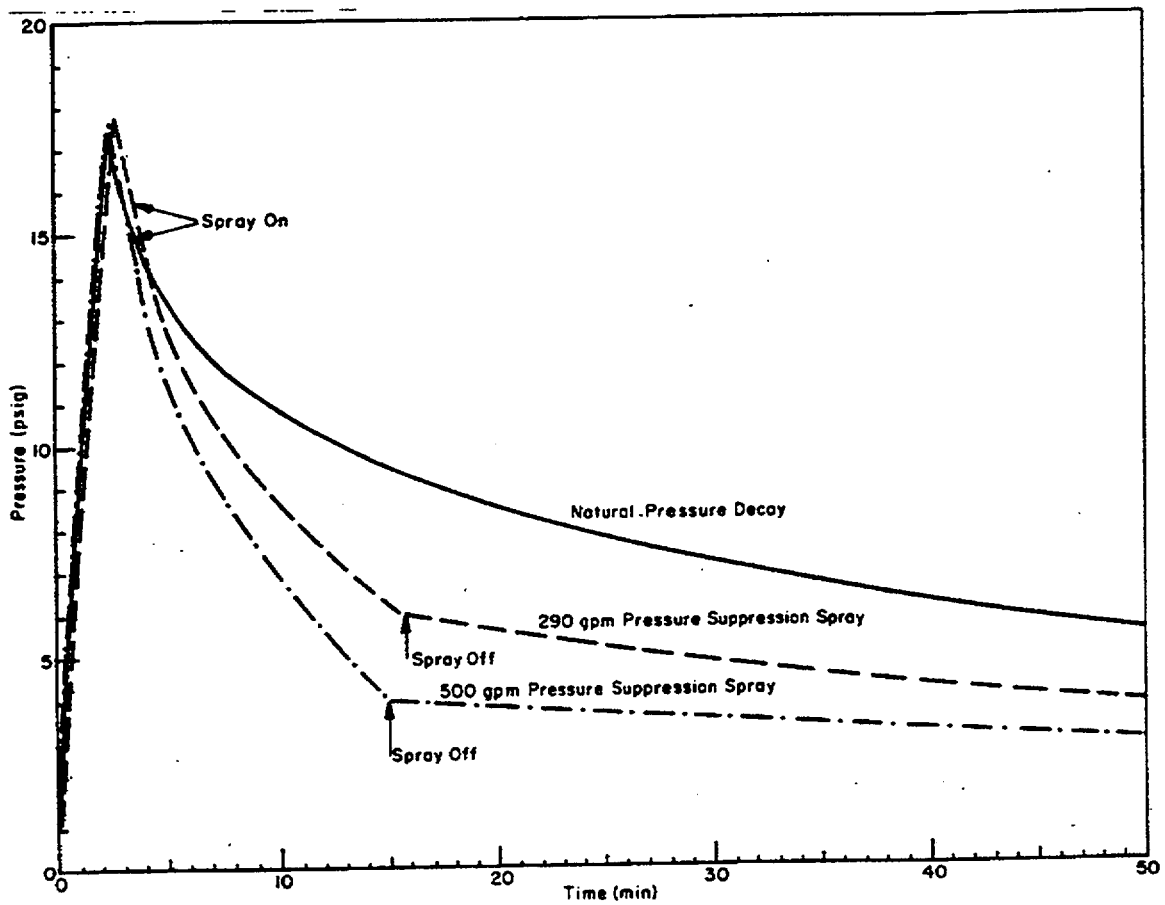


**Figure 9.C.2-42 CVTR containment pressure response (Heise gauge)**

**(reprinted from: R.C. Schmitt, G.E. Bingham, J.A. Norberg, "Simulated design basis accident tests of the Carolinas Virginia Tube Reactor Containment - Final report", Prepared for the U.S. Atomic Energy Commission, Idaho Operations Office, Under Contract No. AT(10-1)-1230)**

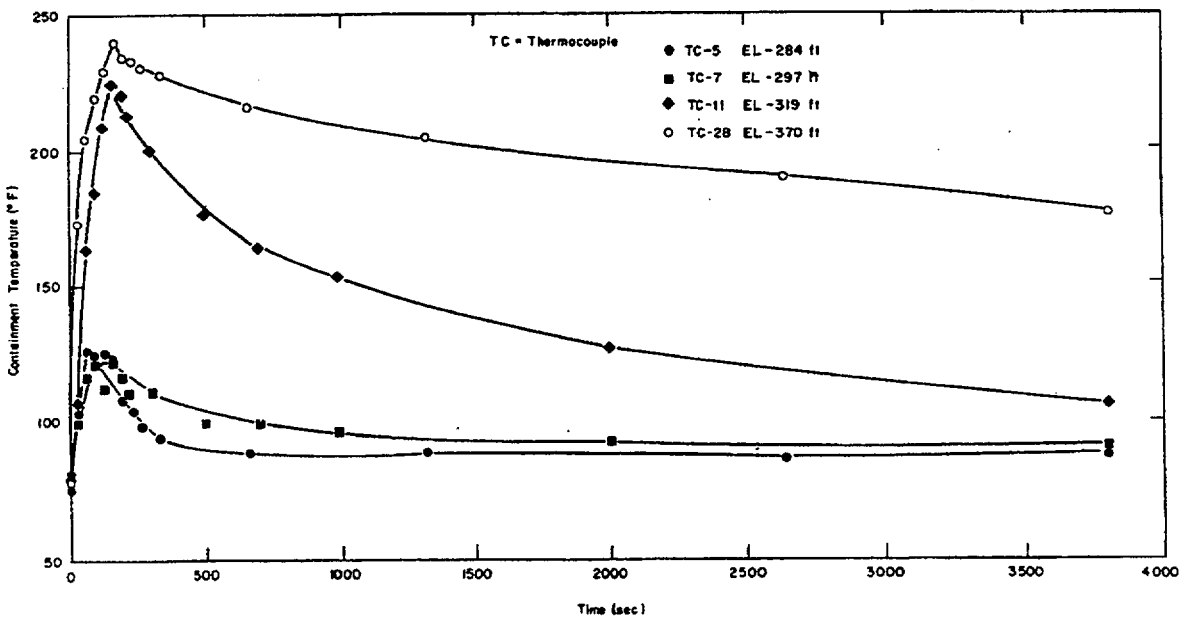


**Figure 9.C.2-43 Atmospheric vertical temperature profile, test 1**

**(reprinted from: R.C. Schmitt, G.E. Bingham, J.A. Norberg, "Simulated design basis accident tests of the Carolinas Virginia Tube Reactor Containment - Final report", Prepared for the U.S. Atomic Energy Commission, Idaho Operations Office, Under Contract No. AT(10-1)-1230)**

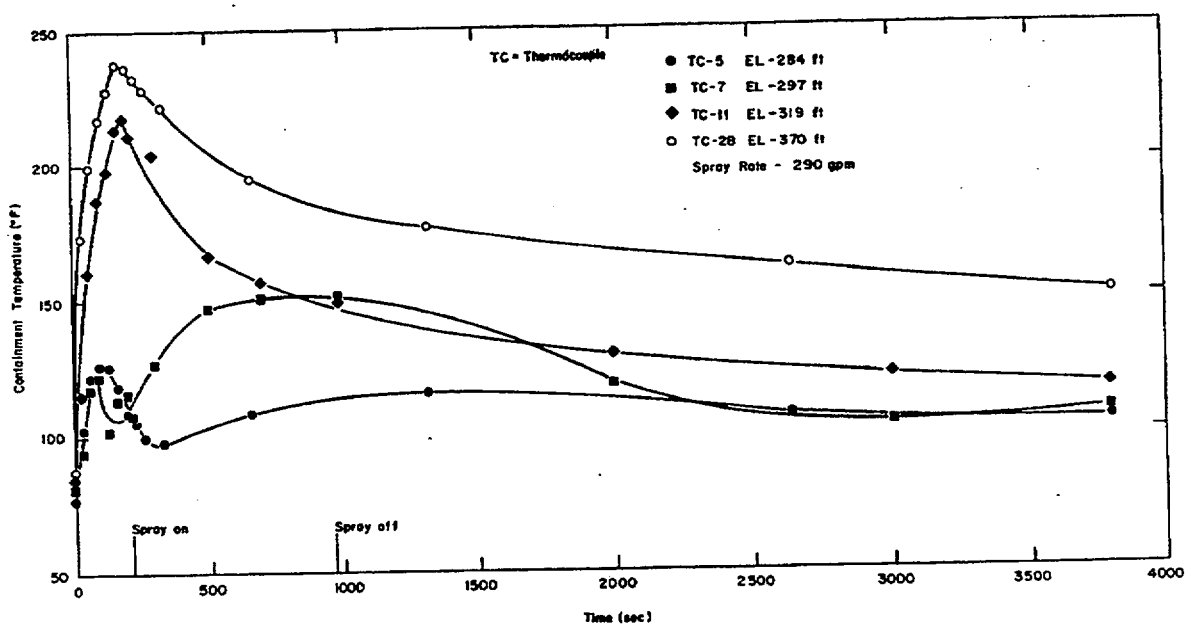


**Figure 9.C.2-44 Atmospheric vertical temperature profile, test 2**

**(reprinted from: R.C. Schmitt, G.E. Bingham, J.A. Norberg, "Simulated design basis accident tests of the Carolinas Virginia Tube Reactor Containment - Final report", Prepared for the U.S. Atomic Energy Commission, Idaho Operations Office, Under Contract No. AT(10-1)-1230)**

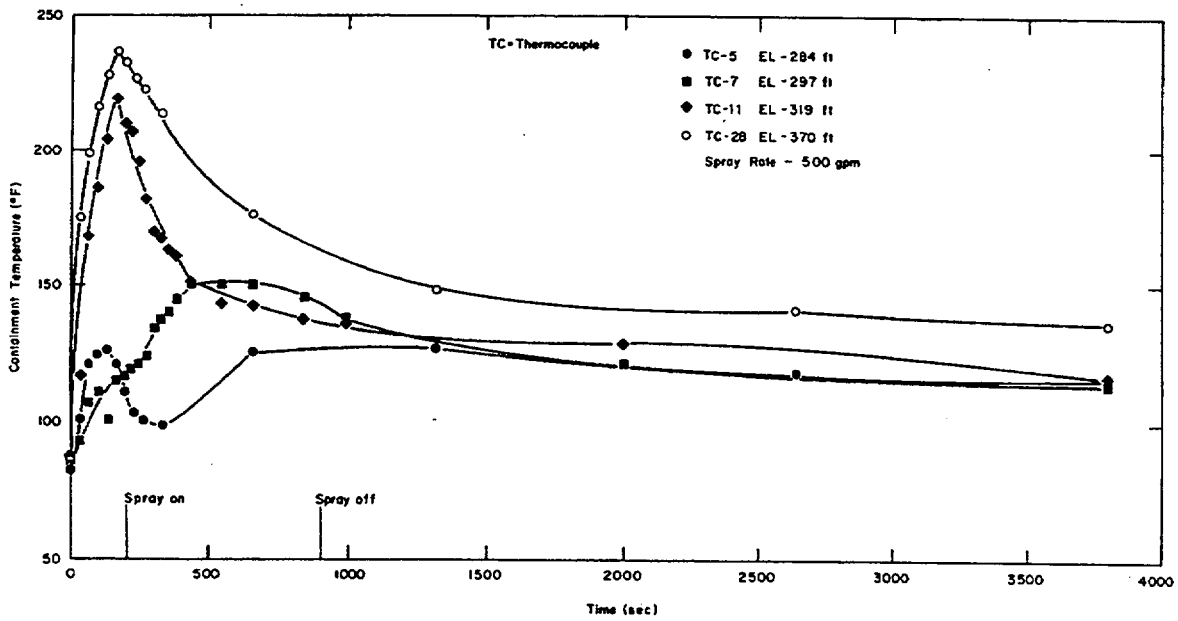


**Figure 9.C.2-45 Atmospheric vertical temperature profile, test 3**

**(reprinted from: R.C. Schmitt, G.E. Bingham, J.A. Norberg, "Simulated design basis accident tests of the Carolinas Virginia Tube Reactor Containment - Final report", Prepared for the U.S. Atomic Energy Commission, Idaho Operations Office, Under Contract No. AT(10-1)-1230)**

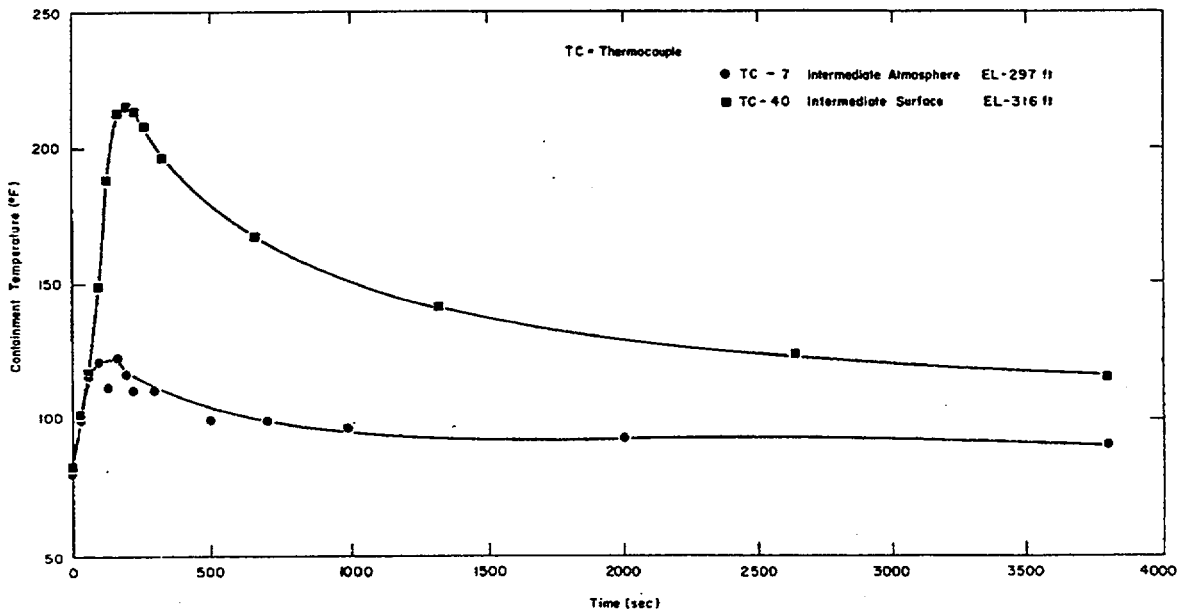


**Figure 9.C.2-46 Surface and atmosphere temperatures - intermediate region, test 1**

**(reprinted from: R.C. Schmitt, G.E. Bingham, J.A. Norberg, "Simulated design basis accident tests of the Carolinas Virginia Tube Reactor Containment - Final report", Prepared for the U.S. Atomic Energy Commission, Idaho Operations Office, Under Contract No. AT(10-1)-1230)**

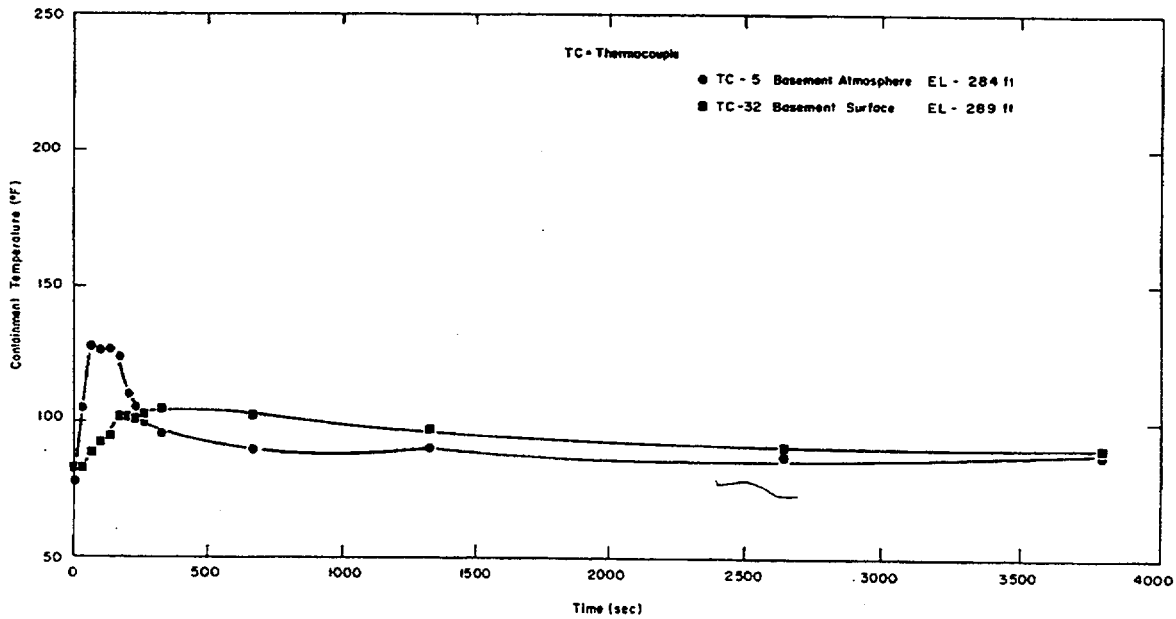


**Figure 9.C.2-47 Surface and atmosphere temperatures - basement region, test 1**

**(reprinted from: R.C. Schmitt, G.E. Bingham, J.A. Norberg, "Simulated design basis accident tests of the Carolinas Virginia Tube Reactor Containment - Final report", Prepared for the U.S. Atomic Energy Commission, Idaho Operations Office, Under Contract No. AT(10-1)-1230)**

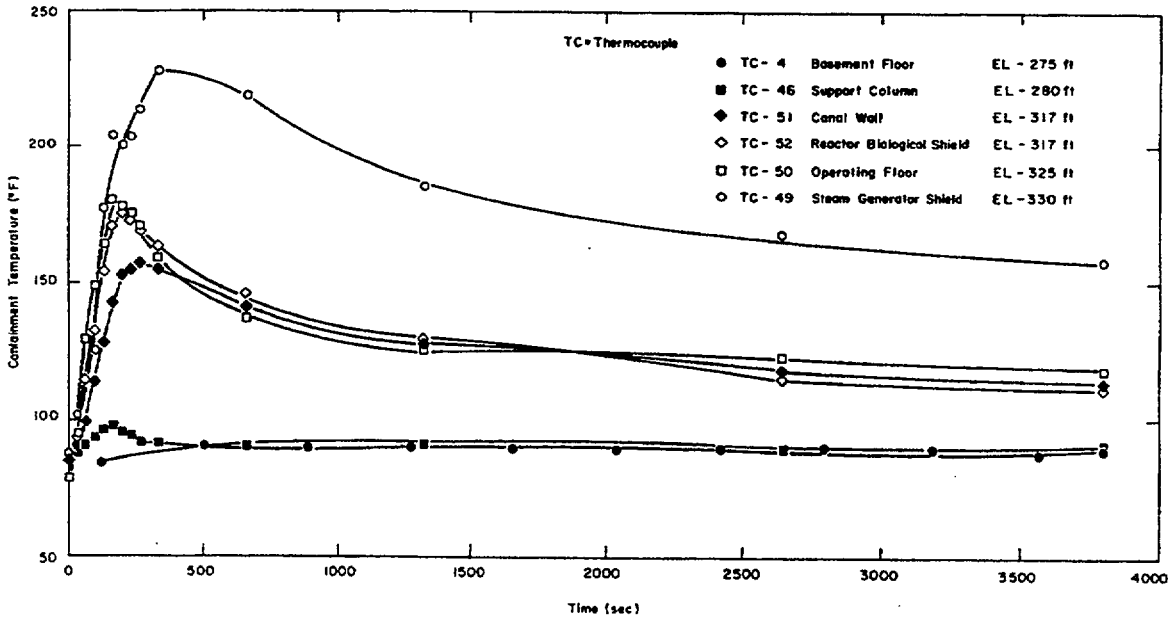


**Figure 9.C.2-48 Concrete surface temperatures, test 1**

**(reprinted from: R.C. Schmitt, G.E. Bingham, J.A. Norberg, "Simulated design basis accident tests of the Carolinas Virginia Tube Reactor Containment - Final report", Prepared for the U.S. Atomic Energy Commission, Idaho Operations Office, Under Contract No. AT(10-1)-1230)**

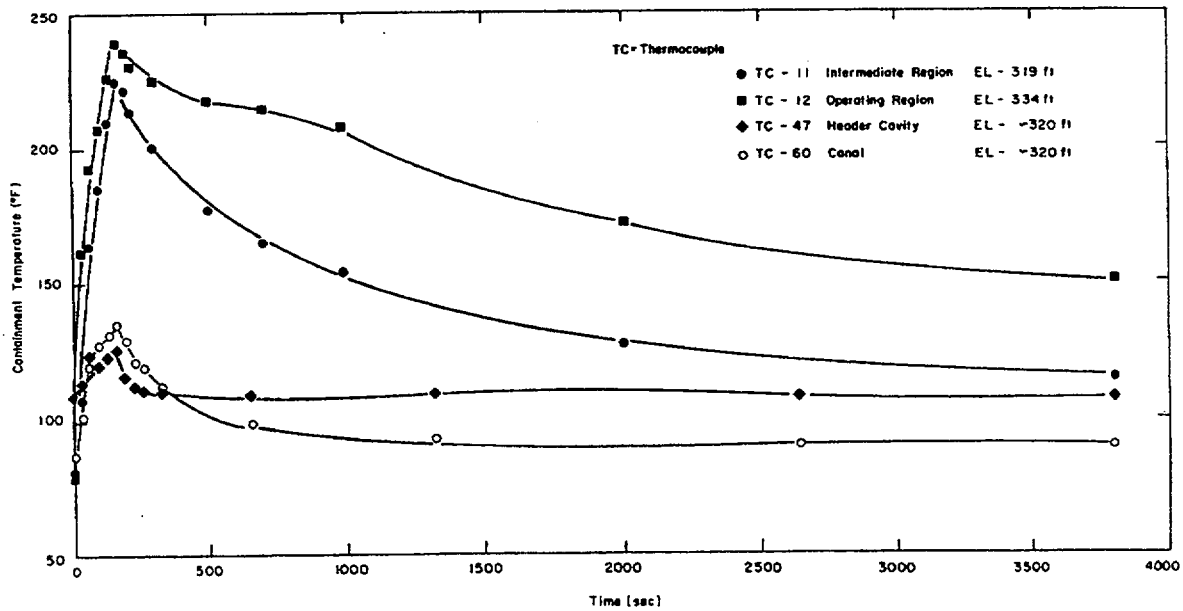


**Figure 9.C.2-49 Isolated containment region temperatures**

**(reprinted from: R.C. Schmitt, G.E. Bingham, J.A. Norberg, "Simulated design basis accident tests of the Carolinas Virginia Tube Reactor Containment - Final report", Prepared for the U.S. Atomic Energy Commission, Idaho Operations Office, Under Contract No. AT(10-1)-1230)**

## 9.C.2.4 DESCRIPTION OF THE AVAILABLE HDR DATABASE

The HDR containment (Figure 9.C.2-50) is 20 m in diameter and 60 m high with a total free volume of 11,300 $m^3$. It is made of steel and concrete with a total surface area of 30,000 $m^3$ available for heat transfer (condensation). The dome volume, including a crane structure, is about 42 percent of the total volume or 5,000 $m^3$. The main and spiral staircase form the dominant vertical flow paths connecting the dome with sump. The containment can be subdivided into 62 to 72 subcompartments containing pipes, pumps, and valves etc. The subcompartments are interconnected by numerous openings. The numbers and locations of thermocouples and anemometers for the HDR-E test series are presented in Figure 9.C.2-51.

### 9.C.2.4.1 HDR E11 Test Series

Test group E11 (the hydrogen distribution and mixing experiments) is included as a part of the HDR-Safety Program Phase III that was conducted in the summer of 1989 (Cron and Schrammel, 1993). This test series simulated severe accident scenarios. The tests provide insights on DBA circulation and stratification. A review of the natural circulation flows formed in experiments E11.0 - E11.5 is presented in Wolf et al., 1996. Circulation is indicated by examination of the recorded temperatures and velocities.

Seven of the eight E11 experiments are initiated with small steam releases. The one exception, the E11.5 experiment, is initiated with a large-break, two-phase LOCA blowdown. The tests provide data for the transient and spatial distribution of the gas concentration (hydrogen/helium mixture) under various initial and boundary conditions.

The following features are considered:

- The large scale of the experimental facility and the multi-compartment geometry with a relatively large dome
- High hydrogen release rates typical of severe accidents
- Superheated steam injection into the containment - single and multiple steam and hydrogen injection phases
- Internal concrete and metal structures and surfaces
- Different axial positions for hydrogen and steam releases

- The efficiency of hydrogen mitigating features, including venting (for example blockage of one major vertical flow path)
- The impact of internal and external sprays
- Sump heat up effects
- Air heater operation effects

#### 9.C.2.4.1.1 Experiment E11.0

Experiment E11.0 is performed with an external steam supply and without a gas mixture release. However, the external steam supply is not able to produce typical severe accident conditions. Therefore, a blowdown of the primary system is used for all other experiments. The results of E11.0 are not discussed here.

#### 9.C.2.4.1.2 Experiment E11.1

Experiment E11.1 includes a high-positioned, small break LOCA, followed by additional steam and gas releases. The effectiveness of the internal spray for decreasing the pressure and temperature inside the containment is also tested. Since this experiment included internal sprays that are not a part of the passive containment design, the results are not discussed here.

#### 9.C.2.4.1.3 Experiment E11.2

Experiment E11.2 also includes a high-positioned release point. However, instead of internal spray as in experiment E11.1, external spray is applied to the dome shell. A detailed presentation of this experiment is given in Wolf, Mun, Floyd, 1995. This experiment, together with E11.4, provides results used as benchmark problems to validate numerical models (Wolf et al., 1994. The verification of the GOTHIC code by Holzbauer and Wolf, 1994, is also based on E11.2 results.

Figure 9.C.2-52 provides the sequence of the experimental procedures. This includes the duration of the heatup and the blowdown of steam (p=110 bar and T=318°C) in the compartment R1805 (in the main stairway at elevation 21.05-25.3 m, see Figure 9.C.2-51, right side). The consecutive steam and gas (mixture of 85 percent He and 15 percent $H_2$) injections are also presented in Figure 9.C.2-52. Compartment 1405, in the spiral stairway at elevation 4.5 m (see Figure 9.C.2-52 right side), receives steam at 770 minutes.

The change in the containment pressure with time is shown in Figure 9.C.2-53. The temperatures, steam concentrations, and $He/H_2$ gas mixture concentrations at various axial positions of the main staircase are presented in Figures 9.C.2-54, 9.C.2-55, and 9.C.2-56, respectively. Temperature differences between the same axial positions of the two vertical flow paths (main and spiral staircases) are pronounced during the heatup phase. Later, temperature differences decrease and change signs. The crossing temperature histories in Figures 9.C.2-57, 9.C.2-58, 9.C.2-59, 9.C.2-60 indicate a change in the flow directions.

A steep thermal gradient indicates the presence of the stratification that exists between the lower compartments and the containment dome (see Figure 9.C.2-61). Even an additional steam release in the lower portion of the containment (compartment R1405) at 770 minutes is not able to completely eliminate the vertical thermal gradient, although it is greatly reduced.

The injection of steam into the lower level, together with the effects of cooling the dome with the external spray, causes redistribution of the $He/H_2$ gas mixture (see Figure 9.C.2-56). The increase in the gas concentration in the upper part of the dome is a consequence of the steam condensation on the inside dome surface. Later, the decrease in temperatures in the upper dome promote global circulation (causing unstable stratification) and homogenize the dome atmosphere. Even after the external spray is stopped, global circulation affects the lower parts of the containment (see Figures 9.C.2-54, 9.C.2-55, 9.C.2-56). Overall, the external spray causes a reduction of 0.44 bar in the containment pressure (see Figure 9.C.2-53).

The application of external sprays at the dome surface promotes global circulation, homogenizes hydrogen concentrations, and decreases the containment pressure. The water film applied to the external surface of the AP600 and AP1000 shell produces similar effects.

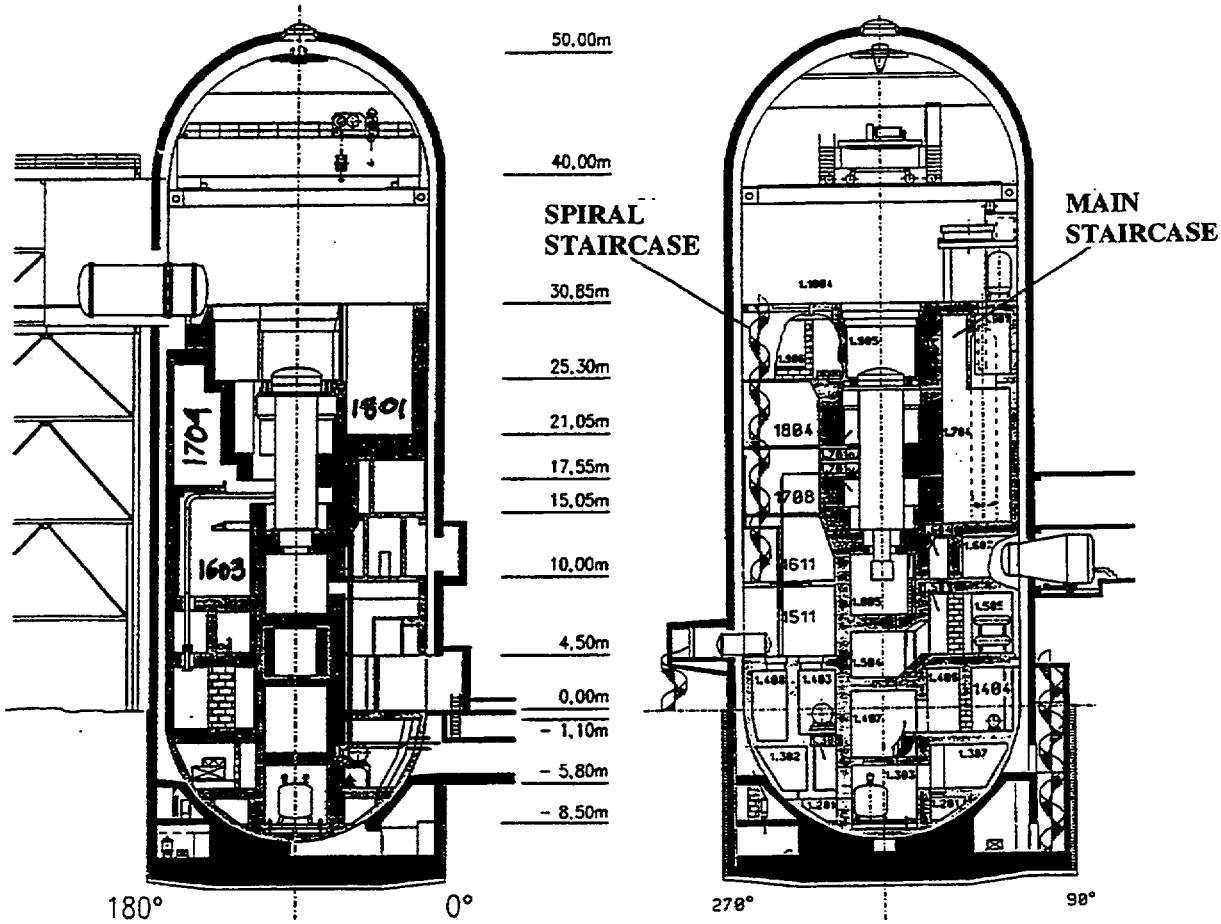


**Figure 9.C.2-50** **Cross-sections, elevations and numbers of compartments of the HDR containment, left (180°-0° cross-section), right (270°-90° cross-section)**

**(reprinted from: L. Wolf, K. Mun, J. Floyd, "HDR hydrogen mixing evaluation for containment safety evaluations" - Phase 1, University of Maryland at College Park, Final Report for DOE-Project Order Number: DE-AP07-951D81401, July 1995)**

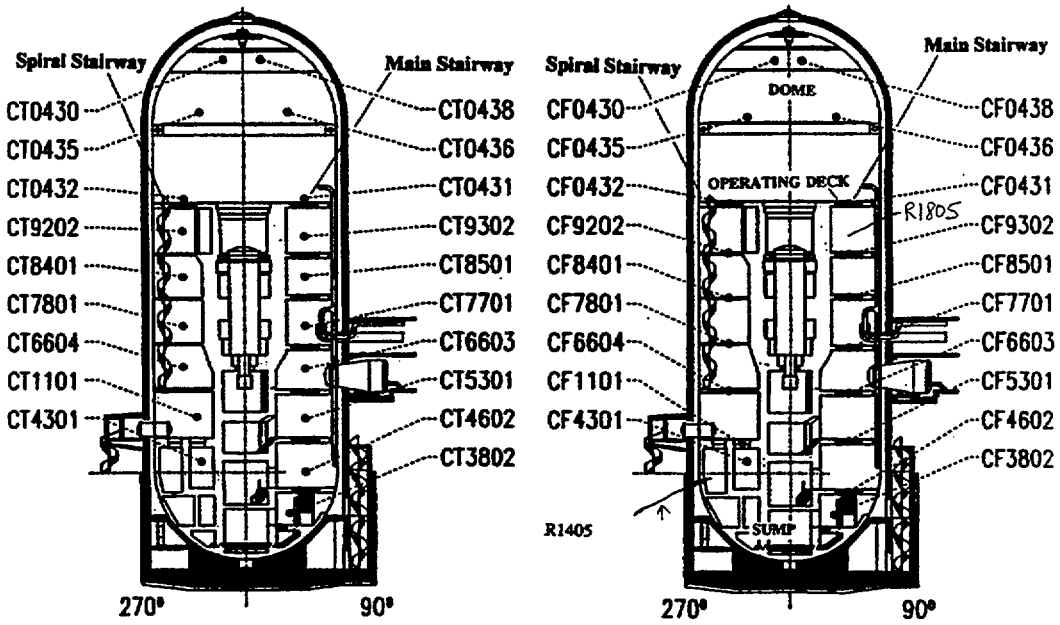


**Figure 9.C.2-51** **Locations and Enumerations of Thermocouples (left) and Anemometers (right) for HDR-E-Test Series**

**(reprinted from: L. Wolf, M. Gavrilas, K. Mun, "Overview of experimental results for long-term, Large-scale natural circulations in LWR-containments after large LOCAs", University of Maryland at College Park, Final Report for DOE - Project, Order Number: DE-AP07-96ID10765", July 1996)**

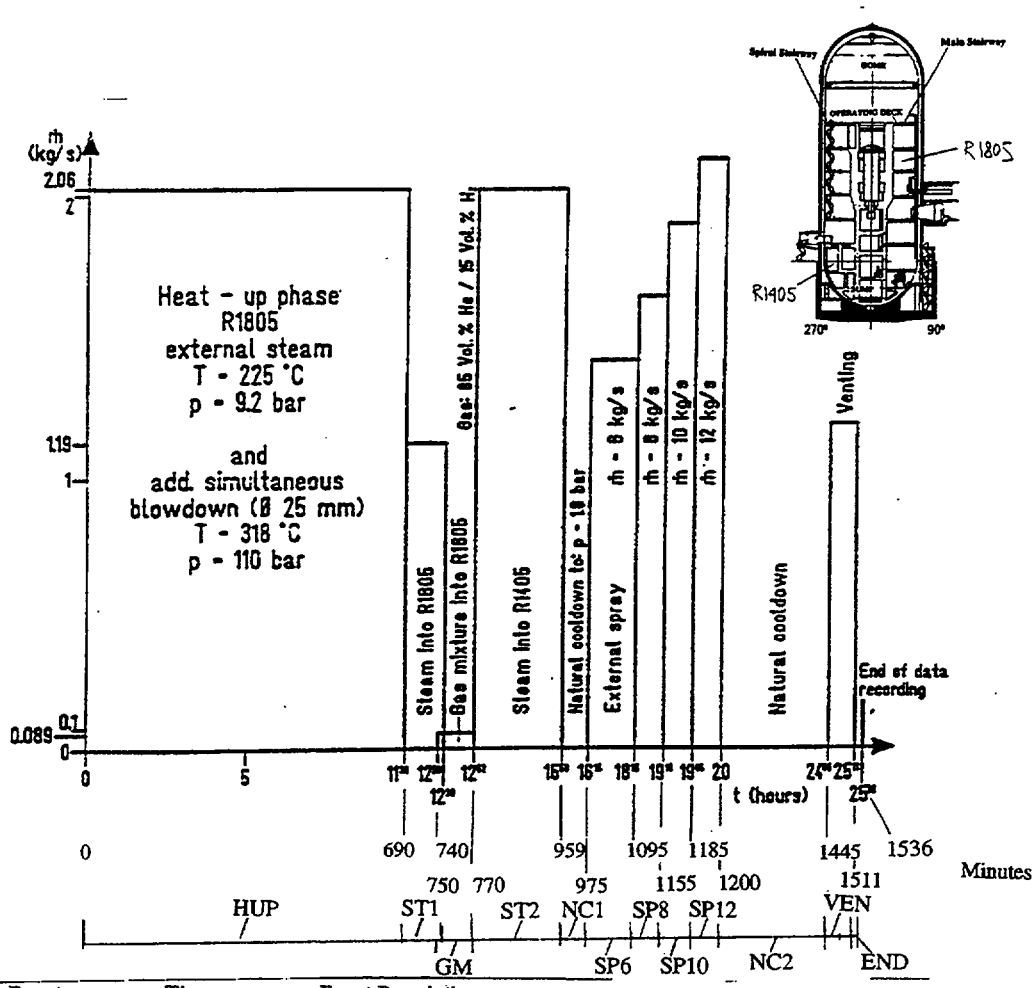


| Event | Time minutes | Event Description |
|---|---|---|
| HUP | 0-690 | RPV-blowdown plus external steam supply with m = 2.06 kg/s |
| ST1 | 690-750 | Reduced external steam with m = 1.19 kg/s in R1.805 |
| GM | 740-770 | $H_2$/He gas mixture release into R1.805 with 0.089 kg/s |
| ST2 | 770-959 | Steam release into R1.405 with 2.06 kg/s |
| NC1 | 959-975 | Natural cooldown |
| SP6 | 975-1095 | External spray m = 6 kg/s |
| SP8 | 1095-1155 | External spray m = 8 kg/s |
| SP10 | 1155-1185 | External spray m = 10 kg/s |
| SP12 | 1185-1200 | External spray m = 12 kg/s |
| NC2 | 1200-1445 | Natural cooldown |
| VEN | 1445-1511 | Containment venting |
| END | 1536 | End of data acquisition |

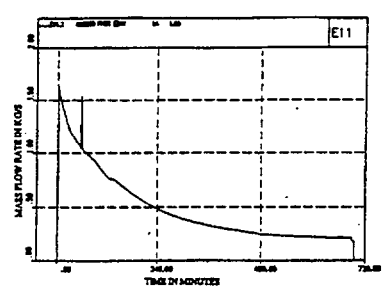


**Figure 9.C.2-52 HDR-E11.2 Sequence of Experimental Test Procedures**

**(reprinted from: L. Wolf, K. Mun, J. Floyd, "HDR hydrogen mixing evaluation for containment safety evaluations" - Phase 1, University of Maryland at College Park, Final Report for DOE-Project Order Number: DE-AP07-951D81401, July 1995)**

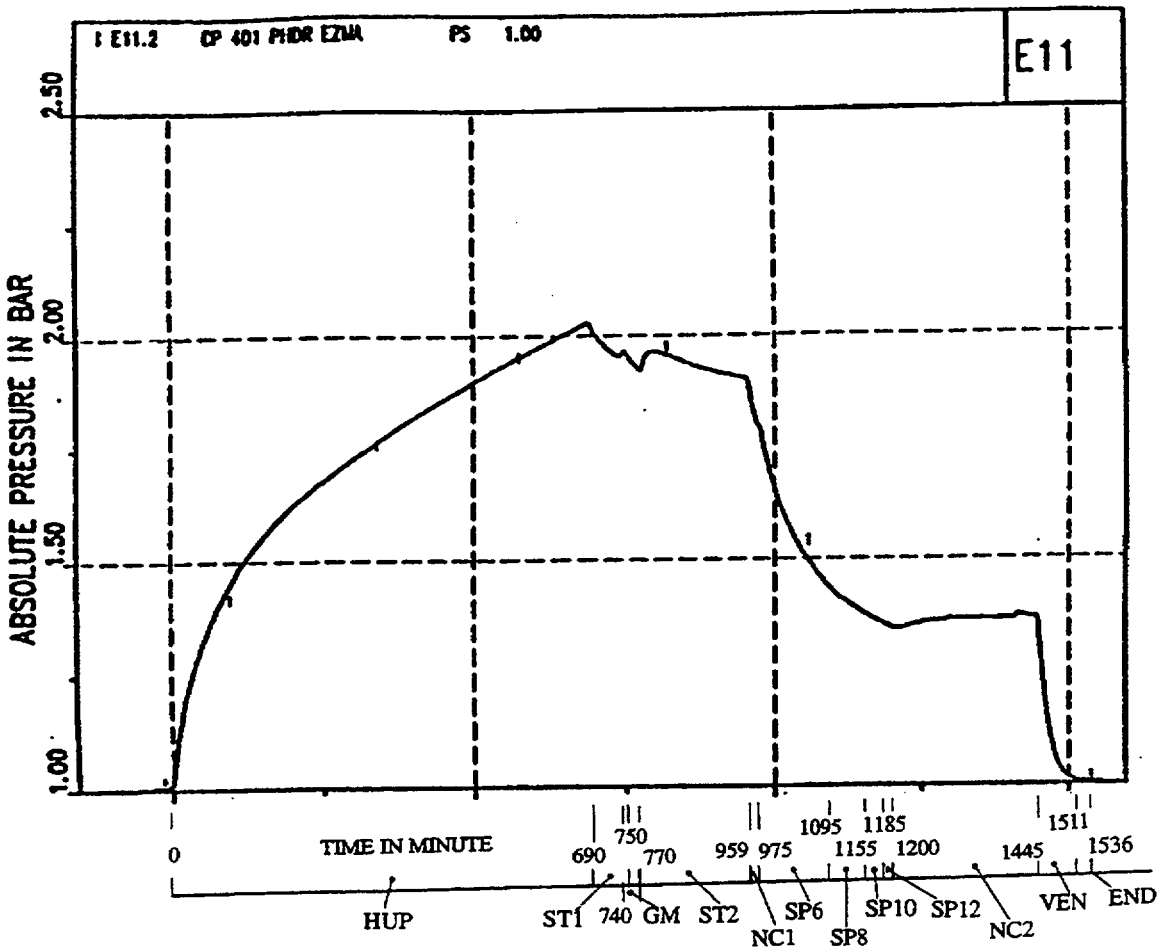


**Figure 9.C.2-53 HDR-E11.2 Containment pressure history**

**(reprinted from: L. Wolf, K. Mun, J. Floyd, "HDR hydrogen mixing evaluation for containment safety evaluations" - Phase 1, University of Maryland at College Park, Final Report for DOE-Project Order Number: DE-AP07-951D81401, July 1995)**

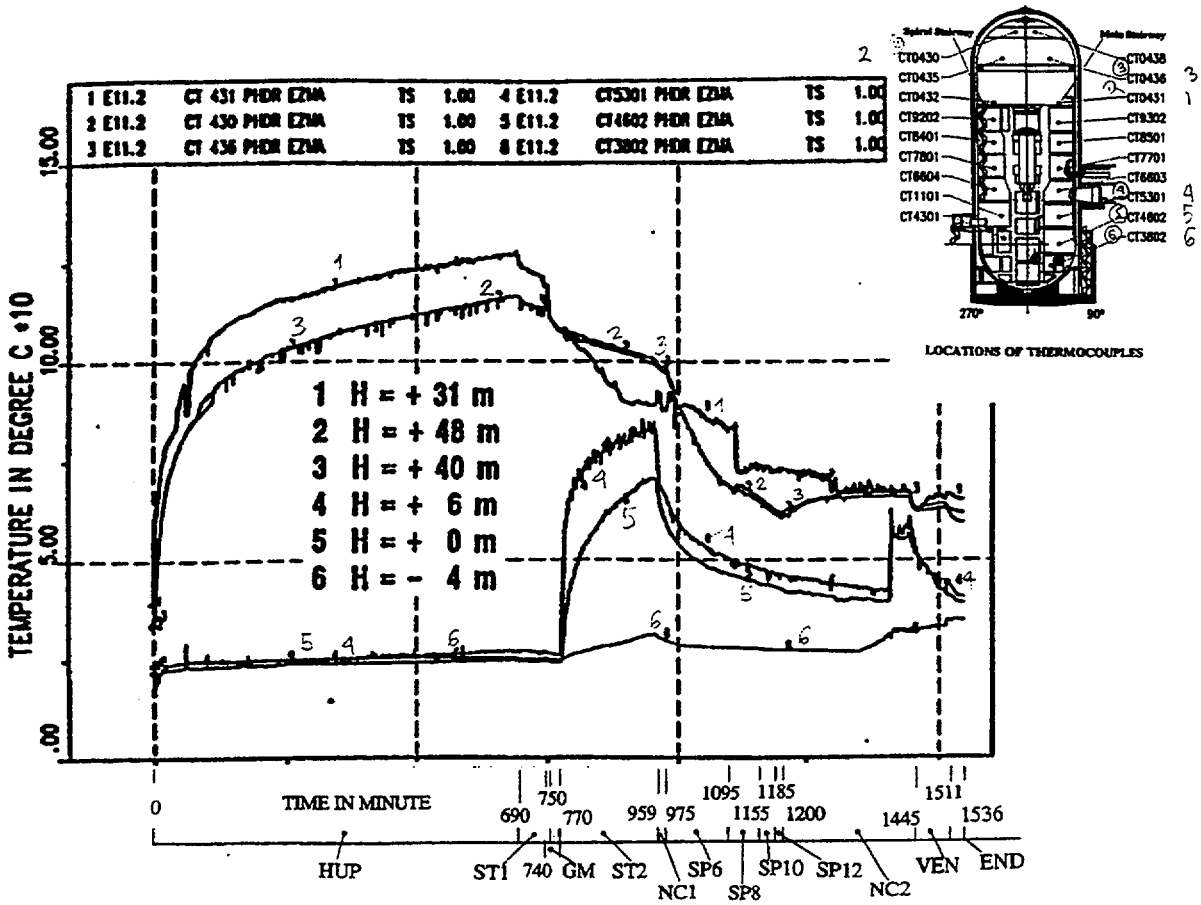


**Figure 9.C.2-54 HDR-E11.2 Atmospheric temperatures along main stairway**

**(reprinted from: L. Wolf, K. Mun, J. Floyd, "HDR hydrogen mixing evaluation for containment safety evaluations" - Phase 1, University of Maryland at College Park, Final Report for DOE-Project Order Number: DE-AP07-951D81401, July 1995)**

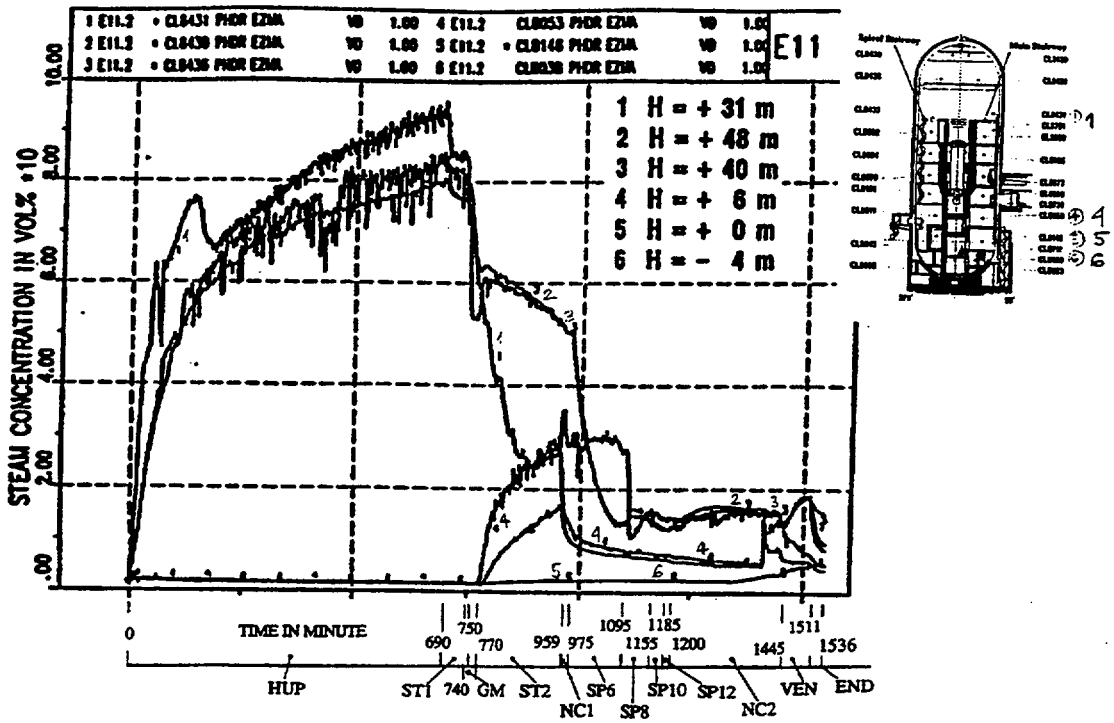


**Figure 9.C.2-55 HDR-E11.2 Steam concentrations along main stairway**

**(reprinted from: L. Wolf, K. Mun, J. Floyd, "HDR hydrogen mixing evaluation for containment safety evaluations" - Phase 1, University of Maryland at College Park, Final Report for DOE-Project Order Number: DE-AP07-951D81401, July 1995)**

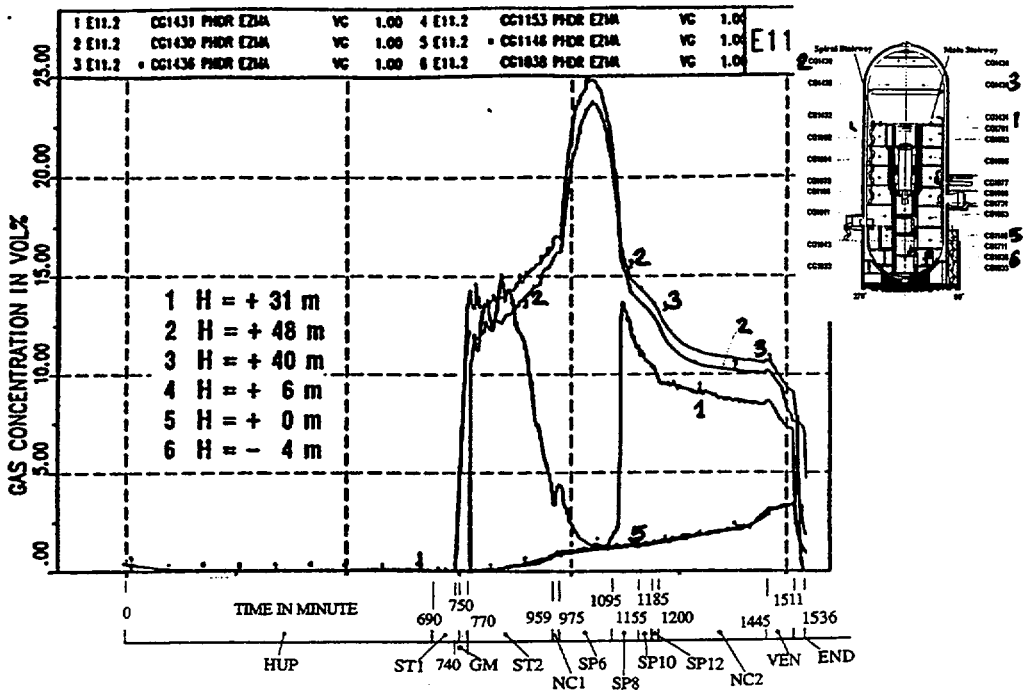


**Figure 9.C.2-56 HDR-E11.2 $H_2$/He Gas concentrations along main stairway**

**(reprinted from: L. Wolf, K. Mun, J. Floyd, "HDR hydrogen mixing evaluation for containment safety evaluations" - Phase 1, University of Maryland at College Park, Final Report for DOE-Project Order Number: DE-AP07-951D81401, July 1995)**

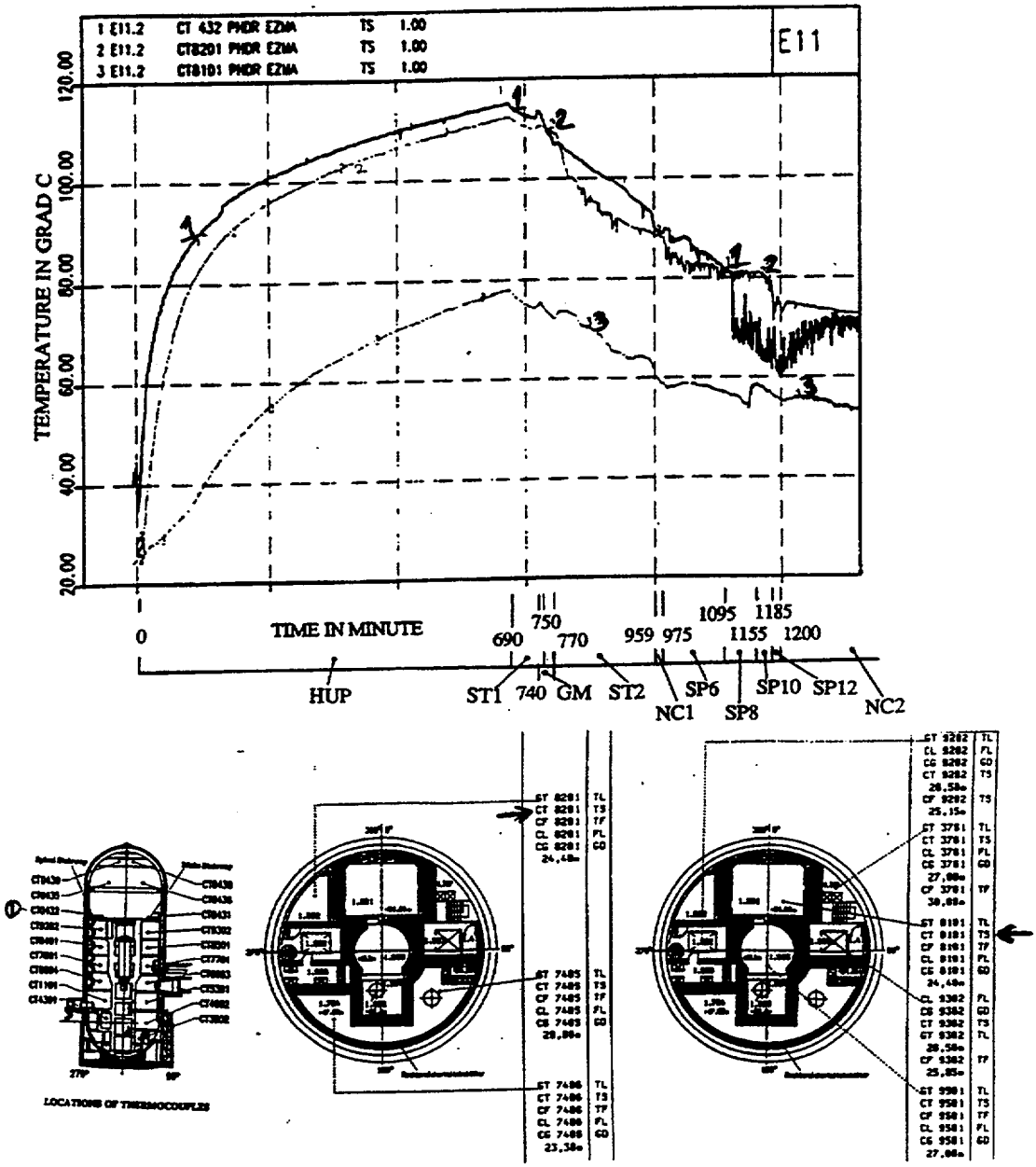


**Figure 9.C.2-57** **HDR-E11.2 Comparison between temperatures in main and spiral stairways at +31.0 m level**

**(reprinted from: L. Wolf, M. Gavrilas, K. Mun, "Overview of experimental results for long-term, Large-scale natural circulations in LWR-containments after large LOCAS", University of Maryland at College Park, Final Report for DOE - Project, Order Number: DE-AP07-96ID10765", July 1996)**

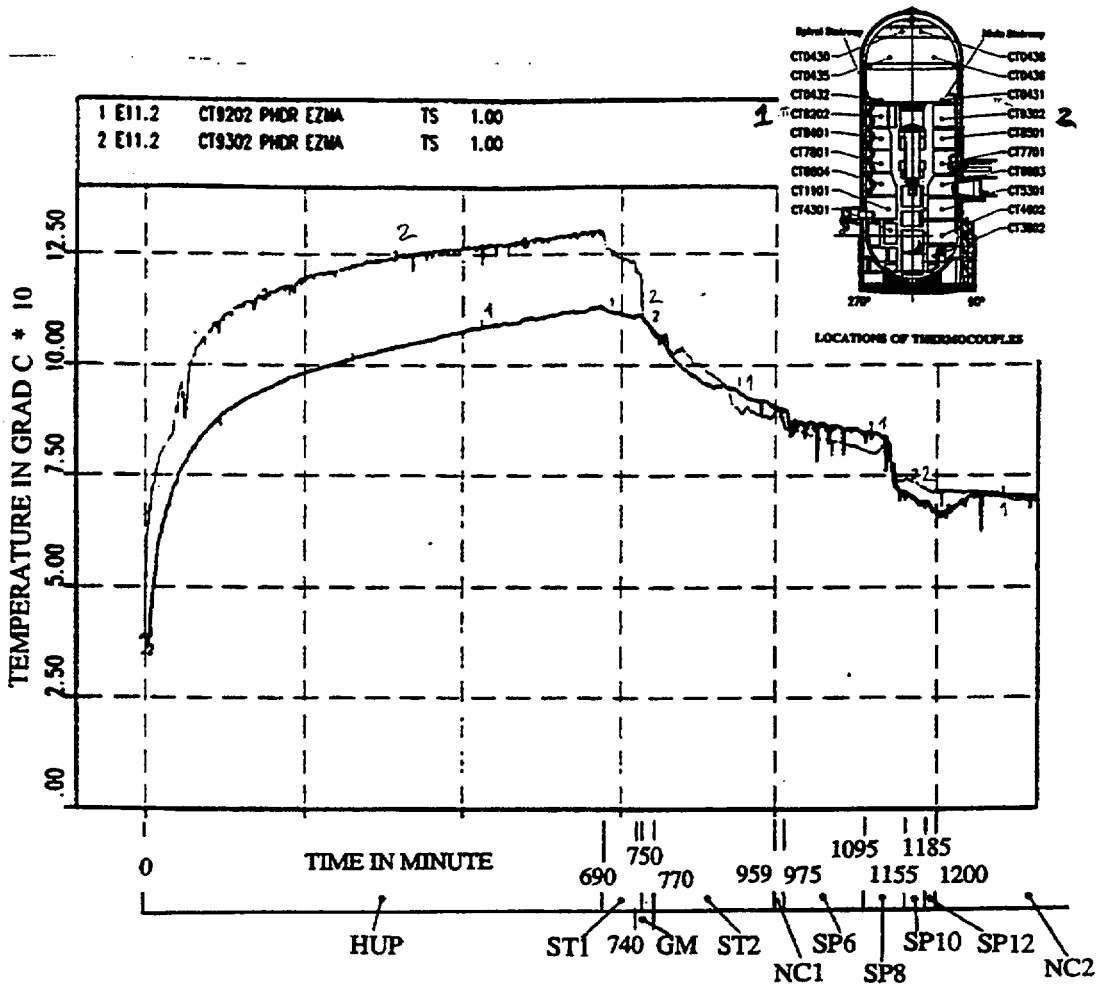


**Figure 9.C.2-58** **HDR-E11.2 Comparison between temperatures in main and spiral stairways at +26.5 m level**

**(reprinted from: L. Wolf, M. Gavrilas, K. Mun, "Overview of experimental results for long-term, Large-scale natural circulations in LWR-containments after large LOCAS", University of Maryland at College Park, Final Report for DOE - Project, Order Number: DE-AP07-96ID10765", July 1996)**

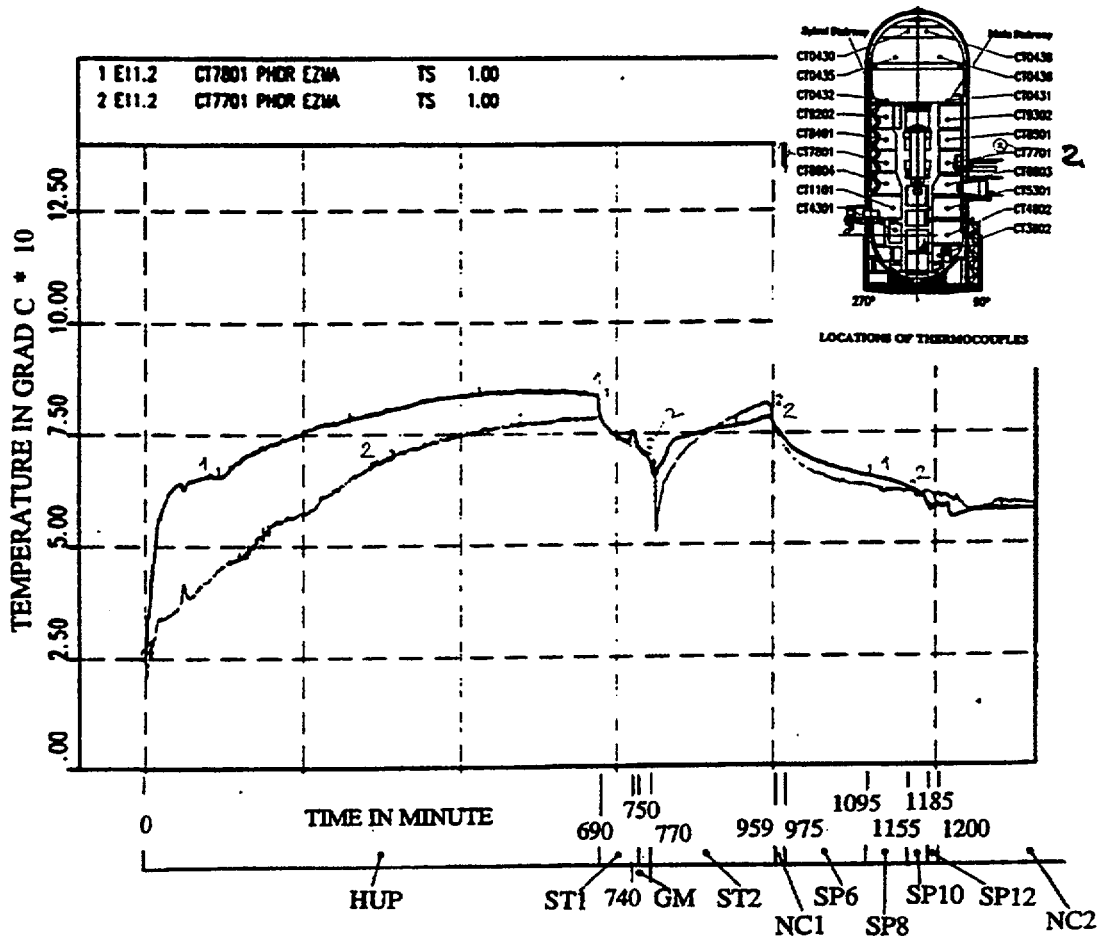


**Figure 9.C.2-59** **HDR-E11.2 Comparison between temperatures in main and spiral stairways at +16.5 m level**

**(reprinted from: L. Wolf, M. Gavrilas, K. Mun, "Overview of experimental results for long-term, Large-scale natural circulations in LWR-containments after large LOCAS", University of Maryland at College Park, Final Report for DOE - Project, Order Number: DE-AP07-96ID10765", July 1996)**

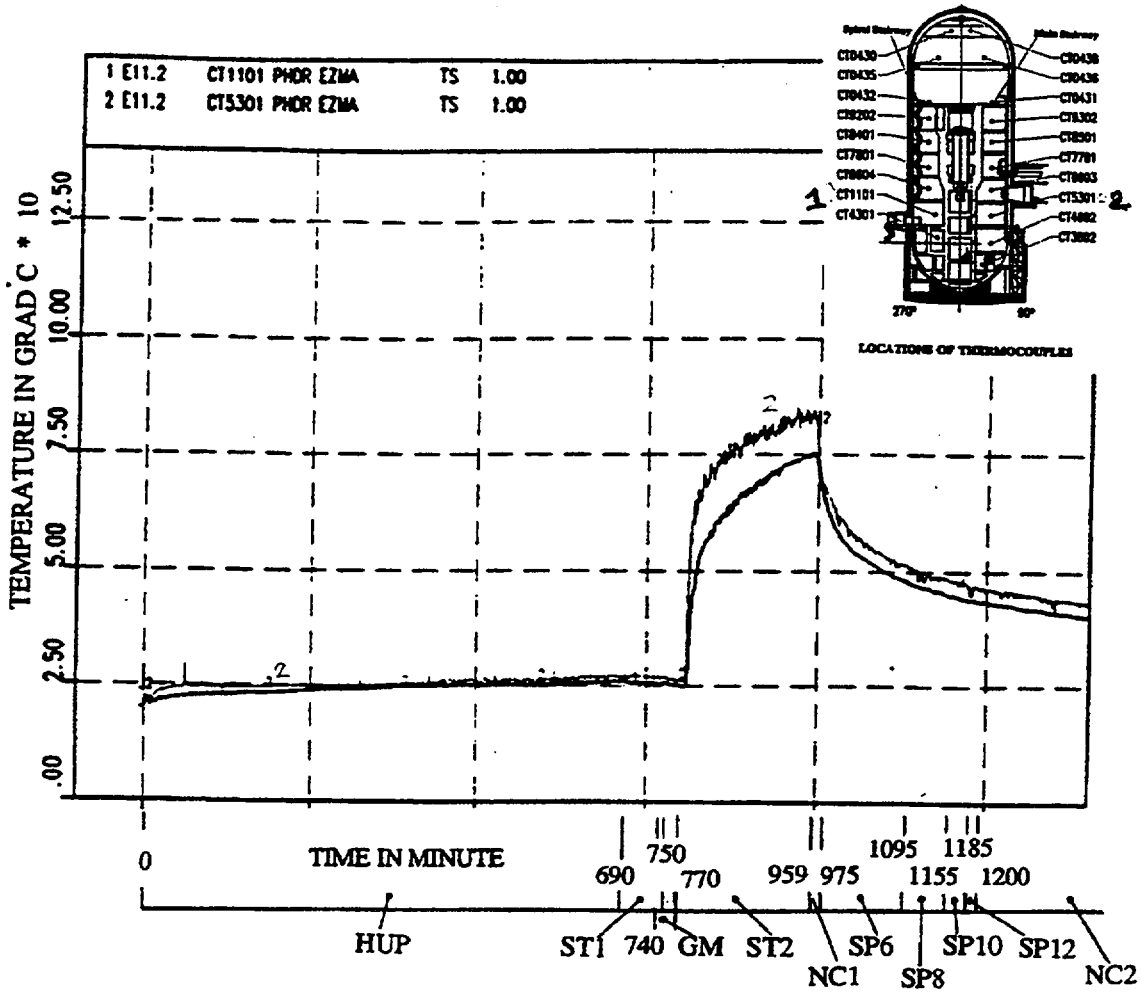


**Figure 9.C.2-60** **HDR-E11.2 Comparison between temperatures in main and spiral stairways at +6 m level**

**(reprinted from: L. Wolf, M. Gavrilas, K. Mun, "Overview of experimental results for long-term, Large-scale natural circulations in LWR-containments after large LOCAS", University of Maryland at College Park, Final Report for DOE - Project, Order Number: DE-AP07-96ID10765", July 1996)**

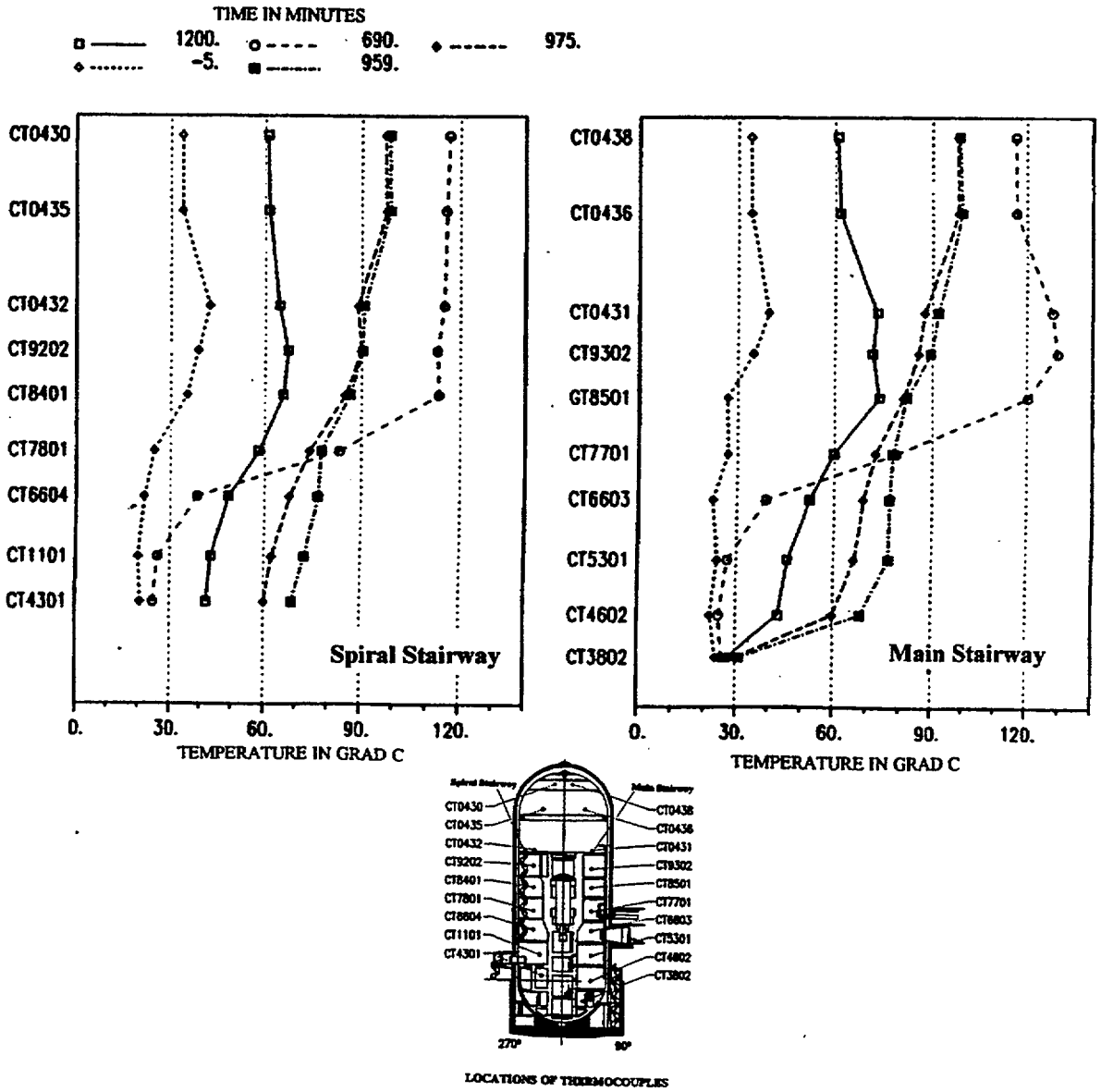


**Figure 9.C.2-61** **HDR-E11.2 Axial temperature profiles in both major flow paths at specific times, left in spiral stairway, right in main stairway**

**(reprinted from: L. Wolf, M. Gavrilas, K. Mun, "Overview of experimental results for long-term, Large-scale natural circulations in LWR-containments after large LOCAS", University of Maryland at College Park, Final Report for DOE - Project, Order Number: DE-AP07-96ID10765", July 1996)**

### 9.C.2.4.1.4 Experiment E11.3

Experiment E11.3 includes a low-positioned small break and gas release, as well as a closed entrance to the spiral stairway at the upper-deck. Although detailed boundary conditions are not available in the literature, this case is included to qualitatively indicate the influence of the injection position on the formation of global circulation. Even with the main vertical flow path from the top of the spiral staircase to the dome closed, global circulation is generated through other horizontal connections between the compartments (see Figures 9.C.2-62 and 9.C.2-63).

Temperature differences exist between the vertical axial flow channels during the heatup phase, the gas release phase, and the long cooldown period. The axial temperature profiles indicate that the temperature field was close to homogeneous with a $\Delta T$ of only 7 °C, except for the region below the release, as indicated by CT8101 in Figure 9.C.2-64 (see Figures 9.C.2-64 to 9.C.2-68).

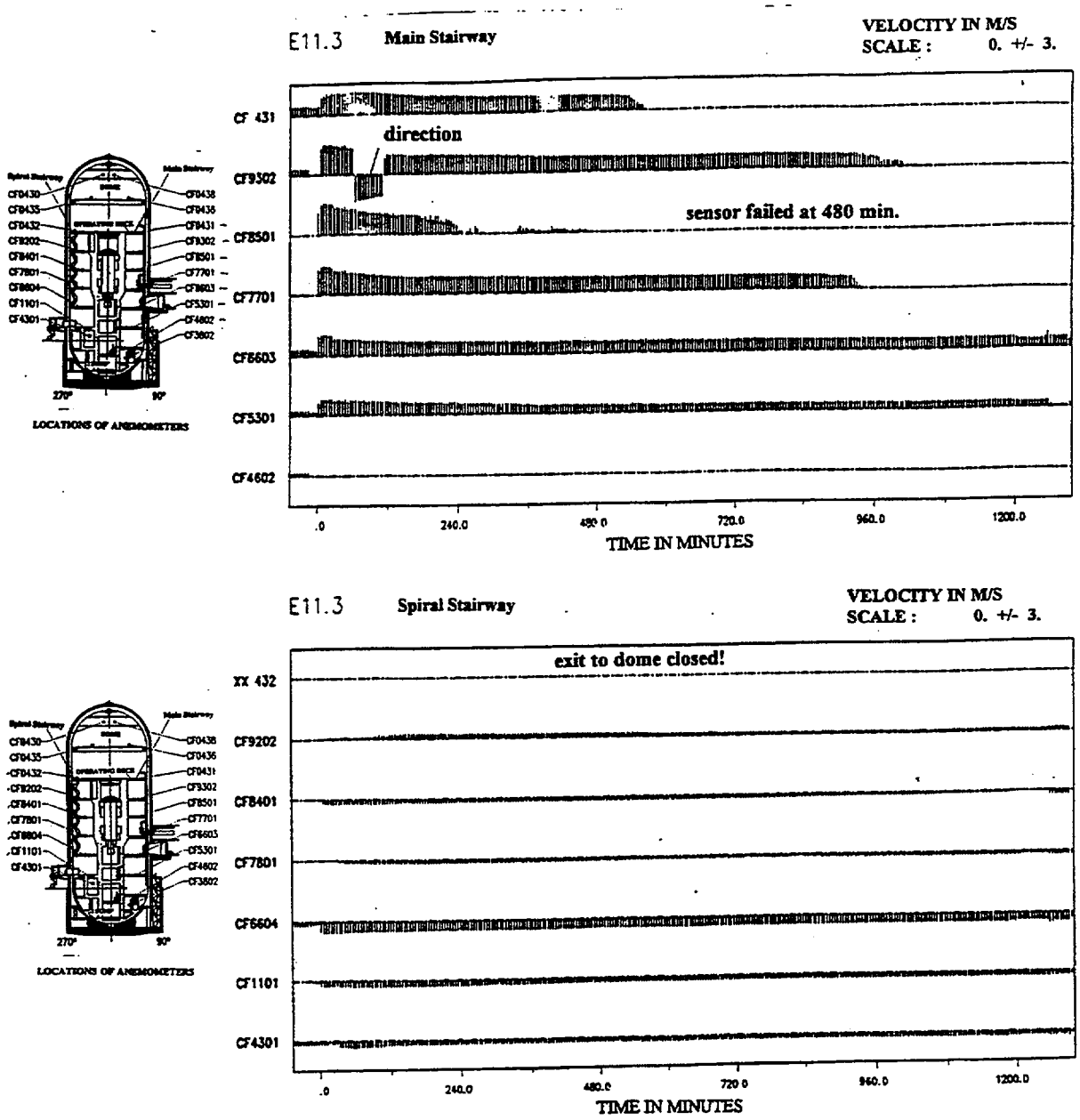


**Figure 9.C.2-62** **HDR-E11.3 Velocities in both major flow paths at different axial positions during containment heatup**

**(reprinted from: L. Wolf, M. Gavrilas, K. Mun, "Overview of experimental results for long-term, Large-scale natural circulations in LWR-containments after large LOCAS", University of Maryland at College Park, Final Report for DOE - Project, Order Number: DE-AP07-96ID10765", July 1996)**

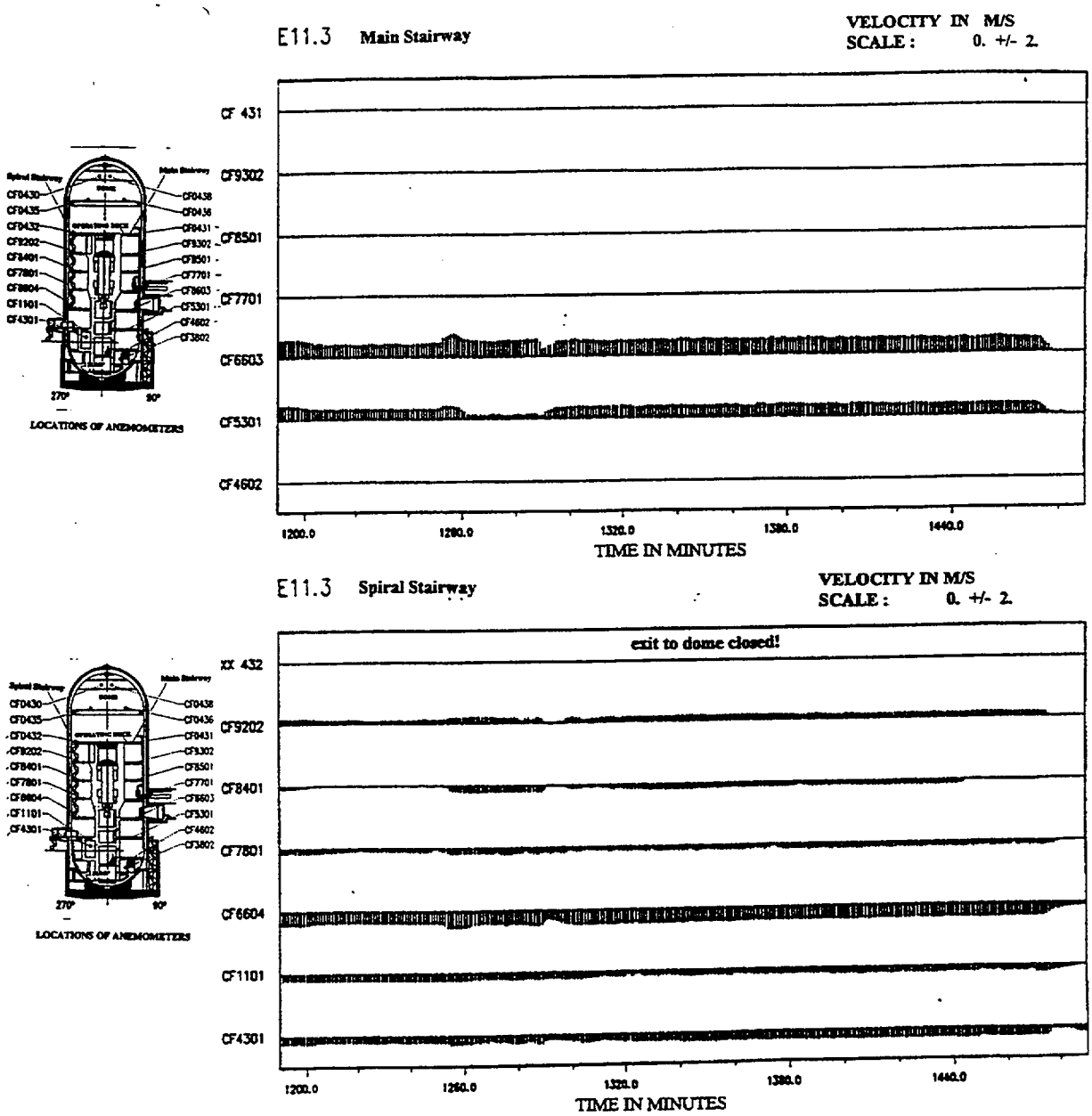


**Figure 9.C.2-63** **HDR-E11.3 Velocities in both major flow paths at different axial positions during $H_2$/He gas mixture release**

**(reprinted from: L. Wolf, M. Gavrilas, K. Mun, "Overview of experimental results for long-term, Large-scale natural circulations in LWR-containments after large LOCAS", University of Maryland at College Park, Final Report for DOE - Project, Order Number: DE-AP07-96ID10765", July 1996)**

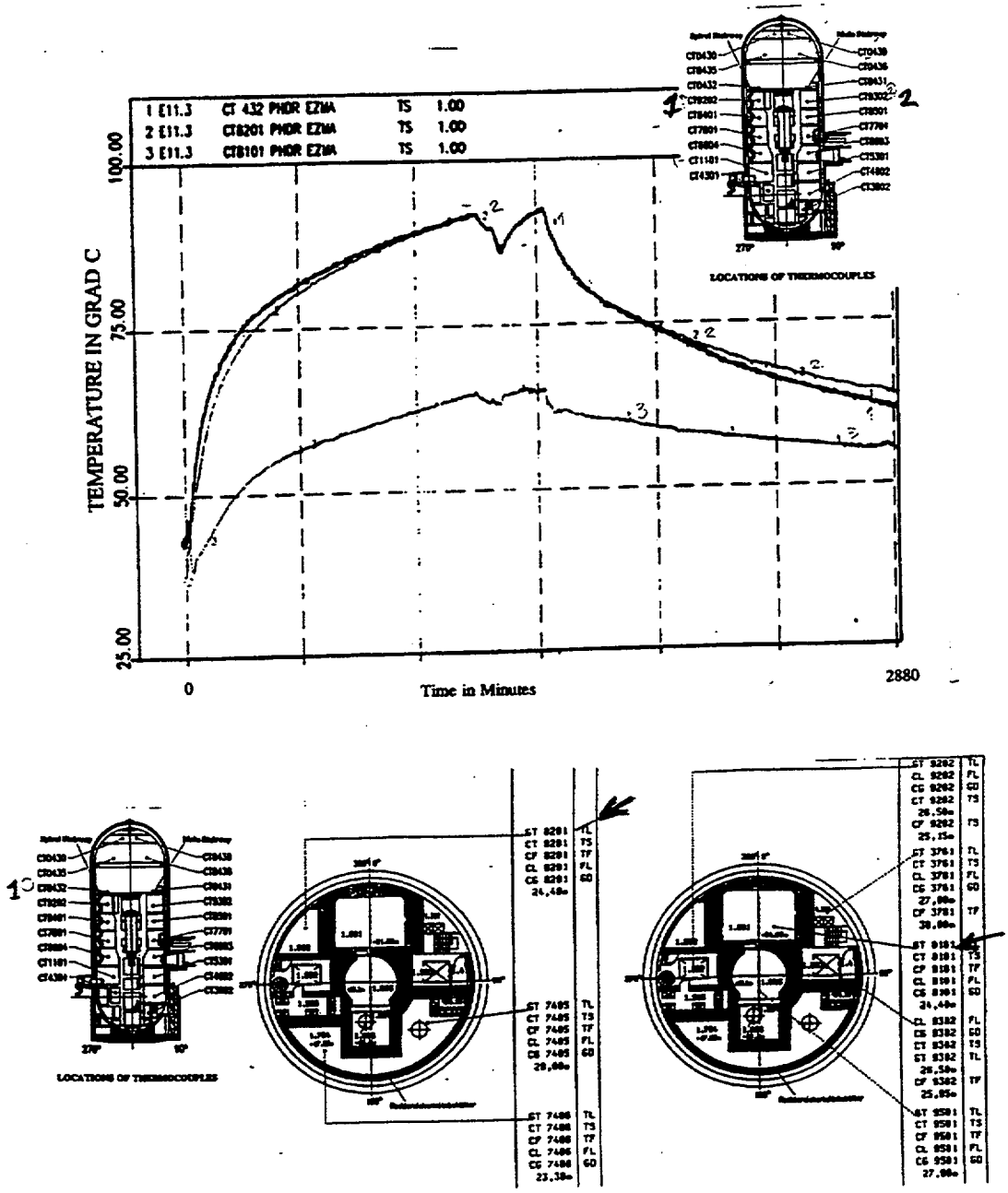


Figure 9.C.2-64 HDR-E11.3 Comparison between temperatures in main and spiral stairways at +31.0 m level

(reprinted from: L. Wolf, M. Gavrilas, K. Mun, "Overview of experimental results for long-term, Large-scale natural circulations in LWR-containments after large LOCAS", University of Maryland at College Park, Final Report for DOE - Project, Order Number: DE-AP07-96ID10765", July 1996)

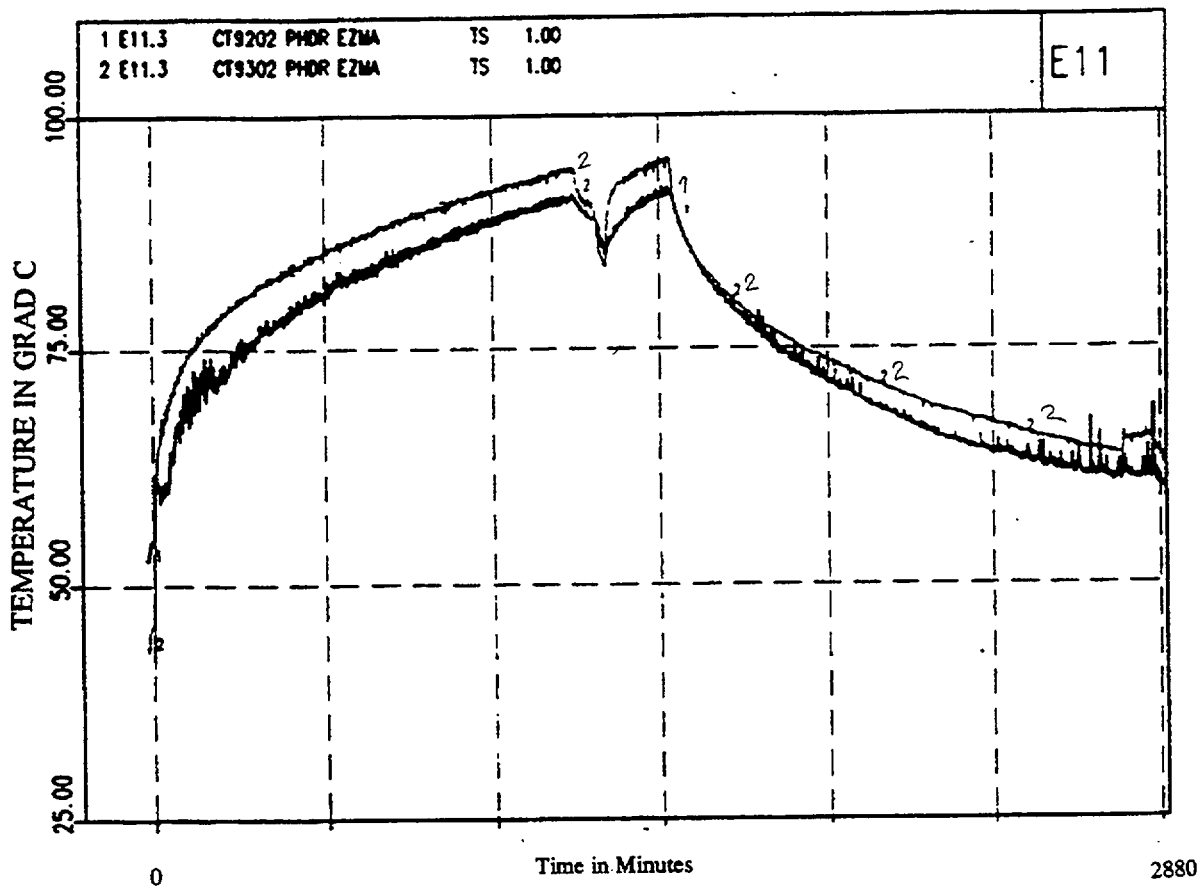


**Figure 9.C.2-65** **HDR-E11.3 Comparison between temperatures in main and spiral stairways at +26.5 m level**

**(reprinted from: L. Wolf, M. Gavrilas, K. Mun, "Overview of experimental results for long-term, Large-scale natural circulations in LWR-containments after large LOCAS", University of Maryland at College Park, Final Report for DOE - Project, Order Number: DE-AP07-96ID10765", July 1996)**

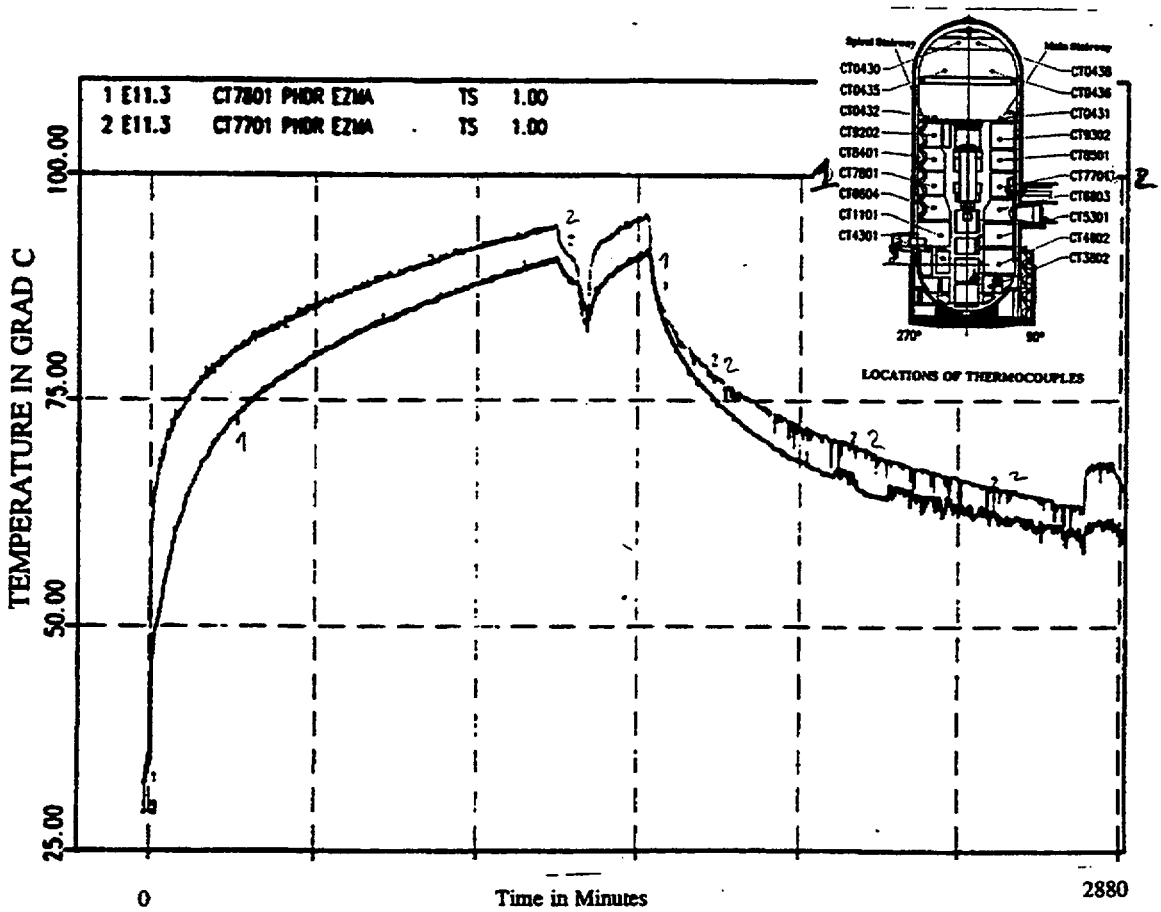


**Figure 9.C.2-66** **HDR-E11.3 Comparison between temperatures in main and spiral stairways at +16.5 m level**

**(reprinted from: L. Wolf, M. Gavrilas, K. Mun, "Overview of experimental results for long-term, Large-scale natural circulations in LWR-containments after large LOCAS", University of Maryland at College Park, Final Report for DOE - Project, Order Number: DE-AP07-96ID10765", July 1996)**

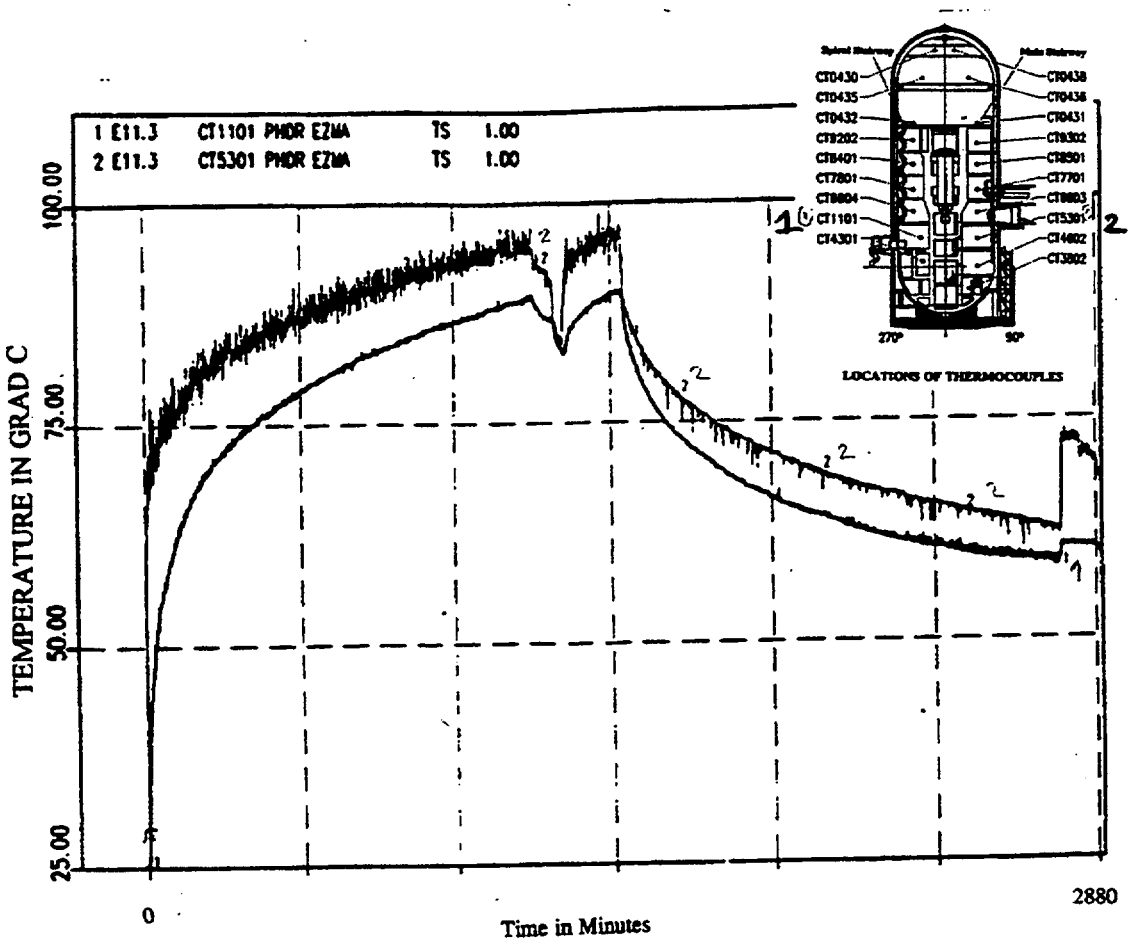


**Figure 9.C.2-67** **HDR-E11.3 Comparison between temperatures in main and spiral stairways at +6 m level**

**(reprinted from: L. Wolf, M. Gavrilas, K. Mun, "Overview of experimental results for long-term, Large-scale natural circulations in LWR-containments after large LOCAS", University of Maryland at College Park, Final Report for DOE - Project, Order Number: DE-AP07-96ID10765", July 1996)**

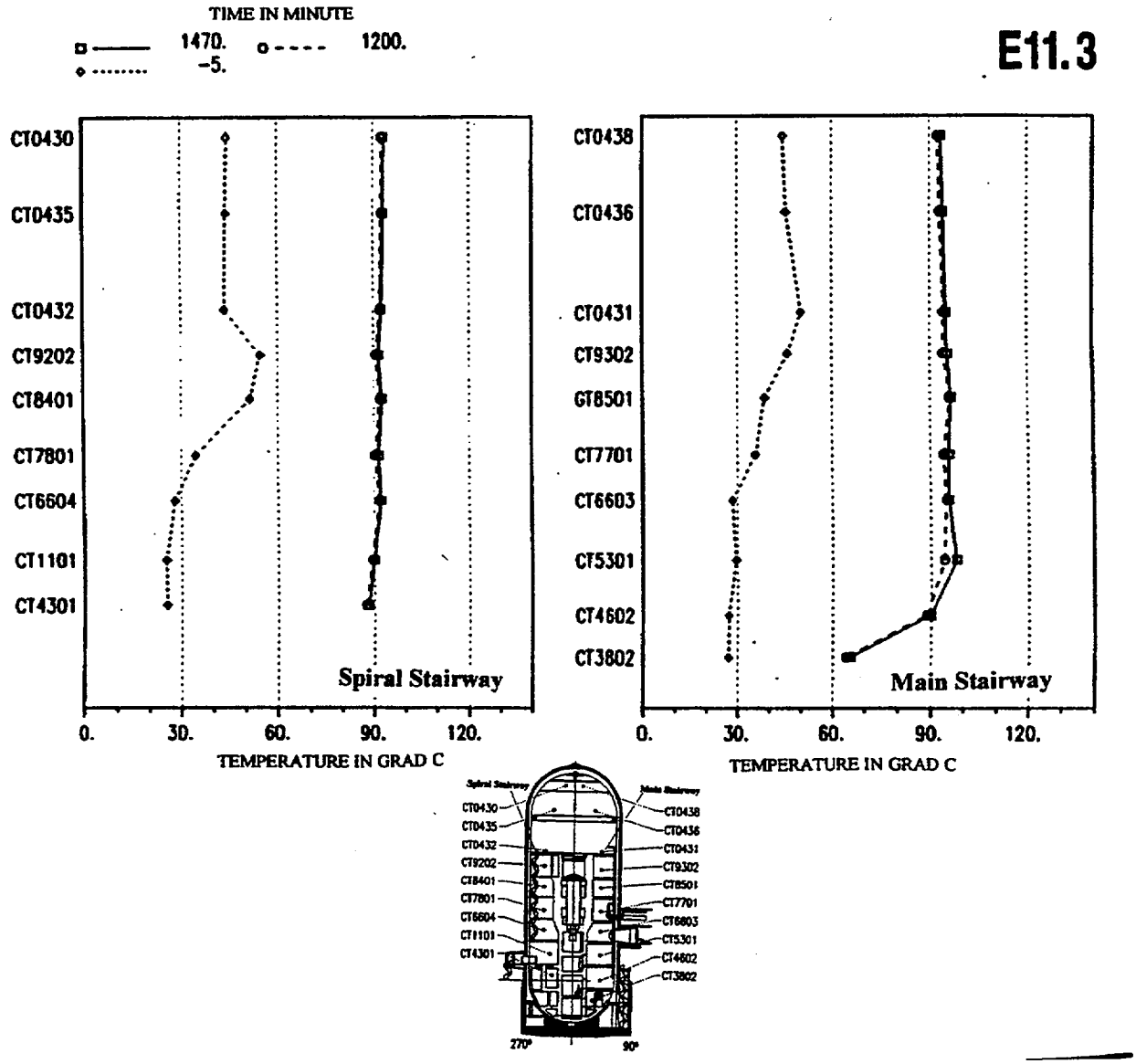


**Figure 9.C.2-68** **HDR-E11.3 Axial temperature profiles in both major flow paths at specific times, left in spiral stairway, right in main stairway**

**(reprinted from: L. Wolf, M. Gavrilas, K. Mun, "Overview of experimental results for long-term, Large-scale natural circulations in LWR-containments after large LOCAs", University of Maryland at College Park, Final Report for DOE - Project, Order Number: DE-AP07-96ID10765", July 1996)**

### 9.C.2.4.1.5 Experiment E11.4

Experiment E11.4 includes a low-positioned break and an active external spray. The spiral stairway entrance to the dome is open. A detailed presentation of this experiment is given by Wolf, Mun, Floyd, 1995. Data from this test is used to validate various numerical containment codes (Wolf et al., 1994, Pisa and Holzbauer and Wolf, 1994, Pisa).

Figure 9.C.2-69 and Table 9.C-5 present the experimental procedure. This includes the duration of heatup and blowdown of steam (p=110 bar and T=318°C in the compartment R1405, (see Figure 9.C.2-51 and 9.C.2-69) and the consecutive steam and gas injections.

The containment pressure history is shown in Figure 9.C.2-70. This figure shows the effects of the external spray application (after 2800 minutes) on the decrease of the containment pressure (by 0.25 bar).

Temperatures at the various axial positions in the main staircase are presented in Figure 9.C.2-71. Note that the shapes of the temperature curves for various levels are similar, but the values are different. Global circulation is indicated by the small temperature differences from the top to the bottom of the dome, $\Delta T$=2-6°C, and from the dome to the sump, $\Delta T$=10-26°C. Figures 9.C.2-72 and 9.C.2-73 provide steam and gas concentration histories for the various levels in the main staircase.

During all phases of the experiment, temperature differences exist between the two vertical channels (main and spiral staircases) enabling the global circulation (see Figures 9.C.2-74 - 9.C.2-77). The temperature differences decrease during the cooldown phase. As in experiment E11.3, the axial temperature distribution indicates a nearly uniform temperature profile, except below the release point (see Figure 9.C.2-78).

During the E11.4 test, the release into the lower-level compartment promotes global circulation and homogenizes the containment atmosphere. In addition, the application of the external sprays causes a decrease in the containment pressure (see Figure 9.C.2-70) and a reduction in the axial temperature gradient (see Figure 9.C.2-71, curves 1-6). The external spray also promotes a more uniform gas concentration (see Figure 9.C.2-73 from 2800 to 3000 minutes).

**Table 9.C-5 Events for E11.4 Experiment**

| Event | Time (minutes) | Event Description |
|---|---|---|
| HUP | 0-2040 | RPV-blowdown plus external steam supply with m = 2.06 kg/s |
| ST1 | 2040-2100 | Reduced external steam with m = 1.19 kg/s in R1.405 |
| GM1 | 2090-2100 | $H_2$/He gas mixture release into R1.405 with 0.089 kg/s |
| ST2 | 2120-2180 | Steam release into R1.405 with 2.06 kg/s |
| DH | 2180-2550 | Dry heat addition into R1.308 |
| GM2 | 2193-2195 | $H_2$/He gas mixture release into R1.405 with 0.2 kg/s |
| GM3 | 2195-2205 | $H_2$/He gas mixture release into R1.405 with 0.089 kg/s |
| ST3 | 2205-2505 | Start of steam release into R1.405 with m = 1.19 kg/s |
| ST4 | 2550-2620 | Steam release into R1.405 with m = 2.06 kg/s |
| SUB | 2620-2800 | Sump boiling |
| NC1 | 2800-2805 | Natural cooldown |
| SP6 | 2805-2925 | External spray m = 6 kg/s |
| SP8 | 2925-2985 | External spray m = 8 kg/s |
| SP10 | 2985-3015 | External spray m = 10 kg/s |
| SP12 | 3015-3016 | External spray m = 12 kg/s |
| NC2 | 3016-3229 | Natural cooldown |
| VEN | 3229-3300 | Containment venting |
| END | 3360 | End of data acquisition |

(reprinted from L. Wolf, M. Gavrilas, K. Mun, "Overview of experimental results for long-term, large-scale natural circulations in LWR-containments after large LOCAS," University of Maryland at College Park, Final Report for DOE - Project, Order Number: DE-AP07-96ID10765")

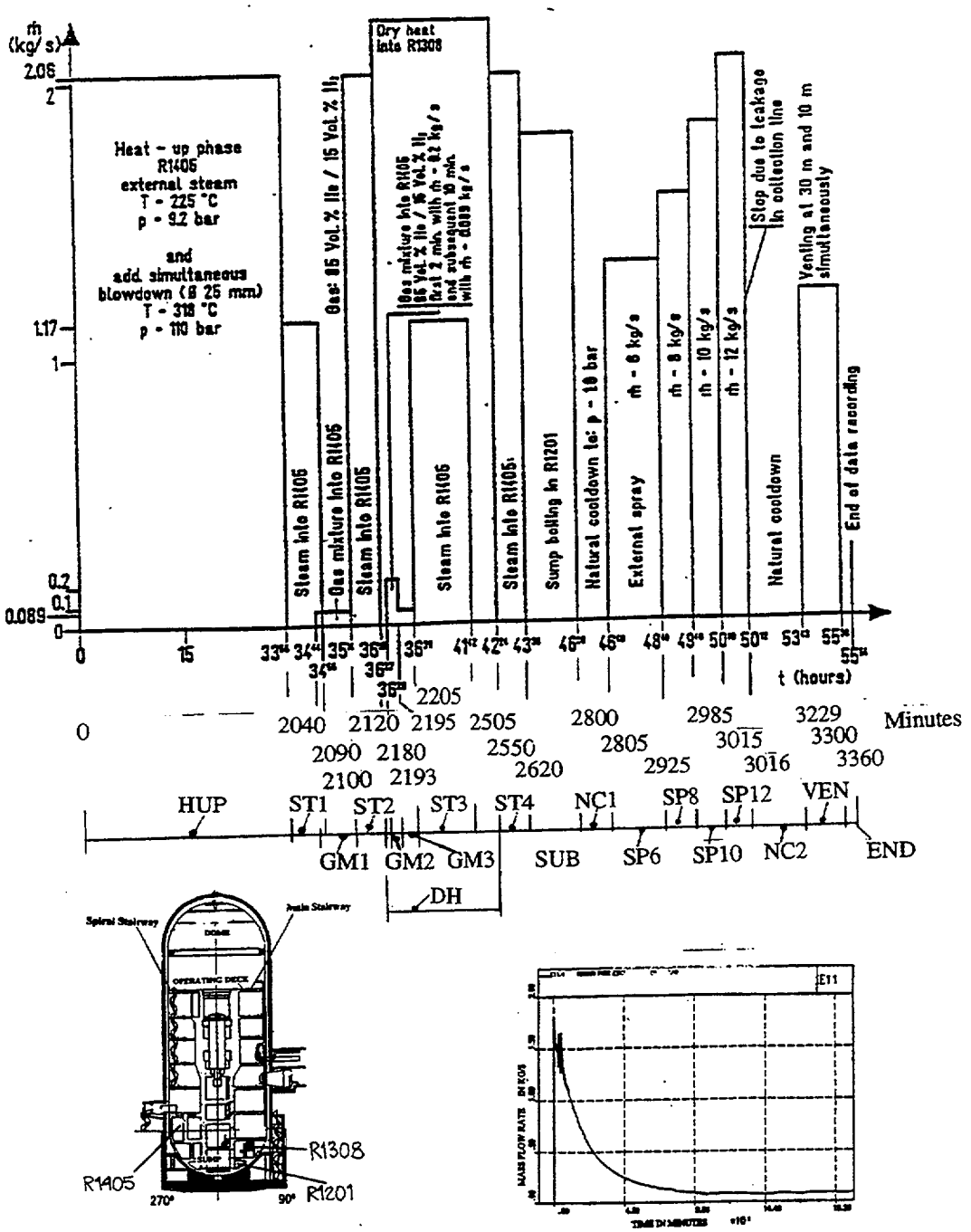


**Figure 9.C.2-69 HDR-E11.4 Sequence of Experimental Test Procedures**

**(reprinted from: L. Wolf, K. Mun, J. Floyd, "HDR hydrogen mixing evaluation for containment safety evaluations" - Phase 1, University of Maryland at College Park, Final Report for DOE-Project Order Number: DE-AP07-951D81401, July 1995)**

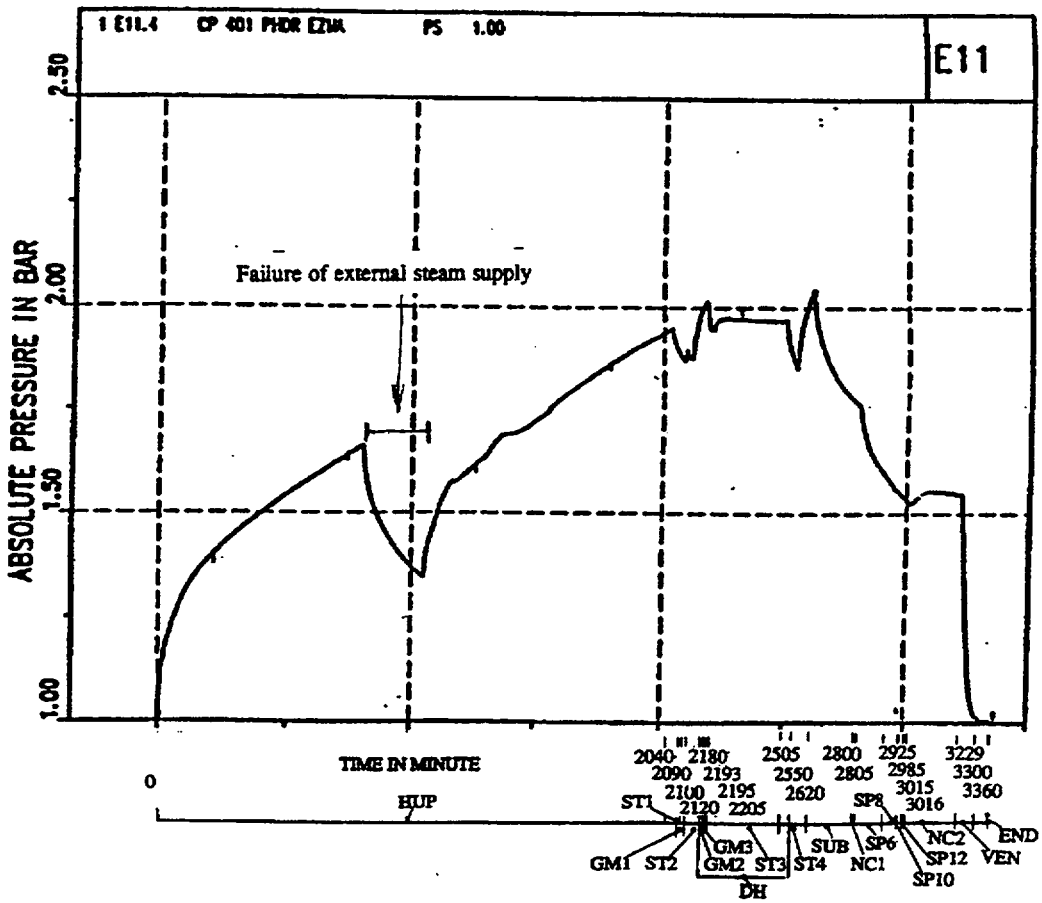


**Figure 9.C.2-70 HDR-E11.4 Containment pressure history**

**(reprinted from: L. Wolf, K. Mun, J. Floyd, "HDR hydrogen mixing evaluation for containment safety evaluations" - Phase 1, University of Maryland at College Park, Final Report for DOE-Project Order Number: DE-AP07-951D81401, July 1995)**

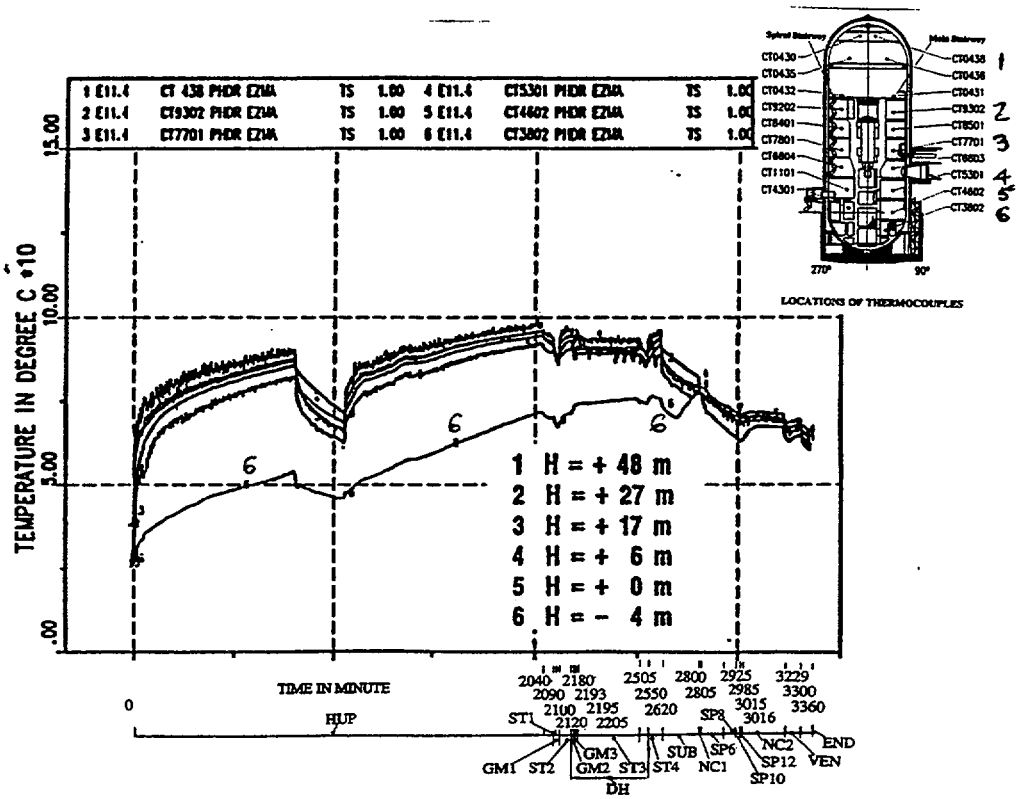


**Figure 9.C.2-71 HDR-E11.4 Atmospheric temperatures along main stairway**

**(reprinted from: L. Wolf, K. Mun, J. Floyd, "HDR hydrogen mixing evaluation for containment safety evaluations" - Phase 1, University of Maryland at College Park, Final Report for DOE-Project Order Number: DE-AP07-951D81401, July 1995)**

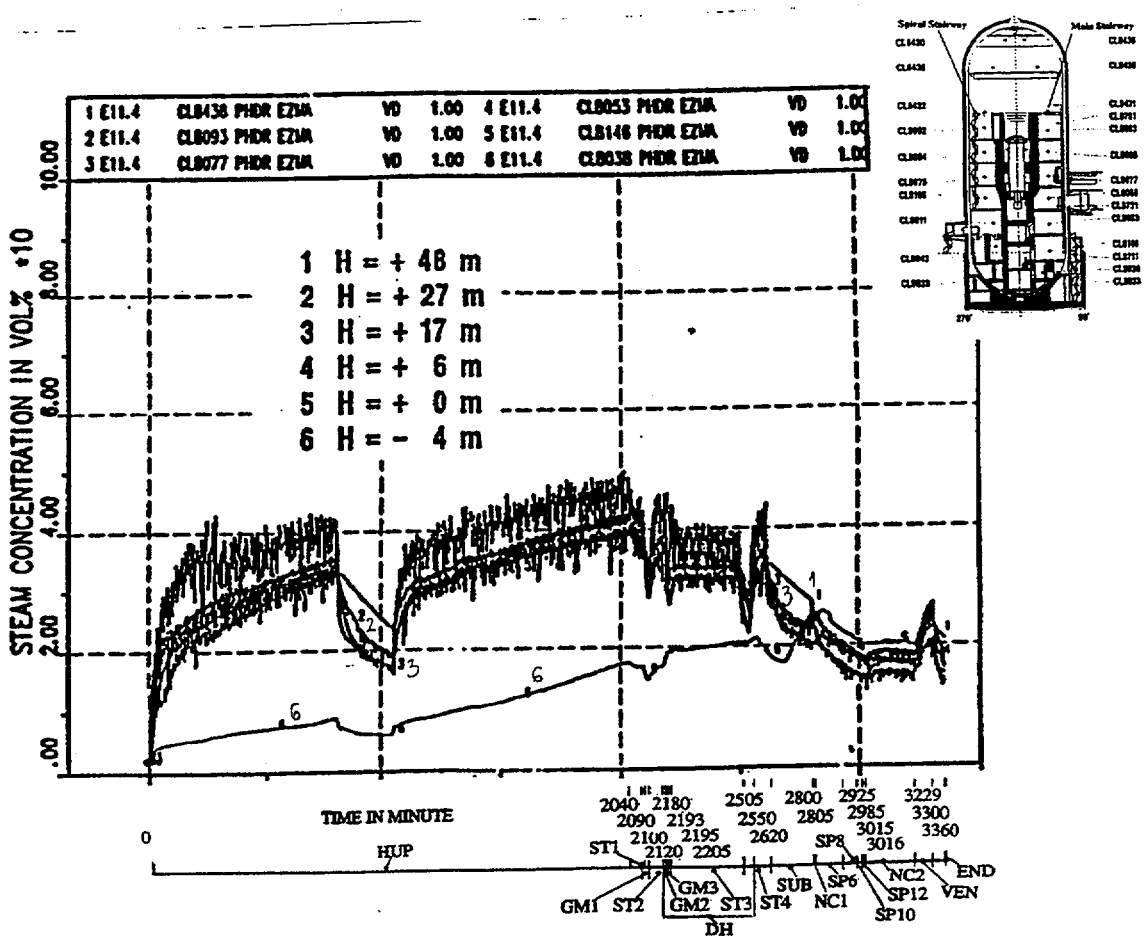


**Figure 9.C.2-72 HDR-E11.4 Steam concentrations along main stairway**

**(reprinted from: L. Wolf, K. Mun, J. Floyd, "HDR hydrogen mixing evaluation for containment safety evaluations" - Phase 1, University of Maryland at College Park, Final Report for DOE-Project Order Number: DE-AP07-951D81401, July 1995)**

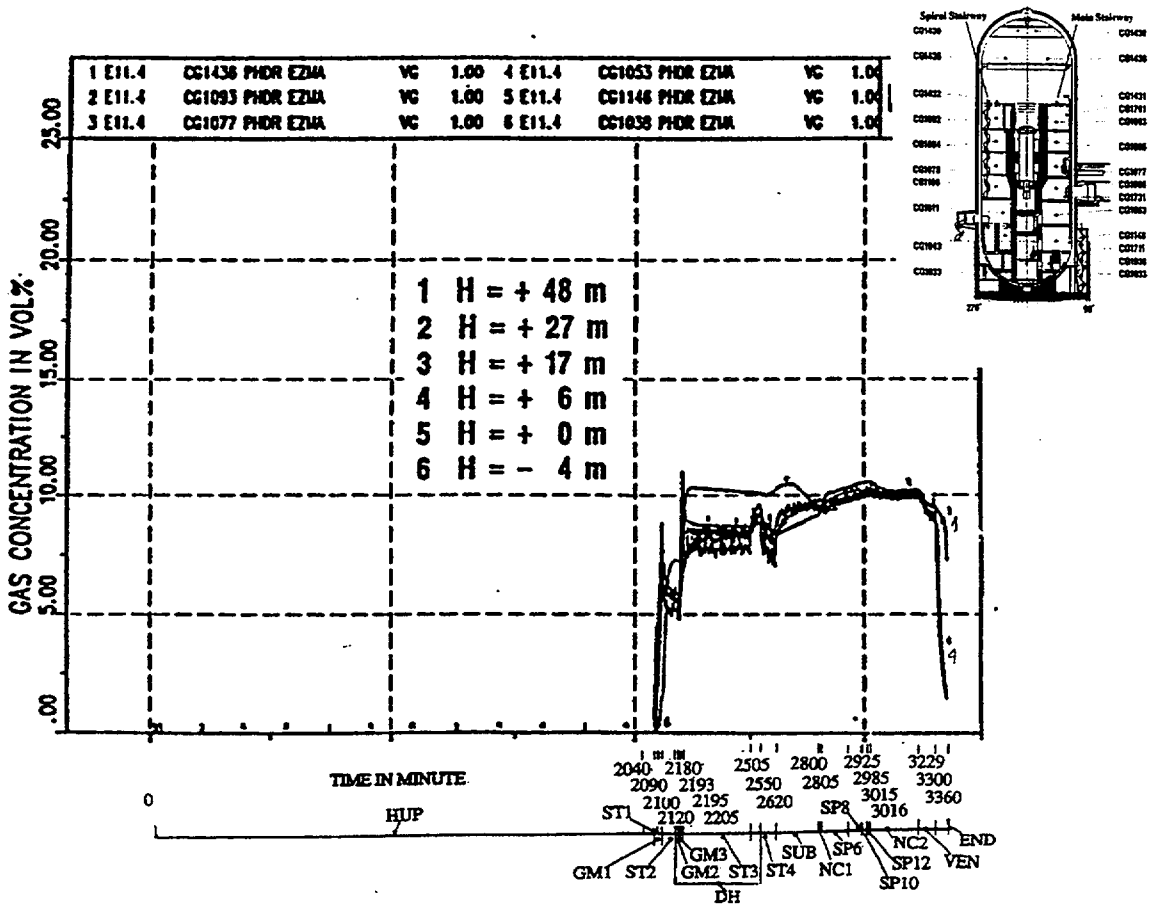


**Figure 9.C.2-73 HDR-E11.4 $H_2$/He Gas concentrations along main stairway**

**(reprinted from: L. Wolf, K. Mun, J. Floyd, "HDR hydrogen mixing evaluation for containment safety evaluations" - Phase 1, University of Maryland at College Park, Final Report for DOE-Project Order Number: DE-AP07-951D81401, July 1995)**

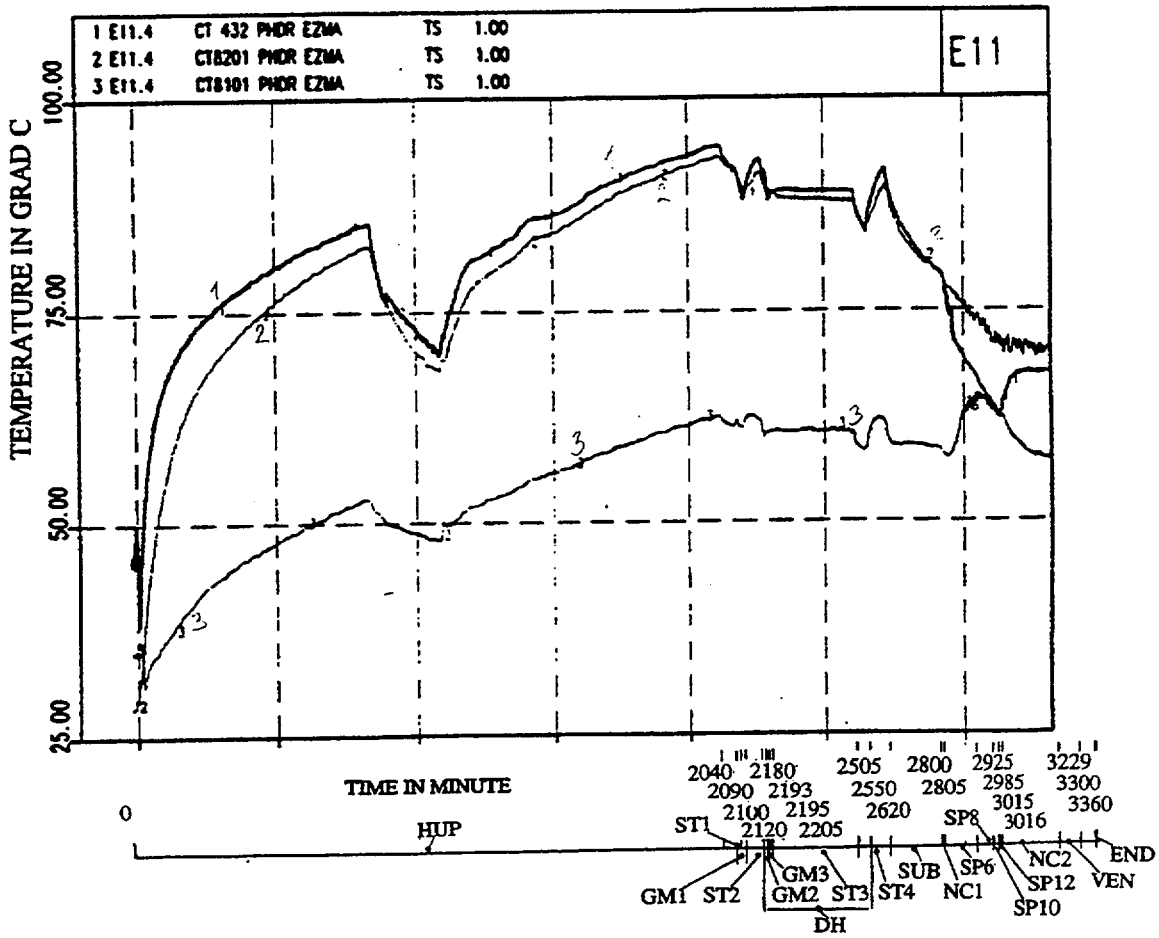


**Figure 9.C.2-74a** **HDR-E11.4 Comparison between temperatures in main and spiral stairways at +31.0 m level**

**(reprinted from: L. Wolf, M. Gavrilas, K. Mun, "Overview of experimental results for long-term, Large-scale natural circulations in LWR-containments after large LOCAs", University of Maryland at College Park, Final Report for DOE - Project, Order Number: DE-AP07-96ID10765", July 1996)**

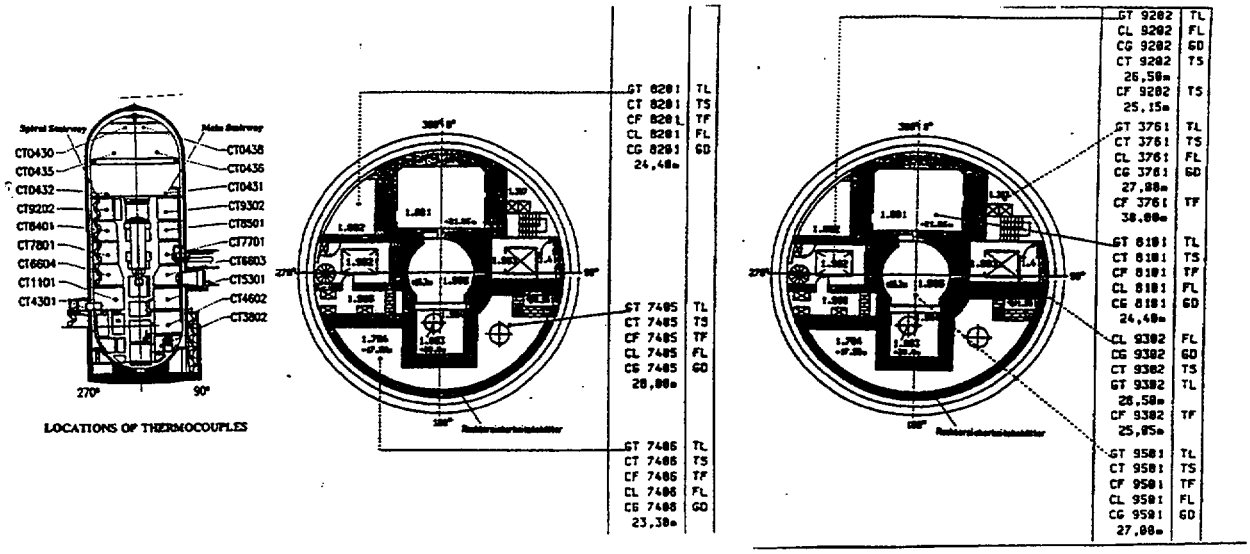


**Figure 9.C.2-74b** **HDR-E11.4 Comparison between temperatures in main and spiral stairways at +31.0 m level**

**(reprinted from: L. Wolf, M. Gavrilas, K. Mun, "Overview of experimental results for long-term, Large-scale natural circulations in LWR-containments after large LOCAs", University of Maryland at College Park, Final Report for DOE - Project, Order Number: DE-AP07-96ID10765", July 1996)**

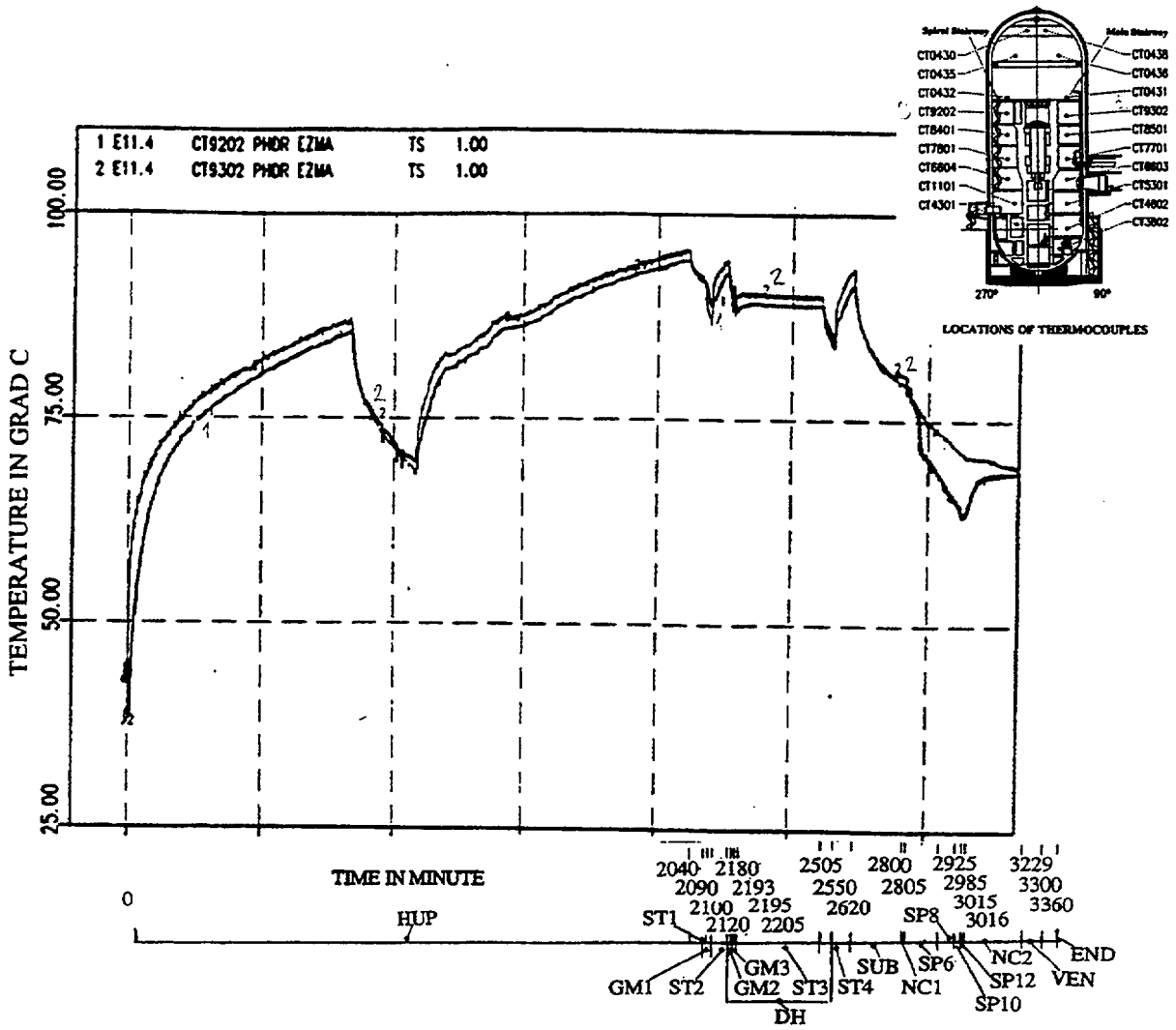


**Figure 9.C.2-75** **HDR-E11.4 Comparison between temperatures in main and spiral stairways at +26.5 m level**

**(reprinted from: L. Wolf, M. Gavrilas, K. Mun, "Overview of experimental results for long-term, Large-scale natural circulations in LWR-containments after large LOCAs", University of Maryland at College Park, Final Report for DOE - Project, Order Number: DE-AP07-96ID10765", July 1996)**

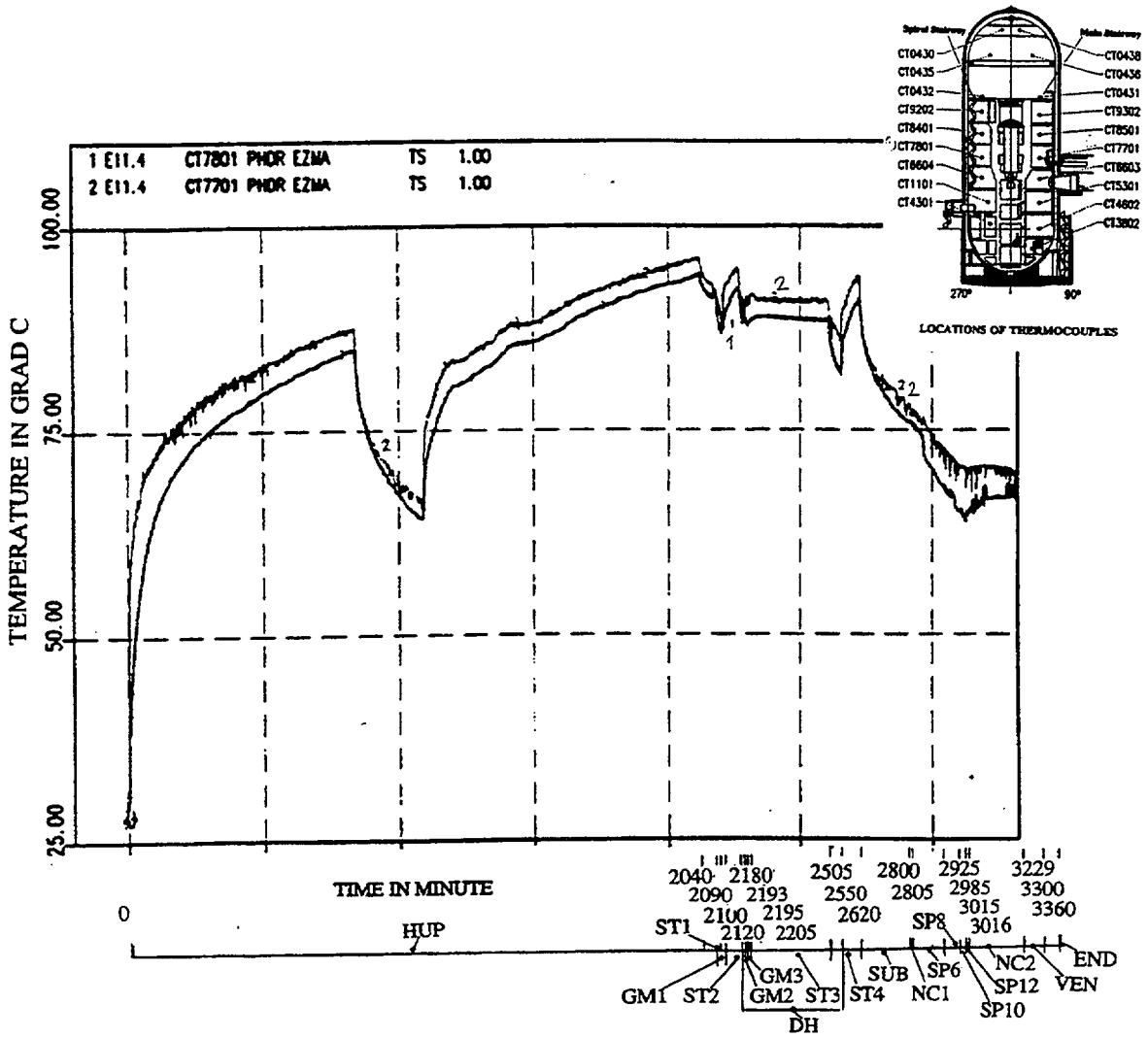


**Figure 9.C.2-76** **HDR-E11.4 Comparison between temperatures in main and spiral stairways at +16.5 m level**

**(reprinted from: L. Wolf, M. Gavrilas, K. Mun, "Overview of experimental results for long-term, Large-scale natural circulations in LWR-containments after large LOCAs", University of Maryland at College Park, Final Report for DOE - Project, Order Number: DE-AP07-96ID10765", July 1996)**

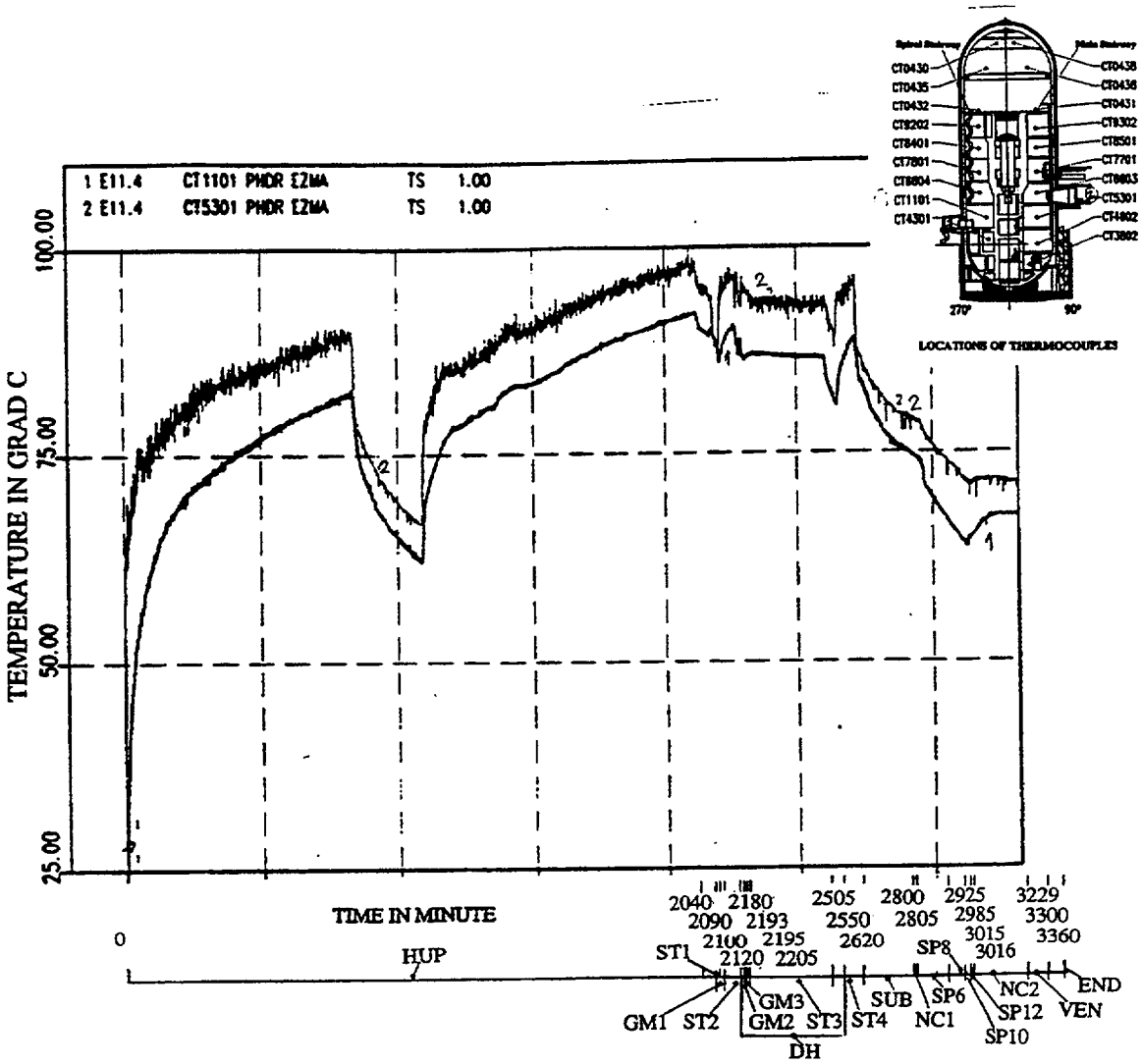


**Figure 9.C.2-77** **HDR-E11.4 Comparison between temperatures in main and spiral stairways at +6 m level**

**(reprinted from: L. Wolf, M. Gavrilas, K. Mun, "Overview of experimental results for long-term, Large-scale natural circulations in LWR-containments after large LOCAs", University of Maryland at College Park, Final Report for DOE - Project, Order Number: DE-AP07-96ID10765", July 1996)**

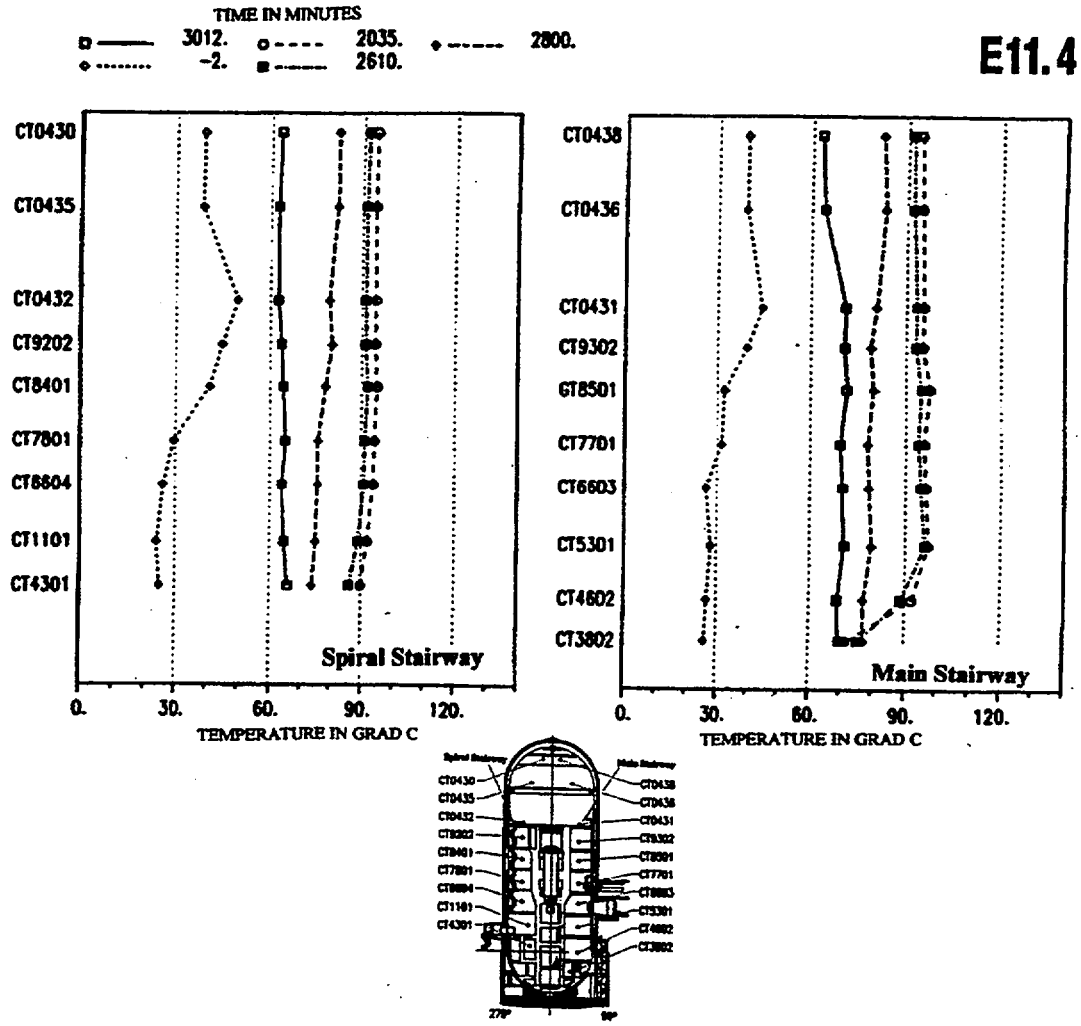


**Figure 9.C.2-78** **HDR-E11.4 Axial temperature profiles in both major flow paths at specific times, left in spiral stairway, right in main stairway**

**(reprinted from: L. Wolf, M. Gavrilas, K. Mun, "Overview of experimental results for long-term, Large-scale natural circulations in LWR-containments after large LOCAs", University of Maryland at College Park, Final Report for DOE - Project, Order Number: DE-AP07-96ID10765", July 1996)**

#### 9.C.2.4.1.6 Experiment E11.5

Experiment E11.5 includes a large-break LOCA at a low position, with subsequent small-break releases. The temperature differences between the vertical flow channels is large enough to obtain global natural circulation. The temperature difference changes sign at some axial positions during some phases.

A more detailed presentation of the E11.5 results will be given in the next chapter, together with the presentation of the other experiments related to large break LOCA.

**Conclusions from the HDR E11 Test Series**

Wolf, et al., 1996, concludes that global natural circulation patterns are established in all E11 experiments, despite the different release positions, the applications of internal and external sprays, and the changes to the flow path geometries. Also, an almost homogeneous temperature field is generated for the low position of the release points (experiments E11.3, E11.4 and E11.5). Higher release positions generated stratified temperature fields.

### 9.C.2.4.2 HDR Large LOCA Experimental Data Base

Experimental results for long-term, large-scale natural circulation in containments after large LOCAs presented by Wolf and Mun, 1996. An assessment of experiments T31.5, V21.1, V43, and E11.5 is provided.

Experiment T31.5 simulates a design basis large LOCA and hydrogen release in the upper section of the containment. Experiment V21.1 simulates a design basis large LOCA in the middle section of the containment, while experiment E11.5 simulates the release of steam and hydrogen in the lowest containment section. Experiment V21.1 is a subcooled blowdown, while all others use steam.

The influence of the break and hydrogen release locations on the containment atmosphere is established by comparing the results of these tests.

#### 9.C.2.4.2.1 Experiment T31.5

The results of containment experiment T31.5 performed by Valencia, 1987 and Wenzel et al., 1987 are reported by Wolf and Valencia, 1988 and 1989. Experiment T31.5 includes a short-term, superheated steam blowdown followed by a long-term, low steam release rate and a $H_2$/He gas mixture injection. The short-term steam mass flow release into the room 1704 of the HDR-containment takes 25 seconds (with the approximate average flow rate of 1200 kg/s - see Figure 9.C.2-79). Room 1704 is at elevation 17.55-25.3 m in the upper

section of the containment, near the spiral staircase (see Figure 9.C.2-50 and 9.C.2-79). The large break position is at +22.3 m (about 8 m bellow the upper deck) and the blowdown pipe is pointing upward.

From 21 to 36 minutes, steam is released at an average mass flow rate 2.3 kg/s (see Figure 9.C.2-80). From 36 to 48 minutes, an $H_2$/He gas mixture is released into the containment with an approximate average mass flow rate of 0.24 kg/s (see Fig. 9.C.2-80). All the releases can be considered as steam blowdowns into a high-positioned compartment in the containment.

The containment pressure, temperature, hydrogen concentration, and velocities histories over 20 hours are presented in Figures 9.C.2-81 - 9.C.2-85. The two pressure peaks correspond to the periods of steam injections (see Figure 9.C.2-81).

Temperature histories at various axial positions are presented in Figure 9.C.2-82. The axial temperature distribution is uniform above the break position, with the exception of local temperatures measuring the break plume. A linearly decreasing temperature (stratification) is present below the break position. The vertical temperature gradient decreases with time due to the global natural circulation, which develops both above and below the break location. The major vertical flow paths are through-compartments in the main and spiral staircases, where small temperature differences of about 5 °C exist at equal heights. Horizontal connections exist at discrete elevations to provide circulation between the vertical flow paths.

The measured hydrogen concentration distributions at various times are presented in Figure 9.C.2-83. The $H_2$/He gas mixture concentration increases to a maximum value (13 percent volume, see Figure 9.C.2-84) in the regions above the release position. This concentration remains uniform over several hours in the upper portion of the dome (above 35 m - see Figure 9.C.2-84), while in the lower positions (34, 31, and 25m) it decreases after reaching maximum values. At the highest position of the dome (49 m), the decrease in the mixture concentration starts about 300 minutes after the start of the experiment and continues until about 360 minutes. After 360 minutes, the concentration above 12 m is a uniform mixture concentration of 10 percent vol. The steady-state profile of the mixture concentration is reached after 900 minutes.

For the first 12 minutes, upward and downward flows are present in the spiral and main staircases, respectively. The measured velocities are presented in Figure 9.C.2-85. The velocities are recorded again after the start of the steam injection (after 21 minute). Staircase flow starts again at approximately 200 minutes, at the same time that the mixture concentration in the upper portion of the containment starts to decrease. It then decreases again around 350 minutes, when upper region reaches a uniform concentration.

**Interpretation of Data**

Even for the case of the high release point with an initially stratified distribution, the final gas concentration through most of the containment is nearly homogenized due to the global natural circulation effects. Only a small, steady stratification gradient exists (about 1 °C over the height of dome, about 18 °C over 25 m below the break, gradient of about 7.5 to 8.8 percent $H_2$/He over the height of dome).

**Applicability to the AP600 and AP1000**

Since the AP600 and AP1000 have significant cooling over the containment dome (which somewhat corresponds to the HDR dome region), additional driving forces for circulation above the operating deck exist.

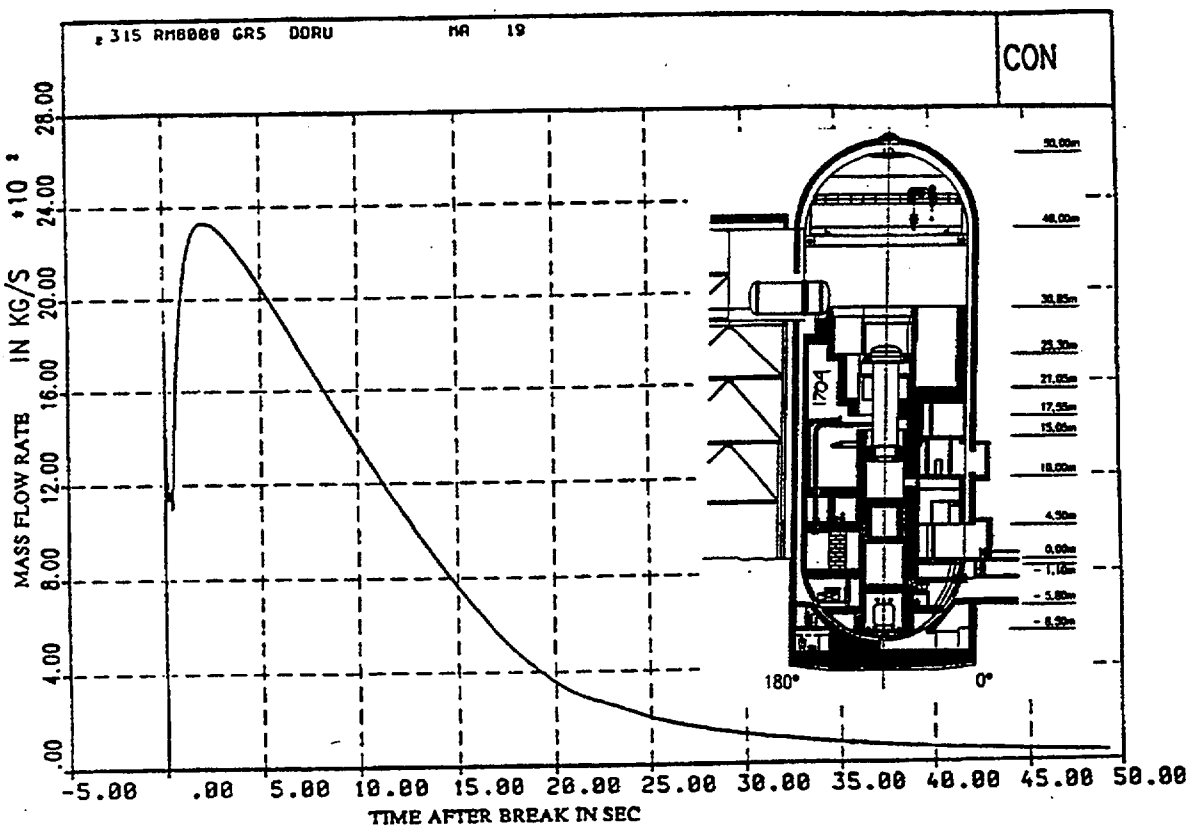


**Figure 9.C.2-79 HDR-T31.5 Blowdown mass flow rate into the containment**

**(reprinted from: L. Wolf, K. Mun, "Overview of experimental results for long-term, Large-scale natural circulations in LWR-containments after large LOCAs, Vol. II: Assessment of HDR Experiments V21.1, V43, T31.5 and E11.5", University of Maryland at College Park, for DOE - Project HDR Hydrogen Mixing Evaluation for Containment Safety Evaluations Natural Global Circulation, Order Number: DE-AP07-96ID10765", April 1996)**

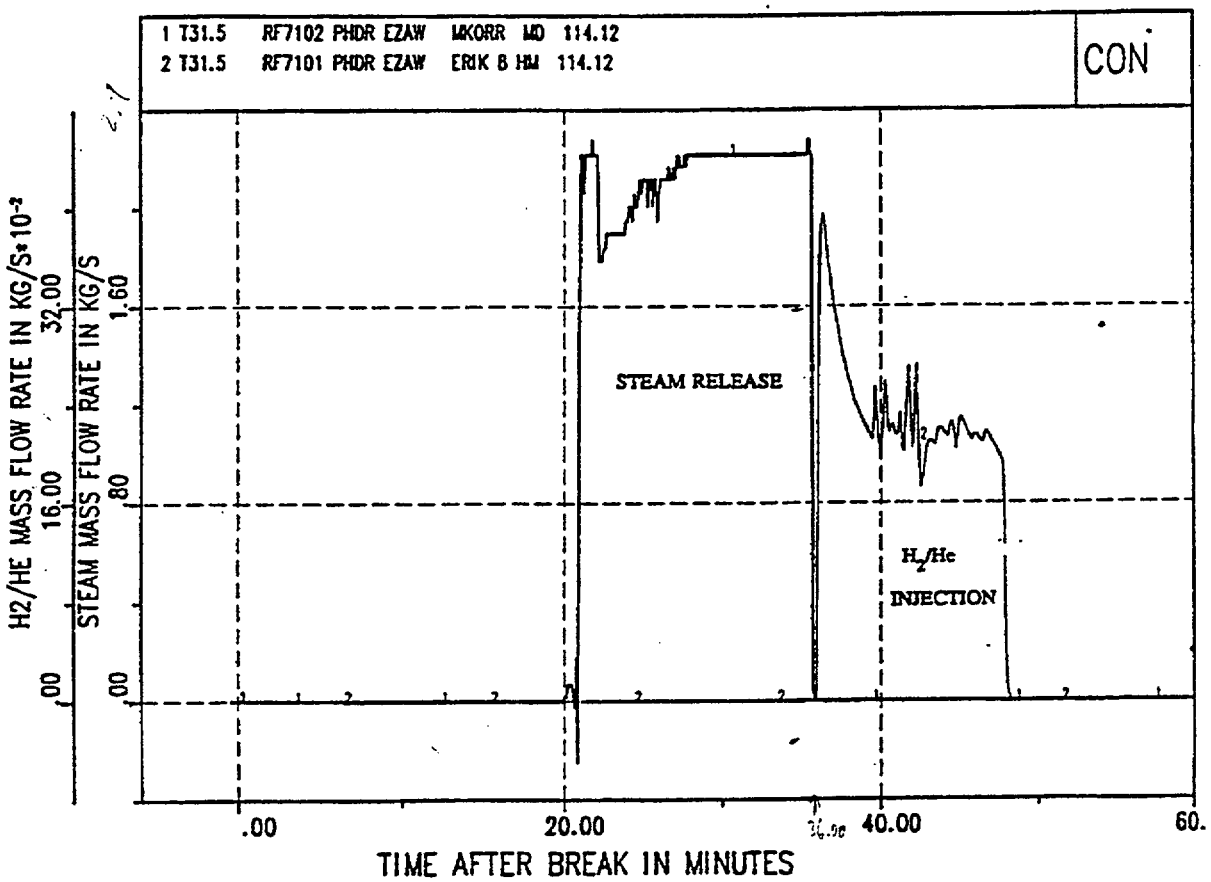


**Figure 9.C.2-80 HDR-T31.5 Steam and $H_2$/He gas mass flow rates into the containment**

**(reprinted from: L. Wolf, K. Mun, "Overview of experimental results for long-term, Large-scale natural circulations in LWR-containments after large LOCAs, Vol. II: Assessment of HDR Experiments V21.1, V43, T31.5 and E11.5", University of Maryland at College Park, for DOE - Project HDR Hydrogen Mixing Evaluation for Containment Safety Evaluations Natural Global Circulation, Order Number: DE-AP07-96ID10765", April 1996)**

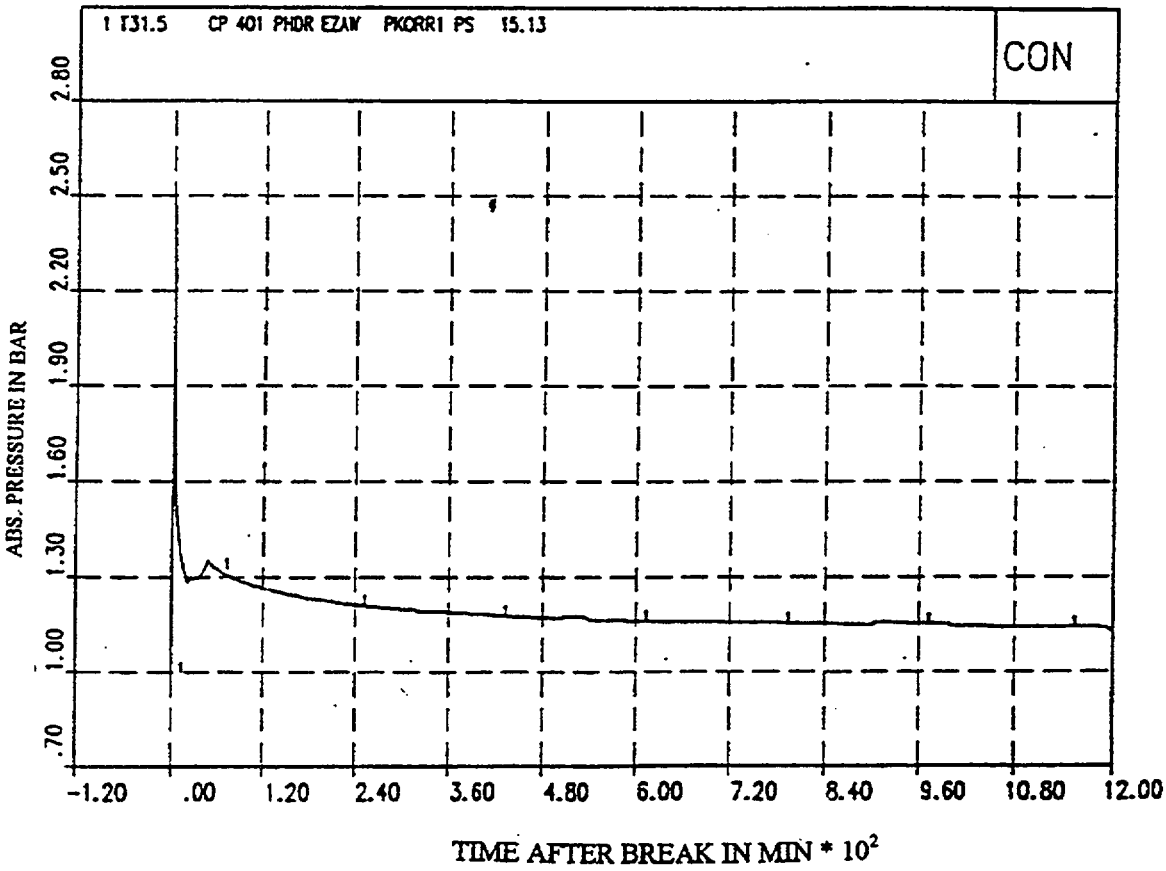


**Figure 9.C.2-81 HDR-T31.5 Pressure history after large LOCA over 1200 minutes**

**(reprinted from: L. Wolf, K. Mun, "Overview of experimental results for long-term, Large-scale natural circulations in LWR-containments after large LOCAs, Vol. II: Assessment of HDR Experiments V21.1, V43, T31.5 and E11.5", University of Maryland at College Park, for DOE - Project HDR Hydrogen Mixing Evaluation for Containment Safety Evaluations Natural Global Circulation, Order Number: DE-AP07-96ID10765", April 1996)**

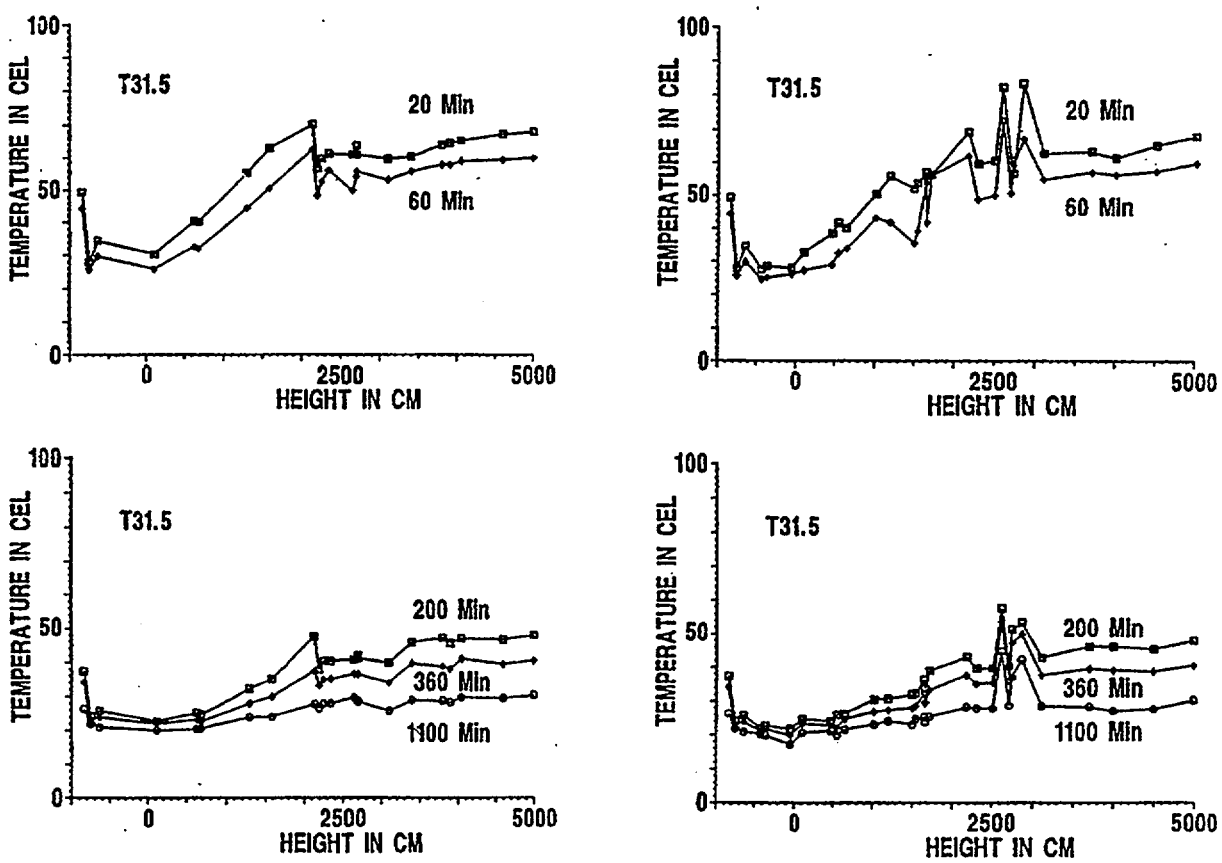


**Figure 9.C.2-82** **HDR-T31.5 Axial temperature profiles along spiral stairway (left) and main stairway (right) for different instants in time**

**(reprinted from: L. Wolf, K. Mun, "Overview of experimental results for long-term, Large-scale natural circulations in LWR-containments after large LOCAs, Vol. II: Assessment of HDR Experiments V21.1, V43, T31.5 and E11.5", University of Maryland at College Park, for DOE - Project HDR Hydrogen Mixing Evaluation for Containment Safety Evaluations Natural Global Circulation, Order Number: DE-AP07-96ID10765", April 1996)**

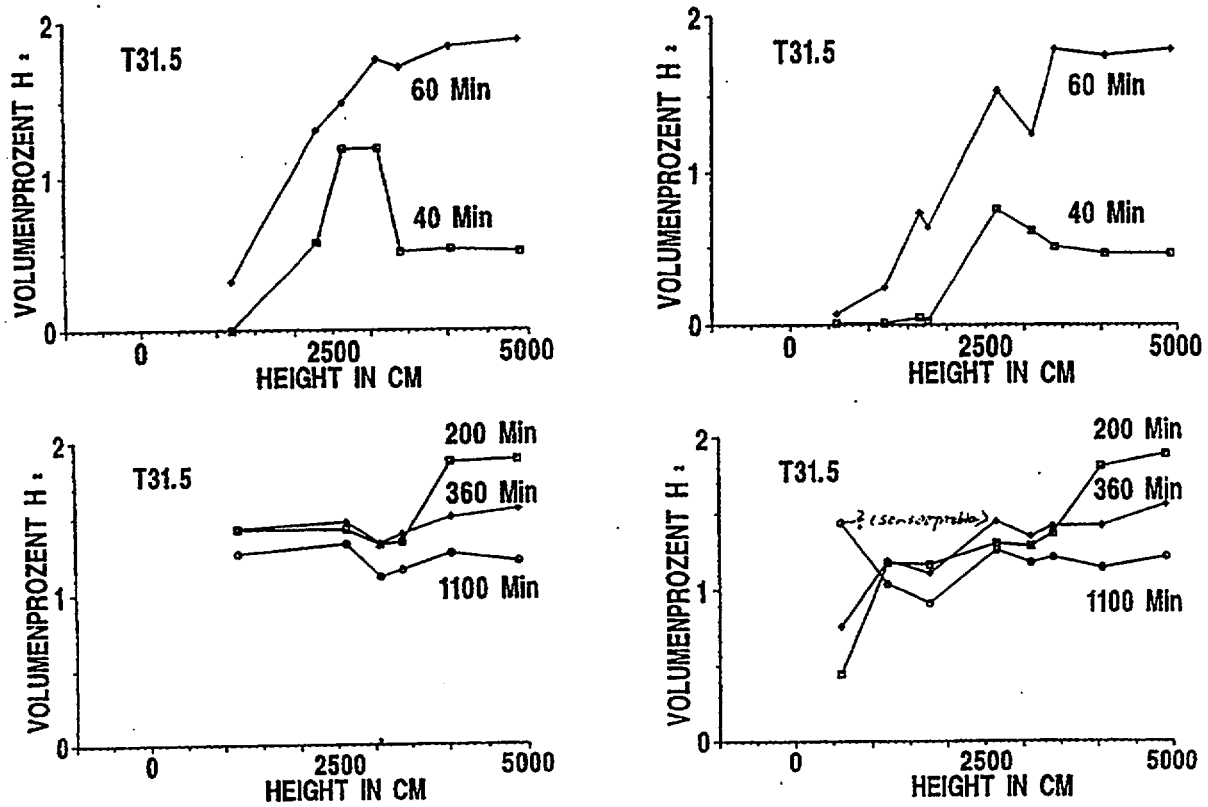


**Figure 9.C.2-83** **HDR-T31.5 Axial gas concentration profiles along spiral stairway (left) and main stairway (right) in upper containment region at different instants in time**

**(reprinted from: L. Wolf, K. Mun, "Overview of experimental results for long-term, Large-scale natural circulations in LWR-containments after large LOCAs, Vol. II: Assessment of HDR Experiments V21.1, V43, T31.5 and E11.5", University of Maryland at College Park, for DOE - Project HDR Hydrogen Mixing Evaluation for Containment Safety Evaluations Natural Global Circulation, Order Number: DE-AP07-96ID10765", April 1996)**

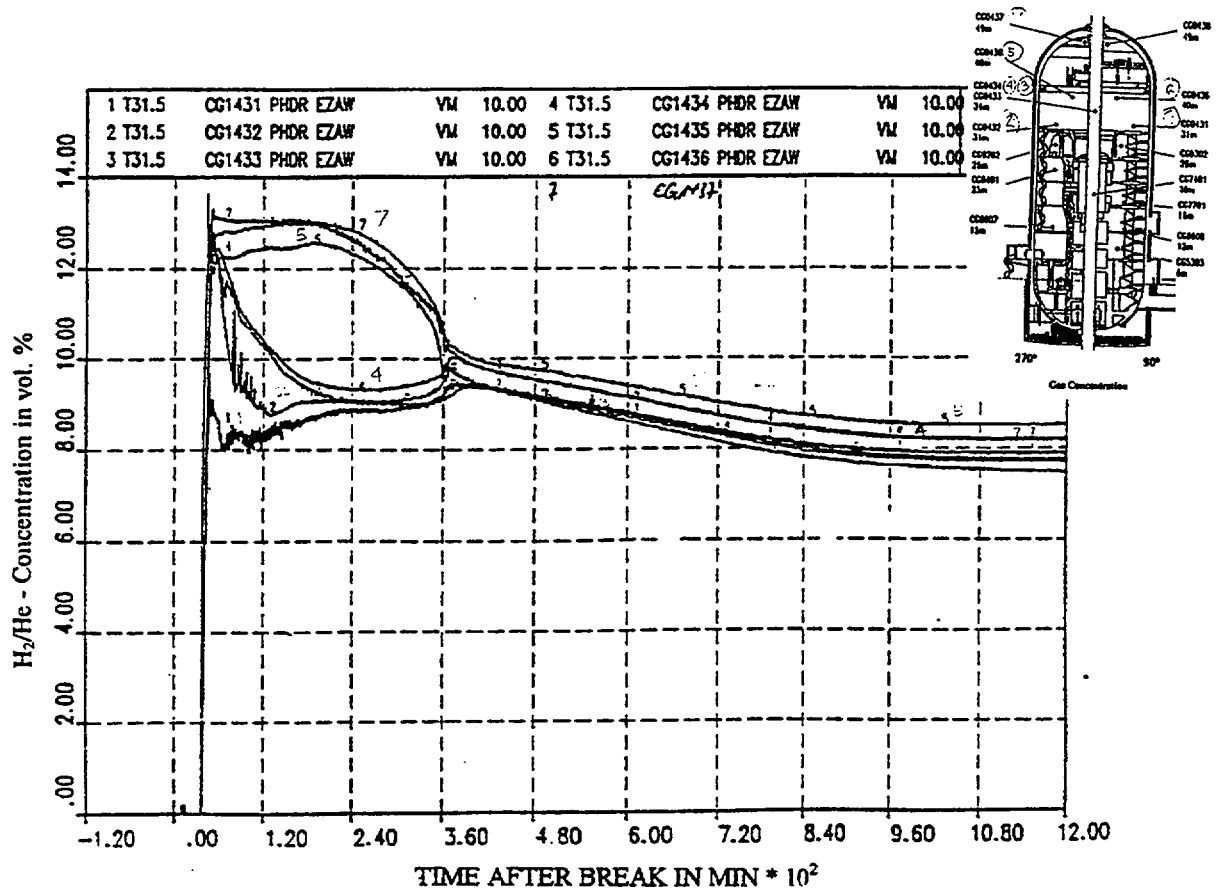


**Figure 9.C.2-84 HDR-T31.5 Gas concentrations inside the containment dome**

**(reprinted from: L. Wolf, K. Mun, "Overview of experimental results for long-term, Large-scale natural circulations in LWR-containments after large LOCAs, Vol. II: Assessment of HDR Experiments V21.1, V43, T31.5 and E11.5", University of Maryland at College Park, for DOE - Project HDR Hydrogen Mixing Evaluation for Containment Safety Evaluations Natural Global Circulation, Order Number: DE-AP07-96ID10765", April 1996)**

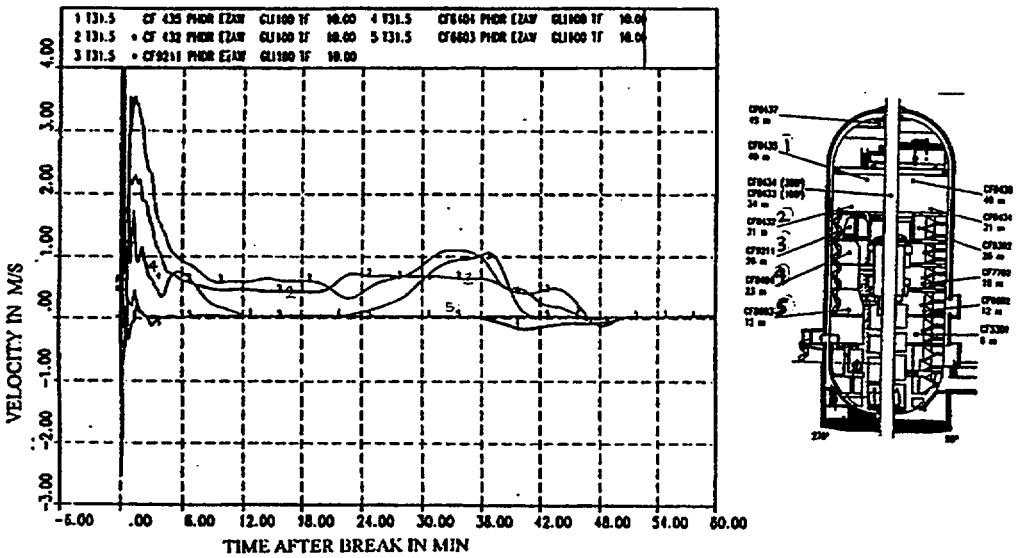


**Figure 9.C.2-85a** **HDR-T31.5 Velocities over 60 minutes along spiral stairways and associated dome regions**

**(reprinted from: L. Wolf, K. Mun, "Overview of experimental results for long-term, Large-scale natural circulations in LWR-containments after large LOCAs, Vol. II: Assessment of HDR Experiments V21.1, V43, T31.5 and E11.5", University of Maryland at College Park, for DOE - Project HDR Hydrogen Mixing Evaluation for Containment Safety Evaluations Natural Global Circulation, Order Number: DE-AP07-96ID10765", April 1996)**

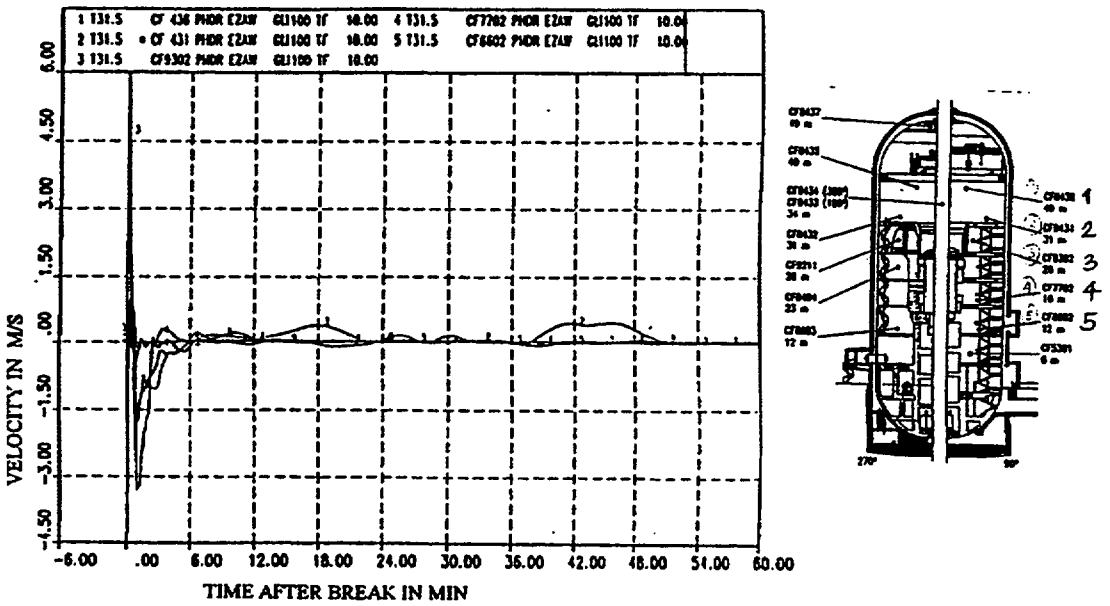


**Figure 9.C.2-85b** **HDR-T31.5 Velocities over 60 minutes along main stairways and associated dome regions**

**(reprinted from: L. Wolf, K. Mun, "Overview of experimental results for long-term, Large-scale natural circulations in LWR-containments after large LOCAs, Vol. II: Assessment of HDR Experiments V21.1, V43, T31.5 and E11.5", University of Maryland at College Park, for DOE - Project HDR Hydrogen Mixing Evaluation for Containment Safety Evaluations Natural Global Circulation, Order Number: DE-AP07-96ID10765", April 1996)**

### 9.C.2.4.2.2 Experiment V21.1

The blowdown for the V21.1 experiment (see Kanzleiter T., Valencia, L., 1984) is initiated inside the R1603 compartment, which is in the middle section of the HDR containment (see Figure 9.C.2-50 and 2-86). The arrangement of reactor pressure vessel, blowdown pipe (break diameter 453 mm), and jet impingement plate for the subcooled water blowdown is shown in Figure 9.C.2-86. Other characteristics of the experiment are given in Table 9.C-6. The total mass and enthalpy of the exiting fluid are 50157 kg and 72320 MJ, respectively. The test could be characterized as a large break cross-section and a short-term blowdown (30 seconds). The maximum peak pressure was 3 bar because of the much higher mass and energy releases during the steam/liquid mixture blowdown (Figure 9.C.2-87). The transient atmospheric temperature for the dome, main and spiral stairway are presented in the Figures 9.C.2-88, 9.C.2-89, and 9.C.2-90.

At the beginning of the V21.1 experiment, the blowdown results in fairly uniform distribution of temperature in the dome (Figure 9.C.2-88). After about 10 seconds, a stratification gradient exists. The maximum temperature gradient over the above-deck height is 10°C at about 100 minutes. Until 420 minutes, the thermal stratification inside the dome volume exists (see Figure 9.C.2-88). At the end of the break release (after 30 seconds) the temperatures inside the dome are decreasing (slower near the top). After 420 minutes, temperature differences inside the dome volume are only around 2-3°C, indicating the presence of natural circulation. The natural circulation in the above-deck region acts to reduce the gradient with time.

The axial temperature distributions in the mean and spiral staircases are presented in Figures 9.C.2-89 and 9.C.2-90. Immediately after the end of the blowdown, a stratification gradient develops. The transient histories of the temperatures at the same axial levels (in the spiral and main staircases) are presented in Figure 9.C.2-91. The large blowdown injected into the middle of the both staircases results in almost equal temperatures in both flow channels, therefore, global natural convection can not be formed. A slightly higher temperature is recorded in the main staircase. A temperature difference of 1-2°C starts at 200 minutes and continues until 800 minutes.

#### Interpretation of Data

The large break with the blowdown penetrating into the middle of both staircases (mean flow paths) minimizes temperature differences among the same axial positions and suppresses the development of the natural circulation.

The small temperature differences of about 1°C (Figure 9.C.2-90) and the slight global natural circulation appear to be established later due to the different heat release rates of the various wall structures. These structures are heated to various temperatures during the early phase of the transient.

The large LOCA HDR tests described should be carefully applied to the passive containment design. The majority of the passive containment compartments are at the lower levels of the containment. Heating of the structures (walls, floors, and equipment) in the middle of the containment height or above is not possible because they do not exist. The formation of the stable stratified layers in the upper portion of the passive containment due to the accumulated heat (in fact the higher temperatures) in the concrete and steel structures is not possible. The temperature of the containment shell, which is the only solid structure in the upper portion of the containment, tends to be lower than the internal containment temperature. This promotes internal global circulation.

**Application to AP600 and AP1000**

Small temperature differences inside the dome, even without dome cooling or additional releases after blowdown, are sufficient to drive natural convection. This leads to more homogenous conditions over time.

**Table 9.C-6 HDR-V21.1 Test Conditions**

| | |
|---|---|
| MEASURED INITIAL CONDITIONS IN REACTOR PRESSURE VESSEL | |
| Pressure | 110.4 bar |
| Temperature | 315 - 319°C |
| Liquid Level | filled |
| Liquid volume prior to blowdown | 74.5 $m^3$ |
| Liquid Mass prior to blowdown | 50233 kg |
| Liquid level in reactor pressure vessel after blowdown | empty |
| Steam volume after blowdown | 74.5 $m^3$ |
| Steam mass after blowdown | 76 kg |
| Mass of exiting fluid | 50157 kg |
| Enthalpy of exiting fluid | 72320 MJ |
| Jet impingement plate distance (LD) | 2 |
| Jet impingement plate inclination angle | 0° |
| Break nozzle diameter | 453 mm |
| Break nozzle length | 6091 mm |
| VENT FLOW OPENINGS FROM BREAK SUBCOMPARTMENT | |
| UO140 | open |
| UO143 | closed |
| UO162 | 6.1 $m^2$ |
| UO177 | open |
| UO178 | closed |
| External spray off (all the time) | |

**(reprinted from: L. Wolf, K. Mun, "Overview of experimental results for long-term, Large-scale natural circulations in LWR-containments after large LOCAs, Vol. II: Assessment of HDR Experiments V21.1, V43, T31.5 and E11.5", University of Maryland at College Park, for DOE - Project HDR Hydrogen Mixing Evaluation for Containment Safety Evaluations Natural Global Circulation, Order Number: DE-AP07-96ID10765", April 1996)**

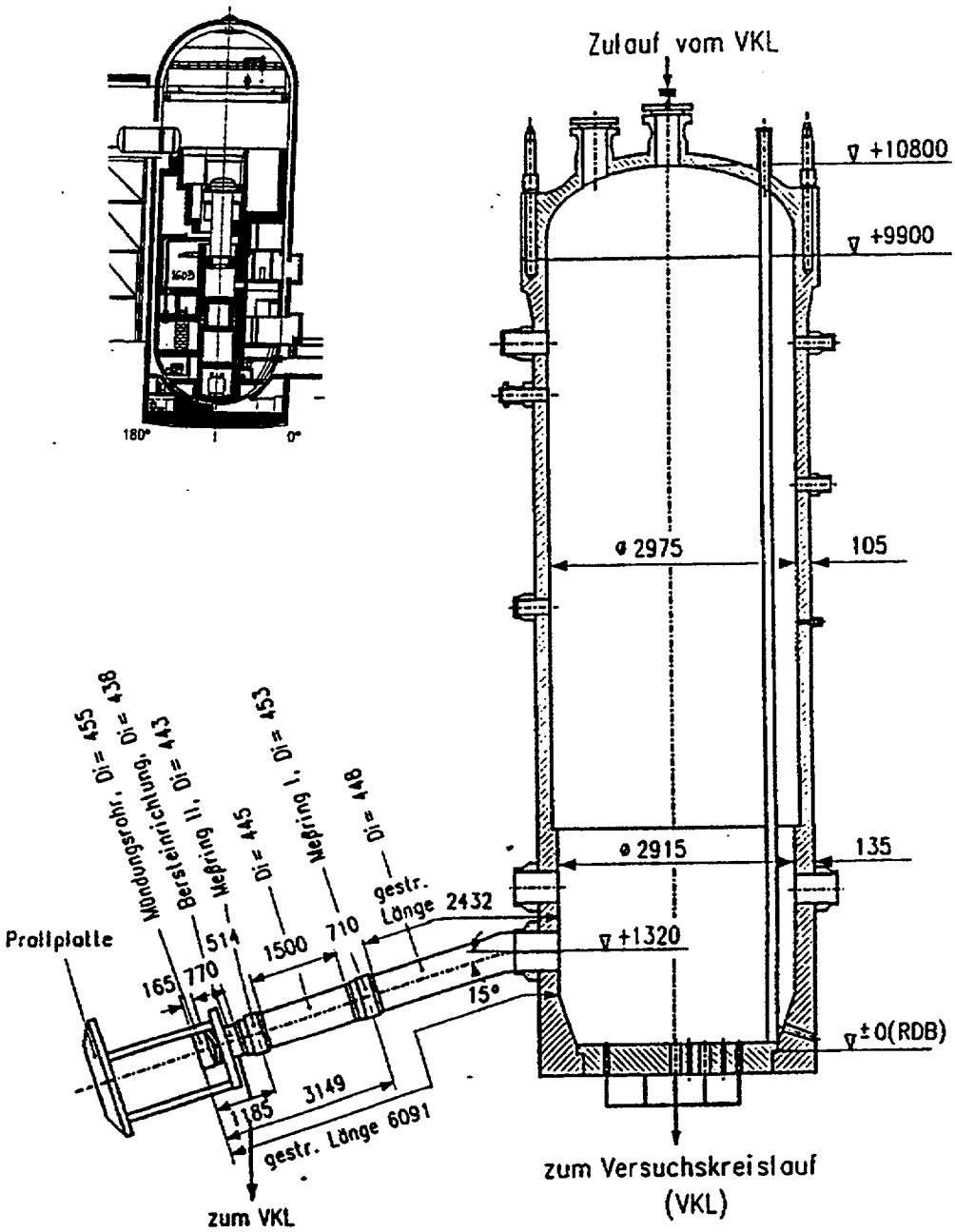


**Figure 9.C.2-86** **HDR-V21.1 Arrangement of reactor pressure vessel, blowdown pipe and jet impingement plate for water blowdown test**

**(reprinted from: L. Wolf, K. Mun, "Overview of experimental results for long-term, Large-scale natural circulations in LWR-containments after large LOCAs, Vol. II: Assessment of HDR Experiments V21.1, V43, T31.5 and E11.5", University of Maryland at College Park, for DOE - Project HDR Hydrogen Mixing Evaluation for Containment Safety Evaluations Natural Global Circulation, Order Number: DE-AP07-96ID10765", April 1996)**

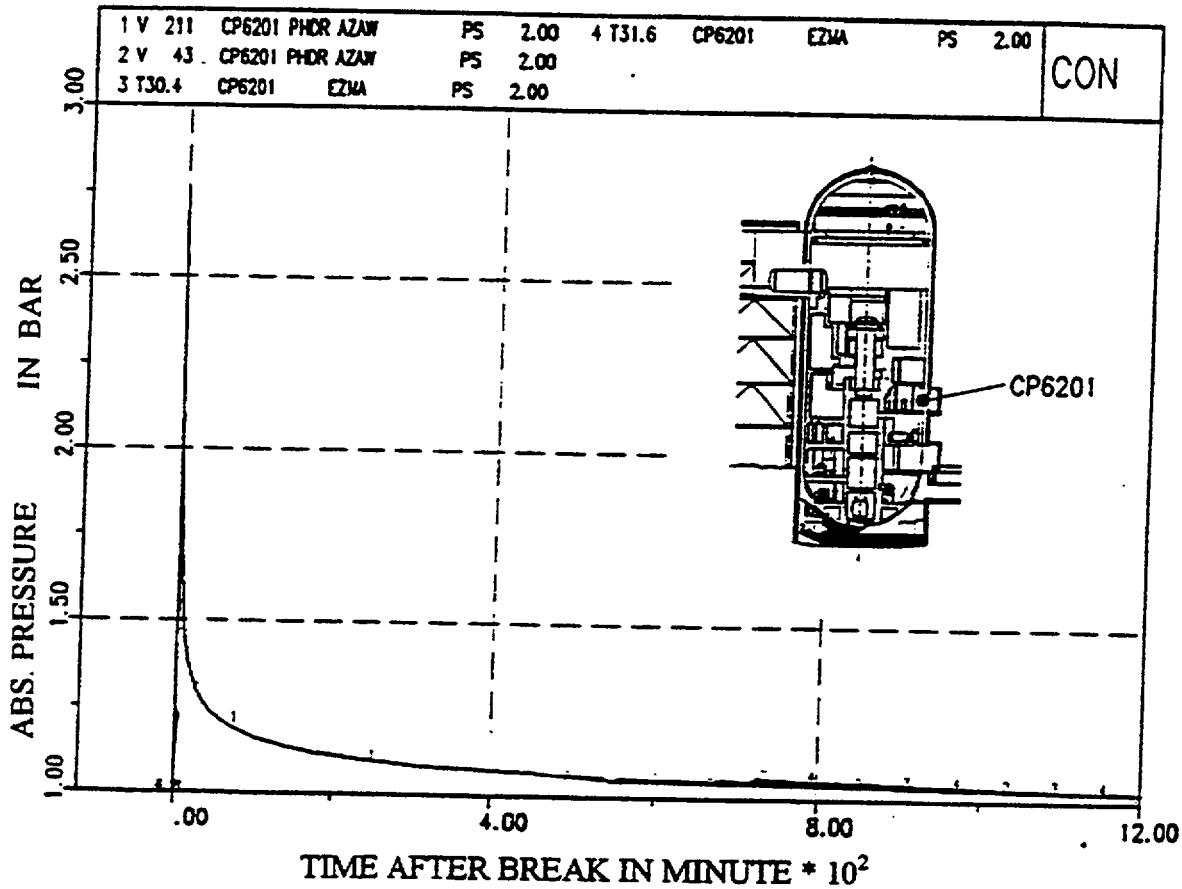


**Figure 9.C.2-87 HDR-V21.1 Containment pressure history**

**(reprinted from: L. Wolf, K. Mun, "Overview of experimental results for long-term, Large-scale natural circulations in LWR-containments after large LOCAs, Vol. II: Assessment of HDR Experiments V21.1, V43, T31.5 and E11.5", University of Maryland at College Park, for DOE - Project HDR Hydrogen Mixing Evaluation for Containment Safety Evaluations Natural Global Circulation, Order Number: DE-AP07-96ID10765", April 1996)**

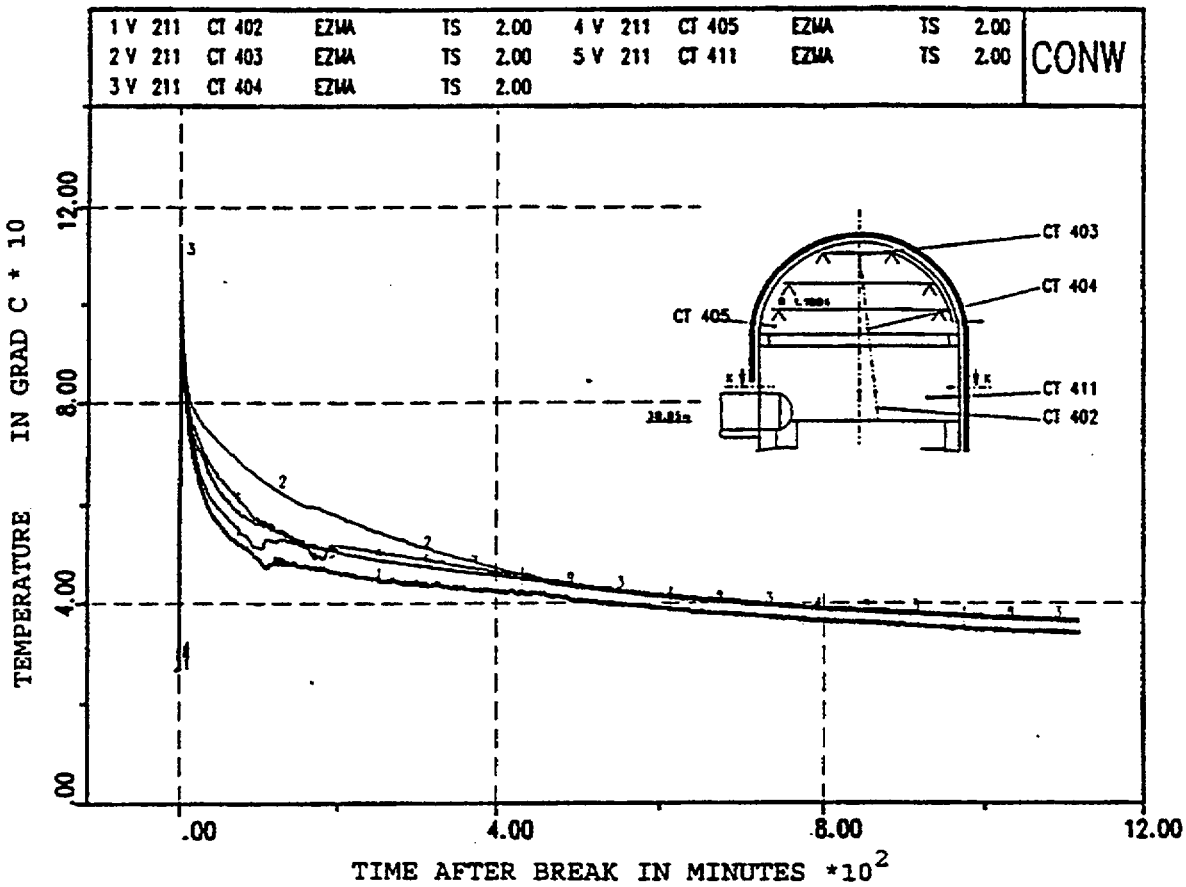


**Figure 9.C.2-88 HDR-V21.1 Temperatures in the containment dome**

**(reprinted from: L. Wolf, K. Mun, "Overview of experimental results for long-term, Large-scale natural circulations in LWR-containments after large LOCAs, Vol. II: Assessment of HDR Experiments V21.1, V43, T31.5 and E11.5", University of Maryland at College Park, for DOE - Project HDR Hydrogen Mixing Evaluation for Containment Safety Evaluations Natural Global Circulation, Order Number: DE-AP07-96ID10765", April 1996)**

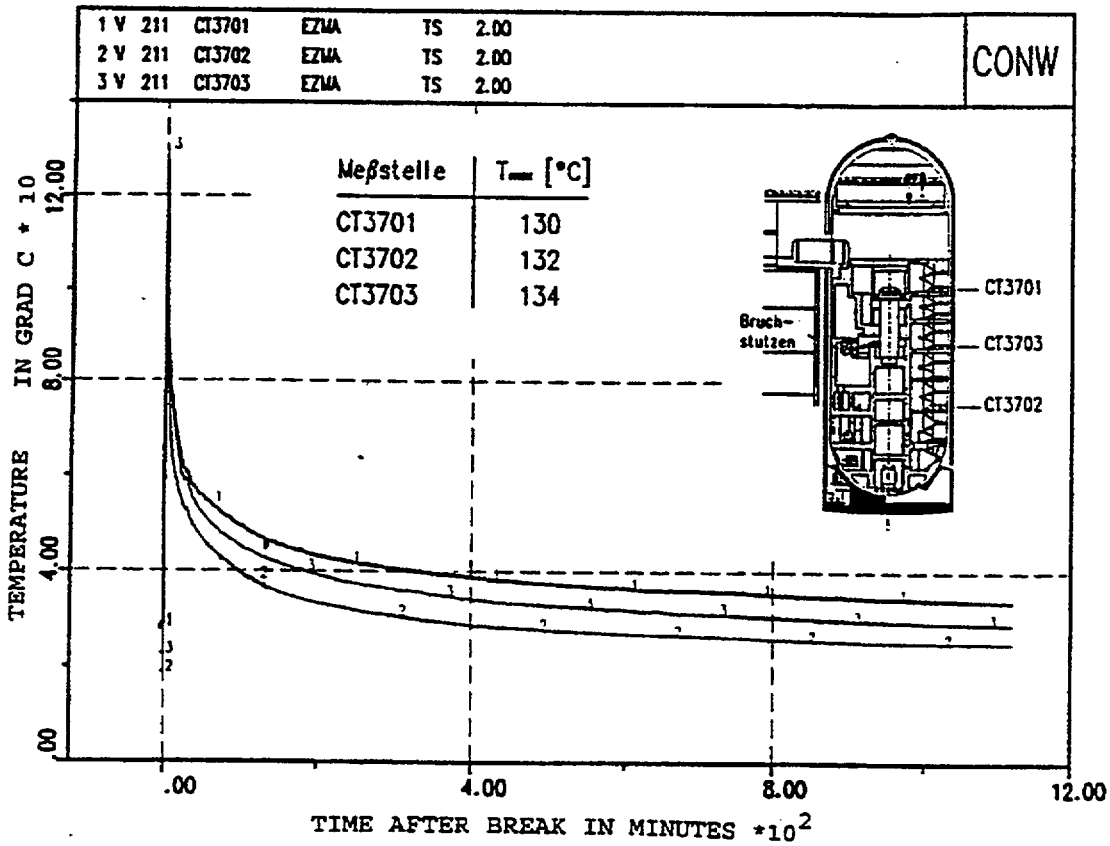


**Figure 9.C.2-89 HDR-V21.1 Temperature along the main staircase at different axial positions**

**(reprinted from: L. Wolf, K. Mun, "Overview of experimental results for long-term, Large-scale natural circulations in LWR-containments after large LOCAs, Vol. II: Assessment of HDR Experiments V21.1, V43, T31.5 and E11.5", University of Maryland at College Park, for DOE - Project HDR Hydrogen Mixing Evaluation for Containment Safety Evaluations Natural Global Circulation, Order Number: DE-AP07-96ID10765", April 1996)**

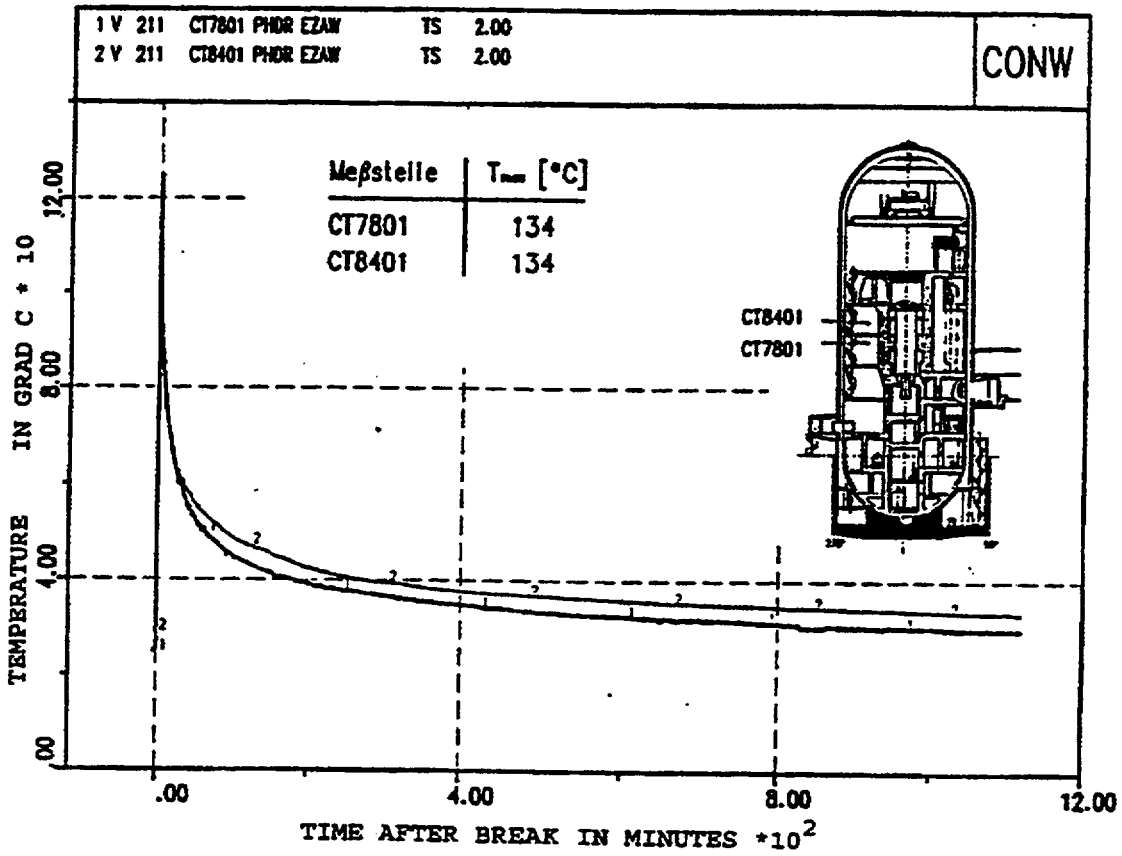


**Figure 9.C.2-90 HDR-V21.1 Temperatures along spiral staircase at different axial positions**

**(reprinted from: L. Wolf, K. Mun, "Overview of experimental results for long-term, Large-scale natural circulations in LWR-containments after large LOCAs, Vol. II: Assessment of HDR Experiments V21.1, V43, T31.5 and E11.5", University of Maryland at College Park, for DOE - Project HDR Hydrogen Mixing Evaluation for Containment Safety Evaluations Natural Global Circulation, Order Number: DE-AP07-96ID10765", April 1996)**

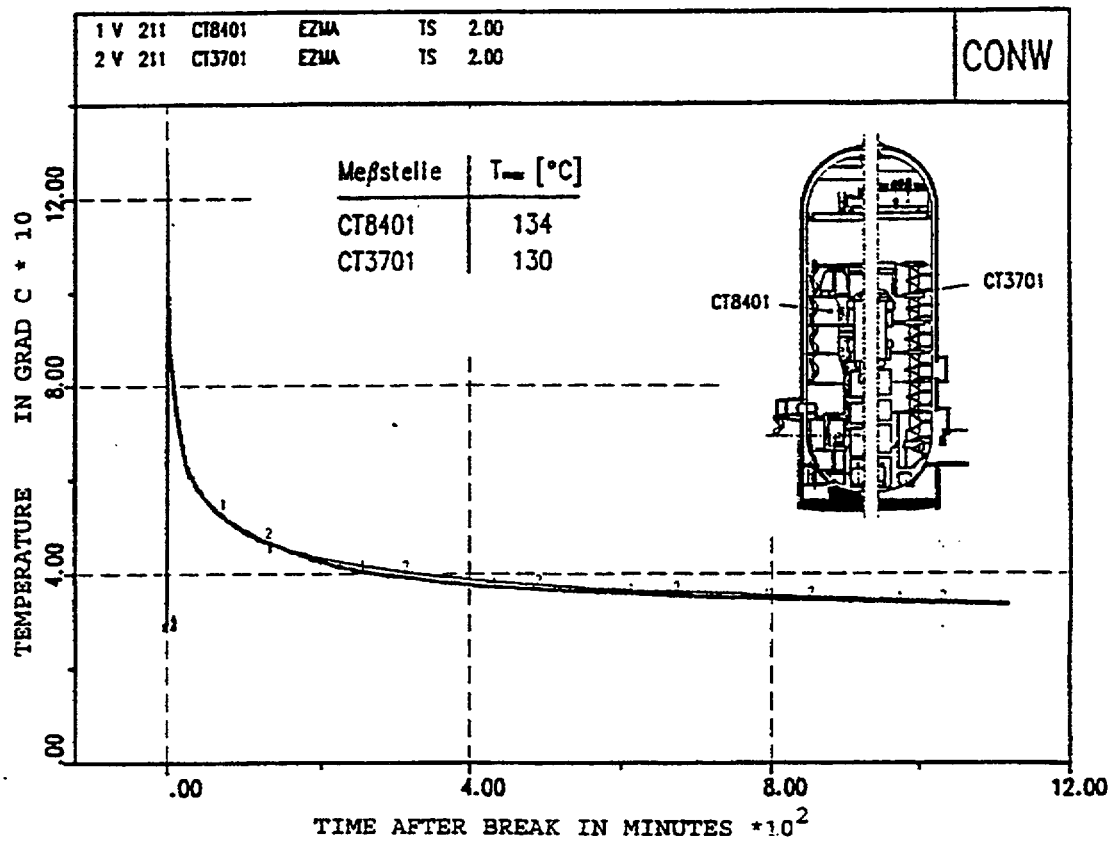


**Figure 9.C.2-91** **HDR-V21.1 Comparison between temperatures in spiral staircase (H=22.5 m) and main staircase (H=25 m)**

**(reprinted from: L. Wolf, K. Mun, "Overview of experimental results for long-term, Large-scale natural circulations in LWR-containments after large LOCAs, Vol. II: Assessment of HDR Experiments V21.1, V43, T31.5 and E11.5", University of Maryland at College Park, for DOE - Project HDR Hydrogen Mixing Evaluation for Containment Safety Evaluations Natural Global Circulation, Order Number: DE-AP07-96ID10765", April 1996)**